Melanoma immunosurveillance by $CD4^+$ T cells

Emma Bawden

ORCID ID:

0000-0002-4772-7675

From Melbourne, Australia

Submitted in total fulfilment of the requirements of the joint degree of

Doctor of Philosophy (PhD)

of

The Medical Faculty

The Rheinische Friedrich-Wilhelms-Universität Bonn

and

The Department of Microbiology and Immunology,

The University of Melbourne

Melbourne, Bonn 2021

Performed and approved by The Medical Faculty of The Rheinische Friedrich-Wilhelms-Universität Bonn and The University of Melbourne.

Supervisors:

1. Prof. Dr. med. Thomas Gebhardt (principal supervisor, Melbourne)
2. Prof. Dr. med. Michael Hölzel (principal supervisor, Bonn)
3. Dr. Katharina Hochheiser (co-supervisor, Melbourne)

Date of submission: 17/12/2020

Date of oral examination: 3/5/2021

Institute of Experimental Oncology (University Hospital Bonn),

Director: Prof. Dr. med. Michael Hölzel

Table of Contents

Abbreviations

ACT	Adoptive cell therapy
ACTB	β-Actin
APC	Antigen presenting cell
ATP5B	ATP synthase F1 subunit beta
BFA	Brefeldin A
BS	Bottom strand
BSA	Bovine serum albumin
CAR	Chimeric antigen receptor
Cat.	Catelog
cbLN	Contralateral brachial lymph node
CD	Cluster of differentiation
cDC	conventional DC
CDK4	Cyclin-dependent kinase 4
Ct	C-terminus
CTLA-4	Cytotoxic T-lymphocyte-associated protein 4
CTLA-4	cytotoxic T-lymphocyte-associated protein 4
CTV	Cell trace violet
d	Day
DAMP	Danger associated molecular pattern
DAPI	4',6-Diamidino-2-Phenylindole, Dihydrochloride
DC	Dendritic cell
DETC	Dendritic epidermal T cell
dH_2O	Distilled water
DMSO	Dimethyl sulphoxide
DNA	Deoxyribonucleic acid
DNase	Deoxyribonuclease
ds	Double stranded
e.c.	Epicutaneous
eGFP	Enhanced green fluorescent protein
Eomes	Eomesodermin
FACS	Fluorescence activated cell sorting
Flt3L	Fms-like tyrosine kinase 3 ligand
FoxP3	Forkhead box P3
gB	Herpes simplex virus glycoprotein b
gD	Herpes simplex virus glycoprotein d

GFP	Green fluorescent protein
GzmB	Granzyme B
h	hours
H&E	Haematoxylin and eosin
HBSS	Hank's balanced salt solution
HEPES	N-2-hydroxyethylpiperazine-N'-2-ethane sulfonic acid
HSV-1	Herpes simplex virus type 1
HVEM	Herpesvirus entry mediator
i.d.	Intradermal
i.p.	Intraperitoneal
i.v.	Intravenous
ibLN	Ipsilateral brachial lymph node
ICB	Immune checkpoint blockade
IFN	Interferon
IFN	Interferon
IL	Interleukin
IL	interleukin
ILC	Innate lymphoid cell
iNOS	Inducible nitric oxide synthase
Int	Intermediate
LAG-3	Lymphocyte activation gene 3
LB	Luria-Bertani
Luc	Luciferase (firefly)
mAbs	Monoclonal antibodies
MAIT cell	Mucosal associated invariant T cell
MDSC	Myeloid derived suppressor cell
MFI	Mean fluorescence intensity
MFI	mean fluorescent intensities
MHC-I	Major histocompatibility complex class I
MHC-II	Major histocompatibility complex class II
Min	Minutes
NK cell	Natural killer cell
NKT cell	Natural killer T cell
OVA	Ovalbumin
PAMP	Pathogen associated molecular pattern

PBS	Phosphate buffered saline
PD-L1	Programmed death-ligand 1
PD-1	Programmed cell death protein 1
PI	Propidium iodide
PMA	Phorbol 12-myristate 13-acetate
PRR	Pattern recognition receptor
qPCR	Quantitative Polymerase Chain Reaction
Rag	Recombination-activating gene
RBC	Red blood cell
RBS	red blood cell
RNA	Ribonucleic acid
RT	Room temperature
RT-PCR	real time polymerase chain reaction
s	seconds
s.c.	Subcutaneous
S1P	Sphingosine 1 phosphate
Seq	Sequence
SLO	secondary lymphoid organ
T-bet	T-cell-specific T-box transcription factor
TAE	Tris-Acetate-EDTA
TAM	Tumour associated macrophage
TBS	Tris-buffered saline
TCM cells	Central memory T cells
TCR	T cell receptor
TCRtg	Transgenic T cell receptor
TEM cells	Effector memory T cells
Tfh	T follicular helper
TGF-b	transforming growth factor-b
TGFβ	Transforming growth factor β
Th	T helper
TIL	Tumour infiltrating lymphocyte
TLS	Tertiary lymphoid structures
TNF	Tumour necrosis factor
TNFR	Tumor necrosis factor receptor
TNFa	Tumor necrosis factor a
TRAIL	Tumor necrosis factor-related apoptosis inducing factor
Treg cells	Regulatory T cells
T_{RM} cells	Tissue-resident memory T cells

TS	Top strand
Tyr	Tyrosinase
TYRP1	Tyrosinase Related Protein 1
U	Units
WEHI	Walter and Eliza Hall Institute of Medical Research
Wk	Week
WT	wild-type
α	Anti

List of tables

List of figures

List of videos

Abstract

The immune system can recognise and control cancer cells in a process termed cancer immunosurveillance. There is increasing evidence that $CD4^+$ T cells play an important role in melanoma immunosurveillance but considerable debate surrounds the underlying anti-tumoral mechanisms. This project thus sought to unravel the role of $CD4^+$ T cell responses to melanoma using a transplantable orthotopic murine melanoma model in conjunction with newly generated genetically modified B16 melanoma cell lines. Remarkably, adoptive transfer of naïve or activated antigen-specific $CD4^+$ T cells was highly protective against the development of melanoma. In addition to a classical “helper” function, $CD4^+$ T cells acted as peripheral anti-tumoral effector cells whereby they migrated into the skin, differentiated into Th1 cells and mediated local suppression of tumor development. Accordingly, we provide evidence that $CD4^+$ T cells can directly kill melanoma cells *in vitro* through several cytotoxic pathways, including TNF superfamily signalling via TNFα and FasL as well as perforin-dependent cell lysis. Finally, we investigated the role of MHC-II expression by melanoma on the antitumoral function of $CD4^+$ T cells. Whilst MHC-II expression by melanoma cells promoted $CD4^+$ T cell infiltration into the primary tumor site it was dispensable for control mediated by $CD4^+$ T cells. This suggested an important role for indirect display of MHC-II-restricted epitopes by antigen-presenting cells within the tumor microenvironment. This was supported by visualization of melanoma-specific $CD4^+$ T cells in the tumor microenvironment using two-photon microscopy, where activated $CD4^+$ T cells appeared to interact with melanoma cells via intermediary cells, presumably professional antigen-presenting cells. Finally, we observed a reduction in metastatic lesions in the tumor-draining lymph node in mice challenged with MHC-II deficient melanoma cells. These data suggest that MHC-II may play context-dependent roles in control of primary tumors and lymph node metastases by $CD4^+$ T cells. In summary, this study demonstrates the important role of $CD4^+$ T cells in melanoma immunosurveillance and provides important insights into underlying antitumoral mechanisms.

Declaration

The work that is presented in this thesis was conducted at the University of Melbourne in the laboratory Prof. Dr. med. Thomas Gebhardt and at the University of Bonn in the laboratory of Prof. Dr. med. Michael Hölzel. This work was funded by the National Health and Medical Research Council. Emma Bawden was supported by an Australian Government Research Training Program Scholarship from the University of Melbourne.

This is to certify that,

(i) the thesis only comprises my original work towards the PhD except where indicated

(ii) due acknowledgement has been made in the text to all other material used

(iii) the thesis is less than 100,000 words in length, exclusive of tables, maps, bibliographies and appendices.

Melbourne, 19th November 2020 Emma Bawden

Preface

(i) Contribution

My contribution to the experiments within each chapter was as follows:

Chapter 3: 90 %

Chapter 4: 80 %

Chapter 5: 85 %

I acknowledge the important contributions of others to the experiments presented herein:

Chapter 3: Tissue processing for histology and staining with H&E was performed by the Histology Facility at the School of Biomedical Sciences at the University of Melbourne.

Chapter 3-5: Bioluminescence imaging was performed by David Freestone, Gebhardt laboratory, the University of Melbourne.

Chapter 4: Light-sheet microscopy was performed by Teagan Wagner and two-photon microscopy was performed in collaboration with Teagan Wagner, Gebhardt laboratory, the University of Melbourne.

Chapter 3, 5: Next-generation sequencing was performed by Maike Effern and Daniel Hinze, Hölzel laboratory, the University of Bonn, Germany.

Acknowledgements

It is with immense gratitude that I acknowledge the leadership of my primary supervisor Professor Thomas Gebhardt. I feel privileged to have been guided by a mentor with expert knowledge and passion for immunology and an open-mindedness to facilitate independent thinking and my development as a scientist. I would like to extend the acknowledgement to my co-supervisor Dr Katharina Hochheiser whose input and encouragement has been valuable to the project and also to my experience as a PhD student. Finally, my thanks go to my supervisor at the University of Bonn, Professor Michael Hözel, who welcomed me into his laboratory and provided the resources and expertise in molecular cloning that was fundamental to advance the project.

I would like to thank the Bonn & Melbourne Research and Graduate School for the opportunity to study for a jointly awarded PhD at the University of Melbourne and the University of Bonn. I would also like to thank my PhD committee, Assoc. Professor Justine Mintern, Dr. Jason Waithman and Professor Andrew Brooks for the insightful discussions and advice.

Thank you to all the members of the Bedoui, Gebhardt and Hölzel laboratories. I consider it a privilege to work with such a supportive team of intelligent and generous people. I would further like to acknowledge the team members who were directly involved in my project; Teagan Wagner, Maike Effern, Daniel Hinze and David Freestone.

Finally, a big thank you to my support network; my family, Jennie, Ross and Harriet, as well as my friends, housemates and colleagues.

List of publications

Protein tyrosine phosphatase non-receptor type 2 and killer cell lectin-like receptor G1 regulate the generation and function of tissue-resident memory T cells in skin.

Journal of Experimental Medicine (in revision).

Katharina Hochheiser, Florian Wiede, Matthias H. Enders, Moshe Olshansky, Brendan Russ, Simone Nuessing, David Freestone, **Emma Bawden**, Asolina Braun, Annabell Bachem, Robyn McConville, Simone L. Park, Claerwen Jones, Gayle Davey, David Gyorki, David Tscharke, Ian Parish, Stephen Turner, Marco Herold, Tony Tiganis, Sammy Bedoui* and Thomas Gebhardt*

Adoptive T Cell Therapy Targeting Different Gene Products Reveals Diverse and Context-Dependent Immune Evasion in Melanoma.

Immunity, 2020 September 15; DOI: 10.1016/j.immuni.2020.07.007

Maike Effern, Nicole Glodde, Matthias Braun, Jana Liebing, Helena N Boll, Michelle Yong, **Emma Bawden**, Daniel Hinze, Debby van den Boorn-Konijnenberg, Mila Daoud, Pia Aymans, Jennifer Landsberg, Mark J Smyth, Lukas Flatz, Thomas Tüting, Tobias Bald, Thomas Gebhardt, Michael Hölzel.

The landscape of *CD28, CD80, CD86, CTLA4*, and *ICOS* DNA methylation in head and neck squamous cell carcinomas.

Epigenetics, 21 Apr 2020; DOI: 10.1080/15592294.2020.1754675

Luka de Vos, Ingela Grünwald , **Emma Grace Bawden** , Jörn Dietrich , Kathrin Scheckenbach , Constanze Wiek , Romina Zarbl , Friedrich Bootz , Jennifer Landsberg & Dimo Dietrich.

Treatment Response Monitoring in Patients with Advanced Malignancies Using Cell-Free SHOX2 and SEPT9 DNA Methylation in Blood: An Observational Prospective Study.

Journal of Molecular Diagnostics, 30 April 2020; DOI: 10.1016/j.jmoldx.2020.04.205

Luka de Vos, Maria Jung, Ruth-Miriam Koerber, **Emma G. Bawden**, Tobias A.W. Holderried, Jörn Dietrich, Friedrich Bootz, Peter Brossart, Glen Kristiansen, Dimo Dietrich.

LAG3 (LAG-3 , CD223) DNA methylation correlates with LAG3 expression by tumor and immune cells, immune cell infiltration, and overall survival in clear cell renal cell carcinoma.

Journal for ImmunoTherapy of Cancer, March 30, 2020; DOI: 10.1136/jitc-2020-000552

Niklas Klümper, Damian J Ralser, **Emma Grace Bawden**, Jenny Landsberg, Romina Zarbl, Glen Kristiansen, Marieta Toma, Manuel Ritter, Michael Hölzel, Jörg Ellinger, and Dimo Dietrich.

Comprehensive analysis of tumor necrosis factor receptor TNFRSF9 (4-1BB) DNA methylation with regard to molecular and clinicopathological features, immune infiltrates, and response prediction to immunotherapy in melanoma.

EBioMedicine, 4 February 2020 DOI: 10.1016/j.ebiom.2020.102647

Anne Fröhlich, Sophia Loick, **Emma Grace Bawden**, Simon Fietz, Jörn Dietrich, Eric Diekmann, Gonzalo Saavedra, Holger Fröhlich, Dennis Niebel, Judith Sirokay, Romina Zarbl, Gerrit H. Gielen Glen Kristiansen, Friedrich Bootz, Jennifer Landsberg, Dimo Dietrich.

Molecular and immune correlates of TIM-3 (HAVCR2) and galectin 9 (LGALS9) mRNA expression and DNA methylation in melanoma.

Clinical Epigenetics, 20 November 2019; DOI: 10.1186/s13148-019-0752-8

Tobias A. W. Holderried, Luka de Vos, **Emma Grace Bawden**, Timo J. Vogt, Joern Dietrich, Romina Zarbl, Friedrich Bootz, Glen Kristiansen, Peter Brossart, Jennifer Landsberg & Dimo Dietrich.

Chapter 1:
Introduction

Chapter 1: Introduction

1.1 A brief overview of the immune system

The immune system, comprising a complex network of different leukocyte populations, functions to protect the host by recognising threats, such as invading pathogens, and mounting appropriate responses to eliminate them. On the other hand, a misguided immune response may cause destruction of healthy tissue which can result in autoimmune disorders. Whilst it has been recognised for centuries that the immune system protects against pathogens, the phenomenon of cancer immunosurveillance, the ability of the immune system to recognise neoplastic cells as “non-self”, has more recently gained broad acceptance.

The immune system can be considered in two branches; innate and adaptive immunity, which work in concert to confer effective immunity. The innate immune system comprises many cell types such as natural killer (NK) cells, innate-lymphoid cells (ILCs), granulocytes and monocytes which make up the first line of host defence. Cells of the innate immune system rapidly execute effector function upon recognising conserved features of foreign pathogens or abnormal cells. Some innate immune cells are phagocytic and able to engulf soluble material from their environment. These include dendritic cells (DCs) and macrophages which recognise danger-associated molecular patterns (DAMPs) and pathogen-associated molecular patterns (PAMPs) which are derived from infected, damaged or transformed cells. DCs and macrophages can function as antigen-presenting cells (APCs) as they are able to phagocytose foreign material and process and present antigens to activate cells of the adaptive immune system. Dendritic cells are particularly proficient in processing and presenting antigens and as such are often considered the bridge between the innate and adaptive immune system.

T cells and B cells make up the adaptive immune system that, unlike innate immunity, is highly specific. Specificity is conferred by T cell receptors (TCR) and

B cell receptors that recognise precise peptide (epitope) sequences of specific cognate antigens. T cells execute cell-mediated immunity whilst B cells produce antibodies and mediate humoral immunity. Conventional αβ T cells express a TCR composed of an α and a β chain and also express a glycoprotein coreceptor, CD4 or CD8. $CD4^+$ T cells and $CD8^+$ T cells are often referred to “T helper (Th) cells” and “cytotoxic T cells,” respectively, based on their most well-known functions. $CD4^+$ T cells are further divided into subsets including Th1, Th2, Th17, Th9, T follicular helper (Tfh) and regulatory T (Treg) cells, which differ in transcriptional profiles, phenotypes and functions. T cells recognise cognate antigen presented on major histocompatibility complex (MHC) molecules; MHC class I (MHC-I) for $CD8^+$ T cells and MHC class II (MHC-II) for $CD4^+$ T cells.

More recently subsets of “unconventional” T cells that do not recognize classical peptide antigens in the context of MHC molecules have been described. Such cells include mucosal associated invariant T cells (MAIT cells) which recognise microbial metabolites of the riboflavin pathway presented on MR1, natural killer T (NKT) cells which recognise lipid antigens presented on CD1d, and γδ T cells which can recognise a variety of host-derived molecules often related to cellular stress (Godfrey et al., 2016). These cells are considered “innate-like” lymphocytes due to their restricted antigen specify and rapid responses. By contrast, conventional αβ T cells exhibit highly diverse TCRs and thus comprise an extremely large pool of cells with different specificities to enable recognition of a diverse array of antigenic peptides. An αβ T cell specific for a particular peptide exists in extremely low abundance in the naïve state but will robustly proliferate upon activation to produce effector and memory cell progeny. The production of memory cells is a key feature of the adaptive immune system and is highly important in enabling the immune system to mount a greater and more rapid response to an antigen upon subsequent encounter. Overall, the diversity of cell types that comprise the immune system has likely developed to provide division of labour as well as some redundancy to mount effective and specific immune responses.

1.2 Dendritic cells and T cell priming

T cell priming is the initial activation of a naïve T cell upon recognition of its cognate antigen presented on an MHC molecule. This is typically carried out by a DC in the secondary lymphoid organs (SLOs). In addition to recognition of cognate antigen via its T cell receptor, a T cell requires two additional signals to become fully activated. The first is co-stimulation which involves the interaction of costimulatory receptors on the surface of the T cell, such as CD28, with costimulatory ligands on the surface of the DC, such as CD80 and CD86. Costimulatory ligands are upregulated by DCs upon sensing DAMPs or PAMPs. If a DC presents antigen in the absence of costimulation it can induce T cell tolerance, deletion or anergy. This mechanism provides a level of regulation to prevent activation of autoreactive T cells in the absence of damage or infection. Finally, signalling via cytokines such as interleukin (IL)-2 is required to expand and differentiate T cells during priming.

Antigens from peripheral tissues may travel directly to SLOs in the lymphatics or may be transported by migratory DCs. Although heterogenous in nature, humans and mice share similar discrete subsets of DCs which, classified based on ontogeny, include monocyte derived DCs, plasmacytoid DCs and conventional DCs (cDCs) (Brown et al., 2019). Conventional DCs can be dichotomised into subsets cDC type 1 (cDC1) or cDC type 2 (cDC2), and both can be further divided into populations which are resident in the lymph node or migrate to the lymph node from the periphery. Both lymph node-resident and migratory DCs have the capacity to prime T cells (Bedoui et al., 2009, Hor et al., 2015) but the precise DC subsets involved in priming can differ for $CD4^+$ and $CD8^+$ T cells. The phenomenon by which DCs take up exogenous peptides and process and present them on MHC-I to $CD8^+$ T cells is known as cross-presentation. The cDC1 subset is particularly proficient in antigen cross-presentation and thus plays an important role in priming $CD8^+$ T cells (Bedoui et al., 2009, Hildner et al., 2008).

Priming of $CD4^+$ T cells is less well characterised. Different subsets of DCs have

been shown to prime different subsets of $CD4^+$ T cells suggesting that the signals derived from the specific DC subset biases $CD4^+$ T cells down certain differentiation pathways (Igyarto et al., 2011). For instance, evidence suggests that cDC2 may dominate priming of Th2 cells (Gao et al., 2013, Pooley et al., 2001) whilst cDC1 may preferentially prime Th1 cells (Harpur et al., 2019). Conflicting results have been found in subcutaneous tumor models whereby one study showed that cDC2 were required for $CD4^+$ T cell priming (Binnewies et al., 2019), whilst another study described the initiation of $CD4^+$ T cell priming by cDC1 (Ferris et al., 2020). In a model of cutaneous HSV infection, lymph node-resident and several skin-migratory subsets of DCs were capable of stimulating $CD4^+$ T cells in the lymph node demonstrating potential redundancy in subsets able to prime $CD4^+$ T cells (Bedoui et al., 2009). Different cell types occupy different anatomical niches and therefore the precise location of the antigen source is likely to influence which migratory DCs deliver antigen to the lymph node. Additionally, better access to antigen by DCs may lead to more efficient T cell priming. For instance, T cells are better primed when melanoma cells are transplanted into the DC-rich dermis, compared to the DC-sparse subcutaneous tissue due to quicker migration of dermal DCs to the draining lymph node (Malissen et al., 2014, Joncker et al., 2016).

1.3 The generation of effector and memory T cells

Upon activation T cells proliferate and undergo clonal expansion resulting in the generation of phenotypically heterogeneous effector and memory T cell populations with identical TCRs. Signalling from DCs during priming and cytokines released into the local lymph node environment drive T cell differentiation and migrational imprinting, that is, changes in adhesion molecules and chemokine receptors on the T cells that direct them to a specific anatomical site (Campbell and Butcher, 2002). The mechanisms by which migratory DCs are able to integrate signals from their local environment in the periphery and translate these into directing T cell differentiation is not well understood. There is

considerable heterogeneity in the DC lineage and the distinct repertoires of receptors able to recognise DAMPs and PAMPs suggest different DC subsets could respond to different stimuli. Therefore, it is likely that both the specific DC subset, as well as its activation state induced by the integration of signals in the periphery, contribute to the differentiation signals conveyed to T cells during priming (Hilligan and Ronchese, 2020).

Effector T (T_{EFF}) cells and effector memory T (T_{EM}) cells acquire the ability to exit the lymphoid compartment and migrate to the source of cognate antigen in the periphery. Whilst the majority of effector T cells die after clearance of the antigen source, a pool of memory T cells survive and remain in the body to mount a superior immune response if a secondary encounter with the cognate antigen occurs. Formerly, memory T cells were considered as two distinct subsets, central memory T (T_{CM}) cells that migrate between secondary lymphoid organs and the blood, and T_{EM} cells that migrate between the blood and non-lymphoid tissues (Sallusto et al., 2014). A third population of memory T cells that reside permanently within peripheral tissues, tissue-resident memory T cells (T_{RM}) cells, has since been discovered (Gebhardt et al., 2009, Schenkel and Masopust, 2014). The precise mechanisms of T_{RM} cell formation and retention are still not fully understood but transcriptional profiling has enabled the discovery of a core set of transcripts for T_{RM} cells which distinguishes them from their circulating counterparts. T_{RM} cells also express tissue-specific transcripts and phenotypic markers suggesting that local environmental factors contribute to the regulation of T_{RM} cell ontogeny (Mackay and Kallies, 2017).

1.4 $CD4^+$ T cell subsets

During activation $CD4^+$ T cells differentiate into specific subsets that are generally distinguished by their specific cytokine and transcription factor profiles which in turn dictates their different functions (Agarwal and Rao, 1998). Conditions that direct differentiation include the local cytokine milieu as well as specific

interactions with APCs, including the nature of co-stimulation and strength of TCR signalling (Bajenoff et al., 2002, Eizenberg-Magar et al., 2017, Harpur et al., 2019, Tubo et al., 2013). The strength of TCR signalling is influenced by the level of antigen presentation, the affinity of the TCR and peptide/MHC complex, and duration of the interaction between the APC and T cell (Tubo et al., 2013). $CD4^+$ T cell subsets were originally dichotomised as either Th1 cells or Th2 cells. Many other subsets including Tfh cells, Treg cells, Th17 cells and Th9 cells have since been described.

Th1 cells express the transcription factor T-bet, secrete the cytokines IFNγ, IL-2 and Tumor necrosis factor α (TNFα), and play an important role in clearance of intracellular pathogens. Th2 cells are characterised by expression of the master transcription factor GATA-3 and the production of IL-4, IL-5 and IL-13. Th2 cells have a protective role in helminth infections but also are known to drive allergic inflammation. Tfh cells are regulated by the transcription factor Bcl6 and are primarily located in secondary lymphoid organs where they support germinal centre formation and the differentiation and function of B cells. Th17 cells are characterised by the expression of the transcription factor RORγT and the production of cytokines IL-17 and IL-22. Th-17 cells are involved in clearance of extracellular bacteria and fungi but can also contribute to autoimmune diseases. Th9 cells, a more recently described subset, produce IL-9 and IL-21. A lineage-specific transcription factor has not been identified for the Th9 subset, but they have been described to express a combination of the transcription factors GATA-3, PU.1 and IRF1 (Malik and Awasthi, 2018). Th9 cells have been discovered to share similar functions with Th2 cells, including a role in controlling helminth infections and promoting asthma. This overlap of functionality has brought into question whether Th9 cells are a distinct $CD4^+$ T cell lineage or a subpopulation of Th2 cells (Caza and Landas, 2015). In addition, Th9 cells can arise from Th2 cells in the presence of transforming growth factor-β (TGF-β) (Dardalhon et al., 2008, Veldhoen et al., 2008).

Treg cells are immunosuppressive and express the lineage specific master

transcription factor FoxP3. These cells are essential for maintenance of tolerance to self-antigens, control of inflammation and prevention of autoimmune disease. On the other hand, they can dampen immune responses to cancers and thus promote cancer development. Treg cells can suppress a broad array of immune cell types through a variety of mechanisms. For instance, they suppress conventional T cells through binding of checkpoint molecules, secreting inhibitory cytokines, consuming IL-2, direct killing, and rendering DCs tolerogenic (reviewed in (Schmidt et al., 2012)). Treg cells can be broadly categorised into two classes based on their developmental origin. Thymic Treg are generated in the thymus from single-positive $CD4^+$ T cells that recognise self-antigen but do not undergo negative selection. Peripheral Tregs develop in the periphery when naïve $CD4^+$ T cells recognise antigen in combination with a specific combination of signals including cytokines TGF-β and IL-2 (Lee and Lee, 2018).

Not only has an increasing number of $CD4^+$ T cell lineages described over time, but additional functions of these cell types continue to be discovered. Importantly, the Th subset paradigm is based upon *in vitro* studies. The advent of powerful technologies such as single-cell proteomic and transcriptional analysis has enabled the heterogeneity that exists within Th subsets *in vivo* to be revealed (Papalexi and Satija, 2018, Becattini et al., 2015). Furthermore, in contrast to the initial hypothesis that lineage committment was a unidirection process, phenotypic plasticity has been demonstrated amongst $CD4^+$ T cell subsets. Some subsets exhibit a higher degree of plasticity such as Th17 cells that can transdifferentiate into Th1, Th2, Treg and T_{FH} cells under certain conditions (Lee et al., 2009, Guery and Hugues, 2015). Varying degrees of plasticity is thought to be important for allowing cells to adapt to their immediate microenvironment, although factors that regulate this process are not well understood (Caza and Landas, 2015).

1.5 Immune landscapes of murine and human skin

The skin is largest organ in the human body and, being interfaced with the environment, it has an important role in protection from external threats. The skin not only serves as a protective barrier but functions as a dynamic immune organ infiltrated by a plethora of immune cells (Bangert et al., 2011). Our understanding of skin immunology has greatly benefitted from the use of murine models. It is, however, important to consider there are some biological differences between human and mouse skin. Both have an outer layer, the epidermis, composed predominately of keratinocytes. The epidermis also contains melanocytes and a restricted repertoire of immune cells. Human skin has a thicker epidermis than mouse skin that forms extensions into the underlying connective tissue. Due to the absence of blood and lymphatic vessels in the epidermis, this site is considered “immune privileged”, and how particular immune cells gain entry to, or exit, the epidermis is an area of ongoing research. Beneath the epidermis lies the dermis, composed largely of collagen and elastic tissue. Blood vessels, nerves and many immune cell types permeate the dermis. Compared to humans, hair follicles are more densely distributed in mice and undergo a program of cyclic growth and degeneration (Tobin, 2011).

Humans and laboratory mice display similar immune landscapes within the skin although some differences have been reported such as the relative proportions of γδ T cells and conventional αβ T cells. The majority of epidermal T cells in mice are γδ T cells, which have been termed dendritic epidermal T cells (DETCs). These are relatively scarce in the human epidermis, in which conventional αβ T cells dominate (Ho and Kupper, 2019). This may partly result from the lack of exposure to environmental stimuli in laboratory mice raised under specific-pathogen-free conditions that would otherwise generate memory αβ T cells in the skin. Indeed, it has been shown that the composition of memory T cells in a laboratory mouse better reflects that of neonates than that of adult humans (Beura et al., 2016).

1.6 Migratory patterns of CD4$^+$ T cells in the skin

T cells play an important role in immunosurveillance against cancers and pathogens in the skin (Ho and Kupper, 2019). It is estimated that adult human skin contains approximately twice as many T cells than found in the circulation, the vast majority of which are memory T cells (Clark et al., 2006). Memory T cells within the skin include recirculating cells that are in equilibrium with the circulation, and T_{RM} cells that are retained permanently within the skin.

Memory CD8$^+$ and CD4$^+$ T cells exhibit differences in their spatial and migratory patterns within the skin. CD8$^+$ T cells readily form T_{RM} in the skin, as demonstrated in numerous infection models (Gebhardt et al., 2009, Jiang et al., 2012) and more recently in melanoma models (Park et al., 2019, Malik et al., 2017). CD8$^+$ T_{RM} cells predominately reside within the epidermis and co-express molecules CD103 and CD69 which are involved in tissue retention. CD69 blocks signalling by tissue egress regulator, S1P1 (Shiow et al., 2006) and CD103 interacts with E-cadherin on epithelial cells (Cepek et al., 1994). It is less clear under what context CD4$^+$ T cells can form permanent, non-recirculating T_{RM} cells. Memory CD4$^+$ T cells locate within the dermis (Collins et al., 2016, Gebhardt et al., 2011, Watanabe et al., 2015) but have also been reported in the epidermis in humans (Watanabe et al., 2015). In a model of cutaneous HSV-1 infection in mice, CD4$^+$ T cells were found in both the epidermis and dermis during the acute phase of infection but memory CD4$^+$ T cells were predominately confined to the dermis at later time points. The memory CD4$^+$ T cells exhibited enhanced retention in the dermis although did not lodge permanently (Collins et al., 2016). This is in contrast to CD8$^+$ T cells which readily formed permanent T_{RM} cells in resolved HSV-1 challenged skin (Gebhardt et al., 2009). Within the dermis memory CD4$^+$ T cells were found patrolling the interfollicular space or localised in clusters with other immune cells, often adjacent to hair follicles (Collins et al., 2016). These structures, termed memory lymphocyte clusters (MLC), have been described in other peripheral tissues and are thought to act as a site for enriched

immune cell retention and activity (Iijima and Iwasaki, 2014).

Other studies support the recirculating nature of memory $CD4^+$ T cells, describing migrating memory $CD4^+$ T cells that retain skin homing molecules and can passage between the skin, lymphatics and circulation (Bromley et al., 2013, Klicznik et al., 2019, Watanabe et al., 2015). However, prolonged or permanent skin residency for $CD4^+$ T cells in humans (Clark et al., 2012, Watanabe et al., 2015) and in mice (Glennie et al., 2015, Park et al., 2018, Beura et al., 2019, Lauron et al., 2019) has also been described. In murine skin, $CD4^+$ T_{RM} formation was reported in response to Leishmania infection, evidenced by their long-term maintenance in transplanted skin grafts (Glennie et al., 2015). Similarly, Th17 cells lodged permanently in the skin of mice infected with the fungus *Candida albicans* and co-existed with a heterogeneous population of migratory $CD4^+$ T cells (Park et al., 2018). The tendency for $CD4^+$ T cells to form long-lived T_{RM} cells has been frequently recorded in other organs such as the lung whereby $CD4^+$ T_{RM} cells play an important role in immunosurveillance in models of infection (Sakai et al., 2014, Teijaro et al., 2011, Wilk et al., 2017). $CD8^+$ and $CD4^+$ T_{RM} cells share similar transcriptional and phenotypic signatures which differ from their circulating counterparts and are greatly influenced by the location in which they reside (Beura et al., 2019). There is thus sufficient evidence to support that $CD4^+$ T cells have the intrinsic capacity to form T_{RM} cells but their propensity to do so is context and tissue dependent.

1.7 Antigen-presentation to $CD4^+$ T cells in the skin

Effector functions exerted by activated T cells at the site of antigen encounter are induced upon TCR engagement with cognate peptide:MHC complex (McLachlan et al., 2009, Macleod et al., 2014). This spatial confinement of the effector response may serve to prevent damage to healthy tissue that activated T cells may encounter on their trajectory to the antigen source. In addition to TCR signalling, T cell effector functions are regulated in the periphery by integration of co-stimulatory signals, cytokines and other soluble factors. As such, the specific

subsets and phenotype of APC populations that present antigen in the periphery can directly impact peripheral T cell responses (Bedoui and Gebhardt, 2011, Clausen and Stoitzner, 2015). Unlike MHC-I, which is expressed on almost all cell types, MHC-II is primarily expressed by professional APCs, which includes B cells, macrophages and DCs. These cells are proficient in processing and presenting antigen in the context of MHC-II. Other cell types, referred to as "non-professional" APCs, can be induced to present MHC-II-restricted peptides to $CD4^+$ T cells under certain conditions. The subsets of APCs involved in priming naïve T cells in LN can differ from those stimulating T cells at the site of the antigen source (Hilligan and Ronchese, 2020).

Heterogeneous populations of professional and non-professional APCs reside in the skin and show varying capabilities in stimulating $CD4^+$ and $CD8^+$ T cells (Macleod et al., 2014). The anatomical location of T cell subsets, as well as differences in the ability of APCs to present peptide on MHC-II and MHC-I may determine which APCs stimulate T cells. In HSV-challenged skin antigen-specific $CD8^+$ T cells produced cytokines upon local antigenic encounter with infected epithelial cells such as keratinocytes, Langerhans cells and DETCs. On the contrary several subsets of professional APCs, most notably dermal DCs, elicited cytokine production in $CD4^+$ T cells. Importantly, the effector $CD4^+$ T cell response in HSV-infected skin was not compromised in transgenic mice deficient in certain populations of professional APCs, including monocyte-derived DCs, Langerhans cells, dermal DCs or B cells (Macleod et al., 2014). This demonstrated redundancy among APC populations capable of stimulating $CD4^+$ T cells in the skin. Despite some degree of redundancy, bias for specific APC subsets to present antigen to $CD4^+$ T cells in the skin has been demonstrated. For instance sustained cytokine production by Treg cells and Th1 cells that shared the same TCR specificity were shown to require local antigen presentation by $CD11b^{high}$ DCs following intradermal injection of the relevant peptide (McLachlan et al., 2009). Furthermore, different DC subsets in the skin can display unique abilities to promote the response of different Th subsets. It has been shown in a model of *Candida albicans* that Langerhans cells were required

for Th17 cell development whereas cDC1 supported Th1 differentiation (Igyarto et al., 2011).

1.8 The multifaceted role of the immune system in cancer

1.8.1 Oncogenesis

The immune system can play different roles at different stages of cancer development. Oncogenesis, the transformation of a normal cell into a its malignant counterpart, involves a series of genetic and cellular changes. The majority of cancers are caused by an accumulation of somatic mutations which can be initiated by environmental carcinogens. One common driver of oncogenesis is chronic infection, and therefore the immune system plays a role in prevention of infection-induced cancers through clearance of pathogens. On the other hand, chronic inflammation driven by immune cells may promote oncogenesis by fostering a tissue microenvironment that promotes DNA damage and survival of malignant cells (Greten and Grivennikov, 2019). Following malignant transformation, the immune system can regulate cancer development. Crosstalk between the immune system and cancer cells can determine the fate of the cancer, a process described by the “cancer immunoediting hypothesis” in three phases; Elimination, Equilibrium, Escape (Dunn et al., 2002).

1.8.2 Elimination – Cancer antigens and immunosurveillance

Cancer immunosurveillance is the recognition and elimination of immunogenic cancer cells by the immune system. Innate immune cells such as NK cells and macrophages can be cytotoxic to cancer cells (Pan, 2012, O'Sullivan et al., 2012, Smyth et al., 2001b, Fauskanger et al., 2018), however T cells are generally considered crucial effectors in immune responses against cancer. The important role of T cells in cancer immunosurveillance is exemplified by the success of T-cell based immunotherapies in cancer treatment (Wirth and Kuhnel, 2017).

The ability of T cells to eliminate cancer cells is contingent on their recognition of tumor-derived antigens. Antigens can be categorised broadly into two types. Firstly, there are unaltered self-antigens that may be recognised because of additional danger signals or altered expression patterns that differ from their normal cell counterparts. For example, NY-ESO-1 is a cancer testis antigen, encoded in the germline that has restricted expression in normal adult tissue but is commonly expressed by multiple cancer types (Raza et al., 2020). Another class of antigens recognised by T cells are tumor-specific antigens that are exclusively expressed by cancer cells and therefore are recognised by the immune system as “non-self”. Tumor-specific antigens include products of oncogenic viruses or endogenous mutated proteins that result from random somatic mutation. The latter, often referred to as neoantigens, represent promising targets of cancer immunotherapy as they are not expressed by healthy cells, minimising the potential for off-target effects (Wirth and Kuhnel, 2017).

1.8.3 Equilibrium – Immune-mediated tumor suppression

Cancer-immune equilibrium describes a situation where the immune system fails to eliminate the cancer cells completely but controls them so that there is no net outgrowth. Mechanisms underlying the equilibrium phase are not well understood. This phase could be dynamic whereby cancer cells continuously divide but at a similar rate to their immune cell-mediated elimination (Holmgren et al., 1995) or could be relatively static whereby the cancer cells remain dormant, neither dividing nor dying (Naumov et al., 2002). Because tumors are generally detected once they are progressively growing, evidence for the equilibrium phase of tumor development in humans is scarce, and mainly deduced from clinical observations. Although rare, malignancies have emerged in transplanted organs from donors who were treated for melanoma but were considered “disease-free” at the time of organ donation (Strauss and Thomas, 2010). It is speculated that the immune system played a role in maintaining cancer cell dormancy during remission but dormant cells present in the transplant reactivated in the

immunocompromised transplant recipients. Indeed, cancer recurrence frequently occurs after prolonged periods of remission and circulating cancer cells can be detected in patients with undetectable disease twenty years after initial treatment (Teng et al., 2008, Meng et al., 2004).

Mouse models have been instrumental for providing evidence of cancer-immune equilibrium (Park et al., 2019, Koebel et al., 2007). In a carcinogen-induced sarcoma model cancer cells were detected more than a year after carcinogenesis and tumor outgrowth could be induced by deleting T cells or blocking IFNγ signalling (Koebel et al., 2007). In an orthotopic transplantable melanoma mouse model, local $CD8^+$ T_{RM} cells played an appreciable role in maintaining melanoma cells in a state of equilibrium (Park et al., 2019). These data provide evidence that T cells can maintain cancer dormancy however the underlying mechanisms have not been elucidated.

The proportion of progressively growing tumors that transition through an equilibrium phase or how long this phase can be maintained is unclear. A process termed “cancer immunoediting” can occur during immune-mediated suppression of cancer outgrowth. This phenomenon describes the process whereby the immune system “sculpts” the tumor landscape as a consequence of a Darwinian selection process. Selective pressure imparted on the cancer cells by the immune system favours the survival of cancer cell clones which have acquired phenotypic and genetic alterations that render them capable of immune evasion (Dunn et al., 2002). Evidence for this micro-evolutionary process first stemmed from the observation that cancer cells from immunodeficient hosts were more immunogenic than those from wildtype hosts (Shankaran et al., 2001, Svane et al., 1996).

1.8.4 Escape – Immune evasion strategies exploited by cancers

Tumor progression occurs when cancer cells escape detection and destruction by the immune system. Cancer cells can coordinate immune-mediated escape

by remodelling their own immunogenicity or by regulating components of the immune system to orchestrate an immunosuppressive microenvironment. T cells are major drivers of immunoediting and a common immune evasion mechanism of cancer cells is loss of antigenicity (DuPage et al., 2012, Matsushita et al., 2012, Effern et al., 2020). The antigen itself can be downregulated if derived from a non-essential gene product (Effern et al., 2020). This is exemplified by the downregulation of melanocyte lineage antigens in melanoma which can be driven through a process of dedifferentiation (Landsberg et al., 2012). Additionally, cancer cells can downregulate molecules involved in antigen presentation such as MHC-I and MHC-II (Hicklin et al., 1999, Vinay et al., 2015). Other evasion strategies include downregulation of costimulatory molecules and upregulation of inhibitory ligands which induce exhaustion or tolerance in anti-tumoral T cells (Zarour, 2016).

Chemokines, cytokines, and metabolites secreted by cancer cells can shift the immune landscape into one that favours tumor progression. The inflammatory tumor microenvironment promotes recruitment and expansion of immunosuppressive immune cells such as myeloid-derived-suppressor cells (MDSCs) and Treg cells (Umansky and Sevko, 2012). MDSC represent a heterogeneous population of immature myeloid cells that expand in the presence of inflammatory mediators and are capable of mediating suppression through multiple mechanisms. These cells can mature into tumor-associated macrophages that also support tumor progression (Kumar et al., 2016). MDSCs have been reported within tumors of different cancer types and their presence in the peripheral blood of cancer patients is strongly associated with poor overall survival (Zhang et al., 2016, Jordan et al., 2017). Acquired resistance to immunotherapy correlates with increased levels of circulating MDSCs in melanoma patients (Martens et al., 2016, Meyer et al., 2014). In melanoma-bearing mice, reversing chronic inflammation in the tumor microenvironment (TME) is associated with a reduction in number and function of infiltrating MDSC, the restoration of T cell function and increased overall survival (Meyer et al., 2011).

As well as recruiting immunosuppressive cells, the TME can reprogram immune cells into subsets that promote tumor progression. For example, “classically activated” M1-type macrophages which secrete proinflammatory cytokines such as IFNγ can be polarised into “alternatively activated” M2-type macrophages which secrete factors such as Arginase-I, IL-10 and TGF-β which can dampen immune responses (Mantovani and Sica, 2010, Ma et al., 2016). Similarly pro-inflammatory Th1 cells have been shown to polarise into immunosuppressive Treg cells in the TME (Ivanova and Orekhov, 2015). In addition, dendritic cells may be rendered tolerogenic within the TME which in turn inhibits T cell function (Gabrilovich, 2004). Mechanisms of immune escape continue to be discovered and immunosuppression within the TME poses a major barrier to the success of cancer immunotherapy.

1.9 Anti-tumoral $CD4^+$ T cell subsets

Whilst the ability of cytotoxic $CD8^+$ T cells to eliminate neoplastic cells is well-established, recognition that $CD4^+$ T cells play a fundamental role in cancer immunosurveillance is more recent. Early studies of $CD4^+$ T cells in tumor immunity focused on their helper role to enhance $CD8^+$ T cell responses. It has since been demonstrated that $CD4^+$ T cells can mediate robust anti-tumoral effector functions in the tumor microenvironment and can directly eliminate tumors in the absence of $CD8^+$ T cells (Shklovskaya et al., 2016, Xie et al., 2010). Furthermore, a study showed that immunogenic mutations of different murine cancers were more frequently recognised by $CD4^+$ T cells than $CD8^+$ T cells and peptide vaccination with the identified MHC-II restricted epitopes resulted in eradication of established tumors (Kreiter et al., 2015).

The numerous $CD4^+$ T cell subsets which exhibit varying degrees of phenotypic plasticity and exert a multitude of unique and overlapping functions have rendered attempts to characterise antitumoral $CD4^+$ T cells challenging. All $CD4^+$ T cell subsets have been implicated in cancer immunosurveillance to varying

degrees. Furthermore, dual roles exist for some $CD4^+$ T cell subsets, whereby they can promote or inhibit tumor development in different contexts. Disparate roles in tumor immunity are evident for the Th2 subset which can display antitumoral (Nishimura et al., 1999) and protumoral activity (Hong et al., 2008). On the other hand, Th1 cells are considered to be central to antitumoral immunity. Th1 cells are the most commonly reported $CD4^+$ T cell subset associated with driving antitumoral immunity in mouse models (Quezada et al., 2010, Xie et al., 2010, Shklovskaya et al., 2016, Haabeth et al., 2018, Malandro et al., 2016) and are associated with a positive response to immunotherapy in cancer patients (Kitano et al., 2013, Chen et al., 2014).

More recently, the role of Th17 cells in cancer immunosurveillance has been examined in mouse models. The antitumoral role of Th17 cells in melanoma has been demonstrated using adoptive transfer of TRP-1 cells, transgenic $CD4^+$ T cells that recognise a melanosomal protein, Tyrosinase-related protein 1 (TYRP1) (Martin-Orozco et al., 2009, Muranski et al., 2008, Bowers et al., 2017). Transfer of Th17-differentiated, but not Th1-differentiated TRP-1 cells mediated complete remission of established subcutaneous B16 melanoma (Muranski et al., 2008, Bowers et al., 2017). In these studies, Th17 cells showed a superior ability to resist senescence and exhaustion and maintained prolonged antitumoral function. Interestingly, the mechanism by which Th17 cells eradicated tumors was dependent on IFNγ and not the Th17-associated cytokines, IL-17 and IL-23. This brings into question the stability of the phenotype of the transferred Th17 cells as their cytokine and transcription factor profiles were not assessed following treatment, and Th17 cells can convert into Th1-like cells under certain polarising conditions (Lee et al., 2009, Guery and Hugues, 2015). Th17-differentiated TRP-1 cells also demonstrated more effective control of melanoma deposits at the lung than Th1-differentiated TRP-1 cells and this affect was dependent on IL-17 and not IFNγ (Martin-Orozco et al., 2009). In this study, IL-17 promoted inflammation and recruitment of various immune cell types including cytotoxic $CD8^+$ T cells into the melanoma deposits.

Further studies showed that mice receiving adoptive transfer of Th9-polarised $CD4^+$ T cells were better able to control subcutaneous B16 melanoma compared to Th1 or Th17-polarised $CD4^+$ T cells (Lu et al., 2018, Purwar et al., 2012). Th9 cells have also been found to control melanoma deposits in the lung (Vegran et al., 2014, Lu et al., 2012). Whilst adoptively transferred Th17 or Th9 cells can mediate robust antitumoral immunity, it should be noted that adoptively transferred naïve $CD4^+$ T cells primed *in vivo* display predominance to polarise into Th1 cells capable of mediate protection against B16 melanoma (Malandro et al., 2016, Xie et al., 2010). This suggests that whilst several $CD4^+$ T cell subsets may exert antitumoral functions, Th1 cells may be the most common subset that naturally provides immunity against cancers.

1.10 Pro-tumoral role of $CD4^+$ T cell subsets

Whilst adoptive transfer of Th17 cells can elicit robust antitumoral immunity, Th17 cells have been shown to promote tumor growth in some cancer models (Ortiz et al., 2015, He et al., 2012). Th17 cells are characterised by the production of IL-17 and this cytokine has been implicated in several protumoral processes. IL-17 can promote oncogenesis by driving inflammation and can support tumor growth by promoting the recruitment of MDSCs into the TME (He et al., 2012). In addition, IL-17 mediates angiogenesis of tumors which can facilitate metastasis (Numasaki et al., 2003). Th17 cells are considered less terminally differentiated than other $CD4^+$ T cell subsets and can be regulated by local environmental cues. This phenotypic plasticity, in combination with the heterogeneity of tumor microenvironments, may provide an explanation for their paradoxical roles in cancer immunosurveillance.

Immunosuppressive Treg cells can drive immune evasion and represent a major barrier to the success of cancer immunotherapies (reviewed in (Paluskievicz et al., 2019)). The presence of Treg cells in melanoma lesions and in lymph nodes from melanoma patients is a frequent occurrence and a high Treg/$CD8^+$ T cell

ratio within tumors correlates with a poor prognosis (Jacobs et al., 2012). Depletion of Treg cells in murine cancer models is associated with better antitumoral responses (Li et al., 2010, Onda et al., 2019). Whilst Treg cells play a role in immune escape by dampening anti-tumoral responses within the established tumors, they may conversely play a role in preventing oncogenesis by suppressing chronic inflammation which is associated with malignant transformation (Greten and Grivennikov, 2019).

1.11 Anti-tumoral mechanisms of $CD4^+$ T cells

1.11.1 $CD4^+$ T cell "help" in secondary lymphoid organs

$CD4^+$ T cells exert multiple "helper" functions by engaging with other cell types to orchestrate immune responses. One well-characterised helper function is the process of DC licensing which functions to enhance priming of $CD8^+$ T cells. DC licencing is cognate antigen-dependent and also requires ligation of CD40 ligand (CD40L) on the surface of an activated $CD4^+$ T cell with its costimulatory receptor, CD40, on a DC (Bennett et al., 1998). This interaction leads to upregulation of antigen-presenting and processing molecules, costimulatory molecules and cytokine production by the DC. $CD4^+$ T cell help via DC licencing has been characterised in models of infection (Greyer et al., 2016, Sun et al., 2004, Shedlock and Shen, 2003, Northrop et al., 2006) and more recently in tumor models (Alspach et al., 2019, Zhu et al., 2015, Ferris et al., 2020).

$CD8^+$ T cells primed in the presence of $CD4^+$ T cell "help" exhibit better effector responses through increased expression of cytotoxic effector molecules, increased production of IFNγ, downregulation of inhibitory receptors and enhanced migratory capacities (Ahrends et al., 2017, Wang and Livingstone, 2003, Alspach et al., 2019). $CD4^+$ T cell help is also important in generating memory $CD8^+$ T cells with improved longevity and recall responses although the underlying mechanisms are not fully understood (Sun et al., 2004, Shedlock and Shen, 2003). Many genes are differentially expressed between "helped" and

“unhelped” $CD8^+$ memory T cells including those that regulate apoptosis and cytokine production (Wolkers et al., 2012, Northrop et al., 2006). Although most studies exploring the pathways involved in DC licencing have been carried out in models of infection, one could hypothesize the same mechanisms are preserved in the context of cancer immunosurveillance. Indeed, a common transcriptional program of “helped” $CD8^+$ T cells was identified for mouse models of therapeutic antitumoral vaccination and viral infection (Ahrends et al., 2017).

Another helper role of $CD4^+$ T cells in the SLOs is that provided by the Tfh cell subset to stimulate humoral immunity (Ma et al., 2012). Interactions between Tfh cells and B cells, promote the formation of germinal centres, the development of short-lived and memory B cell subsets, and the production of high affinity antibodies. The role of Tfh in cancer immunosurveillance has not been well characterised but B cells have been implicated in antitumoral immunity through production of antibodies, provision of antigen to T cells and promoting effector function of NK cells (reviewed in (Sharonov et al., 2020)). Antibodies specific for tumor antigens are frequently reported to be present in the serum of cancer patients and B cells can constitute a proportion of tumor-infiltrating lymphocytes. However, there is evidence that B cells can promote tumor progression through the development of autoantibodies, production of tumor growth factors. In addition, regulatory B cells can directly suppress antitumoral T cell responses (Horii and Matsushita, 2020). It has recently been proposed that Tfh cells could play a role in cancer immunity beyond “help” within the germinal centres. This speculation was driven by the identification of Tfh cells within human breast tumors and colorectal tumors where they were found to promote the organisation of tertiary lymphoid structures (TLS) and their presence correlated with better overall survival (Bindea et al., 2013, Gu-Trantien et al., 2013). Furthermore, B cells, arranged in TLS, were found to be enriched in melanoma patients that responded to immune checkpoint therapy (Helmink et al., 2020).

1.11.2 CD4$^+$ T cell effector functions in the tumor microenvironment

CD4$^+$ T cells constitute a major population of tumor-infiltrating lymphocytes, however the mechanisms by which they orchestrate antitumoral immunity within the TME are not well understood. Intratumoral CD4$^+$ T cells can promote cancer immunosurveillance by regulating other immune cells, such as CD8$^+$ T cells and macrophages, in the TME (Wong et al., 2008, Bos and Sherman, 2010, Alspach et al., 2019, Huang et al., 2005, Martin-Orozco et al., 2009, Church et al., 2014, Corthay et al., 2005, Haabeth et al., 2018, Perez-Diez et al., 2007, Doorduijn et al., 2017). Additionally, several studies have shown that CD4$^+$ T cells can directly kill cancer cells *in vitro* (Quezada et al., 2010, Sashchenko et al., 2007, Lundin et al., 2004) and direct killing has been demonstrated *in vivo* (Quezada et al., 2010). Killing mechanisms of cytotoxic CD4$^+$ T cells are thought to be analogous to those exerted by NK cells and CD8$^+$ T cells, due to shared expression of cytotoxic effector molecules. These include granzymes and TNF superfamily proteins such as FasL and TNFα.

1.11.2.1 Cytotoxicity via granule exocytosis

The granzyme/perforin-dependent killing pathway is commonly exploited by CD8$^+$ T cells and NK cells to kill viral infected cells and cancer cells (Cullen et al., 2010). This pathway involves the release of secretory granules containing perforin and granzymes. Perforin forms pores in the target cell membrane through which granzymes enter and cleave intracellular substrates to initiate cell death. Different granzymes, of which there are five and ten described in humans and mice respectively, can cleave diverse cellular substrates. One well characterised mechanism by which Granzyme B (GzmB), the most abundant and extensively characterised granzyme, induces target cell apoptosis is by cleaving and activating pro-caspase 3 which in turn initiates the executionor caspase cascade (Chowdhury and Lieberman, 2008).

Killing via perforin/granzyme is less well described for CD4$^+$ T cells compared to

$CD8^+$ T cells, with the exception of Treg cells which are known to kill proinflammatory cells via granzyme/perforin mediated killing (Schmidt et al., 2012, Gondek et al., 2005). The ontology of the so-called $CD4^+$ cytotoxic T lymphocytes (CTL) which are proinflammatory and express perforin and granzymes is not well understood. The $CD4^+$ CTL share common features with Th1 cells such as expression of transcription factors T-bet and eomesodermin, which can regulate cytotoxicity, as well as the production of IFNγ. However, it is clear that there is heterogeneity amongst $CD4^+$ CTL and granzymes can also be expressed by Th17, Th9 and Th2 cells (*reviewed in* (Takeuchi and Saito, 2017)). Therefore, cytotoxicity of $CD4^+$ T cells should be considered a differentiation state rather than a uniform subset.

$CD4^+$ CTL that mediate direct cytotoxicity via the granzyme-perforin pathway have been described in the context of viral infection (Takeuchi and Saito, 2017). $CD4^+$ T cells which exhibit antitumoral activity frequently express GzmB and perforin and blocking these molecules can prevent $CD4^+$ T cell-mediating killing of B16 melanoma cells *in vitro* (Quezada et al., 2010). $CD4^+$ T cells associated with response to immunotherapy in cancer patients also display cytotoxic signatures similar to $CD8^+$ T cells including high expression levels of granzymes and perforin (Oh et al., 2020, Kitano et al., 2013). Despite expression of these molecules, the contribution of granule exocytosis to cancer cell killing by $CD4^+$ T cells in mice and humans remains unclear.

1.11.2.2 Cytotoxicity via Fas ligand

FasL is a transmembrane protein in the TNF superfamily that induces Caspase-8 mediated apoptosis in target cells through engagement with its receptor, Fas (Russell and Ley, 2002). FasL has also been reported to induce necroptosis as an alternative cell death pathway independent of caspases (Holler et al., 2000, Vercammen et al., 1998, Ivanova et al., 2017). Membrane-bound FasL can be cleaved from the cell surface to produce soluble FasL and the different forms may differentially regulate downstream pathways. For instance, soluble FasL has

been shown to be less cytotoxic (LA et al., 2009) and can even inhibit cytotoxicity of membrane-bound FasL (Nareznoi et al., 2020, Hohlbaum et al., 2000).

FasL can play contrasting roles in tumor immunology. Activated $CD8^+$ T cells express FasL and can induce cell death in Fas-expressing cancer cells (Ju et al., 1994, Stalder et al., 1994, Ivanova et al., 2017, Sashchenko et al., 2007, Smyth et al., 1998, Kline et al., 2012). $CD4^+$ T cells have also been shown to kill cancer cells *in vitro* via FasL (Sashchenko et al., 2007, Lundin et al., 2004). Whether $CD4^+$ T cells kill cancer cells via FasL *in vivo* is yet to be determined although in a murine model of chronic Friend Virus, $CD4^+$ T cells controlled infection via FasL-depedent killing of viral-loaded targets (Malyshkina et al., 2017). Some cancers downregulate Fas which is speculated to be an escape mechanism from FasL-mediated killing by T cells (Cheng et al., 2005, Bullani et al., 2002).

Activated T cells can also express the receptor Fas which is important for activation-induced cell death, a process that regulates homeostasis and maintenance of self-tolerance (Green et al., 2003). However, FasL expression in tumors can lead to immune escape by inducing apoptosis of Fas-expressing TILs (Zhu et al., 2017, Motz et al., 2014, Li et al., 2002, Yajima et al., 2019, Ryan et al., 2005). FasL is frequently expressed within the tumor microenvironment but not necessarily by the cancer cells themselves (Motz et al., 2014, Yamamoto et al., 2019). Endothelial cells in the tumor vasculature in humans and mice frequently express FasL and have been shown to kill antitumoral T cells (Motz et al., 2014). Additionally, FasL expression by tumor-infiltrating MDSCs was shown to mediate apoptosis of anti-tumoral $CD8^+$ T cells, driving resistance to T cell therapy in a melanoma mouse model (Zhu et al., 2017). Counterintuitively, cancer cells that were geneticaly engineered to express high levels of FasL led to improved anti-tumoral responses, in association with a high level of granulocyte infiltration into the TME (Simon et al., 2002, Shimizu et al., 2001, Chen et al., 2002, Shimizu et al., 1999). However, genetically enforced FasL expression may not represent naturally-occurring FasL signalling events.

1.11.2.3 Cytotoxicity via Tumor Necrosis Factor-Related Apoptosis Inducing Ligand (TRAIL)

TRAIL is a member of the TNF superfamily and has been identified to regulate diverse processes including induction of apoptosis in target cells upon engagement of its death receptors. An antitumoral role for TRAIL was revealed by the increased susceptibility to tumor development and metastasis of mice with genetic ablation of *TRAIL* (Zerafa et al., 2005, Cretney et al., 2002). Several immune cell types have been reported to kill cancer cells via TRAIL *in vitro,* including lymphocytes(Kayagaki et al., 1999), monocytes (Griffith et al., 1999) and neutrophils (Koga et al., 2004). TRAIL is a key antitumoral effector molecule of NK cells in particularly for control of metastatic disease in murine tumor models (Cretney et al., 2002, Smyth et al., 2001a, Takeda et al., 2001).

In a murine model of adenovirus-induced ocular cancer, $CD4^+$ T cells were responsible for tumor clearance and the underlying mechanism was dependent on TRAIL. IFNγ was also required for tumor clearance by $CD4^+$ T cells in this model but did not play a role in direct induction of cell death. The requirement of IFNγ was thus speculated to be due to its effects on upregulating TRAIL on $CD4^+$ T cells (Wang et al., 2003). Despite the ability of TRAIL to kill various cancer types *in vitro* and in mice modes, attempts to harness TRAIL-mediated killing in cancer therapy have shown limited success in clinical trials so far (von Karstedt et al., 2017).

1.11.2.4 Cytotoxicity via TNFα

TNFα is a member of the TNF superfamily which is initially expressed as a transmembrane protein but can be cleaved by a protease to release its soluble form. TNFα is produced by a broad range of immune cells and regulates diverse cellular processes through binding to its receptors, TNF receptor 1 (TNFR1) or TNF receptor 2 (TNFR2). TNFR1 is expressed by most cell types and can be activated by soluble or membrane-bound TNFα (Locksley et al., 2001). TNFR1,

but not TNFR2, has an intracellular death receptor domain and signalling through TNFR1 can induce programmed cell death under certain conditions (Montfort et al., 2019). Expression of TNFR2 is restricted to certain cell types (Carpentier et al., 2004). It has been proposed that TNFR2 is primarily bound by transmembrane TNFα and its major role is in regulating homeostasis and cell survival (Kalliolias and Ivashkiv, 2016, Fontaine et al., 2002, Hurrell et al., 2019).

Due to the pleiotropic effects of TNFα its roles in cancer immunosurveillance are not well understood. TNFα produced by NK cells and $CD8^+$ T cells can kill cancer cells and loss of TNF signalling can drive immune evasion (Kearney et al., 2018). TNFα is a Th1-related cytokine, yet there is scarce evidence to demonstrate that TNFα is a primary mechanism by which $CD4^+$ T cells induce cytotoxicity. TNFα produced by $CD4^+$ T cells was shown to work in combination with chemotherapy to cure colorectal tumors in a mouse model (Habtetsion et al., 2018). This study and others suggest that direct binding of TNFα to melanoma cells induces cell death but requires additional factors (Habtetsion et al., 2018, Nishida et al., 2003). $CD4^+$ T cells have also been shown to induce growth arrest in cancer cells through the combined secretion of Th1 cytokines, IFNγ and TNFα (Matsuzaki et al., 2015, Braumuller et al., 2013).

1.11.2.5 Indirect peripheral effector mechanisms

$CD4^+$ T cells can modulate immune responses through the provision of cytokines or via direct interaction with nearby cells. Several mouse models identified that tumor control driven by $CD4^+$ T cell was dependent on its secretion of IFNγ, but the underlying mechanisms were not fully elucidated (Mumberg et al., 1999, Quezada et al., 2010, Malandro et al., 2016). Some studies demonstrated that the requirement for IFNγ in the antitumoral response was via its reguation of host cells rather than cancer cells (Mumberg et al., 1999, Muranski et al., 2008, Quezada et al., 2010). IFNγ can orchestrate many biological processes within the

TME which may contribute to the antitumoral protection driven by $CD4^+$ T cells including upregulation of MHC molecules by cancer cells (Bohm et al., 1998), inhibition of angiogenesis within tumors (Qin and Blankenstein, 2000) and activation of tumor-infiltrating immune cells (Corthay et al., 2005).

$CD4^+$ T cells "help" $CD8^+$ T cells not only during priming via DC licensing but also during the effector phase of the antitumoral response. $CD4^+$ T cells have been reported to cooperate with $CD8^+$ T cells in the TME by enhancing their recruitment (Wong et al., 2008, Bos and Sherman, 2010, Alspach et al., 2019, Huang et al., 2005) and regulating their effector function (Wong et al., 2008, Bos and Sherman, 2010, Martin-Orozco et al., 2009, Church et al., 2014). The underlying mechanism by which $CD4^+$ T cells regulate $CD8^+$ T cells in the TME are not clear although provision of the cytokine IL-2 by $CD4^+$ T cells was necessary in one study (Bos and Sherman, 2010).

$CD4^+$ T cells have also been shown to activate tumor-infiltrating macrophages through the production of IFNγ (Corthay et al., 2005). Whilst tumor-associated macrophages that exhibit a M2-phenotype are associated with tumor progression, M1-activated macrophages express cytotoxic molecules and can directly kill cancer cells (Pan, 2012, Fauskanger et al., 2018). The cooperation between $CD4^+$ T cells and macrophages in the TME has been shown to orchestrate eradication of subcutaneously transferred myeloma, lymphoma and B16 melanoma (Haabeth et al., 2018, Corthay et al., 2005). Activated macrophages directly killed cancer cells, which was inhibited by blocking inducible nitric oxide synthase (iNOS) *in vitro* (Haabeth et al., 2018) and *in vivo* (Fauskanger et al., 2018). In a recent study, the induced expression of an MHC-II restricted epitope in sarcoma cells resulted in activation of $CD4^+$ T cells and elimination of tumors that would otherwise progress. Tumors expressing the MHC-II restricted epitope correlated with increased levels of tumor infiltrating $CD4^+$ T cells, $CD8^+$ T cells and $iNOS^+$ macrophages, highlighting the possible regulation of multiple intratumoral immune cells by the recruitment of $CD4^+$ T cells into the TME (Alspach et al., 2019). Finally, $CD4^+$ T cells have been shown to

cooperate with NK cells to eliminate tumors. Although the underlying mechanisms were not determined in these studies, inhibition of either NK cells or $CD4^+$ T cells resulted in loss of tumor control (Perez-Diez et al., 2007, Doorduijn et al., 2017).

1.12 The role of MHC-II in melanoma immunosurveillance by $CD4^+$ T cells

Activated $CD4^+$ T cells require stimulation by cognate antigen in the context of MHC-II to execute effector function in peripheral tissue. Unlike MHC-I, which is expressed by all nucleated cells, MHC-II expression is largely restricted to professional APCs. However, some cancer cells express MHC-II and could potentially serve as “non-professional” APCs to directly present endogenously processed antigen to tumor-infiltrating $CD4^+$ T cells (Axelrod et al., 2019). The relative contributions of different cell types in presenting cancer antigens to $CD4^+$ T cells in the TME, and the biological consequence of direct stimulation by cancer cells versus indirect stimulation by professional APCs are not well understood.

Immunohistochemistry of tumor biopsies has revealed that MHC-II expression by cancers cells can occur in variety of cancer types but is highly variable (Axelrod et al., 2019). MHC-II expression by cancer cells is often associated with increased numbers of intratumoral $CD4^+$ T cells as well as better responses to therapy and better overall survival of cancer patients (Johnson et al., 2016, Park et al., 2017, Matsuzaki et al., 2014). However, the extent to which $CD4^+$ T cells directly bind cancer cells in humans remains unknown.

The biological significance of MHC-II expression by cancer cells has been investigated in murine models. $CD4^+$ T cells can directly bind MHC-II-expressing B16 melanoma cells and this direct interaction can lead to the eradication of established subcutaneous melanomas (Quezada et al., 2010, Malandro et al., 2016). However, by using MHC-II-negative cancer cells, several preclinical studies showed that direct display of MHC-II-restricted antigen by cancer cells was dispensable for $CD4^+$ T cell-mediated protection against tumor challenge

(Shklovskaya et al., 2016, Perez-Diez et al., 2007, Haabeth et al., 2018, Mumberg et al., 1999). This highlights the importance of indirect antigen presentation by APCs within tumors for the stimulation of $CD4^+$ T cells. It remains to be established whether direct and indirect stimulation are redundant processes or whether they lead to different biological consequences.

1.13 Current immunotherapies for melanoma

Melanoma is the most aggressive form of skin cancer and arises from the malignant transformation of melanocytes. Melanocytes exist predominately in the skin where their most well-known function is to provide melanin pigment to surrounding cells. In human skin, melanocytes localise near the basal membrane, the junction between the epidermis and the dermis, thus similar to the majority of cancers, cutaneous melanoma originates in epithelial tissue. Like all cancers, the aetiology of melanoma is complex and involves genetic and environmental risk factors (Read et al., 2016).

The incidence of melanoma is increasing worldwide but recent advancements in treatment strategies, including targeted therapy and immunotherapy, have improved the prognosis of metastatic melanoma considerably. Targeted therapy includes drugs directed against components of oncogenic pathways expressed by cancer cells, such as the protein product of the gene *BRAF* which is mutated in 50 % of melanoma (Davies et al., 2002). Target therapy has been successful for some patients, although inherent and acquired resistance remain a major problem. Melanoma bares a high mutational load compared to most cancers (Alexandrov et al., 2013). DNA damage from exposure to UV radiation and the long life-span of melanocytes are thought contribute to the accumulation of mutations over time (Hodis et al., 2012). Although genomic instability can allow melanoma cells to be more aggressive due to increased plasticity, it also facilitates the generation of neoantigens for T cell recognition. Melanoma is thus considered one of the more immunogenic cancer types and immunotherapy has revolutionised the prognosis for melanoma patients, especially those who do not

respond to targeted therapies or those in late stage disease. Most melanoma immunotherapies, FDA-approved or in clinical trials, are directed at enhancing effector T cell responses. These include cytokine administration, vaccination, therapeutic antibodies and adoptive cell transfer.

Administration of proinflammatory cytokines, IL-2 or IFNα, the first FDA approved immunotherapies for melanoma, was aimed at activating anti-tumoral responses of T cells and NK cells. In addition to its immunoregulatory role, IFNα was selected based on evidence that it can inhibit proliferation and oncogenic signalling in cancer cells, whilst positively regulating MHC-I expression (Villikka and Pyrhonen, 1996). However, toxic side-effects and limited efficacy was seen in most patients receiving cytokine therapy (Rosenberg, 2014, Villikka and Pyrhonen, 1996). Therapeutic cancer vaccines represent another avenue for immunotherapy. Administration of melanoma-associated antigens as a vaccine strategy showed limited clinical benefit (Cebon et al., 2020), however, more recently personalised vaccines targeting neoantigens have demonstrated promising results (Boudewijns et al., 2016, Sahin et al., 2017, Ott et al., 2017).

Immune checkpoint blockade (ICB) has demonstrated remarkable efficacy in activation of anti-tumoral responses and has become the most commonly used immunotherapy approach for metastatic melanoma. ICB involves using immunomodulatory antibodies to reverse T cell-exhaustion by blocking inhibitory receptor-signalling. Targets for checkpoint blockade include inhibitory receptors on T cells, such as programmed cell death protein 1 (PD-1) and cytotoxic T-lymphocyte-associated protein 4 (CTLA-4) or ligands for these receptors such as Programmed death-ligand 1 (PD-L1). Some patients treated with anti-PD-1 or anti-CTLA-4 showed a durable response to monotherapy (Callahan et al., 2016). However, combination therapy which targets both receptors has yielded higher response rates, albeit with more adverse effects, compared to monotherapy (Postow et al., 2015, Larkin et al., 2015). The use of agonistic antibodies that target co-stimulatory receptors on T cells and methods to modulate DC function to improve T cell activation are being explored for cancer immunotherapy (Wculek

et al., 2020).

An advantage of ICB is that blocking antibodies are “off-the-shelf” reagents. On the other hand, adoptive cell therapy (ACT) of TILs, which has demonstrated considerable success, is a form of personalised cancer treatment. ACT involves the removal of T cells from a patient, expanding them *in vitro* and then reinfusing them back into the patient. Modifications to the T cells can be made *ex vivo* prior to reinfusion, such as the addition of a chimeric antigen receptors (CAR) for CAR-T cell therapy which has been particularly successful for treating blood malignancies (Barrett et al., 2014). ACT using naturally occurring TILs has mediated complete tumor regressions in patients with metastatic melanoma (Dudley et al., 2002, Hong et al., 2010).

1.14 Exploiting anti-tumoral $CD4^+$ T cells in melanoma immunotherapy

As previously discussed, accumulating data from murine models demonstrates the capacity of $CD4^+$ T cells to eradicate melanoma through diverse mechanisms. In humans, $CD4^+$ TILs are frequently observed in melanoma lesions (Friedman et al., 2012) and high-throughput epitope discovery identified that melanoma-derived neoantigens are frequently recognised by $CD4^+$ T cells (Linnemann et al., 2015). The propensity for $CD4^+$ T cells to infiltrate tumors and recognise neoantigens renders them a promising candidate for cancer immunotherapy. Efforts to harness the anti-tumoral functions of $CD4^+$ T for melanoma immunotherapies are still in early stages. There have been a small number of case studies demonstrating the potential benefit of ACT using $CD4^+$ T cells for late stage cancers. The transfer of autologous $CD4^+$ T cells specific for the cancer testis antigen, NY-ESO-1 resulted in durable disease remission of a patient with metastatic melanoma (Hunder et al., 2008). Tumor regression upon transfer of autologous cancer-specific $CD4^+$ T cells was also observed in a patient with a metastatic gastrointestinal cancer (Tran et al., 2014). Expansion of “bulk” tumor-infiltrating $CD4^+$ T cells *ex vivo* and reinfusion into a patient with metastatic

melanoma mediated a substantial reduction in tumor burden (Friedman et al., 2012).

The majority of immunotherapies for melanoma have been developed to enhance cytotoxic $CD8^+$ T cell responses. However, the mechanisms driving a patient's response to certain drugs with diverse cellular targets, such as cytokine-based therapies or antibody-based therapies, can rarely be ascertained. $CD4^+$ T cells express checkpoint molecules, targeted by ICB, such as CTLA-4 and PD-1, and thus may play a significant role in response to treatment. Differential expression of CTLA-4 may impact the mechanism of anti-CTLA-4 therapy on different cell types (Chan et al., 2014). Anti-CTLA-4 neutralising antibodies can enhance priming or prevent exhaustion of CTLA-expressing antitumoral $CD4^+$ T cells. In addition, Treg cells express high levels of CTLA-4 and can be deleted through antibody-dependent cellular toxicity in response to anti-CTLA therapy (Furness et al., 2014). Indeed, CTLA-4 blockade has been shown to reduce the number of intratumoral Treg cells and enhance Th1-mediated antitumoral immunity in melanoma mice models (Alspach et al., 2019, Quezada et al., 2010). In humans, anti-CTLA-4 therapy was shown to increase the ratio of activated effector $CD4^+$ T cells to Treg cells in bladder tumors (Liakou et al., 2008) and enhance the cytotoxic signature of tumor-specific $CD4^+$ T cells in a small cohort of melanoma patients (Kitano et al., 2013). Furthermore, response to anti-PD-1/PD-L1 therapy was shown to correlate with anti-tumoral $CD4^+$ T cell numbers in bladder cancer (Oh et al., 2020) and with tumor-associated MHC-II expression in metastatic melanoma (Johnson et al., 2016, Rodig et al., 2018). Therefore, in addition to mobilisation of an antitumoral $CD8^+$ T cell response, resounding evidence suggests that checkpoint blockade promotes cancer immunosurveillance by $CD4^+$ T cells.

1.15 Murine models for the study of melanoma

Melanoma mouse models have been invaluable for advancing our understanding of melanoma biology and cancer immunosurveillance. The most suitable model

for a particular study depends on the question to be addressed, and whether that model best approximates the human condition for that particular question. Commonly used mouse models can be divided into either genetically induced tumor models or transplantable tumor models in which melanoma cell lines can be transplanted into syngenic mice.

Genetically induced tumor models have been used for decades to model human melanoma and significant advancements in genetic engineering technologies continue to enable the creation of more sophisticated models. Early genetically induced melanoma models involved the transgenic expression of oncogenes under melanocytic promotors (Mintz and Silvers, 1993). Nowadays models incorporate conditional deletion or activation of tumor suppressor genes or oncogenes respectively, in a tissue-specific manner (Chin et al., 2006). Genetically induced tumor models are useful in studying the initial steps in malignant transformation and can be used in combination with environmental carcinogens, such as UV radiation, to explore gene-environment interactions in melanomagenesis. Genetic models tend to be labour intensive and costly which is why many studies favour the use of transplantable tumor models. Transplantable models also have the additional advantage of flexibility, that is, different combinations of melanoma cell lines and mouse strains can be used. The B16 melanoma cell line is derived from a spontaneous melanoma that arose in a C57BL/6 mouse in 1954 and is still commonly used for transplantation into syngenic mice (Overwijk and Restifo, 2001).

The route of melanoma cell transplantation dictates the location of tumour establishment. This is an important consideration given that the tumor microenvironment is composed of a plethora of cell types and metabolites which can influence cancer cell biology. In addition, different immune subsets reside in different anatomical compartments and even within the different layers of the skin there are vast differences in the composition of resident or infiltrating immune cell subsets (Bangert et al., 2011). It is thus likely that immunosurveillance mechanisms may differ between different sites within the skin. One caveat of

commonly used transplantable melanoma models is that the transfer of tumor cells via intravenous (i.v.), intradermal (i.d.), or subcutaneous (s.c.) routes do not result in tumors permeating the epidermis, which is where cutaneous melanoma arises in humans. Intravenous injection of B16 cells results in primary tumors forming in the lungs. Whilst this method has been used to model pulmonary metastasis (Overwijk and Restifo, 2001) it fails to serve as a model for spontaneous metastasis as it does not recapitulate detachment of melanoma cells from the primary tumor and intravasation into the circulation.

The commonly used s.c. model involves injection of melanoma cells into the subcutaneous tissue residing beneath the dermis. In the s.c. model all inoculated mice develop rapidly growing tumors, unless inhibited by therapeutic intervention, requiring that mice are usually sacrificed within a couple of weeks post-inoculation. This limits the ability to study endogenous immune responses, in particular long-term immune control, as often tumors are too far progressed before the immune system has the time to mount an effective response (Joncker et al., 2016). In addition, s.c. tumors may be less immunogenic as a result of the composition of subcutaneous tissue. The subcutaneous layer is predominately composed of adipose cells and blood vessels and has a low frequency of dendritic cells required for effective priming of T cells and initiating adaptive immune responses (Malissen et al., 2014, Joncker et al., 2016).

In contrast, the dermis is populated by immune cells such as dendritic cells and thus the intradermal model has gained popularity in melanoma immunosurveillance research (Joncker et al., 2016). In addition to more immunogenic primary lesions, intradermal tumors generate lymph node metastases which is not a common feature of the s.c. model. Interestingly, in genetically induced melanoma models, tumors also develop in the dermal compartment. This is because melanocytes in mice are located predominately in the bulb region of the hair follicle, in contrast to human skin whereby melanocytes are distributed throughout the epidermis proper (Tobin, 2011).

1.16 The epicutaneous murine melanoma model

The epicutaneous murine model is a transplantable melanoma model recently developed and characterised in the Waithman and Gebhardt laboratories (Wylie et al., 2015, Park et al., 2019). It involves the transfer of melanoma cells, suspended in a Matrigel, onto the outer layers of the mouse skin, following light abrasion with a Dremel rotary tool. One advantage of this model is that it is orthotopic as melanoma cells are in contact with the epidermal skin layer where melanoma arises in humans. Recently, the e.c. melanoma model was used to demonstrate that $CD8^+$ T_{RM} cells in the epidermis can directly interact with melanoma cells in the epidermis and locally suppress tumor outgrowth (Park et al., 2019). Another advantage of the e.c. model is that the progression of melanomas closely reflects that of cutaneous melanoma in humans. That is, melanoma cells originating in the epidermal and dermal layers of the skin can infiltrate subcutaneous tissue and spontaneously metastasise to the tumor-draining lymph node.

Furthermore, in the e.c. model there is considerable variation in tumor growth kinetics and incidence, which reflects the heterogeneity of human melanoma. Using a B16-F1 melanoma cell line it was found that around 60 % of C57BL/B6 mice challenged epicutaneously developed macroscopic tumors (Park et al., 2019). The immune system was identified as the driving factor for which some immunosufficient mice remained macroscopically tumor-free, as immunocompromised recombination-activating gene (Rag)-deficient mice uniformly developed rapidly growing tumors. The majority of tumors arose at around two to three weeks following inoculation but some arose several weeks later (Park et al., 2019). In approximately half of the remaining macroscopically tumor-free mice, melanoma DNA was detected at the site of inoculation several months after inoculation. In addition, the presence of melanoma cells that were “controlled” in the skin for prolonged periods of time was confirmed by intravital imaging and longitudinal bioluminescence imaging. The remaining macroscopically tumor-free mice in which melanoma cells were not detected

could possibly harbour melanoma cells that were below the detection limit, or alternatively the immune system may have eliminated the entire melanoma cell population. The variability of tumor penetrance and kinetics in the e.c. model presents an interesting paradigm when considering the “cancer immunoediting hypothesis” (Dunn et al., 2002), as all three phases; elimination, equilibrium and escape, can be recapitulated.

1.17 Thesis Aims

Despite growing evidence that $CD4^+$ T cells play an important role in cancer immunosurveillance, there is considerable debate surrounding the underlying mechanisms. The aim of this project was to characterise antitumoral $CD4^+$ T cell responses to melanoma using the recently developed epicutaneous melanoma model. Furthermore, this project aimed to refine the epicutaneous melanoma model by generating modified B16 cell lines for investigating specific mechanisms that underly melanoma immunosurveillance by $CD4^+$ T cells. The mechanism by which $CD4^+$ T cells detect melanoma antigen in the TME, that is whether they can directly bind to MHC-II-positive melanoma cells or are stimulated indirectly by APCs is not well understood. As such this project aimed to examine the role of MHC-II expression in melanoma cells and the relative contributions of antigen presentation by melanoma cells and professional APCs in the TME **(Figure 1.1)**. Furthermore, several mechanisms by which $CD4^+$ T cells orchestrate tumor eradication have been described. We sought to unravel the potential effector mechanisms by which $CD4^+$ T cells contribute to suppression of tumor outgrowth **(Figure 1.2).**

The aims of the project can be summarised as follows:

1. Characterise and refine the epicutaneous melanoma model using B16.gD cell lines.

2. Characterise the role and phenotype of $CD4^+$ T cells in melanoma immunosurveillance.

3. Determine the underlying mechanisms of melanoma immunosurveillance by $CD4^+$ T cells.

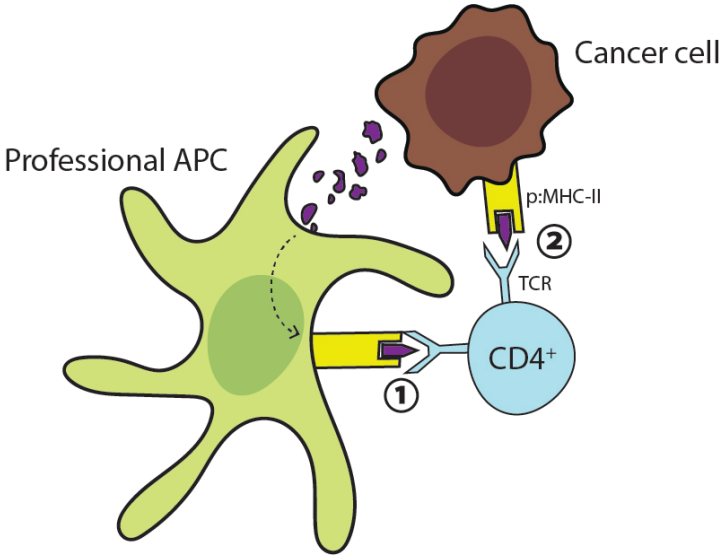

Figure 1.1. Presentation of tumor antigens to CD4⁺ T cells via indirect and direct mechanisms.
$CD4^+$ T cells are stimulated by engagement of their T cell receptor (TCR) with cognate peptide bound to MHC-II (p:MHC-II). Tumor-derived antigens may be taken up by professional APCs such as dendritic cells and presented "indirectly" to $CD4^+$ T cells **(1)**. In addition, cancer cells may express MHC-II and process endogenous peptides onto MHC-II and "directly" stimulate $CD4^+$ T cells **(2)**.

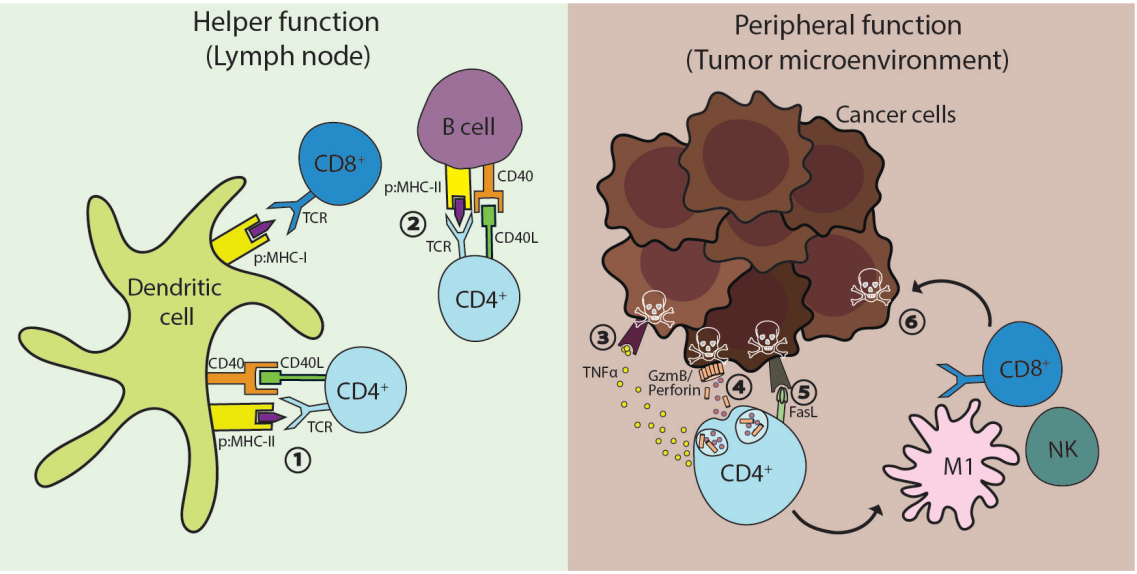

Figure 1.2. Possible antitumoral mechanisms of CD4⁺ T cells.
In the lymph node, CD4⁺ T cells could "help" prime antitumoral CD8⁺ T cells via DC licensing **(1)** and support antitumoral B cell development **(2)**. In the tumor microenvironment CD4⁺ T cells could directly kill cancer cells by secretion of cytokines such as TNFα **(3)**, release vesicles containing granzyme B (GzmB) and perforin **(4)** or engagement of Fas with FasL **(5)**. CD4⁺ T cells could target cancer cells indirectly by modulating the tumor microenvironment and recruiting or activating other antitumoral immune cells including CD8⁺ T cells, NK cells and M1 macrophages **(6)**.

Chapter 2:
Materials and Methods

Chapter 2 – Materials and methods

2.1 Materials

2.1.1 Antibodies

2.1.1.1 Antibodies and dyes for flow cytometry

Name	Conjugate	Clone	Source	Cat. Number	Dilution
Bcl6	BV450	GI191E	eBioscience™	14-9887-82	1:100
CD103	BV510	M290	BD Horizon™	563087	1:200
CD11b	BV711	M1/70	BioLegend	101242	1:300
CD11c	PE-Cy7	N418	eBioscience™	25-0114-82	1:300
CD127	APC	A7R34	eBioscience™	17-1271-82	1:200
CD25	BV605	PC61	BD Horizon™	563061	1:300
CD3e	UV395	145-2C11	BD Horizon™	563565	1:200
CD3e	BV711	17A2	BioLegend	100241	1:200
CD4	BUV805	GK1.5	BD Horizon™	612900	1:200
CD4	BV786	RM4-5	BD Horizon™	563727	1:200
CD40	APC	3-23	BD Pharmingen™	558695	1:200
CD44	BV510	IM7	BD	740215	1:200

			OptiBuild™		
CD44	BUV395	IM7	BD Horizon™	563114	1:200
CD44	PerCP-Cy5.5	IM7	eBioscience™	45-0441-82	1:200
CD45.1	FITC	A20	BD Pharmingen™	553775	1:100
CD45.1	BV785	A20	BioLegend	110743	1:100
CD45.1	BUV395	A20	BD Horizon™	565212	1:100
CD45.1	BV605	A20	BioLegend	110737	1:100
CD45.2	BUV737	104	BD Horizon™	612778	1:100
CD45.2	BV786	104	BD Horizon™	563686	1:100
CD62L	PE-Cy7	MEL-14	eBioscience™	25-0621-82	1:200
CD62L	BV605	MEL-15	BD Horizon™	563252	1:200
CD69	BV421	H1.2F3	BioLegend	104528	1:200
CD8	BV711	53-6.7	BioLegend	100748	1:200
CD8	APC	53-6.7	eBioscience™	17-0081-82	1:200
CD80	Percp710	16-10A1	eBioscience™	46-0801-82	1:200
CD83	PE	Michel-17	eBioscience™	12-0831-80	1:200
CD86	APC	GL1	BioLegend	105012	1:200
CD86	BV510	GL1	BD Horizon™	563077	1:200

DAPI			Thermofisher Scientific	D1306	0.1 µg/mL
FasL	PE	MLF3	eBioscience™	12-5911-82	1:100
FoxP3	eFluor® 450	FJK-16s	eBioscience™	48-5773-82	1:200
GATA-3	PE-Cy7	TWAJ	eBioscience™	25-9966-41	1:100
Granzyme B	FITC	GB11	BioLegend	515403	1:100
Granzyme B	Alexa Fluor® 647	GB11	BioLegend	515405	1:100
IFNγ	PE-Cy7	XMG1.2	BD Pharmingen™	557649	1:200
LIVE/DEAD™ Fixable Near-IR Dead Cell Stain Kit for 633 or 635 nm excitation				L10119	1:400
MHC-II (I-A/I-E)	Alexa Fluor® 700	M5/114.15.2	eBioscience™	56-5321-82	1:200
MHC-II (I-A/I-E)	APC-eFluor 780	M5/114.15.2	eBioscience™	47-5321-82	1:200
MHC-II (I-A/I-E)	APC	M5/114.15.2	eBioscience™	17-5321-82	1:200
MHCI (H2-	APC	AF6-88.5	eBioscience	17-5958-	1:200

Kb)			™	82	
MHCI (H2-Kb)	PE	AF6-88.5	eBioscience™	12-5958-82	1:200
NK1.1	PE-Cy7	PK136	BD Pharmingen™	552878	1:200
NK1.1	FITC	PK136	BD Pharmingen™	553164	1:200
PD-1	PE-Cy7	J43	eBioscience™	25-9985-82	1:200
PD-1	BUV395	J43	BD OptiBuild™	744549	1:200
Perforin	PE	S16009A	BioLegend	154306	1:200
RorgT	APC	B2D	eBioscience™	17-6981-80	1:100
T-bet	BV786	O4-46	BD Horizon™	564141	1:100
TNF	APC	MP6-XT22	BD Pharmingen™	554420	1:200
TNF	APC-Cy7	MP6-XT22	BD Pharmingen™	560658	1:200
Va3.2	PE	RR3-16	BioLegend	135406	1:200

2.1.1.2 Antibodies for $CD4^+$ T cell enrichment

Purified Rabbit anti-mouse	**Clone**
α-erythrocyte	Ter119
α-I-A/E	M5114

α-CD8	53-6.7
α-GR-1	RB6-8C5
α-Mac-1	M1/70
α-F4/80	F4/80

All antibodies for $CD4^+$ T cell enrichment were made in house, Shortman laboratory, WEHI, Australia.

2.1.2 Mice

Strain	Description
C57BL/6 (B6)	Mice that express MHC class I H-2^b and MHC class II I-A^b and the congenic marker Ly5.2/CD45.2.
B6.SJL-PtprcaPep3b/BoyJ (Ly5.1)	Mice that express MHC class I H-2^b and MHC class II I-A^b and the congenic marker Ly5.2/CD45.2.
B6(Cg)-$Tyrc^{-2J}$/J (Albino)	B6 mice that carry a mutation in the tyrosinase gene and therefore cannot produce the pigment melanin.
B6.*Rag1*$^{-/-}$ (*Rag1*$^{-/-}$)	B6 mice that lack expression of Rag1 due to targeted gene deletion.
B6.*Rag2*$^{-/-}$;*Il2rg*$^{-/-}$ (*Rag2*$^{-/-}$;*Il2rg*$^{-/-}$)	B6 mice that lack expression of Rag2 and the common γ chain of the IL-2 receptor due to targeted gene deletions.
B6.gDT-II (gDT-II)	Mice generated on a B6 background express I-A^b-restricted T cell receptor (Vα3.2 Jα16/Vβ2 Dβ2.1 Jβ2.1) specific for HSV-1-derived glycoprotein D peptide ($gD_{(315\text{-}327)}$, IPPNWHIPSIQDA).
gDT-II × Ly5.1 (gDT-II.Ly5.1)	gDT-II mice that express congenic marker CD45.1.
gDT-II × B6.uGFP (gDT-II.uGFP)	gDT-II mice that express green fluorescent protein (GFP) under the control of the ubiquitin C promotor.
gDT-II × Ly5.1 ×	gDT-II.Ly5.1 mice that lack expression of T-bet due to

B6.*Tbx21*$^{-/-}$ (gDT-II.*Tbx21*$^{-/-}$)	gene deletion.
gDT-II × B6.*Prf1*$^{-/-}$ (gDT-II.*Prf1*$^{-/-}$)	gDT-II mice that lack expression of perforin due to gene deletion.
B6.129S2-H2dlAb1-Ea/J (*IAE*$^{-/-}$)	B6 mice that lack expression of MHC class II due to targeted disruption of the IAE gene.
B6.*Cd40*$^{-/-}$ (*Cd40*$^{-/-}$)	B6 mice that lack expression of CD40 due to targeted gene deletion.
B6.*Cd40l*$^{-/-}$ (*Cd40l*$^{-/-}$)	B6 mice that lack expression of CD40L (CD154) due to targeted gene deletion.

2.1.3 Cell lines

Cell line	Origin	Description	Source
B16F10.gD.eGFP (B16.gD)	Mouse melanoma	Polyclonal B16F10 cell line retrovirally transduced with construct containing HSV-derived glycoprotein D and enhanced GFP (eGFP). Gene products are expressed independently.	Waithman laboratory, Telethon Kids Institute, University of Western Australia.
B16F10.Ova.eGFP (B16.Ova)	Mouse melanoma	Polyclonal B16F10 melanoma cell line retrovirally transduced with construct containing Ovalbumin and enhanced GFP (eGFP). Gene	Waithman laboratory, Telethon Kids Institute, University of Western Australia.

		products are expressed independently.	
B16F1.*Tyr*$^{-/-}$.mCherry.gD.eGFP (B16.gD.*Tyr*$^{-/-}$.mCherry)	Mouse melanoma	A B16F1 monoclone with genetic disruption in all *Tyr* alleles (D8) was retrovirally transduced with the prp-mCherry vector followed by the vector encoding full-length, HSV-derived glycoprotein D and enhanced GFP (eGFP). Gene products are expressed independently.	*Tyr* deletion and transduction with mCherry construct performed by Debby van den Boorn-Konijnenberg and Maike Effern, Hölzel laboratory. Transfection with gD.eGFP plasmid performed by Teagan Wagner, Waithman laboratory.
B16F10.gD.Luciferase-mScarlet (B16.gD.Luc-mScar)	Mouse melanoma	B16.gD cells were retrovirally transduced with vector encoding Luciferase and mScarlet. Gene product are expressed as a fusion protein.	Generated in this study. Plasmid vector generated by Daniel Hinze, Hölzel laboratory.
B16F10.gD.MHC-II-mScarlet (B16.gD.MHC-II-mScar)	Mouse melanoma	MHC-II reporter cells generated by CRISPaint using B16.gD cells. Cells	Generated in this study.

		express MHC-II.mScarlet fusion protein.	
B16.gD.*Ciita*$^{-/-}$ (a)	Mouse melanoma	Polyclonal B16.gD cell line with genetic disruption of *Ciita* gene. Generated from vector Px459-*Ciita (a)*.	Generated in this study.
B16.gD.*Ciita*$^{-/-}$ (b) (B16.gD.*Ciita*$^{-/-}$)	Mouse melanoma	Polyclonal B16.gD cell line with genetic disruption of *Ciita* gene. Generated from vector Px459-*Ciita (b).*	Generated in this study.
B16.gD.*Tnfr1*$^{-/-}$ (a)	Mouse melanoma	Polyclonal B16.gD cell line with genetic disruption of *Tnfr1* gene. Generated from vector Px459-*Tnfr1* (a).	Generated in this study.
B16.gD.*Tnfr1*$^{-/-}$ (b) (B16.gD.*Tnfr1*$^{-/-}$)	Mouse melanoma	Polyclonal B16.gD cell line with genetic disruption of *Tnfr1* gene. Generated from vector Px459-*Tnfr1* (b).	Generated in this study.
B16.gD.*Tnfr2*$^{-/-}$ (a)	Mouse melanoma	Polyclonal B16.gD cell line with genetic disruption of *Tnfr1* gene. Generated from vector Px459-*Tnfr2* (a).	Generated in this study.
B16F1.CDK4-mNeon	Mouse	Generated by	Generated in this

	melanoma	CRISPitope.	study.
B16F1.CDK4-mNeon-gD$_{(315 – 327)}$	Mouse melanoma	Generated by CRISPitope.	Generated in this study.
B16F1.CDK4-mNeon-gD$_{(312 – 330)}$	Mouse melanoma	Generated by CRISPitope.	Generated in this study.
B16F1.CDK4-mNeon-gD$_{(312 – 342)}$	Mouse melanoma	Generated by CRISPitope.	Generated in this study.
B16F1.CDK4-mNeon-Ova$_{(324 – 340)}$	Mouse melanoma	Generated by CRISPitope.	Generated in this study.
B16F1.CDK4-mNeon-Ova$_{(321 – 343)}$	Mouse melanoma	Generated by CRISPitope.	Generated in this study.
B16F1.CDK4-mScarlet	Mouse melanoma	Generated by CRISPitope.	Generated in this study.
B16F1.CDK4-mScarlet-gD$_{(315 – 327)}$	Mouse melanoma	Generated by CRISPitope.	Generated in this study.
B16F1.CDK4-mScarlet-gD$_{(312 – 330)}$	Mouse melanoma	Generated by CRISPitope.	Generated in this study.
B16F1.CDK4-mScarlet-gD$_{(312 – 342)}$	Mouse melanoma	Generated by CRISPitope.	Generated in this study.
B16F1.CDK4-mScarlet-Ova$_{(324 – 340)}$	Mouse melanoma	Generated by CRISPitope.	Generated in this study.
B16F1.CDK4-mScarlet-Ova$_{(321 – 343)}$	Mouse melanoma	Generated by CRISPitope.	Generated in this study.
B16F1.TYRP1-mNeon	Mouse melanoma	Generated by CRISPitope.	Generated in this study.
B16F1.TYRP1-mNeon-gD$_{(315 – 327)}$	Mouse melanoma	Generated by CRISPitope.	Generated in this study.
B16F1.TYRP1-mNeon-gD$_{(312 – 330)}$	Mouse melanoma	Generated by CRISPitope.	Generated in this study.
B16F1.TYRP1-mNeon-gD$_{(312 – 342)}$	Mouse melanoma	Generated by CRISPitope.	Generated in this study.
B16F1.TYRP1-mNeon-Ova$_{(324 – 340)}$	Mouse melanoma	Generated by CRISPitope.	Generated in this study.

B16F1.TYRP1-mNeon-Ova$_{(321 – 343)}$	Mouse melanoma	Generated by CRISPitope.	Generated in this study.
B16F1.TYRP1-mScarlet	Mouse melanoma	Generated by CRISPitope.	Generated in this study.
B16F1.TYRP1-mScarlet-gD$_{(315 – 327)}$	Mouse melanoma	Generated by CRISPitope.	Generated in this study.
B16F1.TYRP1-mScarlet-gD$_{(312 – 330)}$	Mouse melanoma	Generated by CRISPitope.	Generated in this study.
B16F1.TYRP1-mScarlet-gD$_{(312 – 342)}$	Mouse melanoma	Generated by CRISPitope.	Generated in this study.
B16F1.TYRP1-mScarlet-Ova$_{(324 – 340)}$	Mouse melanoma	Generated by CRISPitope.	Generated in this study.
B16F1.TYRP1-mScarlet-Ova$_{(321 – 343)}$	Mouse melanoma	Generated by CRISPitope.	Generated in this study.
B16F1.ACTB-mNeon	Mouse melanoma	Generated by CRISPitope.	Generated in this study.
B16F1.ACTB-mNeon-gD$_{(315 – 327)}$	Mouse melanoma	Generated by CRISPitope.	Generated in this study.
B16F1.ACTB-mNeon-gD$_{(312 – 330)}$	Mouse melanoma	Generated by CRISPitope.	Generated in this study.
B16F1.ACTB-mNeon-gD$_{(312 – 342)}$	Mouse melanoma	Generated by CRISPitope.	Generated in this study.
B16F1.ACTB-mNeon-Ova$_{(324 – 340)}$	Mouse melanoma	Generated by CRISPitope.	Generated in this study.
B16F1.ACTB-mNeon-Ova$_{(321 – 343)}$	Mouse melanoma	Generated by CRISPitope.	Generated in this study.
B16F1.ACTB-mScarlet	Mouse melanoma	Generated by CRISPitope.	Generated in this study.
B16F1.ACTB-mScarlet-gD$_{(315 – 327)}$	Mouse melanoma	Generated by CRISPitope.	Generated in this study.
B16F1.ACTB-mScarlet-gD$_{(312 – 330)}$	Mouse melanoma	Generated by CRISPitope.	Generated in this study.
B16F1.ACTB-mScarlet-gD$_{(312 – 342)}$	Mouse melanoma	Generated by CRISPitope.	Generated in this study.

B16F1.ACTB-mScarlet-Ova$_{(324 – 340)}$	Mouse melanoma	Generated by CRISPitope.	Generated in this study.
B16F1.ACTB-mScarlet-Ova$_{(321 – 343)}$	Mouse melanoma	Generated by CRISPitope.	Generated in this study.
B16F1.ATP5B-mNeon	Mouse melanoma	Generated by CRISPitope.	Generated in this study.
B16F1.ATP5B-mNeon-gD$_{(315 – 327)}$	Mouse melanoma	Generated by CRISPitope.	Generated in this study.
B16F1.ATP5B-mNeon-gD$_{(312 – 330)}$	Mouse melanoma	Generated by CRISPitope.	Generated in this study.
B16F1.ATP5B-mNeon-gD$_{(312 – 342)}$	Mouse melanoma	Generated by CRISPitope.	Generated in this study.
B16F1.ATP5B-mNeon-Ova$_{(324 – 340)}$	Mouse melanoma	Generated by CRISPitope.	Generated in this study.
B16F1.ATP5B-mNeon-Ova$_{(321 – 343)}$	Mouse melanoma	Generated by CRISPitope.	Generated in this study.
B16F1.ATP5B-mScarlet	Mouse melanoma	Generated by CRISPitope.	Generated in this study.
B16F1.ATP5B-mScarlet-gD$_{(315 – 327)}$	Mouse melanoma	Generated by CRISPitope.	Generated in this study.
B16F1.ATP5B-mScarlet-gD$_{(312 – 330)}$	Mouse melanoma	Generated by CRISPitope.	Generated in this study.
B16F1.ATP5B-mScarlet-gD$_{(312 – 342)}$	Mouse melanoma	Generated by CRISPitope.	Generated in this study.
B16F1.ATP5B-mScarlet-Ova$_{(324 – 340)}$	Mouse melanoma	Generated by CRISPitope.	Generated in this study.
B16F1.ATP5B-mScarlet-Ova$_{(321 – 343)}$	Mouse melanoma	Generated by CRISPitope.	Generated in this study.
HEK293T	Human embryonic kidney		ATCC (CRL-3216)

2.1.4 Plasmids

Plasmid	Use in this study	Source
gag-pol	Viral tranduction	Gift from Eicke Latz
pCAS9-mCherry-Frame +1	Frame selector plasmid, CRISPitope.	Addgene plasmid #66939
pCAS9-mCherry-Frame +2	Frame selector plasmid, CRISPitope.	Addgene plasmid #66940
pCAS9-mCherry-Frame +3	Frame selector plasmid, CRISPitope.	Addgene plasmid #66941
pCRISPaint-mNeon-BlastR [M1G]	Universal Donor plasmid, CRISPitope.	Generated in this study.
pCRISPaint-mNeon-F-gB-BlastR [M1G]	Backbone to generate Universal Donor plasmids encoding $CD4^+$ T cell epitopes.	Maike Effern, Hölzel laboratory.
pCRISPaint-mNeon-F-gD1-BlastR [M1G]	Universal Donor plasmid, CRISPitope.	Generated in this study.
pCRISPaint-mNeon-F-gD1-PuroR [M1G]	Universal Donor plasmid, CRISPitope.	Generated in this study.
pCRISPaint-mNeon-F-gD2-BlastR [M1G]	Universal Donor plasmid, CRISPitope.	Generated in this study.
pCRISPaint-mNeon-F-gD2-PuroR [M1G]	Universal Donor plasmid,	Generated in this study.

	CRISPitope.	
pCRISPaint-mNeon-F-gD3-BlastR [M1G]	Universal Donor plasmid, CRISPitope.	Generated in this study.
pCRISPaint-mNeon-F-gD3-PuroR [M1G]	Universal Donor plasmid, CRISPitope.	Generated in this study.
pCRISPaint-mNeon-F-ova1-BlastR [M1G]	Universal Donor plasmid, CRISPitope.	Generated in this study.
pCRISPaint-mNeon-F-ova1-PuroR [M1G]	Universal Donor plasmid, CRISPitope.	Generated in this study.
pCRISPaint-mNeon-F-ova2-BlastR [M1G]	Universal Donor plasmid, CRISPitope.	Generated in this study.
pCRISPaint-mNeon-F-ova2-PuroR [M1G]	Universal Donor plasmid, CRISPitope.	Generated in this study.
pCRISPaint-mNeon-gB-PuroR [M1G]	Backbone to generate Universal Donor plasmids encoding $CD4^+$ T cell epitopes.	Maike Effern, Hölzel laboratory.
pCRISPaint-mNeon-PuroR [M1G]	Universal Donor plasmid, CRISPitope.	Generated in this study.
pCRISPaint-mScarlet-BlastR [M1G]	Universal Donor plasmid, CRISPitope.	Generated in this study.

pCRISPaint-mScarlet-F-gB-PuroR [M1G]	Backbone to generate Universal Donor plasmids encoding $CD4^+$ T cell epitopes.	Maike Effern, Hölzel laboratory.
pCRISPaint-mScarlet-F-gD1-BlastR [M1G]	Universal Donor plasmid, CRISPitope.	Generated in this study.
pCRISPaint-mScarlet-F-gD1-PuroR [M1G]	Universal Donor plasmid, CRISPitope.	Generated in this study.
pCRISPaint-mScarlet-F-gD2-PuroR [M1G]	Universal Donor plasmid, CRISPitope.	Generated in this study.
pCRISPaint-mScarlet-F-gD3-PuroR [M1G]	Universal Donor plasmid, CRISPitope.	Generated in this study.
pCRISPaint-mScarlet-F-HSV-BlastR [M1G]	Backbone to generate clone Universal Donor plasmids encoding $CD4^+$ T cell epitopes.	Maike Effern, Hölzel laboratory.
pCRISPaint-mScarlet-F-ova1-PuroR [M1G]	Universal Donor plasmid, CRISPitope.	Generated in this study.
pCRISPaint-mScarlet-F-ova2-PuroR [M1G]	Universal Donor plasmid, CRISPitope.	Generated in this study.
pCRISPaint-mScarlet-PuroR [M1G]	Universal Donor plasmid,	Generated in this study.

	CRISPitope.	
pRP	Viral transduction	Gift from Eicke Latz Addgene plasmid # 41841 ; http://n2t.net/addgene:41841 ; RRID:Addgene_41841)
pRP-Luciferase-mScarlett	Viral transduction	Daniel Hinze, Hölzel laboratory.
pRP-mCherry	Viral transduction	Gift from Eicke Latz
pUC57-gD1	Plasmid backbone containing DNA sequence for cloning into Universal Donor plasmids.	BioCat
pUC57-gD2	Plasmid backbone containing DNA sequence for cloning into Universal Donor plasmids.	BioCat
pUC57-gD3	Plasmid backbone containing DNA sequence for cloning into Universal Donor plasmids.	BioCat
pUC57-Ova1	Plasmid backbone containing DNA sequence for cloning into Universal Donor plasmids.	BioCat

pUC57-Ova2	Plasmid backbone containing DNA sequence for cloning into Universal Donor plasmids.	BioCat
px330-*Actb*-Ct	Target Selector plasmid, CRISPitope.	Maike Effern, Hölzel laboratory.
px330-*ATP5b*-Ct	Target Selector plasmid, CRISPitope.	Maike Effern, Hölzel laboratory.
px330-*Cdk4*-Ct	Target Selector plasmid, CRISPitope.	Maike Effern, Hölzel laboratory.
px330-*Tyrp1*-Ct	Target Selector plasmid, CRISPitope.	Maike Effern, Hölzel laboratory.
Px459 (pSpCas9(BB)-2A-Puro)	Cas9 from S. pyogenes with 2A-Puro, and cloning backbone for short guide (sg)RNA.	Addgene plasmid #62988
Px459-*H2-Ab*-Ct	Target Selector plasmid, CRISPaint.	Generated in this study.
Px459-*Ciita (a)*	Targeted deletion of *Ciita*	Generated in this study.
Px459-*Ciita (b)*	Targeted deletion of *Ciita*	Generated in this study.
Px459-*Tnfr1 (a)*	Targeted deletion	Generated in this study.

	of *Tnfr1*	
Px459-*Tnfr1 (b)*	Targeted deletion of *Tnfr1*	Generated in this study.
Px459-*Tnfr2 (a)*	Targeted deletion of *Tnfr2*	Generated in this study.
Px459-*Tnfr2 (b)*	Targeted deletion of *Tnfr2*	Generated in this study.
VSV-G	Viral transduction	Gift from Eicke Latz

2.1.5 Oligonucleotides

Oligo	**Use in this study**	**Source**
*H2-Ab*_TS CACCGAAAACACTCTGAGTCACTGC	Cloned into Px459	Microsynth
*H2-Ab*_BS AAACGCAGTGACTCAGAGTGTTTTC	Cloned into Px459	Microsynth
Ciita (a)_TS CACCGAGAGGTGGTAGAGATGTAGG	Cloned into Px459	Microsynth
Ciita (a)_BS AAACCCTACATCTCTACCACCTCTC	Cloned into Px459	Microsynth
Ciita (b)_TS CACCGACTGGATGAAGAGACCCGGG	Cloned into Px459	Microsynth
Ciita (b)_BS AAACCCCGGGTCTCTTCATCCAGTC	Cloned into Px459	Microsynth
Trnfr1 (a)_TS CACCGAGTTGCAAGACATGTCGGAA	Cloned into Px459	Microsynth
Trnfr1 (a)_BS AAACTTCCGACATGTCTTGCAACTC	Cloned into Px459	Microsynth
Trnfr1 (b)_TS CACCGATGGGGATACATCCATCAG	Cloned into Px459	Microsynth
Trnfr1 (b)_BS	Cloned into Px459	Microsynth

AAACCTGATGGATGTATCCCCATC		
Trnfr2 (a)_TS *CACCGTGAGGCAAGCATGTATACCC*	Cloned into Px459	Microsynth
Trnfr2 (a)_BS *AAACGGGTATACATGCTTGCCTCAC*	Cloned into Px459	Microsynth
Trnfr2 (b)_TS *CACCGGTGTCAGAGAACGTCCCTG*	Cloned into Px459	Microsynth
Trnfr2 (b)_BS *AAACCAGGGACGTTCTCTGACACC*	Cloned into Px459	Microsynth
Ccl2_forward *CCTGCTGTTCACAGTTGCC*	qPCR	Microsynth
Ccl2_reverse *ATTGGGATCATCTTGCTGGT*	qPCR	Microsynth
Ccl5_forward *GTGCCCACGTCAAGGAGTAT*	qPCR	Microsynth
Ccl5_reverse *CCACTTCTTCTCTGGGTTGG*	qPCR	Microsynth
Vcam1_forward *CCGGCATATACGAGTGTGAA*	qPCR	Microsynth
Vcam1_reverse *ACCAAGGAAGATGCGCAGTA*	qPCR	Microsynth
Tnfr1_forward *AAATGGCCTGAGCAAGTGTC*	qPCR	Microsynth
Tnfr1_reverse *TCTGCACACAGTGTCCTTCC*	qPCR	Microsynth
Tnfr1 (b)_NGS_forward *ACACTCTTTCCCTACACGACGCTCTTC* *CGATCTcaatttgttgctacctctaaggc*	NGS	Microsynth
Tnfr1 (b)_NGS_reverse *TGACTGGAGTTCAGACGTGTGCTCTT* *CCGATCTctcaagacaattctctgctctc*	NGS	Microsynth

2.1.6 Bacteria and virus strains

Strain	Origin / Source
Chemically-competent DH10β Escherichia coli (*E. Coli*)	Hölzel laboratory, the University of Bonn, Germany. Originally obtained from the laboratory of Veit Hornung, University Hospital Bonn
Herpes Simplex Virus Type 1 KOS strain (HSV-1 KOS)	Dr Stanley Person, John Hopkins University, MD, USA

2.1.7 Media

Media/solution	Source
DMEM	Thermo Fisher Scientific
Hanks Buffered Salt Solution (HBSS)	Media Preparation Unit, Dept. Microbiology & Immunology, University of Melbourne, Australia.
KDS-RPMI	Media Preparation Unit, Dept. Microbiology & Immunology, University of Melbourne, Australia.
LB (Luria-Bertani) Broth media (Lennox)	Carl Roth
Opti-MEM	Thermofisher Scientific
Phosphate Buffered Saline (PBS)	Media Preparation Unit, Dept. Microbiology & Immunology, University of Melbourne, Australia.

2.1.8 Peptides and recombinant proteins

Peptides and recombinant proteins	Source
Recombinant human IL-2	Peprotech Inc., USA
Recombinant murine IFNγ	Peprotech Inc., USA
Recombinant murine TNFα	Peprotech Inc., USA
$gD_{(315-327)}$, Seq: IPPNWHIPSIQDA	Auspep, Australia.

2.1.9 Enzymes

Enzyme	Source
10X Trypsin + EDTA	Sigma Aldrich, USA
Antarctic phosphatase	New England Biolabs
AVRII	New England Biolabs
Collagenase Type III	Worthington, USA
DNase I	Roche, Germany
EcoNI	New England Biolabs
Phusion High Fidelity DNA Polymerase	New England Biolabs
Q5® High-Fidelity DNA Polymerase	New England Biolabs
RNAse A	Life Technologies
T4 DNA Ligase	New England Biolabs

2.1.10 Commercially available kits

Kit	Source
cDNA synthesis SuperMix	Bimake
Cytofix/Cytoperm™ Fixation/Permeabilization Solution Kit	BD Biosciences
DNeasy blood and tissue kit	Qiagen, Germany
MEGAquick-spin Plus Total Fragment DNA Purification Kit	iNtRON Biotechnology
PureLink® HiPure Plasmid Midiprep Kit	Life Technologies
RNeasy MicroKit	Qiagen, Germany

2.1.11 Chemicals and reagents

Chemicals	Source
2-B-mercaptoethanol	Sigma-Aldrich
Ampicillin	Carl Roth
Benzylpenicillin	CSL, Australia
Bovine Serum Albumin (BSA)	Sigma-Aldrich
Brefeldin A (BFA)	Sigma-Aldrich

Broad Range Markers	Santa Cruz Biotechnologies
D-Luciferin Potassium Salt	Thermo Fisher Scientific
DETACHaBEAD Mouse CD4	Invitrogen
Dimethyl sulphoxide (DMSO)	Sigma-Aldrich
dNTPs	Thermo Fisher Scientific
Dynabeads mouse CD4 (L3T4)	Invitrogen
EDTA, tetrasodium salt dihydrate	Sigma-Aldrich
Ethidiumbromide	Carl Roth
EvaGreen (R) QPCR-Mix Plus	Bio-Budget Technologies GmbH
Fetal calf serum (FCS)	CSL, Australia
Flt3L (human)	BioXCell
FuGENE ® HD transfection reagent	Promega
Glycine	Carl Roth
Haematoxylin	Australian Biostain
HEPES	Merck
Histodenz	Sigma-Aldrich
Ilium Xylazil	Troy Laboratories, Australia
Ionomycin	Sigma-Aldrich
Isoflurane	Cenvet, Australia
Ketamine	Parnell Laboratories, Australia
L-glutamine	Thermo Fisher Scientific
Matrigel® Basement Membrane Matrix	Corning, USA
N-Methylacetamide	Sigma-Aldrich
Paraformaldehyde	Sigma-Aldrich
Phorbol 12-myristate 13-acetate (PMA)	Sigma-Aldrich
Propidium Iodide	Sigma-Aldrich
Puromycin	Sigma-Aldrich
Red blood cell lysis buffer (Hybri-Max)	Sigma-Aldrich
SPHERO blank calibration beads (6.0-6.4 µm)	BD Pharmingen, USA

Streptomycin	Sigma-Aldrich
Tris	Carl Roth
Tween-20	Carl Roth
Zinc-fixative 10x (formalin free)	BD Biosciences

2.1.12 Consumables

Consumable	Source
10mL syringe	Terumo, Australia
18G needle	Terumo, Australia
1mL syringe	Terumo, Australia
21G needle	Terumo, Australia
24 well flat bottom plate	Corning, USA
26G needle	Terumo, Australia
30G syringe	BD Biosciences, USA
3mL syringe	Terumo, Australia
96 well flat bottom plate (Black plate, clear bottom)	Corning, USA
96 well flat bottom plate (Clear plate, clear bottom)	Corning, USA
96-well plate LightCycler 480 (white)	Roche Life Sciences
Cell strainer, 30µm	Miltenyi Biotec, Germany
Cell strainer, 40µm	Sigma Aldrich, USA
Cell strainer, 70µm	Miltenyi Biotec, Germany
Cotton tip applicator	Livingstone, Australia
Dremel with grindstone attachment	Dremel, USA
Durapore™ surgical tape	3M, USA
Electric shaver	Wahl, USA
Glass coverslips No 1.5 (24 × 50mm)	ProSciTech, Australia
Goat anti-rat IgG magnetic beads	Qiagen, Germany

Lacri-lube™ lubricating eye gel	Allergen Australia, Australia
Magnetic column	Life Technologies, USA
Metal sieve	Sefar Metal Mesh, Australia
Micropore™ surgical tape	3M, USA
Op-Site Flexigrid™	Smith and Nephew, UK
Pap pen	Daido Sangyo, Japan
Polypropylene round-bottom FACS tubes (5mL)	BD Biosciences, USA
Surgical blades	Livingstone, Australia
Transpore™ surgical tape	3M, USA
Vacuum grease Dow	Corning, USA
Veet™	Reckitt Benckiser, UK
Vetbond™ tissue adhesive	3M, USA

2.2 Methods

2.2.1 General molecular cloning techniques

2.2.1.1 Oligonucleotide annealing

Oligonucleotides purchased from Microsynth were reconstituted in dH_2O to a concentration of 100 µM. One microlitre of each of the top strand and bottom strand oligonucleotides were added to 48 µl annealing buffer (100 mM NaCl, 50 mM HEPES in ultrapure water; pH 7.4). Oligonucleotides were annealed in a thermocycler using the following conditions:

90 °C 4 min
70 °C 10 min
69 °C 1 min (decrease 1 °C / 60 s until RT is reached)
20 °C ∞

2.2.1.2 Restriction enzyme digest

Ten micrograms of plasmid DNA was incubated with 10-30 U of a restriction enzyme and the corresponding buffer in a reaction volume of 50 µl. Plasmids were incubated for 4 h at 37 °C. Products of restriction digestions were purified using the MEGAquick-spin Plus Total Fragment DNA Purification Kit.

2.2.1.3 Agarose gel electrophoresis

DNA digested by restriction enzymes was separated using agarose gel electrophoresis. Agarose gels (0.8 % - 2 %) were prepared using 1 × TAE buffer (1 mM EDTA Na_2, 40 mM TRIS, 20 mM acetic acid) + 0.5 µg/mL Ethidium bromide. Gels were run at 140 V for 30 min and DNA was visualised by UV light.

2.2.1.4 Ligation

For the ligation of annealed oligonucleotides into the px459 plasmid backbone, 100 ng of BbsI-digested px459 DNA and 2 µl of the annealed oligonucleotides were incubated with 1 µl T4 DNA ligase and the corresponding buffer in a 10 µl reaction for 10 min to 12 h at room temperature.

For ligation of DNA inserts into universal donor backbone plasmids (CRISPitope), 1 µL of gel-purified DNA insert was added to 0.8 µL of Antarctic phosphatase-treated plasmid backbone (30 ng) and incubated with 0.5 µL T4 DNA ligase and the corresponding buffer in a 10 µl reaction for 12 h at room temperature then 1 h at 37 °C.

2.2.1.5 Transformation

Chemically-competent DH10β Escherichia coli (*E. coli*) was transformed with DNA plasmids using the heat-shock method. E .coli (50 µL) were thawed on

ice and mixed with ligated plasmid (5 µl from ligation reaction). Samples were incubated for 10 min on ice followed by 45 seconds at 42 ° C and then 2 min on ice. Transformed *E. coli* were streaked on LB (Luria-Bertani) agar plates containing 100 mg/ml ampicillin. The agar plates were incubated upside down overnight at 37°C.

2.2.1.6 Plasmid DNA preparation from Escherichia coli cultures

For small-scale or medium-scale plasmid preparations, 1.5 ml or 100 ml LB broth containing 100 mg/ml ampicillin were inoculated with a single *E. coli* colony. Cultures were incubated overnight at 37 °C shaking (180 rpm). For small-scale plasmid preparations, the bacteria were pelleted in a table-top centrifuge at 6,000 × g for 10 min and were resuspended in 180 µl resuspension buffer P1 containing RNAse A. Following resuspension, 180 µl lysis buffer P2 was added and the solution was mixed by inverting the tube six times. 250 µl of neutralisation buffer N3 was added and the solution was again mixed by inverting the tube six times. The solution was centrifuged in a table-top centrifuge at full speed for 10 min and the supernatant was transferred to a spin column for DNA isolation. The spin column was centrifuged at 10,000 rpm in a table-top centrifuge and the membrane was washed twice with 750 µl PE washing buffer. Plasmid DNA was eluted in 40 µl ultrapure H_2O.

Resuspension buffer P1:	50 mM Tris-HCl (pH 8.0), 10 mM EDTA, 50 µg/ml RNAseA
Lysis buffer P2:	200 mM NaOH, 1 % SDS
Neutralisation buffer N3:	4.2 M Guanidine hydrochloride, 0.9 mM potassium acetate; pH 4.8
Wash buffer PE:	10 mM Tris-HCl (pH 7.5), 80 % Ethanol

Medium-scale plasmid preparations were processed using the PureLink® HiPure Plasmid Midiprep Kit according to the manufacturer's instructions.

Plasmid DNA was reconstituted in 100 µl ultrapure H_2O. DNA concentrations of plasmid preparations were measured using the spectrophotometer NanoDrop 2000.

2.2.1.7 Retroviral transduction

1.8×10^6 HEK293T cells were plated in a 6-well plate in DMEM-10. Six hours later, the HEK293T cells were transfected using the calcium phosphate method. Two hundred microliters of HBS (25 mM HEPES, 140 mM NaCl, 0.71 mM $Na_2HPO_4$7H2O; pH 7) were mixed with 2 µg gag-pol plasmid, 220 ng VSV-G plasmid, 2 µg of the desired retroviral overexpression plasmid and 10 µl $CaCl^2$ (2.5 M). This mixture was incubated for 20 min and added to the adherent HEK293T cells. Two days later the media of the HEK293T cells was changed twice and the target B16 cells were plated in a 6-well plate. The next day the supernatant of the HEK293T cells was harvested and filtered (0.45 µm). The target B16 cells were cultured in the filtered supernatant containing the viral particles for four days. Cells were passaged twice before sorting by flow cytometry.

2.2.2 Generation of universal donor plasmids encoding CD4+ T cell epitopes

DNA encoding epitope sequences of Glycoprotein D (gD) or Ovalbumin (Ova) specific for transgenic $CD4^+$ T cells, gDT-II and OT-II cells, respectively, were cloned into universal donor plasmids. In addition to sequences encoding the minimal epitope recognised by gDT-II or OT-II cells, sequences encoding the epitope plus additional flanking amino acid residues were used in case of a possible requirement of flanking residues for correct cleavage or folding **(Table. 1).** Sequences were sourced from GenBank, references AAA19631.1 (glycoprotein D) and AUD54707.1 (Ovalbumin) available from

www.ncbi.nlm.nih.gov)

Table 1. CD4⁺ T cell epitope sequences cloned into universal donor plasmids.

Epitope	Sequence
gD1$_{(315 – 327)}$	IPPNWHIPSIQDA
gD2$_{(312 – 330)}$	APQIPPNWHIPSIQDAATP
gD3$_{(312 – 342)}$	APQIPPNWHIPSIQDAATPYHPPATPNNMGL
Ova1$_{(324 – 340)}$	ISQAVHAAHAEINEAGR
Ova2$_{(321 – 343)}$	SLKISQAVHAAHAEINEAGREVV

Universal donor plasmids encoding CD4⁺ T cell epitopes were generated using the backbone vectors pCRISPaint-mNeon/mScarlet-F-gB-PuroR/BlastR, provided by Maike Effern, Hölzel laboratory. The sequence encoding a gB peptide was excised from pCRISPaint-mNeon/mScarlet-F-gB-PuroR/BlastR plasmids by digestion with AVRII and EcoNI. Cut plasmids were purified by gel electrophoresis and treated with an alkaline phosphatase (Antarctic phosphatase) to prevent re-ligation. Prior to ligation of inserts, backbone plasmids were heated to 80 °C for 5 min to heat inactivate the Antarctic phosphatase.

Customised DNA plasmids encoding the CD4⁺ T cell epitopes (listed in **Table 1**), flanked by restriction sites for AVRII and EcoNI, were generated (BioCat) to facilitate molecular cloning into the universal donor backbone plasmids. BioCat plasmids were digested with EcoNI and AVRII and the oligo inserts encoding the CD4⁺ T cell epitopes were purified by gel electrophoresis. Inserts were ligated into digested pCRISPaint-mNeon/mScarlet-F-gB-PuroR/BlastR plasmids using T4 DNA ligase as described above. A full list of universal donor plasmids generated in this study are presented in **Table 2.**

Table 2. List of universal donor plasmids generated for CRIPSitope.

Plasmid name	Fluorescence protein	Tag	Selection marker
pCRISPaint-mNeon-PuroR [M1G]	mNeon		Puromycin
pCRISPaint-mNeon-F-gD1-PuroR [M1G]	mNeon	Flag-gD$_{(315 – 327)}$	Puromycin
pCRISPaint-mNeon-F-gD2-PuroR [M1G]	mNeon	Flag-gD$_{(312 – 330)}$	Puromycin
pCRISPaint-mNeon-F-gD3-PuroR [M1G]	mNeon	Flag-gD$_{(312 – 342)}$	Puromycin
pCRISPaint-mNeon-F-Ova1-PuroR [M1G]	mNeon	Flag-Ova$_{(324 – 340)}$	Puromycin
pCRISPaint-mNeon-F-Ova2-PuroR [M1G]	mNeon	Flag-Ova$_{(321 – 343)}$	Puromycin
pCRISPaint-mScarlet-PuroR [M1G]	mScarlet		Puromycin
pCRISPaint-mScarlet-F-gD1-PuroR [M1G]	mScarlet	Flag-gD$_{(315 – 327)}$	Puromycin
pCRISPaint-mScarlet-F-gD2-PuroR [M1G]	mScarlet	Flag-gD$_{(312 – 330)}$	Puromycin
pCRISPaint-mScarlet-F-gD3-PuroR [M1G]	mScarlet	Flag-gD$_{(312 – 342)}$	Puromycin
pCRISPaint-mScarlet-F-Ova1-PuroR [M1G]	mScarlet	Flag-Ova$_{(324 – 340)}$	Puromycin
pCRISPaint-mScarlet-F-Ova2-PuroR [M1G]	mScarlet	Flag-Ova$_{(321 – 343)}$	Puromycin
pCRISPaint-mNeon-BlastR [M1G]	mNeon		Blastocidin
pCRISPaint-mNeon-F-gD1-BlastR [M1G]	mNeon	Flag-gD$_{(315 – 327)}$	Blastocidin

pCRISPaint-mNeon-F-gD2-BlastR [M1G]	mNeon	Flag-gD$_{(312 – 330)}$	Blastocidin
pCRISPaint-mNeon-F-gD3-BlastR [M1G]	mNeon	Flag-gD$_{(312 – 342)}$	Blastocidin
pCRISPaint-mNeon-F-Ova1-BlastR [M1G]	mNeon	Flag-Ova$_{(324 – 340)}$	Blastocidin
pCRISPaint-mNeon-F-Ova2-BlastR [M1G]	mNeon	Flag-Ova$_{(321 – 343)}$	Blastocidin
pCRISPaint-mScarlet-BlastR [M1G]	mScarlet		Blastocidin
pCRISPaint-mScarlet-F-gD1-BlastR [M1G]	mScarlet	Flag-gD$_{(315 – 327)}$	Blastocidin
pCRISPaint-mScarlet-F-gD2-BlastR [M1G]	mScarlet	Flag-gD$_{(312 – 330)}$	Blastocidin
pCRISPaint-mScarlet-F-gD3-BlastR [M1G]	mScarlet	Flag-gD$_{(312 – 342)}$	Blastocidin
pCRISPaint-mScarlet-F-Ova1-BlastR [M1G]	mScarlet	Flag-Ova$_{(324 – 340)}$	Blastocidin
pCRISPaint-mScarlet-F-Ova2-BlastR [M1G]	mScarlet	Flag-Ova$_{(321 – 343)}$	Blastocidin

2.2.3 Transfection

For standard transfections with px459 plasmids, 1×10^5 B16.gD cells were seeded in 12-well plates. Six hours later cells were transfected with 200 ng of plasmid DNA in reduced serum media (OptiMEM®) using 0.6 µl of FuGENE® HD transfection reagent according to the manufacturer's instructions.

For CRISPaint and CRISPitope transfections, 2×10^4 cells (B16.gD for CRISPaint or B16F1 for CRISPitope) were seeded in a 96-well plates. Six hours later, cells were transfected with 200 ng of DNA (50 ng target selector, 50 ng

frame selector and 100 ng universal donor) in OptiMEM® using 0.6 µl of FuGENE® HD transfection reagent according to the manufacturer's instructions.

2.2.4 Puromycin treatment for selection of transfected cells

B16.gD cells transfected with the plasmids generated on the Px459 backbone were selected by puromycin (2 µg/ml) in RP-10 for three days. Puromycin was removed and cells were cultured in RP-10 for 4 days and then passaged into T25 flasks.

2.2.5 Enrichment of B16 cell lines by flow cytometry single cell sorting

Melanoma cells were harvested using Trypsin and resuspended in RP-10 for cell sorting. For cell lines that were sorted based on MHC-II expression, cells were treated with IFNγ (1000 U/mL, 3 days) prior to sorting. Cells were stained in FACS buffer with primary antibody α-MHC-II-APC (eBioscience). B16.gD cells were sorted on GFP expression and additionally on the MHC-II negative population to generate B16.gD.*Ciita*$^{-/-}$ cells lines. Cells transduced with pRP-mCherry, pRP-luciferase-mScarlett were sorted on mCherry or mScarlet expression, respectively. For CRIPSitope generated cell lines, cells were sorted on mNeon or mScarlet expression depending on the fluorophore encoded in the universal donor plasmid. Cells were sorted into 10 mL tubes and plated in flasks to generate polyclonal cultures. Sorting was carried out by the Core Facility, UKB, the University of Bonn.

2.2.6 Cytokine treatment to enrich polyclonal B16.gD.*Tnfr1*$^{-/-}$ cell lines

To enrich *Tnfr1* gene-deleted cells, B16.gD cells transfected with Px459-*Tnfr1* (a) or Px459-*Tnfr1* (b) were plated in RP-10 at 1×10^4 cells/well in a 96 well

plate. The following day, RP-10 containing IFNγ (500 U/mL) and TNFα (1000 U/mL) was added to the plate. Cytokine media was replaced daily for 5 days. To generate the control cell line, B16.gD cells transfected with Px459 were plated at the same conditions but treated with IFNγ (500 U/mL) alone for 5 days.

2.2.7 Next generation sequencing using Illumina MiSeq platform

Next generation sequencing (NGS) using Illumina MiSeq platform was caried out to analyse indels (insertions/deletions) in the region of *Tnfr1* targeted by Px459-*Tnfr1 (b)*. B16.gD.*Tnfr1*$^{-/-}$ cells were analysed directly following enrichment *in vivo* and from *ex vivo* cultures derived from tumors of mice inoculated (e.c.) with the enriched B16.gD.*Tnfr1*$^{-/-}$ cell line. *Ex vivo* tumors were processed (as described in **2.2.14**) and plated in RP-10. After approximately 3 days cells were passaged using standard trypsin protocol to remove cells other than melanoma cells, and then replated in RP-10 for another 2 days. DNA was extracted from cells using the DNeasy blood and tissue kit (Qiagen) according to the manufacturer's instructions. Two PCRs were performed to prepare DNA samples for NGS. The first PCR used primers specific to *Tnfr1* to amplify the region targeted by Px459-*Tnfr1* (b) and the second PCR involved the addition of barcodes to the amplicons. PCR reactions and NGS sequencing was carried out by Maike Effern and Daniel Hinze, Hölzel laboratory, the University of Bonn, Germany. MiSeq PCRs were performed according to the following protocol:

1st MiSeq PCR

2.5	µl	5 × Phusion buffer HF
0.25	µl	dNTPs (10 mM each)
0.625	µl	Forward primer and reverse primer for target region (5 µM each)
1	µl	Template gDNA
0.125	µl	Phusion High-Fidelity DNA Polymerase
8	µl	ultrapure H_2O

The PCR reaction was incubated in a PCR thermocycler using the following

thermocycling conditions:

Initial denaturation	98	°C	30 s	
Denaturation	98	°C	10 s	× 18
Annealing	57	°C	15 s	
Extension	72	°C	30 s	
Final extension	72	°C	3 min	
Hold	12	°C	∞	

2nd MiSeq PCR

5	µl	5 × Phusion buffer HF
0.5	µl	dNTPs (10 mM each)
2.5	µl	Forward primer and reverse barcode primer (5 µM each)
2	µl	DNA product from 1st MiSeq PCR
0.25	µl	Phusion High-Fidelity DNA Polymerase
14.75	µl	ultrapure H_2O

The PCR reaction was incubated in a PCR thermocycler using the following thermocycling conditions:

Initial denaturation	98	°C	30 s	
Denaturation	98	°C	10 s	× 18
Annealing	57	°C	15 s	
Extension	72	°C	30 s	
Final extension	72	°C	3 min	
Hold	12	°C	∞	

The 2nd MiSeq PCR product was analysed by gel electrophoresis. Samples were pooled and sequenced by NGS using the Illumina MiSeq platform. Sequences were aligned against the region of *Tnfr1* targeted by Px459-*Tnfr1* (b) using the web tool Outknocker 3.0 alignment tool.

2.2.8 Quantitative Real Time Polymerase Chain Reaction.

Quantitative real time polymerase chain reaction (RT-PCR) was used for functional validation of B16.gD.*Tnfr1*$^{-/-}$ cell lines. Enriched B16.gD.*Tnfr1*$^{-/-}$ cell lines or the control B16.gD cell line were plated in 12 well plates (3×10^5 cells) and treated with TNFα (1000 U/mL) for 18 hours. RNA was extracted using a RNeasy MicroKit (Qiagen). RNA (1000 ng) from each sample was converted to cDNA using cDNA synthesis SuperMix kit (Bimake) with the following thermocycler conditions:

42	°C	15 min
85	°C	2 min
		Cool down

cDNA was diluted in 40 μL dH_2O and samples were added (1 μL/well) to white 96 well plates (Lightcycler). EvaGreen Dye was mixed with annealed primers (*Ccl2, Vcam1, Ccl5, Tnfr1, GAPDH*) and added to samples. Plates were run on a LightCycler using the LC480 program with the following settings:

Initial denaturation	95	°C	10 min	
Denaturation	95	°C	10 s	× 40
Annealing	60	°C	15 s	
Extension	72	°C	15 s	

Relative mRNA expression was calculated as fold change (2-ΔΔCt), normalized to GAPDH.

2.2.9 Cell culture

B16 melanoma cell lines were cultured in RPMI media supplemented with 10 % fetal calf serum (FCS), 5 mM HEPES, 2 mM L-glutamine, 50 U/ml penicillin, 100 mg/mL streptomycin and 0.05 mM 2-mercaptoethanol (RP-10). HEK293T

cells were cultured in DMEM supplemented with 10 % FCS, 2 mM L-Glutamine, 100 U/ml penicillin and 100 µg/ml streptomycin (DMEM-10). All cells were maintained in an incubator at 37 °C in 6.5 % CO_2.

2.2.10 Mice

Mice were bred and housed under Specific-pathogen-free conditions at the Bioresource Facility of the Department of Microbiology and Immunology, University of Melbourne. All transgenic strains were generated on a C57BL/6 (B6) background. All mice used in experiments were female, aged between 6 to 14 weeks. Euthanasia was performed by carbon dioxide (CO_2) administration at a fill rate of 1.6 g/L. All animal experiments were approved by the University of Melbourne Animal Ethics Committee.

2.2.11 Epicutaneous inoculation of B16 melanoma cells

Melanoma cells were cultured in RP-10 were collected from tissue culture flask using Trypsin. Cells were washed 3 times in HBSS, resuspended in Corning® Matrigel® Basement Membrane Matrix and maintained on ice until ready for application. Mice were anesthetised by i.p. injection of a mixture of ketamine (100 mg/kg bodyweight) and xylazine (15 mg/kg bodyweight) and lubricating gel was applied to the eyes to prevent them from drying. The left flank of the mouse was shaved with clippers and depilated using Veet hair removal cream. Veet was removed by gently wiping skin with a tissue soaked in water. A Dremel rotary tool with grindstone attachment was used for 10-12 seconds to create a light abrasion site on the skin. The abrasion site was wiped with a cotton topped applicator soaked in PBS prior to application of 10 µL of Matrigel, containing B16 melanoma cells (1×10^5 cells, unless otherwise indicated). Once the Matrigel solidified (~10 min), it was covered by a transparent waterproof film (Op-Site Flexigrid). Mice were bandaged with Micropore and Transpore surgical

tape for 4 days. Tumors were measured using a digital calliper and tumor volume calculated using the formula: Volume = ((width^2 × length)/2).

2.2.12 HSV flank infection

Mice were anesthetised by i.p. injection of a mixture of ketamine (100 mg/kg bodyweight) and xylazine (15 mg/kg bodyweight) and lubricating gel was applied to the eyes to prevent them from drying. The left flank of the mouse was shaved with clippers and depilated using Veet hair removal cream. Veet was removed by gently wiping skin with a tissue soaked in water. A Dremel rotary tool with grindstone attachment was used for 8-10 seconds to create a light abrasion site on the skin. The abrasion site was wiped with a cotton topped applicator soaked in PBS. HSV-KOS (10^6 PFU) in PBS was applied to the abrasion site and covered by a transparent waterproof film (Op-Site Flexigrid). Mice were bandaged with Micropore and Transpore surgical tape for 2 days.

2.2.13 Preparation of mouse tissue for flow cytometric analysis

Blood (~100μL) was sampled from the lateral tail vein or the submandibular vein and passed through a heparinised capillary tube to prevent clotting. Blood was treated with red blood cell (RBC) lysis buffer twice for 5 min and washed once with FACS buffer (PBS + 10 % (w/v) BSA + 5mM EDTA).

Spleens and brachial lymph nodes were harvested into cold HBSS and single cell suspensions were generated by pressing organs through a fine metal sieve. Cells were washed once with FACS buffer. Half of the lymph node or 1/40 of the spleen were stained for flow cytometric analysis.

Prior to harvesting **skin and tumor samples,** skin was shaved with clippers and depilated using Veet hair removal cream. Tumors or skin (1 × 1 cm^2)

were harvested directly into 3 mg/ml Collagenase Type III in RPMI media supplemented with 2 % FCS, 5 mM HEPES, 2 mM L-glutamine, 50 U/ml penicillin, 100 mg/mL streptomycin, 0.05 mM 2-mercaptoethanol and 5 μg/ml DNAse I. Skin or tumors were cut into small pieces for 3 min and incubated for 90 min in a 37 °C water bath. For experiments in which cells were stained with Granzyme B, 10 μg/mL Brefeldin A (BFA) was added to the Collagenase Type III media to prevent release of granzyme-containing vesicles. Following digestion, samples were resuspended in RP-10 and further homogenised with a transfer pipette. Samples were passed through 70 μm nylon filters followed by 30 μm nylon filters and washed once with FACS buffer. Whole skin samples were stained for flow cytometric analysis. The whole tumor was stained when tumor volume <100 m^3 and half the tumor was stained when tumor volume >100 m^3.

Samples were stained with antibodies specific for surface markers (and in some experiments a fixable viability dye) in 100 μL of FACS buffer in polypropylene round-bottom FACS tubes for ~45 min on ice in the dark. For intracellular staining, cells were permeabilized and stained using a Fixation/Permeabilization kit (BD Biosciences) according to the manufacturer's instructions. Cells were washed with 1 × FACS buffer and for some experiments 0.1 μg/mL DAPI was added prior to analysis. A known number of SPHERO Blank Calibration Particles were added to each sample prior to analysis for enumeration. Samples were run on an LSRFortessa (BD Biosciences) and analysed using FlowJo software.

2.2.14 Enrichment of gDT-II cells

Spleens and brachial lymph nodes (bLN) of gDT-II mice were harvested into cold HBSS and a single cell suspension was generated by pressing organs through a fine metal sieve. Cells were washed in HBSS + 2.5 % FCS (HBSS-2.5), resuspended in RBC lysis buffer for 3 min and then washed again in HBSS-2.5. gDT-II cells were enriched by positive and negative selection using magnetic

beads. For negative enrichment, cells were incubated for 30 min on ice with purified rat mAbs α-Mac-1 (M1/70), α-F4/80 (F4/80), α-erythrocyte (TER-119), α-GR-1 (RB6-8C5), α-I-A/E (M5114) and α-CD8. Cells were then incubated for 20 min on a roller at 4 °C with goat α-rat IgG-coupled magnetic beads at an approximate concentration of 8 beads: 1 cell. Following incubation, cells bound to beads were removed using a magnetic column and the supernatant was collected for positive enrichment using the Dynabeads® Mouse CD4 kit (L3T4) (Invitrogen). Dynabeads were added at a ratio of 1 bead: 1 cell and incubated for 20 min on a roller at 4 °C. The bead-cell solution was placed on a magnetic column and unbound cells were discarded. DETACHaBEAD (Invitrogen) was used, per manufacturer's instructions, to release $CD4^+$ T cells from beads.

2.2.15 *In vitro* activation of gDT-II cells

gDT-II cells were enriched from lymph nodes and spleen of a gDT-II mouse as described above. Splenocytes were harvested from a C57BL/6 mouse, washed twice in HBSS and pulsed with 5 μM of the $gD_{(315-327)}$ peptide (IPPNWHIPSIQDA) for 45 min in a 37 °C water bath. Pulsed splenocytes were mixed with enriched gDT-II cells at a ratio of 1:1. Cells were co-cultured in RP-10 containing LPS (0.15 μg/mL) for 5-7 days in incubator (37 °C, 6.5 % CO^2). After 48 hours, cells were split 1:2 and recombinant human IL-2 (12.5 U/mL) was added every 24 hours.

2.2.16 Adoptive gDT-II cell transfer

A viable cell count was performed with a hemocytometer using trypan blue exclusion. gDT-II cells were injected intravenously (i.v.) via the lateral tail vein. Naïve gDT-II cells (1×10^4, unless otherwise indicated) were transferred following enrichment at a purity between 55-68 % ($V\alpha3.2^+$ $CD4^+$). Activated gDT-II cells (1

× 10^6) were transferred 5-7 days post-activation at a purity of 75-99 %.

2.2.17 *In vitro* differentiation of bone marrow derived dendritic cells

Bone marrow was collected from C57BL/6 mice, centrifuged and resuspend in 1 mL RBC lysis buffer for 20 seconds. Cells were resuspended and cultured at 1.5 × 10^6 cells/mL in KDS-RPMI supplemented with 10 % FCS, 0.2 g/L streptomycin, 100 U/ml penicillin, 90 µM 2-β-mercaptoethanol and 1.32 mM L-glutamine and 150 ng/mL of human Flt3L (BioXCell) for 8 days in an incubator (37 °C, 5.2 % CO^2).

2.2.18 *In vitro* functional assay for gDT-II cells

B16 cell lines were plated at 1 × 10^4 cells/well in 96-well plates with or without IFNγ (500 U/mL) for 2.5 days. Bone marrow derived DCs (2.5 × 10^5) were incubated with cell lysate from B16 cells (7.5 × 10^5). Cell lysate was generated in PBS by 3 × freeze-thaw cycles on dry-ice and in a 37 °C water bath. Immediately prior to coculture, B16 cells were gently washed twice with warm RP-10 to remove IFNγ. *In vitro* activated gDT-II cells (2.5 × 10^5) or lysate-pulsed DCs (2.5 × 10^5) were suspended in in RP-10 containing 10 µg/mL BFA and added to the wells containing B16 cells. B16 and gDT-II cells were cocultured for 5 hours, during which time the plate was gently agitated twice. Cells were collected for intracellular staining and analysis by flow cytometry.

2.2.19 *In vitro* gDT-II killing assay for analysis by flow cytometry

B16 cell lines were plated at 1 × 10^4 cells/well in 96-well plates with or

without IFNγ (500 U/mL) in RP-10 for 2.5 days. Prior to co-culture, the cell culture media was removed and the B16 cells were gently rinsed twice in warm RP-10. B16 cells were cultured in RP-10 containing *in vitro* activated gDT-II cells (2.5 × 10^5) in RP-10 media alone (control) for 24 hours. In some experiments, blocking antibodies, α-IFNγ (10 μg/mL) or α-TNF (10 μg/mL) were added to the gDT-II cells 20 min prior to co-culture and incorporated in the media during co-culture. After 24 hours co-culture, gDT-II cells were gently rinsed from the wells using pre-warmed RP-10. B16 cells were detached using Trypsin and wells were rinsed twice to collect all B16 cells. Samples were stained for flow cytometric analysis and a known number of SPHERO Blank Calibration Particles were added to each sample to determine the number of surviving melanoma cells following co-culture. Samples were run on an LSR Fortessa (BD Biosciences) and analysed using FlowJo software.

2.2.20 Real-time *in vitro* gDT-II killing assay measured by PI uptake

B16 cell lines were plated at 1 × 10^4 cells/well in clear-bottom, black 96-well plates with or without IFNγ (500 U/mL) in RP-10 for 2.5 days. Prior to co-culture, the cell culture media was removed and the B16 cells were gently rinsed twice in warm RP-10. B16 cells were cultured in RP-10 + 6 μg/ml PI with *in vitro* activated gDT-II or gDT-II.*Prf1*$^{-/-}$ or in RP-10 + 6 μg/ml PI alone (control) for 24 hours. In some experiments blocking antibodies, α-TNF (10 μg/mL) or α-FasL antibody (2 μg/mL) were added to the gDT-II or gDT-II.*Prf1*$^{-/-}$ cells 20 min prior to co-culture and incorporated in the media during co-culture. PI fluorescence intensity was measured every 5 minutes by the CLARIOstar Plus microplate reader (BMG Labtech) over the 24 hours co-culture.

2.2.21 Bioluminescence imaging

To validate bioluminescence emission from the B16.gD.Luc-mScar cell

line *in vitro*, cells were plated in RP-10 at varying densities and five hours later D-luciferin was added to the cell culture media at a final concentration of 75 μg/ml. Imaging started immediately after luciferin administration to wells at an exposure time of 300 seconds.

For *in vivo* bioluminescence imaging mice were inoculated with B16.gD.Luc-mScar (1×10^5 e.c.) and mice were injected (i.p.) with 150 mg/kg of D-luciferin potassium salt dissolved in PBS. Mice were anaesthetized with isoflurane (2.5 %) vaporized at an 80:20 mixture of O_2 and air. The left flank of the mouse was shaved and depilated. Five minutes after injection of D-luciferin, mice were imaged at an exposure time of 300 seconds. Bioluminescence was measured using the IVIS Lumina XRMS Series III imaging system (Perkin Elmer). Images were analysed with Living Image v4.4.5 software. Bioluminescence signals were measured at site of tumor inoculation and calculated as total flux (Radiance, photons/second, p/s).

2.2.22 Histology

Skin was harvested from mice and fixed for 24 h in 1 × zinc-fixative. The fixed tissue was paraffin embedded and the tissue was cut into 4 μm sections onto glass slides. Haematoxylin and Eosin (H&E) staining was carried out using a Leica AutoStainer XL with the following protocol;

Staining solution	**Time**
Deparaffinise and rehydrate sections	
Xylene	4 minutes
Xylene	2 minutes
Xylene	2 minutes
100 % Ethanol	1 minute
100 % Ethanol	2 minutes
90 % Ethanol	2 minutes

70 % Ethanol	2 minutes
Wash in running tap water	1 minute or more
Stain	
Stain nuclei with Harris haematoxylin	4 minutes
Wash in running tap water	2 minutes
Blue nuclei in Scott's tap water	1 minute
Wash in running tap water	3 minutes
Stain with 1 % eosin	4 minutes
Wash in running tap water	1 minute
Dehydrate, clear and mount	
100 % Ethanol	1 minute
100 % Ethanol	30 seconds
100 % Ethanol	30 seconds
100 % Ethanol	30 seconds
100 % Ethanol	30 seconds
Xylene	2 minutes
Xylene	2 minutes
Xylene	2 minutes

Coverslips were added (Leica CV5030 Coverslipper) and tissue sections were scanned using the slide scanner Pannoramic SCAN II. Tissue processing and staining with H&E was performed by the Histology Facility at the School of Biomedical Sciences at the University of Melbourne.

2.2.23 Intravital two-photon microscopy

Intravital imaging using two-photon microscopy was carried out as described previously (Gebhardt et al., 2011). Mice were anaesthetized with isoflurane (2.5 % for induction, 1-1.5 % for maintenance), vaporized in an 80:20 mixture of oxygen and air. The left flank was shaved and depilated with Veet hair removal cream. Two parallel incisions, 15 mm apart, were made on the left flank either

side of the melanoma inoculation site. The skin was separated from the peritoneum, and an 18 mm-wide, 1 mm thick piece of stainless steel was inserted under the dermis and adhered using Vetbond tissue adhesive (3M). Vacuum grease (Dow Corning) was applied around the edges of the elevated skin. PBS was used to cover the skin and glass coverslip was placed on the skin forming a seal with the vacuum grease. Incision sites were regularly irrigated with PBS to prevent dehydration of the peritoneum during imaging. Images were acquired with an upright FV-MPERS multiphoton microscope with a 25x/1.05NA Water Immersion objective enclosed in a heated chamber maintained at 35°C. Fluorescence excitation was provided by Mai-Tai (690-1040nm) and InSight (680-1300) lasers and Galvano laser scanner (4fps). mCherry was excited at 1100nm (InSight laser) and eGFP and collagen from the skin dermis visualized by the second harmonic generation (SHG) were excited at 950nm (Mai-Tai laser). For four-dimensional data sets, three-dimensional stacks were captured at a resolution of 512 × 512 every 60 seconds over a period of 1-4 h with 3µm intervals. Raw imaging data were processed and movies generated in Imaris 9 (Bitplane) and edited using Adobe Premier Rush.

2.2.24 Light-sheet microscopy

Lymph nodes were harvested and fixed in 4 % paraformaldehyde (Sigma-Aldrich) for 24 hours at 4 °C. Lymph nodes were cleared to a refractive index of 1.49-1.5 by immersion in Ce3D medium (Li et al., 2017) containing 1.455 g/mL Histodenz (Sigma-Aldrich), 0.5 % 1-Thioglycerol and 0.1 % Triton-X100 in 40 % N-Methylacetamide (Sigma-Aldrich). Tissues were incubated at room temperature on a shaker and after 24 hours the clearing medium was replaced with fresh Ce3D medium and incubated for a further 4-5 days. The cleared lymph nodes were embedded in 2 % low melting agarose in glass capillaries (2.15 mm diameter; Zeiss). Samples were submerged in clearing medium for 24 hours for refractive index matching before imaging. Images were acquired on a Zeiss Z.1 Light-sheet Microscope, with a 5x/0.16 air objective and processed using 9.5.1

Imaris (Bitplane). Multiview Z-stacks were acquired at 180 degree angles and fused using ZEN for Light-sheet Z.1 (Zeiss).

2.2.25 Statistical analysis

Statical analysis was performed using the Graphpad Prism 7 software. P values were determined by the Log-rank Mantel Cox test for comparison of tumor incidence or by the Mann-Whitney test, as indicated in figure legends. P values less than 0.05 were considered statistically significant. Statistical analysis was only performed when n >5 and data was obtained from two or more independent experiments.

Chapter 3:
Characterisation and refinement of the epicutaneous melanoma model using B16.gD cell lines.

Chapter 3: Characterisation and refinement of the epicutaneous melanoma model using B16.gD cell lines.

3.1 Background

The recently developed murine epicutaneous melanoma model has several advantages over other models for the study of melanoma immunosurveillance. Firstly, being a transplantable model provides the flexibility to use different melanoma cell lines in combination with different mouse strains. Secondly, being an orthotopic model means that the local tumor microenvironment is a better anatomical approximation of human cutaneous melanoma. This is important because the tumor microenvironment has a direct impact on melanoma biology and immunogenicity. Thirdly, in the epicutaneous model, tumor incidence and the kinetics of tumor development recapitulate the variation seen in human melanoma. This variation is largely a result of disparities in immune responses as highly immunodeficient mice display a uniform susceptibility to melanoma challenge in the epicutaneous model (Park et al., 2019). Interestingly, this variation recapitulates the three E's of the cancer immunoediting hypothesis; elimination, equilibrium and escape (Casey et al., 2012). The underlying mechanisms driving different fates of epicutaneously transplanted melanoma cells are still largely unknown. An additional feature of this model is the occurrence of spontaneous metastasis to the tumor-draining lymph node. Together, these features render the epicutaneous model highly valuable for the study of immune cell-melanoma cell interactions at different stages of cancer progression. This chapter showcases the molecular cloning strategies that have been used to generate different melanoma cell lines to refine the epicutaneous melanoma model.

The epicutaneous model has been previously characterised using a B16F1 melanoma line that expresses HSV-derived glycoprotein B (B16.gB) (Park et al., 2019). This cell line was used primarily to study $CD8^+$ T cell responses through the use of transgenic gBT-I cells that recognise an epitope of glycoprotein B. gDT-

II cells are transgenic $CD4^+$ T cells that are specific for an MHC-II-restricted epitope of glycoprotein D (gD) (Bedoui et al., 2009). To study melanoma-specific $CD4^+$ T cell responses using gDT-II cells, we used the B16.gD cell line generated by retroviral transduction to overexpress full-length HSV-derived glycoprotein D (gD).

Engineering melanoma cell lines to express proteins which harbour immunological epitopes for the use of TCR transgenic T cells is one example of the utility of molecular cloning. Another common tool for molecular cloning is the use of the CRISPR/Cas9 to manipulate the host genome (de la Fuente-Nunez and Lu, 2017). CRISPR/Cas9 utilises a bacterial derived endonuclease (Cas9) to cut the genome at a precise location targeted by short-guide RNA sequences. This system can be readily used to disrupt genes or insert genetic material into a gene of interest. CRISPR/Cas9 is now the gold standard approach to disrupt genes and therefore is routinely used to investigate the importance of gene products in cell biology. A useful approach to investigate the underlying mechanisms of cancer immunosurveillance is to block receptor-ligand interactions that mediate immune-cancer cell crosstalk. Inhibition can be achieved through various techniques including neutralisation antibodies, that function on a protein level, or disrupting genes on a DNA level. Blocking antibodies have the limitation that they are not always fully specific for the cell type of interest. This project exploited CRISPR/Cas9 to disrupt the *Ciita* and *Tnfr1* genes in the B16.gD cell line.

A topic of ongoing debate is the impact of MHC-II expression by cancer cells on immunosurveillance. This is of particular relevance for $CD4^+$ T cells that bind their cognate antigen in the context of MHC-II molecules. In both humans and mice, expression of MHC-II, and other molecules in the MHC-II peptide procressing pathway, are controlled primarily at the transcriptional level by the inducible co-activator CIITA (Steimle et al., 1994). Whilst professional APCs express MHC-II under basal conditions, for other cell types, including some cancers, MHC-II expression is inducible (Steimle et al., 1994, Johnson et al., 2016). IFNγ is a well-known inducer of *Ciita* transcription, and subsequent MHC-II upregulation, in

some cell types including B16 melanoma (Bohm et al., 1998). To determine whether $CD4^+$ T cell can directly bind to MHC-II-expressing melanoma cells and to investigate the downstream consequences of this potential interaction, *Ciita* was deleted from the genome of the B16.gD cell line.

The role of TNFα in cancer immunosurveillance is an ongoing area of confliction. The multifaceted role of TNFα stems from its ability to target many cell types and modulate many signalling pathways. Of note, TNFα induces vasculature permeability, regulates immune responses and can induce apoptosis in various cell types, including cancers (Montfort et al., 2019). In the epicutaneous model it was found that mice deficient in the production of TNFα, but not effector molecules perforin or IFNγ, were more susceptible to tumor outgrowth than their wild-type counterparts (Park et al., 2019). Whilst this finding intimates an anti-tumoral role of TNFα in this model, the underlying mechanisms have not been elucidated. The cell type responsible for the production of TNFα, which is normally protective against melanoma outgrowth, remains to be determined. Additionally, it is not clear whether TNFα mediates its antitumoral role by targeting melanoma cells directly or by regulating host cells. Of note, TNFα produced by antigen-specific $CD4^+$ T cells has been reported to induce oxidative stress and cell death by directly binding TNFR1 on cancer cells (Habtetsion et al., 2018). To address the role of TNFR1-signalling in melanoma cells on immunosurveillance, in particular whether this pathway is involved in the anti-tumoral $CD4^+$ T response, the *Tnfr1* gene was functionally deleted in B16.gD cells.

All cell lines described in this chapter were generated using a polyclonal gene-editing approach. Monoclonal cell lines can show vast differences in protein expression, growth characteristics and morphology to the parental cell line. Polyclonal cell lines are therefore favourable to avoid monoclonal bias and maintain phenotypic heterogeneity.

3.2 Results

3.2.1 Characterisation of the B16.gD cell line in the murine epicutaneous melanoma model

Tumor growth characteristics depend on properties of the cancer cell line and of the tumor microenvironment. Characterisation of the B16.gD cell line was carried out in the epicutaneous model in wild-type (C57BL/6) mice. Approximately half of the mice developed tumors in the epicutaneous model, in contrast to the 100 % tumor incidence in mice challenged subcutaneously (**Figure 3.1a**). The majority of progressively growing tumors arose between seven and 20 days p.i. but a small percentage arose later. There was variation in growth kinetics of tumors and generally tumors which arose later grew more slowly than those which were detected earlier (**Figure 3.1b**). As reported previously in the epicutaneous model (Park et al., 2019), there was considerable interexperimental variation regarding tumour incidence, whereby the percentage of mice developing tumours ranged from 20-100 % (**Figure 3.1c**).

In a small proportion of mice, miniscule black lesions that remained at a similar size over the course of several weeks were observed at the site of inoculation (**Figure 3.1 e, f**). Detection and monitoring of small lesions that were difficult to see by eye was aided by the use of a dermoscopy camera (Dermlight). It seemed likely that most observed lesions comprised melanoma cells as previous characterisation of the epicutaneous model showed that melanoma cells can persist in macroscopically tumor-free skin over long periods of time (Park et al., 2019). Additionally, proof that persistant lesions harbour melanoma cells comes from the fact that occassionally the lesions escape and develop into progressively growing tumors after a prolonged period of time (**Figure 3.1d**). There was variation in the appearance of the controlled lesions (**Figure 3.1 e, f and Appendix figures 1-10**). In most cases the lesion borders showed changes in shape over time but the overall size of the lesion did not dramatically change.

Rarely did a lesion disappear, although often the strength of colour faded over time.

A number of tumors or non-progressing lesions were resected for histological analysis. Hematoxylin and eosin (H&E) staining revealed structural information of the melanoma microenvironment. Melanoma cells in small, albeit progressively growing tumors resided within the epidermis, dermis and subcutaneous layers (**Figure 3.1d**). In the lesions that did not develop into progressively growing tumors, large, pigmented cells consistent with the morphology of melanoma cells were identified in the dermis where they were often localised in small clusters (**Figure 3.1e, f**). Although histology suggested these non-progressing lesions comprise melanoma cells, the identity of these cells cannot be definitively ascertained from H&E staining and visual examination alone.

Another feature of the epicutaneous model is the occurrence of spontaneous metastasis in lymph nodes draining the site of initial inoculation (Park et al., 2019, Wylie et al., 2015). Metastasis was monitored by the observation of black deposits at the tumor-draining lymph node. There was variation in the size and spread of seeding in the lymph node. The surface area of pigment observed ranged from small black regions, only detectable under a microscope, to enlarged lymph nodes that were almost entirely black.

To stratify lymph node metastasis by size a scoring system ranging from 0-3 was devised based on the surface area of the black pigment that could be observed using a scale bar on the Stereo microscope (**Figure 3.1g**). The absence of black pigment was scored a 0 although it could not be assumed that these lymph nodes were completely devoid of melanoma cells which may have been present at undetectable levels. Miniscule metastasis (score=1) corresponded to pigment <0.5 mm^2. Overt metastasis (score=2) corresponded to pigment 0.5-1.5 mm^2 and dominant metastasis (score=3) corresponded to pigment >1.5 mm^2. This grading system was employed in future experiments to make a preliminary

assessment of the level of metastasis in different treatment groups.

There was a high incidence of metastasis (88 %) in mice with progressively growing B16.gD melanomas (**Figure 3.1h**). Nodal disease was not observed in mice with macroscopically tumor-free skin (data not shown) and only one in four mice harbouring non-progressing primary lesions showed signs of lymph node metastasis. Validating that live B16.gD cells constituted the black nodules in the lymph node of melanoma-bearing mice, GFP^+ cells with a characteristic size and granularity of melanoma cells could be detected by flow cytometry. In addition, black nodules from the lymph node were cultured *ex vivo* and monolayers of GFP^+ melanoma cells were able to be grown *in vivo* (data not shown).

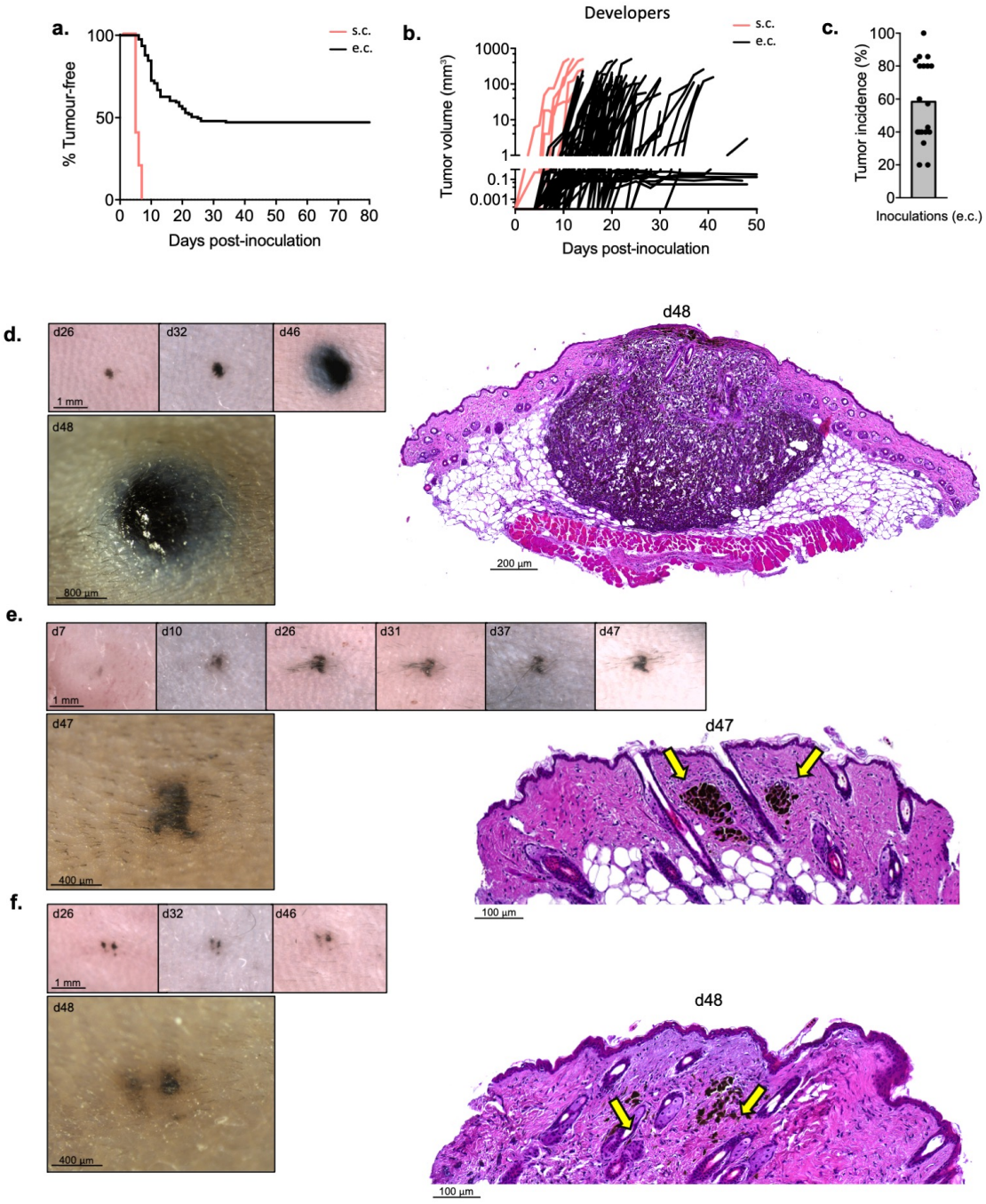
a.
% Tumour-free
Days post-inoculation
s.c.
e.c.
b.
Developers
Tumor volume (mm³)
Days post-inoculation
c.
Tumor incidence (%)
Inoculations (e.c.)
d.
d26
d32
d46
1 mm
d48
800 µm
d48
200 µm
e.
d7
d10
d26
d31
d37
d47
1 mm
d47
400 µm
d47
100 µm
f.
d26
d32
d46
1 mm
d48
400 µm
d48
100 µm

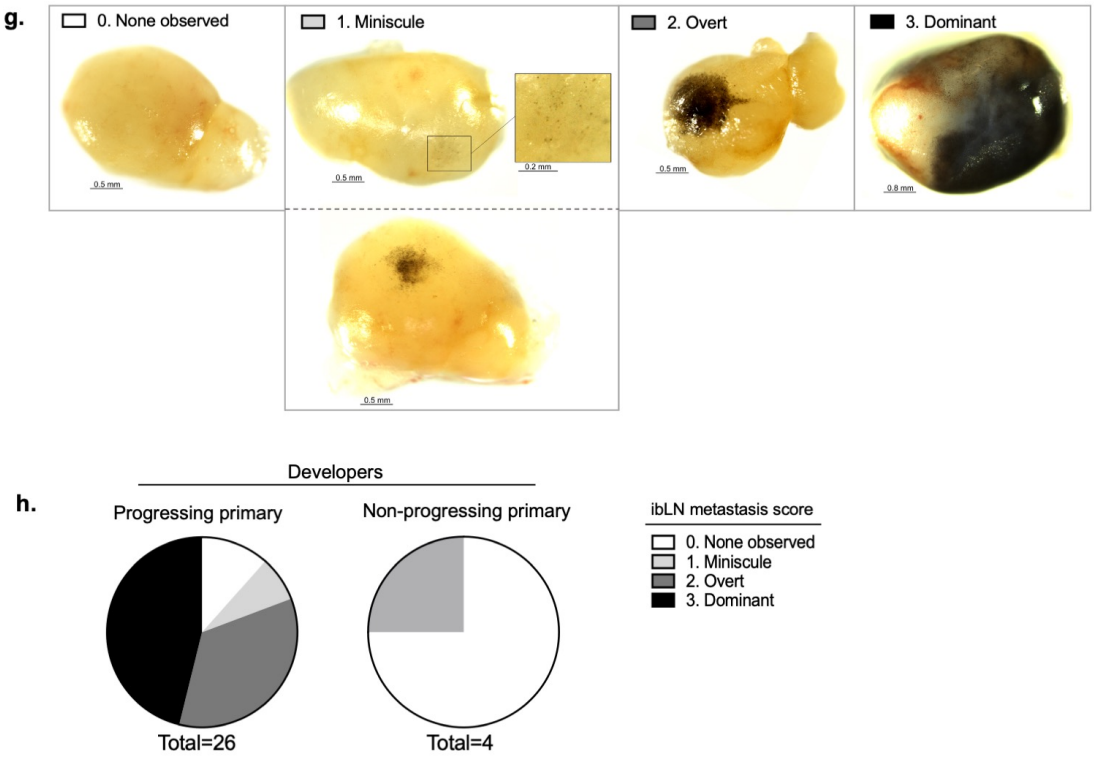

Figure 3.1. Characterisation of B16.gD growth kinetics in the epicutaneous model.

a, Primary tumor incidence and **b,** Primary tumor volumes measured with calipers in C57BL/6 mice challenged with B16.gD (1×10^5 cells), epicutaneously (e.c., n=133, 20 experiments) or subcutaneously (s.c., n=5, 1 experiment). **c,** Proportion of mice that developed primary tumors, where each point represents an individual experiment of 48 days with 5-10 mice per group. Bar shows mean tumor incidence. **d-f,** Photos and H&E staining of melanoma lesions corresponding to those labelled d-f in **(b)**. Photos taken by Dermlight camera (top panels) or by Stereo microscope camera (bottom) and H&E stain (right) of corresponding lesion taken at day (d) indicated. **g,** Examples of brachial lymph nodes from melanoma (developer) mice. Metastases scored from 0-3 based on the surface area of black pigment observed; 0 (none observed) corresponds to no observable pigment, 1 (miniscule) corresponds to pigment <0.5 mm^2, 2 (overt) corresponds to pigment 0.5-1.5 mm^2, 3 (dominant) corresponds to pigment >1.5 mm^2. **h,** Incidence of ibLN metastasis observed by eye in mice with progressively growing primary B16.gD tumors, assessed in tumors ranging from 20-180 mm^3 (progressing primary) or with non-progressing primary lesions, whereby lesion dimensions remained below 1 × 1 mm^2 for 45 days or more. Metastases scored 0-3 based on criteria described in **(g)**, data pooed from 8 biologicaly independent experiments.

3.2.2 *In vitro* validation that B16.gD cell lines are recognised by gDT-II cells.

An *in vitro* co-culture assay was used to confirm that B16.gD melanoma cells expressed gD and were capable of stimulating gDT-II cells through provision of cognate antigen (**Figure 3.2a**). The B16.Ova melanoma cell line that does not express glycoprotein D was used as a negative control. Melanoma cells were treated with IFNγ to induce expression of MHC-II, required for presentation of MHC-II restricted epitopes (**Figure 3.2b**). Additionally, MHC-II-expressing DCs were pulsed with melanoma cell lysates. *In vitro*-activated gDT-II cells were co-cultured with melanoma cell lines (+/- IFNγ pre-treatment) or lysate-pulsed DCs and stimulation of gDT-II cells was determined by their production of cytokines, TNFα and IFNγ.

As expected melanoma cells that were not pre-treated with IFNγ did not directly stimulate gDT-II to produce cytokines. However, gDT-II cells produced cytokines upon co-culture with IFNγ-treated B16.gD cells but not IFNγ-treated B16.Ova cells. gDT-II cells could also be stimulated by DCs which were pulsed with the cell lysate of B16.gD but not that of B16.Ova. An additional observation was that the relative percentages of TNFα and IFNγ production by gDT-II cells was greater for TNFα (**Figure 3.2c**). This assay showed that gDT-II specifically recognised gD expressed by B16.gD cells in the context of MHC-II and validated that gDT-II cells and B16.gD cells can be used to in combination to model an antigen-specific $CD4^+$ T cell response to melanoma.

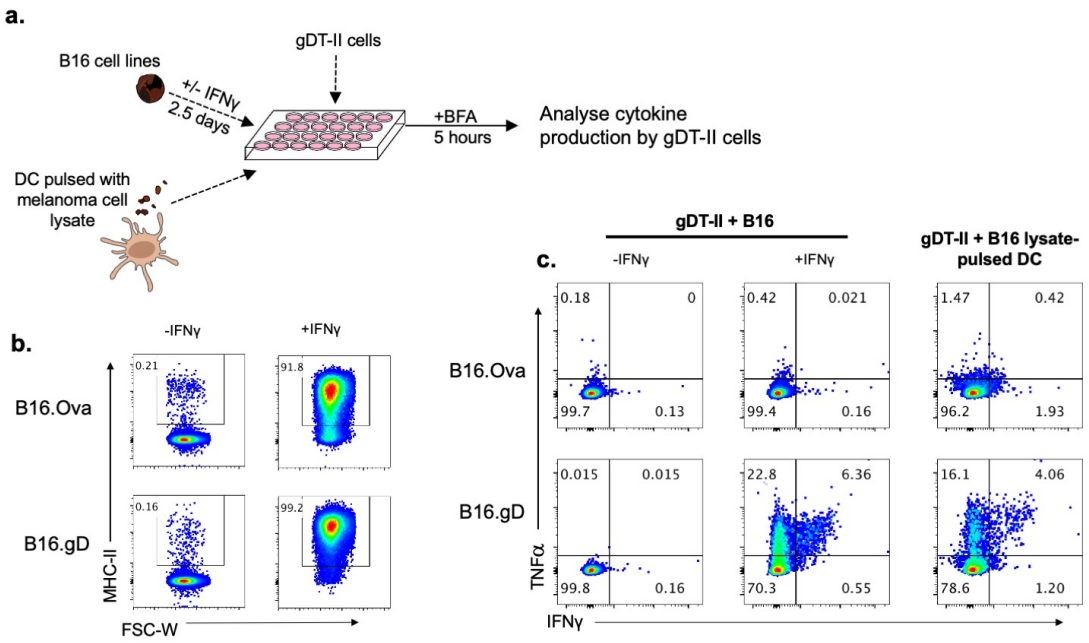

Figure 3.2. gDT-II cells are directly stimulated by B16.gD.
a, Experimental schematic of co-culture assay. **b**, MHC-II expression of B16 cell lines +/- IFNγ pre-stimulation (500 U/mL, 2.5 days) prior to co-culture with gDT-II cells. **c,** Production of IFNγ and TNFα by *in vitro*-activated gDT-II cells following 5 hours co-culture with either B16 cell lines alone (+/- pre-treatment with IFNγ) or with dendritic cells pulsed with B16 cell lysates. Data from a single experiment, representative of three individual experiments.

3.2.3 Generation and validation of B16.gD.*Ciita*$^{-/-}$ cell lines.

To address the role MHC-II expression by melanoma cells in melanoma immunosurveillance the gene *Ciita* was disrupted using a conventional CRISPR/Cas9 approach **(Figure 3.3a)**. Multiple isoforms of CIITA exist therefore sgRNA was designed to target an exon expressed in all alternatively spliced variants. Two sgRNA pairs were designed in case of potential off-target effects. The sgRNA sequences were cloned separately into the px459 plasmid which encodes the Cas9 endonuclease and a puromycin resistance cassette. The resulant vectors (px459-*Ciita* (a) or px459-*Ciita* (b)) were transfected into the B16.gD cell line and stably transfected cells that had incorporated the transgene into their genome were selected via puromycin treatment.

To test whether the gene deletion was successful, the cell lines were treated with 1000 U/mL IFNγ for three days, conditions previously established to upregulate MHC-II in 100 % of the parental B16.gD cell line**.** In contrast to the control px459 vector, both px459-*Ciita* (a) and px459-*Ciita* (b) appeared to successfully disrupt *Ciita* as a proportion of the transfected cells were unable to express MHC-II in response to IFNγ stimulation. Transfection with px459-*Ciita* (b) was more effective in producing a higher proportion of cells with a functional deletion of *Ciita* compared to px459-*Ciita* (a) at frequencies of 76 % and 25 % respectively (**Figure 3.3b**). To further enrich the proportion of gene-disrupted cells in the polyclonal cultures, MHC-II-negative cells were enriched by flow cytometry sorting following IFNγ treatment. Enrichment yielded frequencies of 94 % and 83 % of cells that were not capable of expressing MHC-II in response to IFNγ treatment in the polyclonal cultures generated by px459-*Ciita* (b) and px459-*Ciita* (a), respectively **(Figure 3.3c).** Enriched B16.gD.*Ciita*$^{-/-}$(b) (henceforth referred to as B16.gD.*Ciita*$^{-/-}$) thus appeared to have a higher frequency of *Ciita* gene deletion (94 %) and was selected for use in subsequent experiments. To generate an appropriate control cell line for downstream applications the parental line was transfected with a Px459 (empty) vector lacking the guide RNA sequences. These control-transfected cells were also treated with the same

conditions of puromycin and IFNγ, and then enriched by flow cytometry sorting on GFP$^+$MHC-II$^+$ cells. Of note, the absence of *Ciita* did not prevent IFNγ-induced expression of MHC-I, thereby confirming B16.gD.*Ciita*$^{-/-}$ cells were still responsive to IFNγ (**Figure 3.3d**)

In a next step, variants of B16.gD.*Ciita*$^{-/-}$ and parental control B16.gD cell lines were generated which expressed the fluorochrome mCherry. The cells were retrovirally transduced with a plasmid containing the mCherry construct under the CMV promotor (pRP-mCherry) and transduced cells were enriched by flow cytometry sorting on GFP$^+$mCherry$^+$ cells **(Figure 3.3e)**. Control cell lines were generated by transduction with the empty control plasmid (pRP-empty) and sorting on GFP$^+$ cells. Analysis of IFNγ stimulated cells by flow cytometry indicated that frequencies of successful gene targeting ranged between 94-97 % and that mCherry expression was greater than 98 % in both the B16.gD.*Ciita*$^{-/-}$.mCherry and the B16.gD.mCherry cell lines **(Figure 3.3f)**.

Previously it was shown in an *in vitro* co-culture assay that B16.gD cells pre-treated with IFNγ, but not untreated cells, upregulated MHC-II and were capable of stimulating gDT-II cell directly **(Figure 3.2c).** The *in vitro* co-culture assay was repeated using B16.gD.*Ciita*$^{-/-}$ cells to confirm that the functional deletion of *Ciita* prevented direct presentation of cognate antigen to gDT-II cells **(Figure 3.3g)**. Indeed, IFNγ-stimulated B16.gD.*Ciita*$^{-/-}$ cells failed to stimulate the gDT-II cells to produce TNFα or IFNγ. Pulsing bone-marrow derived DCs with the B16.gD.*Ciita*$^{-/-}$ cell lysate stimulated gDT-II cells confirming that the gD peptide was produced in this cell line and could be indirectly presented to gDT-II cells by APCs.

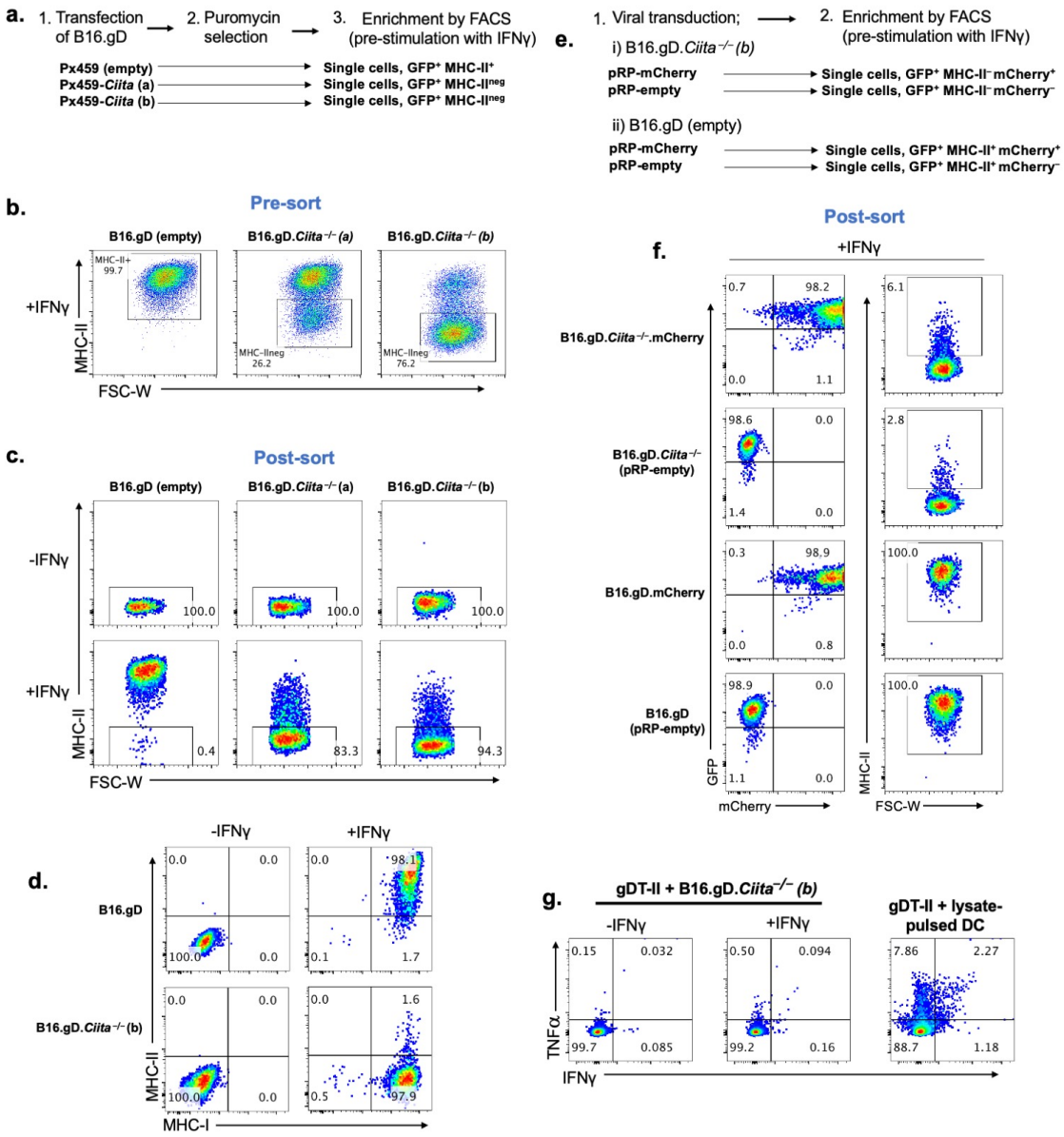

Figure 3.3. Generation of polyclonal B16.gD.*Ciita*$^{-/-}$ cell lines.
a, Workflow for the generation and enrichment of B16.gD.*Ciita*$^{-/-}$ cell lines. Transfection vectors and respective sorting gates used for enriching cell lines by flow cytometry shown in bold. **b,** MHC-II expression upon stimulation with IFNγ (1000 U/mL, 3 days) of cells following transfection and puromycin selection (pre-sort). Gates on FACS plots depict the gates used for sorting. **c,** MHC-II expression with or without IFNγ treatment (1000 U/mL, 3 days) of sorted cell lines from **(b)**. **d,** Analysis of MHC-I and MHC-II expression of cells by FACS with or without IFNγ stimulation (1000 U/mL, 3 days) **e,** Workflow for the generation and enrichment of a polyclonal B16.gD.*Ciita*$^{-/-}$.mCherry cell line (and controls) using cells generated in **(c)** as parental cell lines. Retroviral vectors and respective gates used for enriching cell lines by flow cytometry sorting shown in bold. **f,** mCherry and GFP expression (left column) and MHC-II expression (right column) following IFNγ stimulation (1000 U/mL, 3 days) of cell lines generated by method

described in **(e)**. **g,** Production of IFNγ and TNFα by *in vitro*-activated gDT-II cells following 5 hours co-culture with either B16.gD.*Ciita*$^{-/-}$ cells (+/- pre-treatment with IFNγ) or with dendritic cells pulsed with B16.gD.*Ciita*$^{-/-}$ cell lysates.

3.2.4 Generation of the B16.gD.*Tnfr1*$^{-/-}$ cell line.

TNFα initiates intracellular signalling through binding to its receptors, TNFR1 or TNFR2. To determine the role of TNFα signalling in melanoma CRISPR/Cas9 was used to disrupt *Tnfr1* and *Tnfr2* in B16.gD cells. These cells could be used in combination with gDT-II cells in the epicutaneous melanoma model to determine whether TNFα is a requirement for melanoma immunosurveillance by $CD4^+$ T cells.

Although it is well established that B16 cells respond to TNFα (Kearney et al., 2018, Boecke et al., 2013), expression of neither TNFR1 nor TNFR2 on the cell surface of B16.gD cells could be detected by flow cytometry (data not shown). Since TNFR1-signalling has been documented in melanoma cells, the inability to detect this receptor by flow cytometry was most likely because its protein expression was below the limit of detection by currently available antibodies. This prevented the use of flow cytometry to validate and to enrich cells with successful TNF receptor gene disruption.

Instead, a cytokine treatment strategy was devised to enrich for cells that harboured disrupted TNF receptor genes. This strategy exploited the phenomenom of TNF-induced cell death, as cells with defective TNF-receptors would be resistant to TNF signalling. Cells in which the TNF receptor genes were not successfully disrupted following transfection would be sensitive to TNF-signalling and thus could be eliminated from the culture under conditions that initiate TNF-induced apoptosis.

TNF signalling can have diverse outcomes within a cell, and the capacity for TNFα to induce cell death can depend on the presence of other environmental factors (Habtetsion et al., 2018, Nishida et al., 2003). Treatment of B16.gD cells with TNFα alone (1000 U/mL) did not result in cell death (**Figure 3.4a**, **b)** consistent with a previous study that showed B16 cells were resistant to TNF-induced apoptosis unless pre-treated with a PKC inhibitor (Nishida et al., 2003).

IFNγ has been shown to cooperate with TNFα to induce death in different cell types (Kim et al., 2005a, Kim et al., 2005b). To test whether IFNγ could sensitise B16.gD cells to TNF-induced apoptosis IFNγ and TNFα were titrated into cultures of wild-type B16.gD cells. Cell death was observed in the B16.gD cell culture treated for 72 hours with a combination of TNFα (1000 U/mL) and IFNγ (50 or 500 U/mL) by microscopy. Accordingly, combined cytokine treatment resulted in the presence of a substantial amount of cellular debris and any remaining cells in these wells were rounded and formed clumps (**Figure 3.4a**), consistent with morpological features of cell death (Ziegler and Groscurth, 2004). Counting the cells by flow cytometry confirmed that co-treatment resulted in a reduction in the number of propidium iodide-negative B16.gD cells in the plate by more than 90 % compared to untreated cells after 72 hours (**Figure 3.4b**). IFNγ treatment alone resulted in a 45-55 % reduction in cell numbers, using 50 or 500 U/mL IFNγ, respectively, relative to the untreated control cells after 72 hours. This reduced cell number could be a combination of retarded cell growth and increased cell death. The relative contributions of either process cannot be fully discerned by microscopy as there was a combination of cells with normal morphology but also some rounding and clumping, particularly in the group treated with higher concentration of IFNγ (500 U/mL). Regardless, compared to TNFα and IFNγ co-treatment, IFNγ treatment alone induced substantially less cell death after 72 hours. These results provided evidence that IFNγ and TNFα co-treatment could be implemented as a strategy to enrich cells with deletion of TNF receptor genes.

A conventional CRISPR/Cas9 approach was used to disrupt the TNF receptor genes in B16.gD cells (**Figure 3.4c**). Two sgRNA pairs were designed for each gene in case of potential off-target effects. The sgRNA sequences were cloned into the Px459 plasmid which encodes the Cas9 endonuclease and a puromycin resistance cassette. The vectors were transfected into the B16.gD cell line and stably transfected cells were selected for via puromycin. Cytokine enrichment was carried out using previously optimised conditions of TNFα (1000 U/mL) and IFNγ (500 U/mL). Four days following combined cytokine treatment

there was less cell death in the B16.gD.*Tnfr1*$^{-/-}$ cell lines compared to the parental B16.gD cell line, which served as initial evidence that a proportion of cells were deficient in TNFR1-signalling **(Figure 3.4d)**. Treatment was continued for 6 days by which time all the control-transfected cells (cells transfected with Px459 (empty)) that had been co-treated with TNFα and IFNγ were dead. Cytokine-treated cells that had been transfected with Px459-*Tnfr2* (a) showed an equivalent amount of cell death upon microscopic examination when compared to the B16.gD parental line. Whether B16.gD expresses TNFR2 was not determined, however neither the encoding mRNA or protein was detected in RT-qPCR or in Western blot, respectively, (data not shown).

IFNγ can have broad effects on cells and epigenetic changes can be carried into future generations. To control for exposure of B16.gD.*Tnfr1*$^{-/-}$ cells to IFNγ, a control cell line was generated by transfection of B16.gD with Px459 (empty) and treated with IFNγ alone.

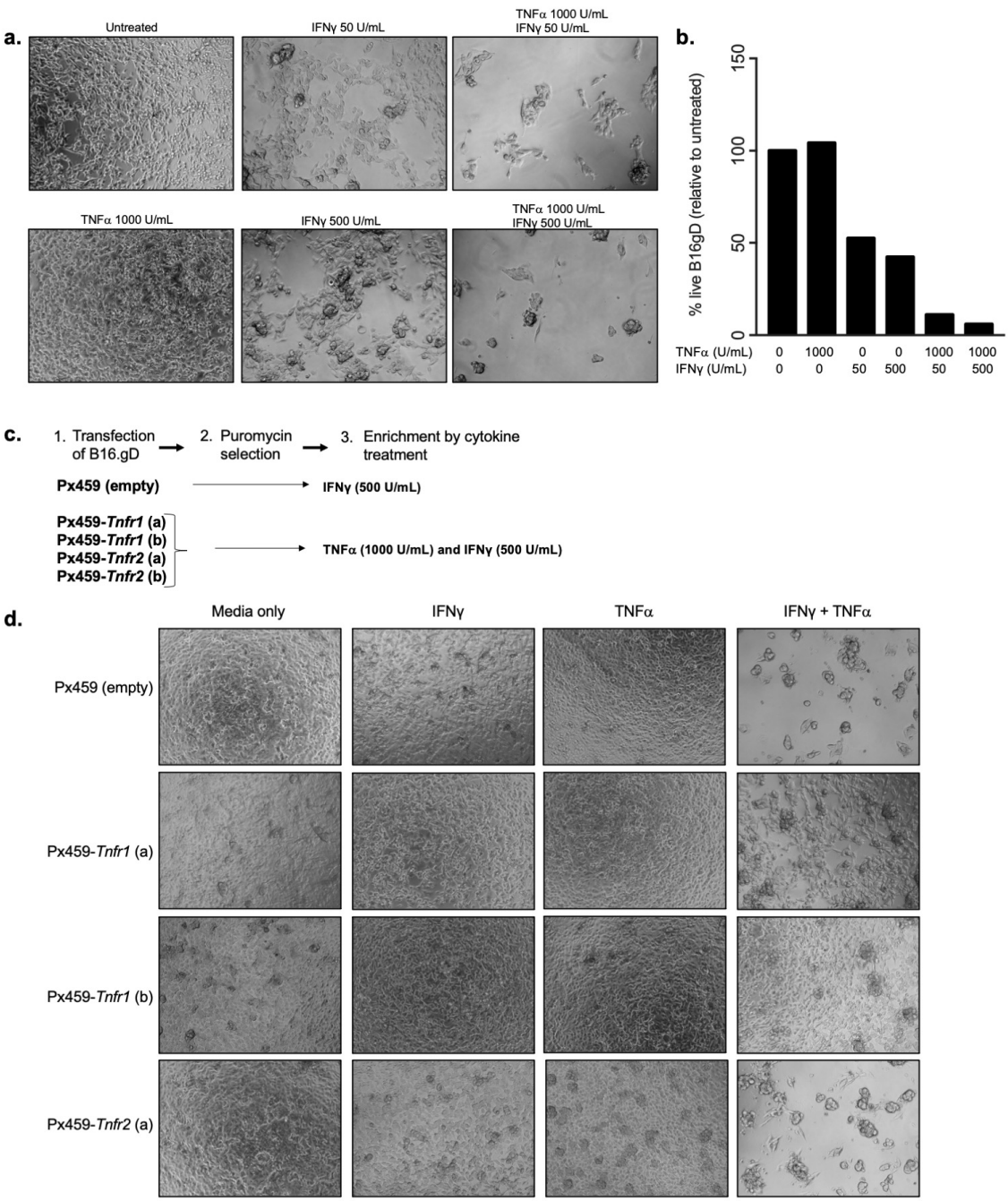

Figure 3.4 Generation of polyclonal B16.gD.Tnfr1$^{-/-}$ cell lines.

a, b, Analysis of cell death in B16.gD cells culture in the presence of indicated cytokines to optimise enrichment strategy for the generation of B16.gD.*Tnfr1*$^{-/-}$ cells. B16.gD cells treated with murine IFNγ and TNFα at concentrations indicated for 72 hours. **a**, Photos and **b,** cell death quantified by flow cytometry (number of DAPI^{neg} GFP^{+} cells) following cytokine treatment. Treatment groups normalised as percent of the number of untreated cells. Data are mean of duplicates from one experiment. **c-d,** Generation and enrichment of B16.gD.*Tnfr1*$^{-/-}$ and control cell lines. **c,** Schematic of experimental protocol; Transfection vectors and respective cytokine treatment conditions for enrichment

listed in bold. **d**, Photos of transfected cells on day 4 of cytokine treatment**.** Cell lines were treated with media only, or media containing cytokines, (1000 U/mL TNFα, 500 U/mL IFNγ) alone or in combination.

3.2.5 Validation of the B16.gD.*Tnfr1*$^{-/-}$ cell line

Experiments were carried out to validate successful deletion of *Tnfr1* in the two enriched B16.gD.*Tnfr1*$^{-/-}$ cell lines generated by different sgRNAs. To do this, melanoma cells were treated with TNFα and components of the downstream TNFR1-signalling pathway were examined. RNA sequencing analysis previously carried out in the Hölzel laboratory identified that, in response to 18 hours TNFα exposure, transcription of *Ccl2*, *Ccl5* and *Vcam* were substantially upregulated (> 5 Log 2 fold change) in B16 cells. Accordingly, mRNA expression of these genes was upregulated in response to 18 hour-TNFα treatment in the control B16.gD cell line **(Figure 3.5 a)**. In contrast, in the B16.gD.*Tnfr1*$^{-/-}$ cell lines neither *Ccl2* nor *Vcam* mRNA expression was detected after treatment with TNFα. *Ccl5* mRNA transcripts could be detected in all cell lines at baseline. Following TNFα treatment there was a robust increase in CCL5 mRNA expression in the wild-type cells, but no changes in *Ccl5* mRNA expression in the B16.gD.*Tnfr1*$^{-/-}$ cultures. The changes in mRNA expression of the TNF response genes in the wild-type B16.gD cell line, but not in the B16.gD.*Tnfr1*$^{-/-}$ cell lines, provided functional evidence for impaired TNFR1-signalling and successful genetic targeting and deletion.

Tnfr1 mRNA expression was also analysed and transcripts were expressed at lower levels in the B16.gD.*Tnfr1*$^{-/-}$ cell lines compared to the parental line. mRNA expression level of *Tnfr1* cannot be used as a measure of gene deletion frequency, because mRNA can still be transcribed from genes which have been disrupted by the insertion or deletion of DNA base pairs. A possible reason for which there may be a reduction of *Tnfr1* mRNA expression in the B16.gD.*Tnfr1*$^{-/-}$ cell lines compared to the control cell line, is that non-functional mRNA that harbors a premature stop codon can be quickly degraded through cell intrinsic mechanisms, a phenomenon known as nonsense-mediated decay (Brogna and Wen, 2009).

No difference in growth kinetics nor in functional impairment of TNF-

signalling, as assessed in qPCR, was observed between the B16.gD.*Tnfr1*$^{-/-}$ cell lines generated by Px459-*Tnfr1* (a) or Px459-*Tnfr1* (b). The B16.gD.*Tnfr1*$^{-/-}$*(b)* cell line (henceforth referred to as B16.gD.*Tnfr1*$^{-/-}$) was selected for use in subsequent experiments. Next Generation Sequencing (NGS) using the MiSeq illumina platform was carried out to confirm that *Tnfr1* was disrupted on the genomic level and to determine the indel frequency of *Tnfr1* in the final enriched polyclonal culture. (**Figure 3.5 b**). As expected, the control cell line had greater than 99 % wild-type reads at the site in the *Tnfr1* gene targeted by Px459-*Tnfr1* (b). Conversely, 91.4 % of B16.gD.*Tnfr1*$^{-/-}$ cells harboured DNA indels at the Px459-*Tnfr1* (b) target sequence, the majority of indels were out-of-frame. It can be assumed that cells harbouring these frame-shift mutations would not be capable of generating a functional protein as translation of the original sequence would be disrupted. A small fraction of cells harboured in-frame indels (indels of triplets) and therefore could possibly produce a functional protein with a slight change in structure due to the addition or deletion of a single or few amino acids. The allele frequency of wild-type reads (unmutated sequences) was 6 %.

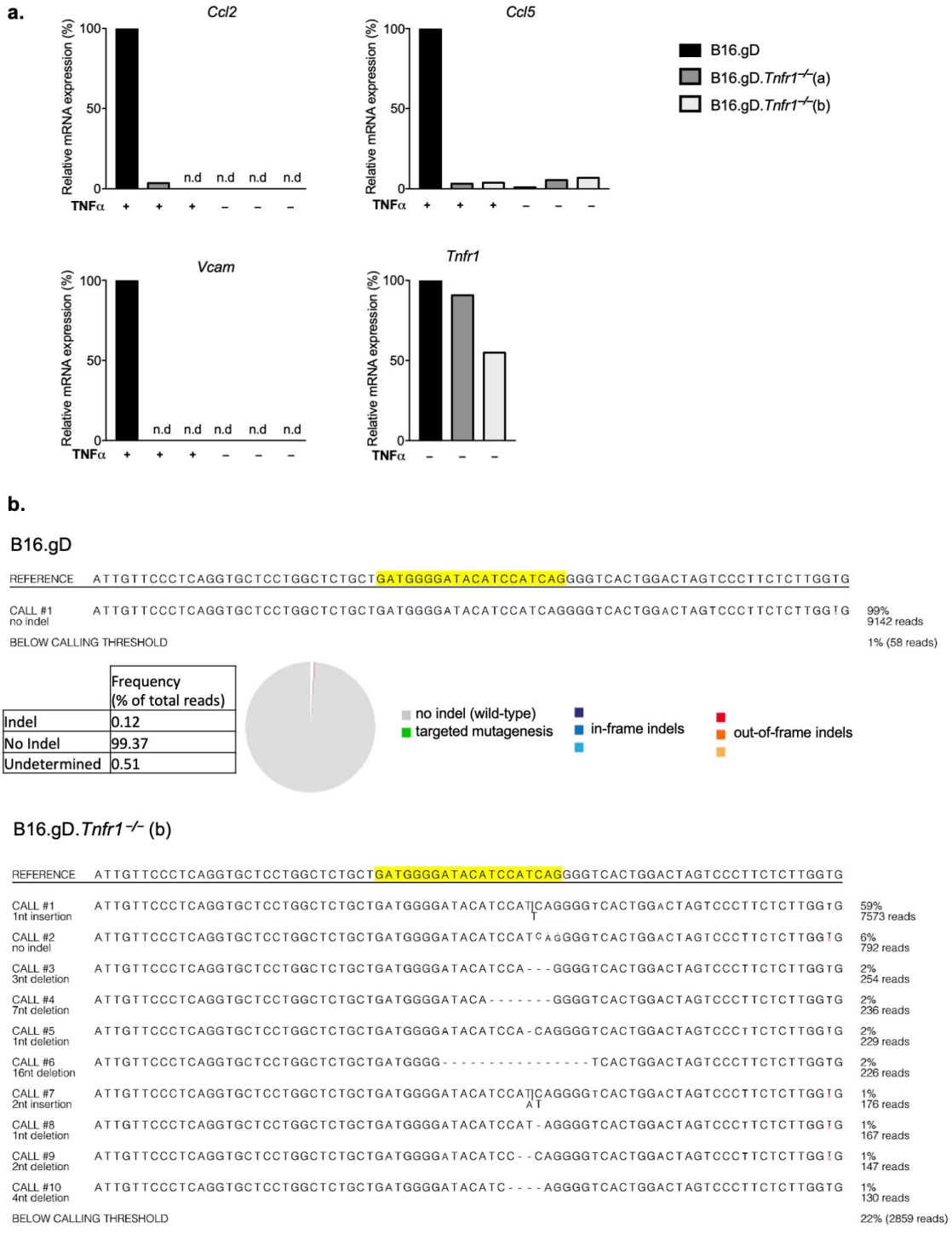

Figure 3.5. Functional validation of B16.gD.*Tnfr1*$^{-/-}$ cell lines by analysis of TNFR1-signalling molecules.

Analysis of B16.gD.*Tnfr1*$^{-/-}$ (a) and B16.gD.*Tnfr1*$^{-/-}$ (b) (enriched by TNF/IFNγ treatment) and B16.gD control cells. Data from a single analysis. **a,** qRT-PCR

analysis of *Ccl2*, *Vcam*, *Ccl5* and *Tnfr1* 18 hours after TNFα treatment (1000 U/mL). Relative mRNA expression was calculated as fold change ($2^{-\Delta\Delta Ct}$), normalized to GAPDH. n.d indicates no transcript detected. **b,** Analysis of *Tnfr1* gene insertion/deletion (indel) frequency in the enriched B16.gD.*Tnfr1*$^{-/-}$ (b) cell line by Next Generation Sequencing (NGS) using the Illumina MiSeq platform. Reference sequence contains region of *Tnfr1* gene complementary to sgRNA encoded in Px459-*Tnfr1* (b) (highlight in yellow). Frequency of indels shown in table and depicted in pie charts with different types of indels categorized by color as indicated in key. NGS data were analyzed using the web tool Outknocker 3.0 alignment tool.

3.2.6 Generation of the B16.gD.MHC-II-mScarlet cell line.

Reporter systems are useful tools for tracking expression of a gene of interest. A reporter gene encodes a protein, such as a fluorescent molecule, whose expression is easily monitored by microscopy and flow cytometry. Generally, a reporter gene would insert downstream of a gene of interest and be transcribed independently. Therefore, its expression acts as a surrogate marker for transcription of the gene of interest. An advancement on reporter systems is the generation of fusion molecules between the protein of interest and the reporter protein. This enables tracking expression at the protein level, and can be used to investigate protein turnover, protein subcellular localisation and protein-protein interactions.

To generate a tool to enable tracking MHC-II expression by melanoma cells, B16.gD cells were used to generate a reporter cell line in which MHC-II was tagged with the fluorescent molecule mScarlet (B16.gD.MHC-II-mScarlet). A CRISPR/Cas9 based approach called CRISPR-assisted insertion tagging (CRISPaint), first described by Schmid-Burgk *et al* (Schmid-Burgk et al., 2016), was used. CRISPaint is a modular cloning approach which involves the transfection of cells with three plasmids. The first plasmid, the target selector, contains sgRNA targeting the sequence immediately upstream of the stop codon of the gene of interest, where a double stranded break (DSB) is introduced by the Cas9 endonuclease also encoded in the first plasmid. The second plasmid, the frame selector, ensures that the third plasmid, the universal donor, is cut in frame for insertion at the DSB. The universal donor encodes the gene for a fluorescent marker resulting in the generation of a fluorescently tagged gene product within the transfected cells. The universal donor also encodes a FLAG-tag and an antibiotic resistant cassette (**Figure 3.6a**).

Following CRISPaint transfection, selection and enrichment were carried out by puromycin treatment and flow cytometry, respectively (**Figure 3.6b**). The initial tagging efficiency was approximately 4 % which was assessed by mScarlet

and MHC-II co-expression following treatment with IFNγ (1000 U/mL, 3 days) (**Figure 3.6c**). The low tagging efficiency was not particularly surprising considering that MHC-II is not expressed by B16.gD cells under basal conditions, and therefore the DNA for the encoding gene, *H2-Aβ,* was probably condensed and not easily accessible to the CRISPaint plasmids. mScarlet^{+} cells were sorted by flow cytometry following IFNγ treatment and the resultant polyclonal cell line had a tagging frequency of approximately 95 %. Results from flow cytometry suggest that there is high specificity of tagging because less than 1 % of cells expressed mScarlet in the absence of MHC-II expression (**Figure 3.6d**).

To test whether fusion of mScarlet to MHC-II would impair presentation of the gD epitope to gDT-II cells an *in vitro* co-culture assay was carried out as described in **Figure 3.2**. IFNγ-pre-stimulated, but not unstimulated, B16.gD.MHC-II-mScarlet cells were able to stimulate gDT-II cells indicating that MHC-II was functional (**Figure 3.6e**).

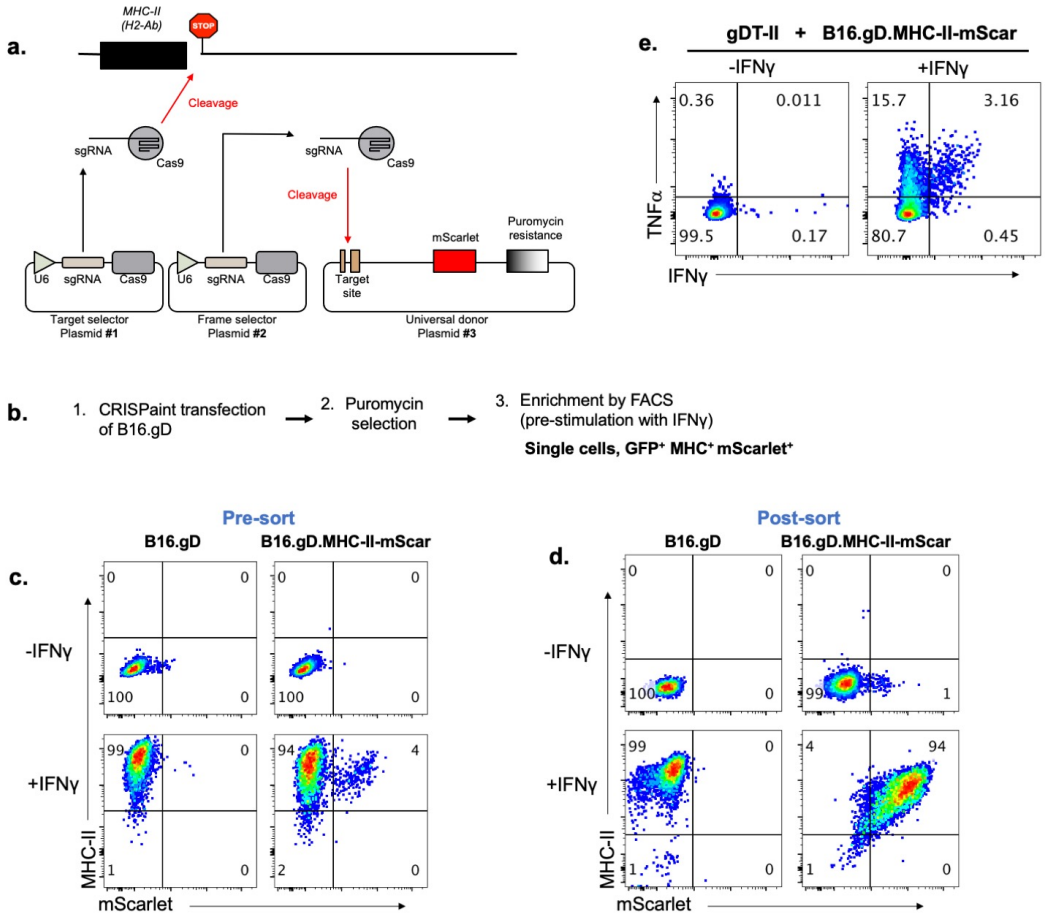

Figure 3.6. Generation of B16.gD.MHC-II-mScarlet reporter cell line using CRISPaint.

a, Diagrammatical representation of the CRISPaint technology (Schmid-Burgk et al., 2016) used to tag MHC-II with mScarlet. *Figure adapted from Maike Effern (Holzel laboratory, the University of Bonn).* **b,** Schematic of experimental protocol for generation and enrichment of B16.gD.MHC-II-mScarlet cells. Gates used to enrich tagged cells by flow cytometry shown in bold. **c, d,** MHC-II and mScarlet expression analysed by flow cytometry with or without IFNγ treatment (1000 U/mL 3 days) **c,** prior enrichment and **d,** post enrichment. **e,** Production of IFNγ and TNFα by *in vitro*-activated gDT-II cells following 5 hours co-culture with B16.gD.MHC-II-mScar cells (+/- pre-treatment with IFNγ).

3.2.7 Generation and validation of the B16.gD.Luciferase-mScarlet cell line.

The epicutaneous melanoma model has the advantage that tumors originate within the outer layers of skin facilitating visual monitoring of tumor growth kinetics. However, visual monitoring comes with the limitations that low numbers of melanoma cells within the skin may not be detectable by eye and that tumor depth and metastatic spread can also not be measured longitudinally. *In vivo* bioluminescence imaging can circumvent these limitations through sensitive and semi-quantitative detection of luciferase-expressing melanoma cells. Luciferase is an enzyme that oxidises luciferin, generating photons of light as a product of the reaction. These photons can be detected by a high-sensitivity camera which displays the signals as pixels on a photo, at the site in which bioluminescence is detected. To make use of bioluminescent imaging technology, B16.gD cells were retrovirally transduced with a plasmid encoding the Firefly luciferase gene (**Figure 3.7a**). This plasmid also encodes the gene for the fluorophore mScarlet, allowing for enrichment of successfully transduced cells by flow cytometry. Following enrichment, the polyclonal B16.gD.Luciferase-mScarlet (B16.gD.Luc-mScar) cell line had a purity of 99 % transduced cells, as determined by percent of mScarlet-expressing cells (**Figure 3.7b**). To test whether the luciferase enzyme was functional within these cells they were titrated *in vitro* and their production of bioluminescence was analysed upon addition of luciferin (**Figure 3.7c**). As expected, the magnitude of the bioluminescence signal correlated to the number of cells in the wells. Signal was detectable in the well with the lowest cell number (~31 cells) but not detectable in the absence of the cells.

The B16.gD.Luc-mScar cell line was tested *in vivo* in the epicutaneous melanoma model and bioluminescence was frequently observed at the primary skin inoculation site and also at the tumor-draining lymph node (**Figure 3.7d**). In general, the size of melanomas at the primary site, as observed using a

dermoscopy camera, correlated to the strength of bioluminescence signal however this was not strictly the case. Additionally, a bioluminescence signal at the primary site occasionally was detected in the absence of a lesion observed by the dermoscopy camera. Whilst a direct correlation between luminescence counts and cell number was observed *in vitro*, there are many factors besides the exact cell number, which may impact the strength of the bioluminescence signal *in vivo*. This could include the distribution of cells, the cells' availability to luciferin in the bloodstream, the cells‘ metabolism and affects of the local microenvironment. Overall the B16.gD.Luc-mScar cell line showed strong bioluminescence production in the epicutaneous model validating them for use in longitudinal monitoring experiments.

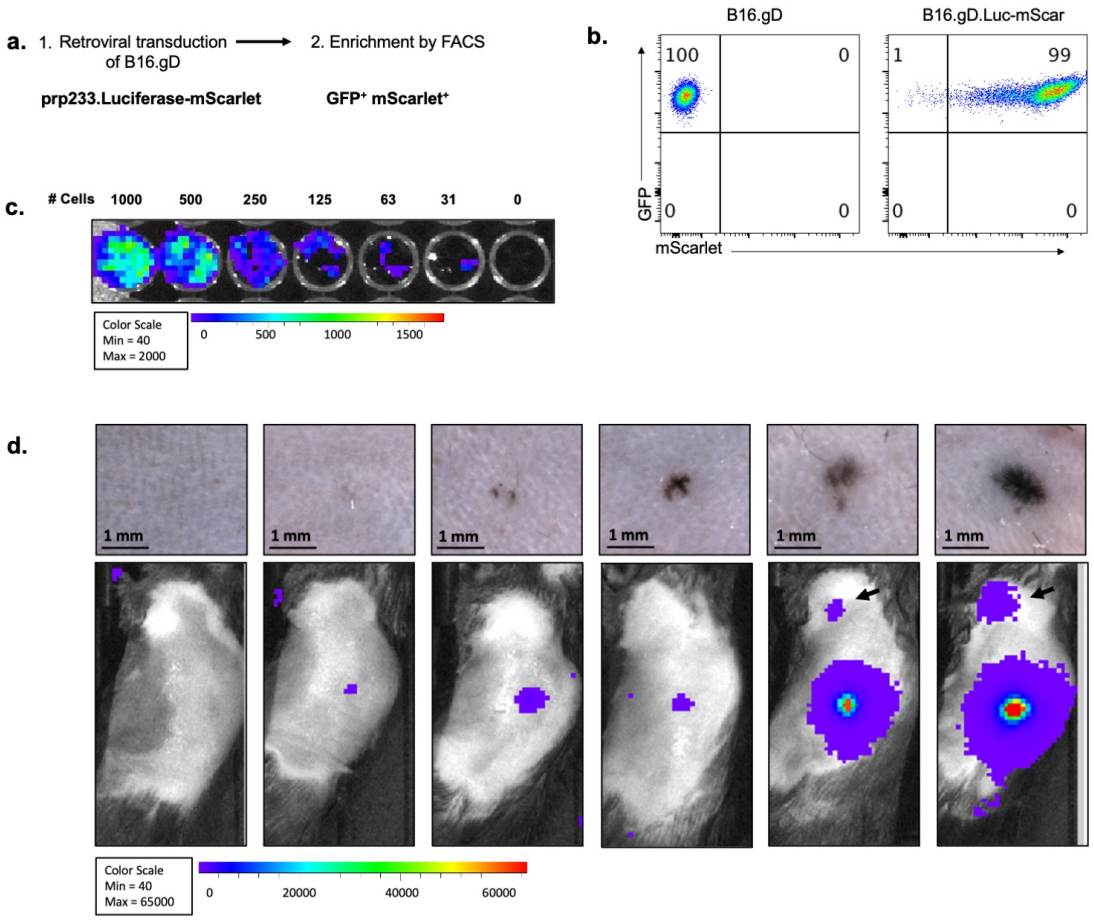

Figure 3.7. Generation of the B16.gD.Luciferase-mScarlet line.
a, Workflow for the generation and enrichment of B16.gD.Luciferase-mScarlet (B16.gD.Luc-mScar) cells. Plasmid used for retroviral transduction and gates for enrichment by flow cytometry listed in bold. **b,** GFP and mScarlet expression of the B16.gD parental cell line and the enriched B16.gD.Luc-mScar cell line. **c,** *In vitro* validation of bioluminescence signals from B16.gD.Luc-mScar. B16.gD.Luc-mScar plated at cell numbers indicated and bioluminescence measured using an in vivo imaging system (IVIS) following administration of luciferin (75 μg/mL). **d,** Examples of 5 wild-type C57BL/6 mice inoculated with B16.gD.Luc-mScar cells (1×10^5 e.c.) and analysed at day 11 post-inoculation. Top; Photos of the mouse flank at the site of inoculation taken with dermoscopy camera camera. Bottom; corresponding bioluminescence signals measured by IVIS. *IVIS imaging performed by David Freestone.*

3.2.8 Characterisation of B16.gD.Luciferase-mScarlet cells in the epicutaneous melanoma model.

B16.gD.Luc-mScar cells were characterised in the epicutaneous melanoma model using C57BL/6 mice and radiance of bioluminescence signals were monitored by in vivo imaging system (IVIS) (**Figure 3.8a**). Of note, the incidence of tumor development was lower using the B16.gD.Luc-mScar cell line compared to the parental B16.gD cell line (**Figure 3.8b, Figure 3.1a**), although data are comprised from only seventeen mice challenged with B16.gD.Luc-mScar and additional experiments would be required to confirm this difference.

Four days following melanoma challenge 94 % (16/17) of mice presented with a bioluminescence signal at the site of the inoculation, indicating that grafting of the cells was successful (**Figure 3.8a**). The radiance of the signal at the inoculation site decreased or was lost completely in 75 % (12/16) of mice by day 11. For most mice that lost the primary signal, once the signal disappeared it could not be detected again at a later time point. However, there was recurrence of bioluminescent signal at the primary site in 3/12 mice that did not develop a progressively growing tumor. The radiance of this signal was low, consistent with the fact that melanoma cells could not be observed by eye. It cannot be definitely concluded that the signal corresponded to the presence of B16.gD.Luc-mScar cells as there was a low level of background luminescence which could lead to false positive signals. A signal that occurs repeatedly at the same location provides more robust evidence that the melanoma cells are the true source of luminescence hence weekly monitoring by IVIS was carried out. Of the seventeen C57BL/6 mice monitored by IVIS, only one macroscopically tumor-free mouse that had a recurring signal on two consecutive weeks was identified (**Figure 3.8e**).

In half of the mice challenged epicutaneously with B16.gD.Luc-mScar a signal in the tumor-draining lymph node could be detected on day four p.i.. This

was a higher frequency of early dissemination to the brachial lymph node than previously observed using luciferase-expressing B16-F1 lines (data not shown). A particularly interesting observation was that none (0/8) of the mice which presented with a signal at the brachial lymph node on day 4 p.i. developed a progressively growing tumor (**Figure 3.8 d-g**). On the other hand, half (4/8) of the mice that had a signal at the primary site but not at the brachial lymph on day four p.i. developed a progressively growing tumour (**Figure 3.8 c, f, g**). The appearance of brachial lymph node metastasis occurred later in mice with progressing tumors and did not appear to impede primary tumor growth.

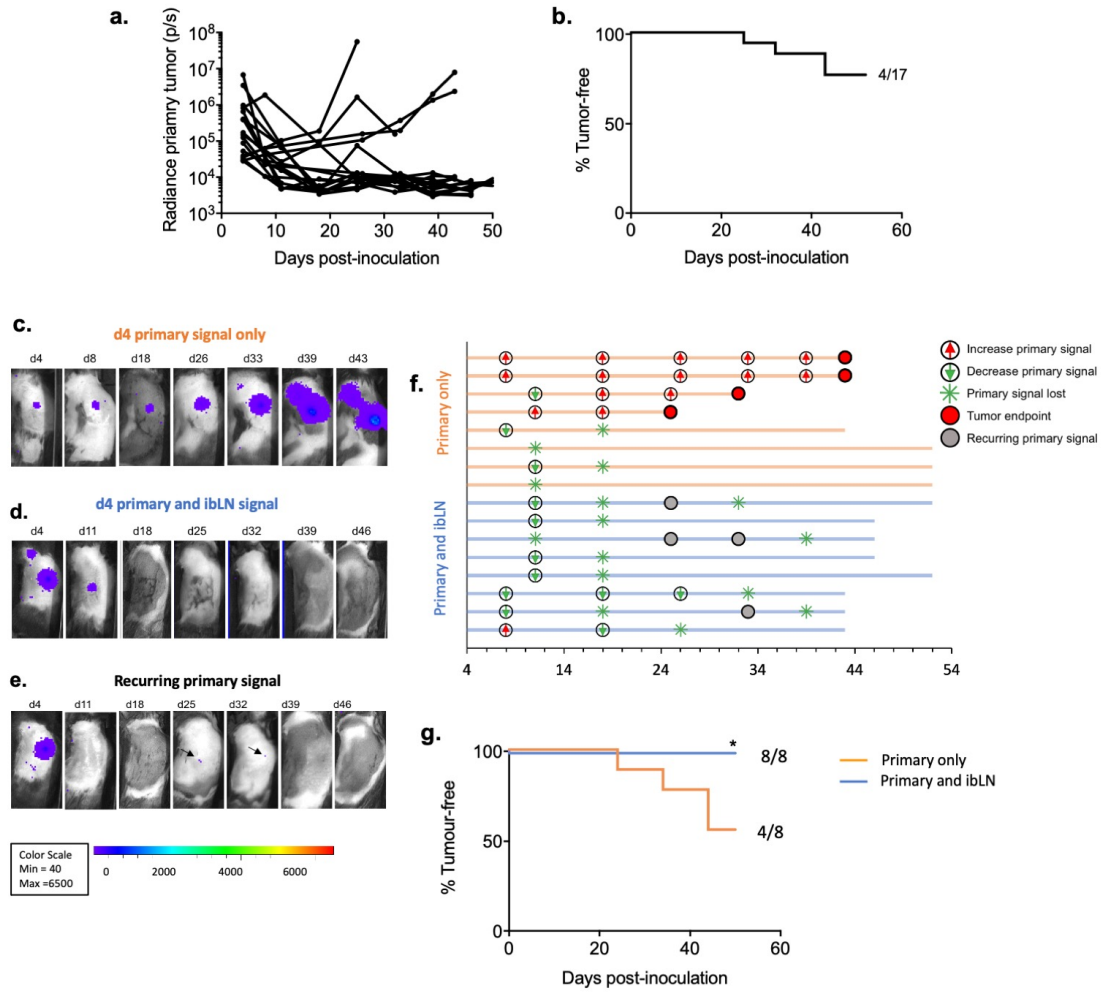

Figure 3.8. Characterisation of B16.gD.Luc-mScar growth kinetics in the epicutaneous melanoma model using In Vivo Imaging Software.
C57BL/6 mice were inoculated with 1 × 10^5 B16.gD.Luc-mScar (e.c.) and monitored on days (d) indicated for bioluminescence signal using In Vivo Imaging Software (IVIS). **a,** Bioluminescence signals measured at site of tumor inoculation and calculated as total flux (Radiance, photons/second, p/s). **b,** Proportion of mice that did not develop a progressing primary tumor. **c-e,** Representative photos of bioluminescence monitoring for individual mice over time. **c,** Mouse presenting with bioluminescence signal at primary site (site of tumor inoculation) but not at the ibLN at day 4 p.i. **d,** Mouse presenting with bioluminescence signal at primary site and at the ibLN on day 4 p.i. **e,** Mouse with recurring bioluminescence signal at primary site, indicated by black arrows**. f,** Swimmer plot depicting progression of bioluminescence signals in C57BL/6 mice stratified by the presence of primary and ibLN signal (blue) or only primary signal (orange) on day 4 p.i. detected by IVIS, where each horizontal line represents an individual mouse **g.** Incidence of mice developing tumors stratified by the presence of primary and ibLN signal (blue) or only primary signal (orange) on day 4 p.i. detected by IVIS. **f, g**, n=16, pooled from 3 biologically independent experiments.

3.2.9 Fusion of CD4$^+$ T cell epitopes to endogenous gene products using CRISPitope.

It is not currently well understood how variations in antigen biology such as expression level or subcellular localisation effect CD4$^+$ T cell responses. To generate tools to address this question, the gene-editing platform CRISPR-assisted insertion of epitopes (CRISPitope) (Effern et al., 2020) was used to engineer cell lines in which defined epitopes recognised by transgenic CD4$^+$ T cell were fused to the C-termini of different endogenous gene products. The CRISPitope platform was successfully applied previously in the Hölzel laboratory to tag proteins with epitopes recognised by CD8$^+$ transgenic T cells. However, due to differences in the pathways of endogenous peptide processing for loading onto MHC-II and MHC-I, it remained to be established whether this technology could also be applied using CD4$^+$ T cells epitopes.

CRISPitope was adapted from the CRISPaint platform developed by Schmid-Burgk *et al.* as previously described (Schmid-Burgk et al., 2016) and similarly follows a 3-plasmid transfection protocol (**Figure 3.9a**). The target selector plasmids, which encodes the protein to be tagged, can be used interchangeably between the CRISpaint and CRISpitope system. What makes CRISPitope different from CRISPaint is that the universal donor plasmid encodes an epitope sequence adjacent to the FLAG-tag and the gene encoding a fluorescent protein (mNeon or mScarlet). Therefore, a fusion protein is generated between the gene product (encoded in the target selector plasmid), the epitope sequence, FLAG-tag and fluorescent marker. Of note, the antibiotics resistance gene (puromycin or blatocidin) encoded in the universal donor plasmid to enable selection of transfected cells is separated from the epitope sequence by a T2A cleavage sequence and thus would be expressed independently of the fusion protein.

To generate B16 cells expressing CD4$^+$ T cell epitopes using the CRISPitope platform, universal donor plasmids were engineered to encode the

epitope sequences of gD and ovalbumin that are specific for transgenic gDT-II and OT-II cells, respectively (**Figure 3.9b**). CRISPitope constructs encoding the minimal epitope sequences as well as the minimal sequence plus additional flanking amino acids were generated (**Table 1**) in case flanking residues were required for correct cleavage, folding or loading of peptides onto MHC-II. A full list of universal donor plasmids generated in this study can be found in **Table 2**.

The proteins tagged with epitope sequences were β-Actin (ACTB), ATP synthase F1 subunit beta (ATP5B), Cyclin-dependent kinase 4 (CDK4) and TYRP1. These proteins were selected in part because they reside in in different intracellular compartments (cytoskeleton, mitochondira, nucleus, melanomsomes, respecitively) (**Figure 3.9c**) and it remained to be determined whether the subcellular localisation of the tagged protein would affect processing of the epitope into the MHC-II loading pathway. Following transfection and selection using antibiotics, cell lines were enriched by flow cytometry sorting as all successfully tagged cells would express the fluorescent marker encoded in the universal donor plasmid.

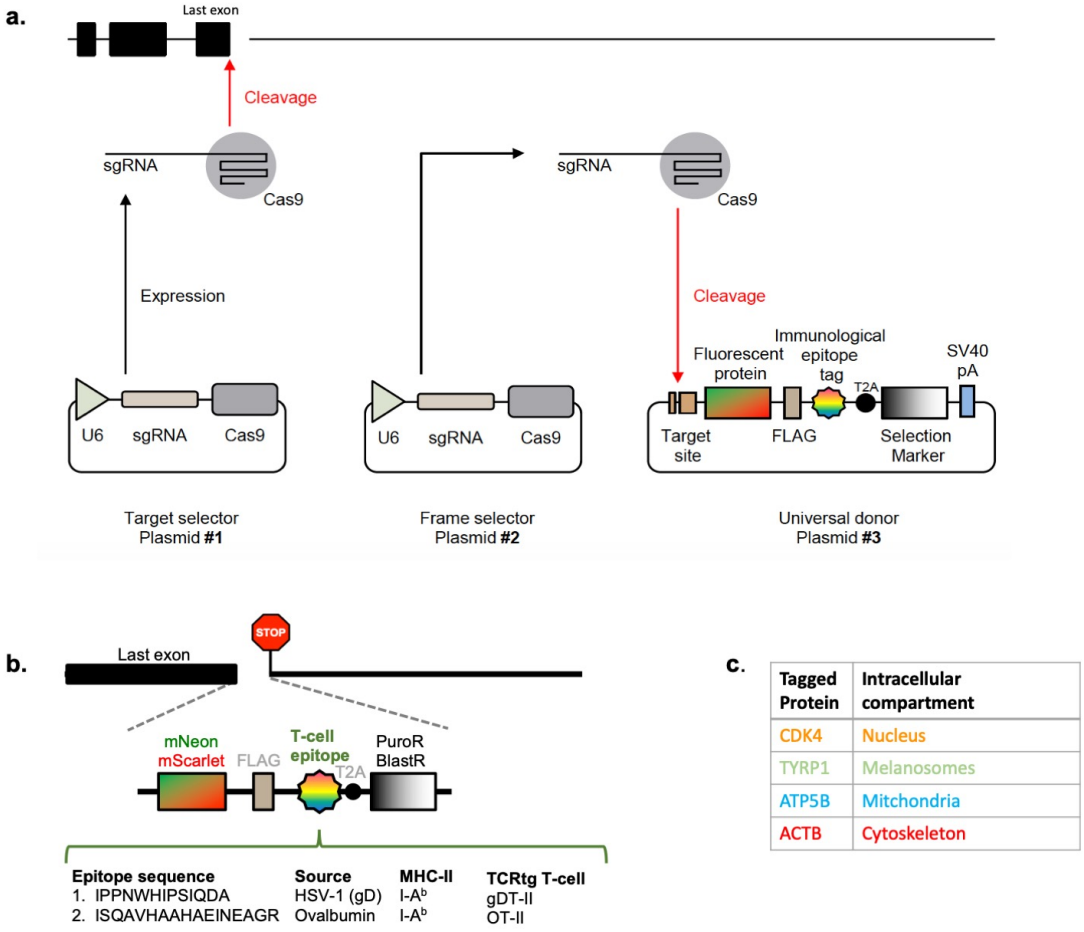

Figure 3.9. CRIPSitope toolbox used for generating cell lines with T cell epitope fusion proteins.

a, Graphical representation of the CRISPitope molecular cloning technique that uses a 3-plasmid system to generate a fusion product between a gene of interest (last exon) and a T cell epitope (immunological epitope tag) encoded by the universal donor (plasmid 3) (Effern et al., 2020). **b,** Graphical representation of the fusion cassettes encoded in the Universal donor plasmid. Cassettes encoded two $CD4^+$ T cell epitopes sourced from either gD or Ovabumin. Respective epitope peptide sequences, MHC class II restrictions and cognate TCR transgenic (tg) T cells are listed. **c.** List of proteins tagged with $CD4^+$ T cell epitopes in this study and their subcellular locations. *Figures adapted from Maike Effern (Holzel laboratory, the University of Bonn).*

3.2.10 Validation of CRISPitope-engineered B16 cell lines

Cell lines generated using the universal donor encoding the minimal gD and epitope ($gD_{(315-327)}$) and mNeon were used for subsequent validation experiments. In flow cytometry the cell lines with different tagged proteins exhibited different mean fluorescent intensities (MFI) of mNeon (**Figure 3.10a**). The MFI likely corresponds to expression level of the tagged protein and therefore could be used as a surrogate measurement for antigen ($gD_{(315-327)}$) epression level. Cells were imaged using confocal microscopy to validate that the fusion protein, which could be visualised by mNeon, was in the expected subcellular localisation (**Figure 3.10b**). As expected mNeon was detected in the nucleus of B16.CDK4-mNeon-$gD_{(315-327)}$ cells and in the cytoplasm of B16.TYRP1-mNeon-$gD_{(315-327)}$, B16.ACTB-mNeon-$gD_{(315-327)}$ and B16.ATP5B-mNeon-$gD_{(315-327)}$ cells. Using the mitotracker stain we were further able to validate that the mNeon signal in the B16.ATP5B-mNeon-$gD_{(315-327)}$ colocalised with mitochondria **(Figure3.10c)**.

The CRISPitope cell lines expressing $gD_{(315-327)}$ were validated in an *in vitro* functional assay to determine whether they could be recognised by gDT-II cells (**Figure 3.10d**). Melanoma cells were prestimulated with IFNγ to upregulate MHC-II prior to co-culture and antigen recognition by gDT-II cells was measured by their production of TNFα and IFNγ. As expected, in the absence of IFNγ pretreatment, gDT-II cells did not produce TNFα or IFNγ. However, all cell lines expressing $gD_{(315-327)}$ pretreated with IFNγ were capable of directly stimulating gDT-II cells regardless of the protein to which the epitope was fused. The control cell line which expressed a fusion protein between ACTB and mNeon, but not $gD_{(315-327)}$, did not stimulate the gDT-II cells corroborating that the response to the other cell lines was antigen-specific. Interestingly, this assay demonstrated that endogenous tumor antigens arising in diverse compartments of the cell can gain access to the MHC class II loading pathway for direct presentation to $CD4^+$ T cells. From a single experiment, the proportions of gDT-II cells producing cytokines upon coculture with different cell lines cannot be used to infer quantitative differences between the ability of cell lines to stimulate gDT-II cells. Cell lines expressing the extended epitope sequences $gD_{(312-330)}$ and $gD_{(312-342)}$ were also tested *in vitro* and were found to be capable of stimulating the gDT-II cells directly (data not shown). Overall, the CRISPitope platform demonstrated to be a highly valuable tool to generate melanoma cells in which epitopes specific for $CD4^+$ T cells are expressed under specific promotors and can be tracked by microscopy and flow cytometry.

a.

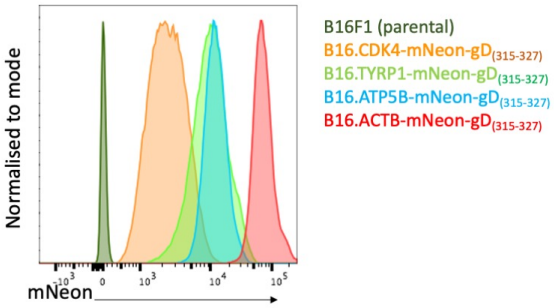

b. B16.CDK4-mNeon-gD$_{(315-327)}$

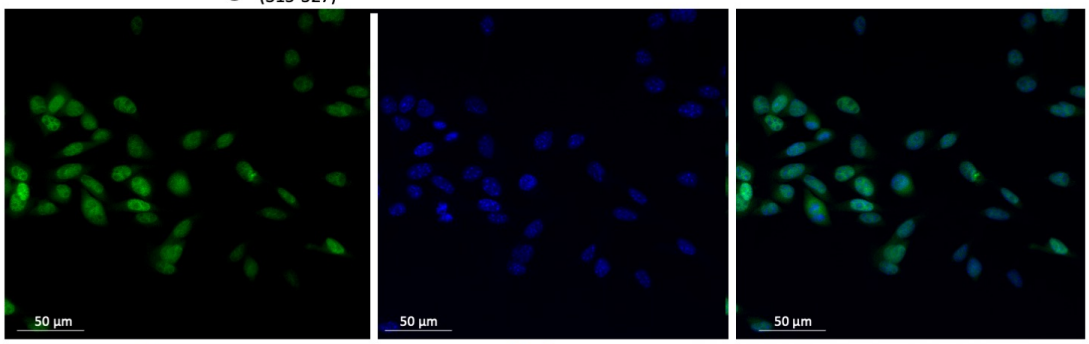

B16.TYRP1-mNeon-gD$_{(315-327)}$

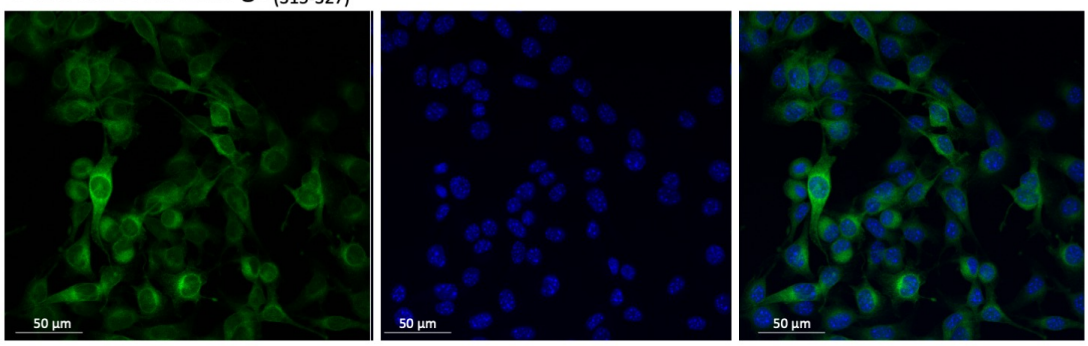

B16.ACTB-mNeon-gD$_{(315-327)}$

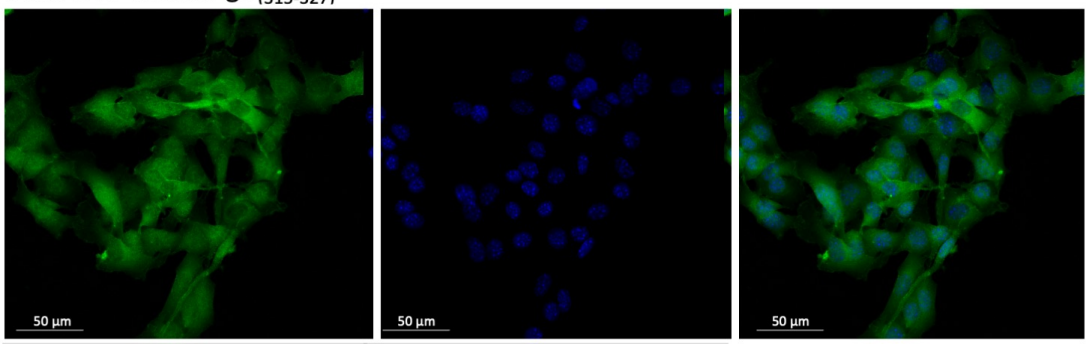

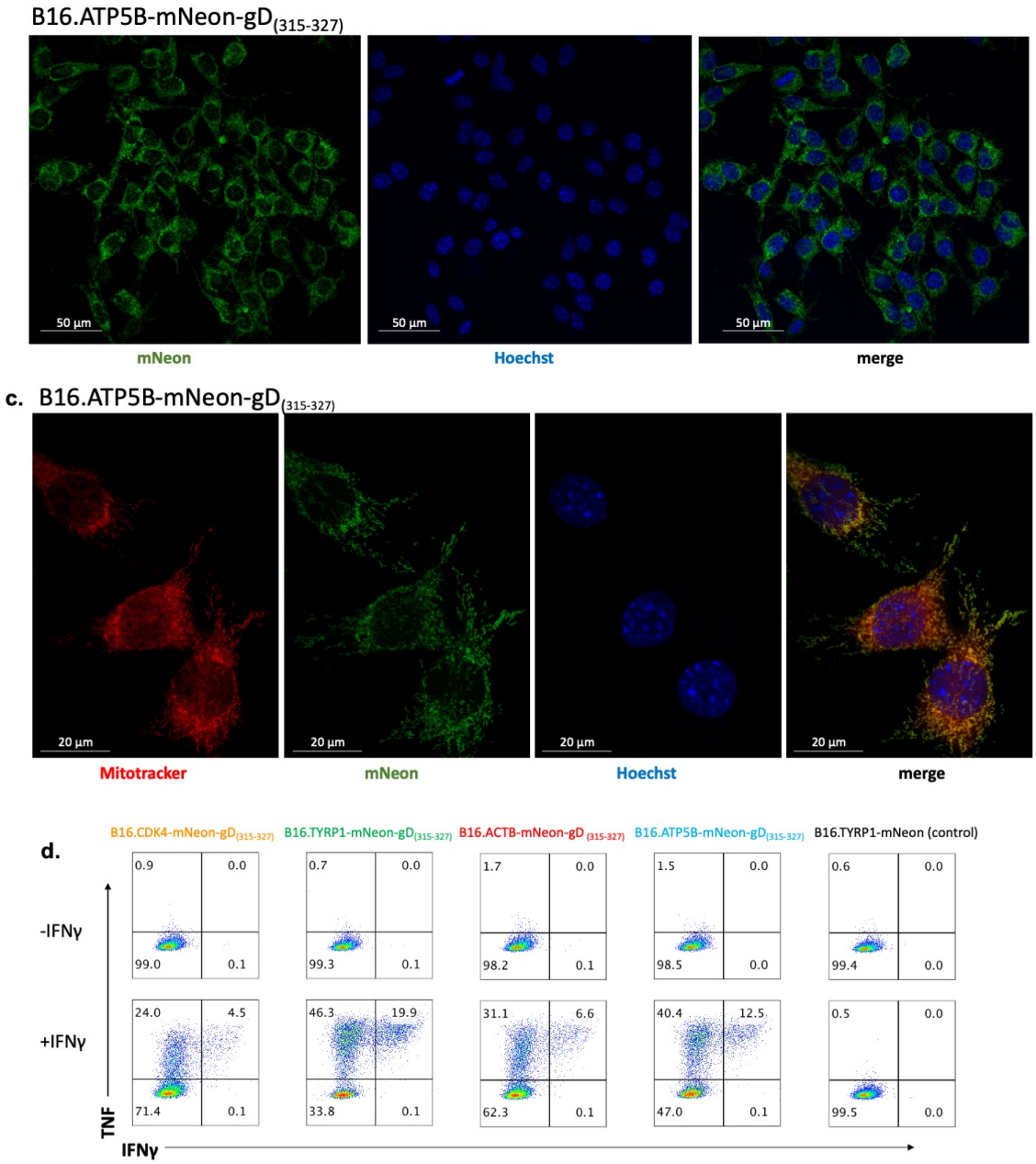

Figure 3.10. Characterisation and validation of CRISPitope-generated cell lines that express minimal gD epitope (gD(315-327)).
a, mNeon expression in indicated cell lines measured by flow cytometry **b,** Confocal microscopy of CRISPitope-generated cell lines to show subcellular location of endogenous mNeon expression (green). Cells stained by Hoechst to visualize cell nuclei (blue). **c,** Confocal microscopy of B16.ATP5B-mNeon-gD(315-327) showing endogenous mNeon expression (green), stained by Hoechst to visualize cell nuclei (blue) and stained by Mitotracker (red) to visualize mitochondria. **d,** *In vitro* co-culture assay to confirm gD(315-327) expression in CRISPitope-generated cell lines and their capacity to directly stimulate gDT-II cells. Production of IFNγ and TNFα by *in vitro*-activated gDT-II cells following 5 hours co-culture CRIPitope-generated cell lines (+/- IFNγ pre-stimulation).

3.3 Discussion

The epicutaneous melanoma model has been recently shown to better approximate characteristics of human melanoma than the more traditional model of subcutaneous (s.c.) inoculation (Park et al., 2019). The e.c. model is orthotopic, exhibits variation in primary tumor incidence and growth kinetics and can produce spontaneous metastasis, thus enabling the study of immunosurveillance at different stages of disease. The epicutaneous model is a transplantable model which has the advantage that there is flexibility regarding mouse strains and melanoma cell lines which can be used. Some commonly used murine melanoma lines are derivatives of the B16-F0 cell line which was first isolated from a spontaneous melanoma in a C57BL/6 mouse. The B16-F1 and B16-F10 sublines of B16-F0 were generated by a one-time or ten-time selective procedure, respectively. This procedure, first described by Fidler, involved intravenously injecting melanoma cells into mice, harvesting tumor nodules from the lung and culturing the melanoma cells *ex vivo* (Fidler, 1973). Fidler reported that less than 1 % of cells injected intravenously survive *in vivo*, and therefore the clonal composition of tumor cells that form at the lung could be considerably different to that of the original cell line injected. This procedure favoured selection of clones that are better able to survive and colonise the lung *in vivo* thus leading to the generation of more aggressive sublines (Nakamura et al., 2002, Fidler, 1973). In general, cancer cell lines exhibit a high degree of genetic instability and can easily acquire mutations even in culture without the selective pressure from an *in vivo* environment (Kaufmann et al., 2014). The epicutaneous model has been characterised using various B16.gB cell lines which express glycoprotein B (Park et al., 2019). These cells were generated on a B16-F1 background. In contrast, B16.gD cells express glycoprotein D and were generated on a B16-F10 background. For this project, the B16.gD cell line was characterised in the epicutaneous model as tumor growth characteristics and immunogenicity could differ from those of B16.gB cell lines previously used in the model.

Epicutaneous inoculation with B16.gD cells resulted in a tumor incidence

between 50-60 %, similar to what was found using the B16.gB cell line (Park et al., 2019). However, the majority of B16.gD tumors arose slightly earlier, around 10 days p.i, than B16.gB tumors, of which the majority arose between two and three weeks p.i. The mechanisms underlying the variation in tumor onset and growth kinetics that occurs in the epicutaneous model remain to be determined. The fact that late onset tumors tended to grow more slowly may reflect a level of host pressure that is ultimately outpaced by the proliferation of melanoma cells. In contrast, early arising, rapidly developing tumors may result from the failure to mount an initial anti-tumoral response. This is supported by the fact that immunodeficient mice develop tumors very rapidly in the e.c. model (Park et al., 2019). Clonal variation of the melanoma cells which survive transplantation may additionally affect tumor growth kinetics. It is likely a balance of melanoma cell biology and host factors, including immunosurveillance mechanisms, which dictates the fate of tumor development within immunocompetent mice.

Persistence of B16.gB was previously shown using a combination of techniques including intravital imaging, bioluminescence longitudinal monitoring and detection of melanoma-specific DNA (Park et al., 2019). Here, persistence of non-progressively growing B16.gD lesions was documented through longitudinal photography. This represents a refinement of visual detection through the implementation of technologies such as the Dermlight demoscopy camera and Stereo microscope. Cells with the morphology of melanoma cells were detected in lesions analysed by H&E staining. However, melanoma have a similar morphology to melanophages, macrophages that take up melanin pigment (Busam et al., 2001, Behrens et al., 2019), and therefore additional methods, such as longitudinal bioluminescence imaging can be used to ascertain the presence of melanoma cells within these lesions. Recurrence of bioluminescent signals at the site of inoculation was observed in a few mice with macroscopically tumor-free skin however the rate of persistence from initial experiments cannot be determined due to a small sample size and a limited number of imaging sessions. Future experiments will be carried out using bioluminescene to better characterise the rate and kinetics of persistance of

melanoma cells. The prevailing evidence that at least some persisting lesions contain bonafide melanoma cells is that in some mice, lesions which persisted over prolonged periods eventually developed into progressively growing tumors (Park et al., 2019).

The underlying mechanisms which may prevent outgrowth of B16.gD cells in persistent lesions remains to be determined. One possibility is that the immune system is controlling melanoma cells in a state of immune-melanoma "equilibrium," in which the melanoma cells are either dormant or dividing at the same rate as their immune-mediated elimination (Dunn et al., 2002). In a previous study, depletion of T_{RM} specific for B16.gB resulted in 20 % outgrowth of macroscopically tumor-free mice indicating a role for T_{RM} in maintaining the state of equilibrium (Park et al., 2019). In the remaining mice that did not develop tumors upon T_{RM} depletion melanoma cells may have been completely eliminated prior to depletion. Alternatively, depletion can be highly variable and may not have effectively removed all the T_{RM} from the skin. However, it is also possible that T_{RM}-independent mechanisms were mediating melanoma-immune equilibrium in the skin. The level of protection mediated by the endogenous repertoire of $CD8^+$ T_{RM} was not determined in this study (Park et al., 2019). Whether there are differences in the mechanism underpinning persistence of B16.gD or B16.gB in the skin, or even differences in mechanisms amongst mice challenged with the same melanoma cell line, remains to be elucidated. Deciphering the underlying mechanisms mediating a melanoma-immune equilibrium is an area of intense research in the Gebhardt laboratory, which has been made possible by the development of the epicutaneous melanoma model.

Melanoma is a highly metastatic disease. Since primary melanoma can be cured by surgery, it is the occurrence of metastasis which poses the greatest threat to survival. It is therefore imperative to have a robust experimental model in which spontaneous metastasis can be recapitulated. The use of B16.gD cell in the epicutaneous model demonstrated to be a valuable model for studying spontaneous metastasis as a high frequency of nodal disease was observed.

There was a high degree of variability regarding the appearance of metastases and a grading system was devised based on the size of black pigment observed under a microscope. As this process was based on observation it poses limitations for quantification. Firstly, multiple seeding events may occur giving rise to multiple metastatic nodules rendering the overall pigmented surface area difficult to measure. Furthermore, metastasis is often observed in the superficial layers of the lymph node but seeding that occurs more internally may be difficult to observe. Additionally, it is possible that melanoma cells lose their pigment in the process of dedifferentiation rendering them undetectable under the microscope or merely that the number of cells is below the limit of detection by observation. Using bioluminescence imagaing facilitated a semi-quantitative analysis of tumor growth kinetics not only at the primary site but also of metastatic disease at the tumor-draining lymph node. An interesting finding was the correlation between early detection of melanoma cells in the lymph node and subsequent regression of the primary lesion. This suggests that the presence of melanoma cells at the brachial lymph node early following inoculation may be protective against tumor development. It is tempting to speculate that the presence of melanoma cells at the lymph node early in disease leads to better priming and a stronger immune response. Accordingly, it has been shown in a previous study that melanoma cells transferred directly into lymphoid organs effectively primed naïve $CD8^+$ T cells resulting in tumor eradication, whereas peripherally injected melanoma cells did not induce effective priming and mice were unable to control tumors (Ochsenbein et al., 2001).

To investigate mechanisms underlying melanoma immunosurveillance, a series of genetically modified cell lines were generated on the B16.gD background. Firstly, B16.gD cells unable to express MHC-II were generated by functional genetic deletion of *Ciita.* These cells serve as a useful tool to elucidate the role of MHC-II expression by melanoma cells on the melanoma immunosurveillance. In particular, these cells were used in subsequent chapters to determine whether melanoma cells in the epicutaneous model can directly present antigens to $CD4^+$ T cells and whether this interaction is required for the

anti-tumoral response mediated by $CD4^+$ T cells.

Secondly, B16.gD.*Tnfr1*$^{-/-}$ cells were generated to investigate the role of TNFR1-signalling in melanoma cells. TNFα can mediate induction of cell death in different cancer cell types under certain conditions (Montfort et al., 2019, Kearney et al., 2018, Kimura et al., 2003). In this study, combined exposure to TNFα and IFNγ, but neither cytokine alone, resulted in B16.gD cell death. This phenomenon was harnessed to implement a cytokine enrichment strategy to select for cells with non-functional *Tnfr1* gene which would be unresponsive to TNFα-induced cell death. The frequency of gene-deleted cells in the final enriched polyclonal culture was approximately >90 %, as determined by NGS. Whilst present at a low frequency, the small proportion of wild-type cells in the final polyclonal culture should be taken into account in future experiments, as the relative proportions of *Tnfr1* gene-deleted and wild-type cells could change if TNFR1-signalling drives a selective growth advantage or disadvantage under certain conditions.

Tnf$^{-/-}$ mice have been shown to be more susceptible to tumor development in the epicutaneous model but the underlying mechanism was not determined (Park et al., 2019). B16.gD.*Tnfr1*$^{-/-}$ cells are a valuable tool to determine whether TNFα directly targets melanoma cells or contributes to melanoma immunosurveillance by modulating host cells. $CD4^+$ T cells have been reported to kill cancer cells directly through TNFα-induced apoptosis (Habtetsion et al., 2018). Since gDT-II cells are protective in the epicutaneous model and produce a high level of TNFα upon co-culture with MHC-II-positive B16.gD cells, one could postulate that TNFα produced by gDT-II cells may play a role in direct killing of B16.gD cells. The B16.gD.*Tnfr1*$^{-/-}$ cell line was used in subsequent chapters to address this question.

B16.gD cells were transfected with guide RNAs targeting *Tnfr2,* however, unlike cells transfected with guide RNAs targeting *Tnfr1,* these cells were killed by co-treatment with IFNγ and TNFα, indicating that they are not resistant to TNF-

induced cell death. It is possible that the guide RNAs were ineffective at targeting *Tnfr2*. However, likely explanations would be that TNF-induced cell death does not occur via signalling through TNFR2 in B16.gD cells and/or TNFR2 is simply not expressed by B16.gD cells. In line with these postulations, signalling through TNFR2 is typically associated with pro-survival pathways (Fontaine et al., 2002, Hurrell et al., 2019) and, whilst TNFR1 is ubiquitously expressed, TNFR2 expression is restricted to certain cell types (Carpentier et al., 2004). From this knowledge, one could speculate that TNF primarily signals through TNFR1 in B16.gD cells, and it was shown that signalling through this receptor, in the presence of IFNγ, promotes cell death.

Thirdly, an MHC-II-reporter cell line, B16.gD.MHC-II-mScarlet, was generated using the CRISPaint platform. These cells were validated for the ability to functionally form peptide/MHC-II complex despite the fusion of mScarlet and MHC-II molecules. Now that the technique used to generate a polyclonal MHC-II reporter cell line has been validated, the same technique can be applied to melanoma cells deficient in tyrosinase to use in two-photon microscopy, as the deletion of tyrosinase is necessary to avoid quenching of the fluorescent signal. This could be used to visualize how the expression of MHC-II by melanoma cells affects interactions with $CD4^+$ T cells.

A luciferase-expressing melanoma cell line, B16.gD.Luc-mScar, was generated to enable *in vivo* longitudinal monitoring of melanoma via bioluminescence imaging. Initial characterisation of these cells in the epicutaneous model demonstrated their utility in tracking melanoma development, including persisting lesions that cannot be seen by eye, and metastasis. It was observed that the incidence of tumor development was lower in mice challenged with B16.gD.Luc-mScar cells compared to the B16.gD cells. It is possible that the B16.gD.Luc-mScar cell line is more immunogenic than the parental line due to the addition of the luciferase-mScarlet construct which may harbour xenoantigens that can be targeted by the adaptive immune system. Another explanation is that the process of generating the cells, including retroviral

transduction and sorting by flow cytmetry, could impact the intrinsic viability of the cells due to genetic or epigenetic alterations. A selective procedure involving injecting the B16.gD.Luc-mScar cells into mice and culturing them *ex vivo* (Nakamura et al., 2002, Fidler, 1973) could be used enable the cells to better adapt to an *in vivo* environement and increase the penetrance of the cell line in the e.c. melanoma model.

The B16.gD cell line used in this study was generated by retroviral transduction with a vector encoding full-length gD. This has the limitation that retroviral-mediated overexpression of gD is likely to represent antigen levels above those naturally expressed in cancer cells. The CRISPitope toolkit was used to generate B16 cell lines that express fusion proteins between selected gene products and defined $CD4^+$ T cell epitopes. A major advantage of the CRISPitope-generated cells is that antigen expression is regulated under a selected promotor at biologically relevant levels. In addition, since the epitope is directly fused to a fluorescent protein, antigen expression can be specifically monitored by flow cytometry or microscopy. MFI values of the fluorescent protein tags in flow cytometry indictated that tagging different proteins led to differences in epitope expression levels. Future experiments will characterise these cell lines *in vivo* to determine how different antigen expression levels may confer different levels of protection by $CD4^+$ T cells. The choice endogenous gene product can additionally be used to investigate other variables of antigen biology. For instance, Effern *et al*, 2020 showed that fusing a $CD8^+$ T cell epitope to a melanomsal protein (GP100) or an oncogenic protein (CDK4R24C) affected the immune landscape in the tumor microenvironment and ultimately led to different relapse mechanisms in response to adoptive T cell therapy. Similar to the study by Effern *et al.*, 2020, both essential and non-essential gene products were selected for tagging with $CD4^+$ T cell epitopes in this study. TYRP1 is a melanosomal protein and can be downregulated during a process known as melanoma dedifferentiation (Landsberg et al., 2012). On the other hand, proteins such as ATP5B, which is the essential catalytic subunit of the mitochondrial ATP synthase, CDK4, which is an important regulator of the cell cycle, and β-Actin, an integral componenent

of the cytoskeleton, represent “essential” gene products that cannot be readily switched off.

In addition to the level of antigen expressed by cancer cells, the amount of antigen secreted into the TME could impact the immune response. Secretion of antigen renders it readily available for uptake by surrounding APCs that may travel to the lymph node to initiate priming. In addition, particularly for MHC-II-negative tumors, secretion of antigen may be important for the stimulation of $CD4^+$ T cells by APCs within tumors. Indeed, it was demonstrated in a murine model of myeloma that secretion of a model antigen was required for effective priming and in turn the elimination of tumors orchestrated by $CD4^+$ T cells (Corthay et al., 2009). It would thus be interesting to investigate whether fusion of the epitope to TYRP1, could lead to better $CD4^+$ T cell priming, given that TYRP1 is localised in melansomes which are readily secreted from melanocytes.

Another potential limitation of retroviral overexpression of full-lenth gD, is that it cannot be ascertained whether the protein may play a physiological role in the B16.gD cell line. The canonical function of gD in HSV-1 is to bind to Herpesvirus entry mediator (HVEM) on lymphocytes to facilitate viral entry. However, HVEM can act as a costimulatory receptor for T cells and thus the possibility that full-lenth gD could regulate T cell activation should be considered (Whitbeck et al., 1997, Mauri et al., 1998). Furthermore, full-length gD harbours several immunological epitopes and could thus stimulate a broader repetoir of antigen-specific $CD8^+$ and $CD4^+$ T cells and B cells, thereby altering the immunogenicity of the cells (BenMohamed et al., 2003, Mikloska and Cunningham, 1998, Koelle et al., 2003, Welling-Webster et al., 1991). As CRISPitope introduces specific epitope sequences into cells, this can overcome limitations of introducing full-length model antigens which may be highly immunogenic and play unknown functions.

Confocal microscopy confirmed that the fluorescently tagged proteins localised in the expected subcellular compartment. To definitely confirm that the

correct protein was tagged, identification of the FLAG-tag encoded in fusion cassette of the universal donor plasmid can be used for antibody-dependent detection approaches such as immunoblotting, as shown previously (Effern et al., 2020).

Overall, cells generated by CRISPitope in this project will be highly valuable for investigating the effects of antigen biology on $CD4^+$ T cells responses in the context of melanoma. This knowledge could assist in future design of T cell-based immunotherapy, particularly for deciding on appropriate antigens to be targeted by adoptively transferred $CD4^+$ T cells.

Chapter 4: Characterising the role of $CD4^+$ T cells in melanoma immunosurveillance.

Chapter 4. Characterising the role of CD4$^+$ T cells in melanoma immunosurveillance.

4.1 Background

Several studies in preclinical models have demonstrated the important role of anti-tumoral CD4$^+$ T cells in cancer immunosurveillance (Perez-Diez et al., 2007, Quezada et al., 2010, Xie et al., 2010, Shklovskaya et al., 2016, Malandro et al., 2016, Hirschhorn-Cymerman et al., 2012, Haabeth et al., 2018, Alspach et al., 2019). Recent evidence in humans also suggests that CD4$^+$ T cells are critical for controlling cancers (Oh et al., 2020, Tran et al., 2014). On the other hand, a heterogenous subset of immunosuppressive CD4$^+$ T cells, Treg cells, can promote tumor development and thus remain a major barrier to the success of cancer immunotherapies (Paluskievicz et al., 2019). Attempts to characterise melanoma immunosurveillance by CD4$^+$ T cells have led to inconsistent findings, obscured by the high degree of phenotypic and functional heterogeneity within the CD4$^+$ T cell lineage. Additionally, CD4$^+$ T cells are sensitive to regulation by the surrounding microenvironment, which may explain discrepancies seen among studies using different models.

Several studies have demonstrated the therapeutic benefit of adoptive transfer of *in vitro* activated antigen-specific CD4$^+$ T cells. These protocols however preclude characterisation of CD4$^+$ T cell priming to melanoma antigens *in vivo*. Therefore, the processes involved in the formation of spontaneous responses to melanoma by endogenous CD4$^+$ T cells is not well understood. Importantly, the signals that T cells receive during priming impact their differentiation, their memory potential and migratory characteristics (Hilligan and Ronchese, 2020). The transfer of trackable naïve antigen specific CD4$^+$ T cells that are primed *in vivo* in tumour challenged mice is thus a preferential model to mimic endogenous CD4$^+$ T cells.

In chapter 3, TCR transgenic CD4$^+$ T cells, gDT-II cells, were demonstrated to

specifically recognise B16.gD cells *in vitro*. In addition, B16.gD cells were characterised in the epicutaneous melanoma model whereby tumor development was shown to closely approximate the anatomical location and growth kinetics of human melanoma. The focus of the work described in this chapter was to determine the role of $CD4^+$ T cell in melanoma immunosurveillance in the epicutaneous melanoma model and to characterise the $CD4^+$ T cell response to B16.gD melanoma challenge using *in vivo* primed gDT-II cells.

4.2 Results

4.2.1 Resolved HSV infection confers protection against B16.gD tumor development.

HSV-derived gD harbours several MHC-II-restricted epitopes recognised by $CD4^+$ T cells in mice and humans (BenMohamed et al., 2003, Mikloska and Cunningham, 1998). Immunisation of mice with MHC-II restricted epitopes derived from gD can prime $CD4^+$ T cell responses that protect against a lethal model of ocular HSV-1 (BenMohamed et al., 2003). $CD8^+$ T cell and B cell epitopes of gD have also been identified (Koelle et al., 2003, Welling-Webster et al., 1991), although the major immunodominant epitope recognised by $CD8^+$ T cells is derived from glycoprotein B (Wallace et al., 1999). To determine whether adaptive immunological memory specific to gD could afford protection against epicutaneous challenge with B16.gD, wild-type (C57BL/6) mice were infected with HSV-1 on the flank skin and challenged with B16.gD at the same site several months later (**Figure 4.1a**). Mice previously challenged with HSV-1 (HSV memory) but not aged-matched controls, were completely protected against B16.gD melanoma development (**Figure 4.1b**). Following resolution of HSV-1 infection, the skin at the site of prior inoculation has been shown to maintain an inflammatory immune landscape, including a sustained increase in the number of APCs, compared to unchallenged skin (Collins et al., 2017). To test if protection against B16.gD melanoma in HSV-memory mice was indeed due to

immunological memory formed against gD, and not a result of non-specific changes to the immune contexture in HSV-challenged skin, HSV-memory mice were inoculated with B16.Ova, a cell line expressing an unrelated model antigen, ovalbumin. As shown in **Figure 4.1c**, these mice were not protected from melanoma development demonstrating that protection against B16.gD challenge was antigen-specific**.** Since gD contains several different $CD4^+$ T cell epitopes it appeared likely that long-term protection was driven by memory $CD4^+$ T cells. However, the underlying mechanism, and the relative contributions of adaptive immune cells driving protection were not further examined.

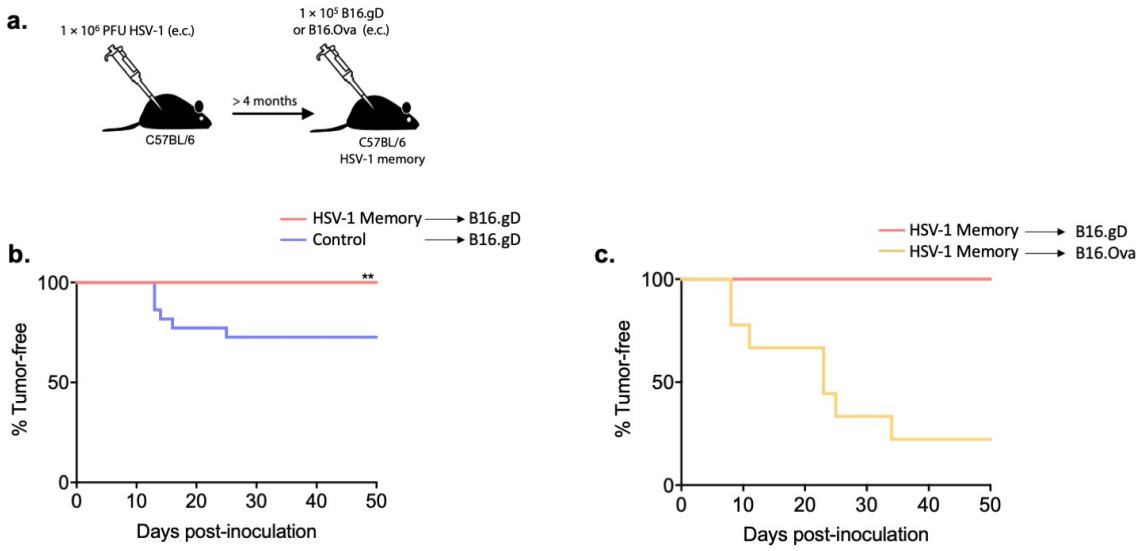

Figure 4.1. Resolved HSV infection confers protection against epicutaneous challenge with B16.gD.
a, Schematic of experimental protocol; C57BL/6 mice were challenged with HSV-1 KOS (1×10^6 PFU e.c.) on the left flank and rested for 4-10 months (HSV Memory) prior to melanoma challenge (e.c.) at the same site. **b,** Primary tumor incidence of HSV memory mice or naïve, aged-matched mice (Control) challenged with B16.gD (1×10^5). Data pooled from 3 biologically independent experiments, total of 22-24 mice per group. **P = 0.0064, statistics determined by log-rank Mantel–Cox test. **c**, Primary tumor incidence of HSV memory mice challenged with B16.gD or B16.Ova (1×10^5). Data from 1 experiment, 8-9 mice/group.

4.2.2 Transfer of naïve CD4$^+$ T cells confers protection against tumor development in wild-type mice.

CD4$^+$ T cells with transgenic expression of a gD-specific TCR (gDT-II cells) were used in combination with gD-expressing melanoma cells (B16.gD) to characterise melanoma immunosurveillance by CD4$^+$ T cells. Prior to epicutaneous melanoma challenge, 1 × 10^4 naïve gDT-II cells were adoptively transferred into wild-type C57BL/6 mice (**Figure 4.2a**). This transfer dose was selected as it has been used in previous studies to model an endogenous CD4$^+$ T cell response to cutaneous HSV-1 infection (Collins et al., 2016, Macleod et al., 2014, Gebhardt et al., 2011). The transfer of this number of naïve gDT-II cells resulted in a significant reduction in tumor incidence whereby in total only 35 % of gDT-II-recipient mice developed tumors, compared to 65 % tumor-development in control (naïve) mice (**Figure 4.2b**). Tumor growth kinetics were variable amongst developer mice, including some early developing tumors, late developing tumors and some persistent lesions, however, overall there were no obvious differences in tumor growth patterns between the gDT-II cell-recipients and control mice (**Figure 4.2c**). The significant reduction in tumor incidence resulting from a low transfer dose of naïve gDT-II cells indicated that CD4$^+$ T cells can play a potent anti-tumoral role in the epicutaneous model. Furthermore, metastatic spread into brachial lymph nodes was less frequently observed and less pronounced in mice with progressively growing melanoma that received gDT-II cells compared to controls, suggesting that gDT-II cells may not only protect from primary tumor development but may also play a role in prevention or control of nodal disease (**Figure 4.2d**). In a separate dose titration experiment, a trend that gDT-II cells may protect against primary tumor development in a dose-dependent manner was observed (**Figure 4.2e, f**). As expected, tumor incidence was highest in the naïve controls, followed by the lowest dose of gDT-II cells (1 × 10^3). However, 1/11 and 1/12 mice developed tumors in the groups receiving 1 × 10^4 and 1 × 10^5 gDT-II cells, respectively, so a greater number of mice would be required to ascertain whether doses higher than 1 × 10^4 mediate a higher level of protection. Finally, kinetics of melanoma immunosurveillance in the presence or absence of gDT-II cells was

analysed with bioluminescence imaging using the B16.gD.Luc-mScar melanoma cell line (**Figure 4.3a**). Thirty-three percent (4/12) of control mice developed progressively growing B16.gD.Luc-mScar tumors, whereas the entire cohort (12/12) of gDT-II cell-recipient mice remained free from the development of progressively growing tumors (**Figure 4.3b**). In both groups, 11/12 mice presented with a bioluminescence signal at the primary site on day 4 following inoculation. Between day 8 and 11 p.i., bioluminescence signal was detected at the primary site in 55 % (6/11) of the gDT-II cell-recipients compared to 91 % (10/11) in the control group **(Figure 4.3c, d)**.

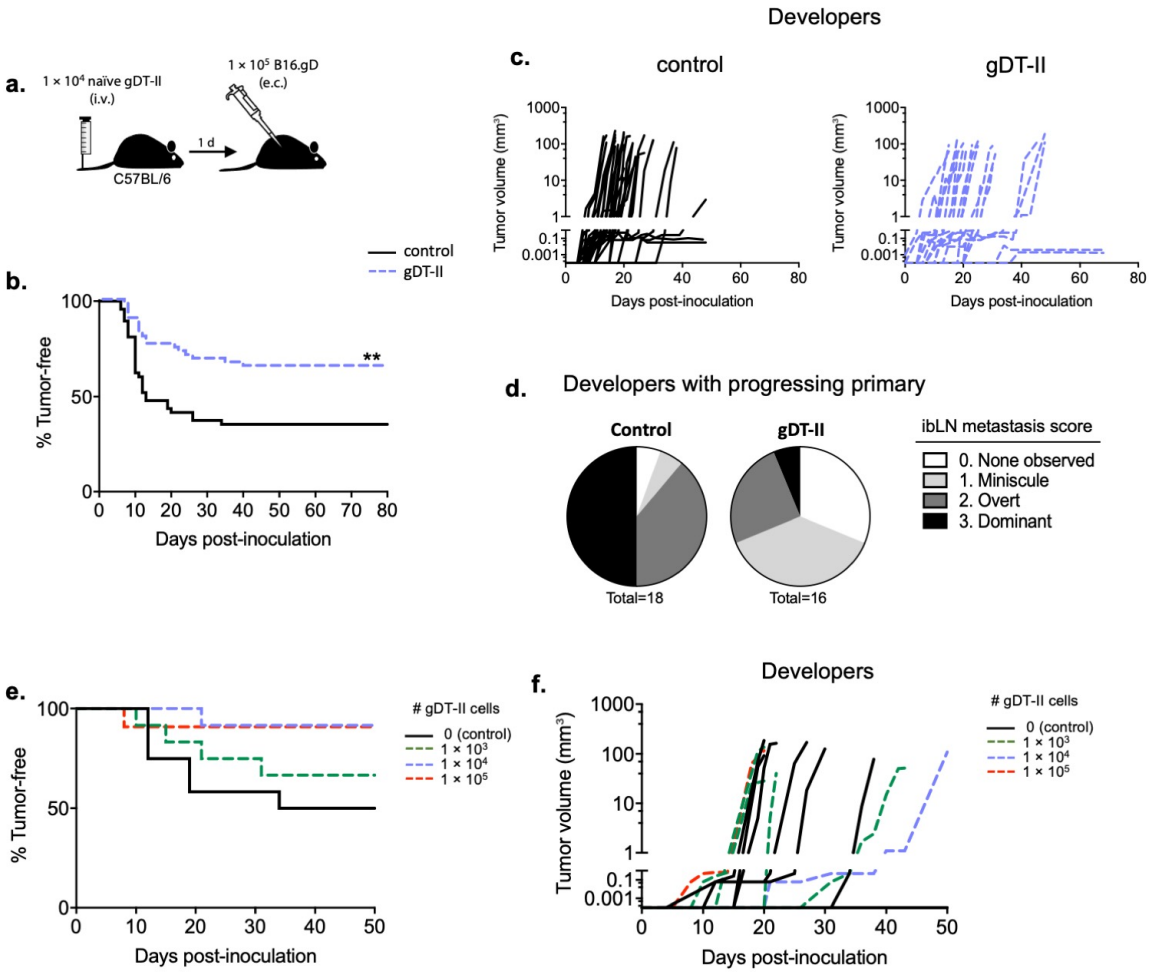

Figure 4.2. Naïve gDT-II cells protect against development of B16.gD melanoma in C57BL/6 mice.

a, Schematic of experimental protocol for (b-d); C57BL/6 mice received 1 × 10^4 naïve gDT-II cells i.v. (gDT-II) and were challenged the following day with B16.gD cells (1 × 10^5 e.c), in parallel to aged-matched, naïve C57BL/6 mice (control). **b,** Primary tumor incidence (**p=0.0021) and **c,** primary tumor growth kinetics; n=48-53 mice/group, pooled from 8 biologically independent experiments. **d,** Incidence of ibLN metastasis observed by eye in mice with progressively growing primary B16.gD tumors, assessed in tumors ranging from 20-180 mm^3. Metastases scored from 0-3 based on the surface area of black pigment observed; 0 (none observed) corresponds to no observable pigment, 1 (miniscule) corresponds to pigment <0.5 mm^2, 2 (overt) corresponds to pigment 0.5-1.5 mm^2, 3 (dominant) corresponds to pigment >1.5 mm^2. **e, f,** Same experimental protocol as in **(a)** except mice received different doses of naïve gDT-II cells as indicated in key. **e,** Primary tumor incidence and **f,** primary tumor growth kinetics, n=11-12 mice/group, pooled from 2 biologically independent experiments.

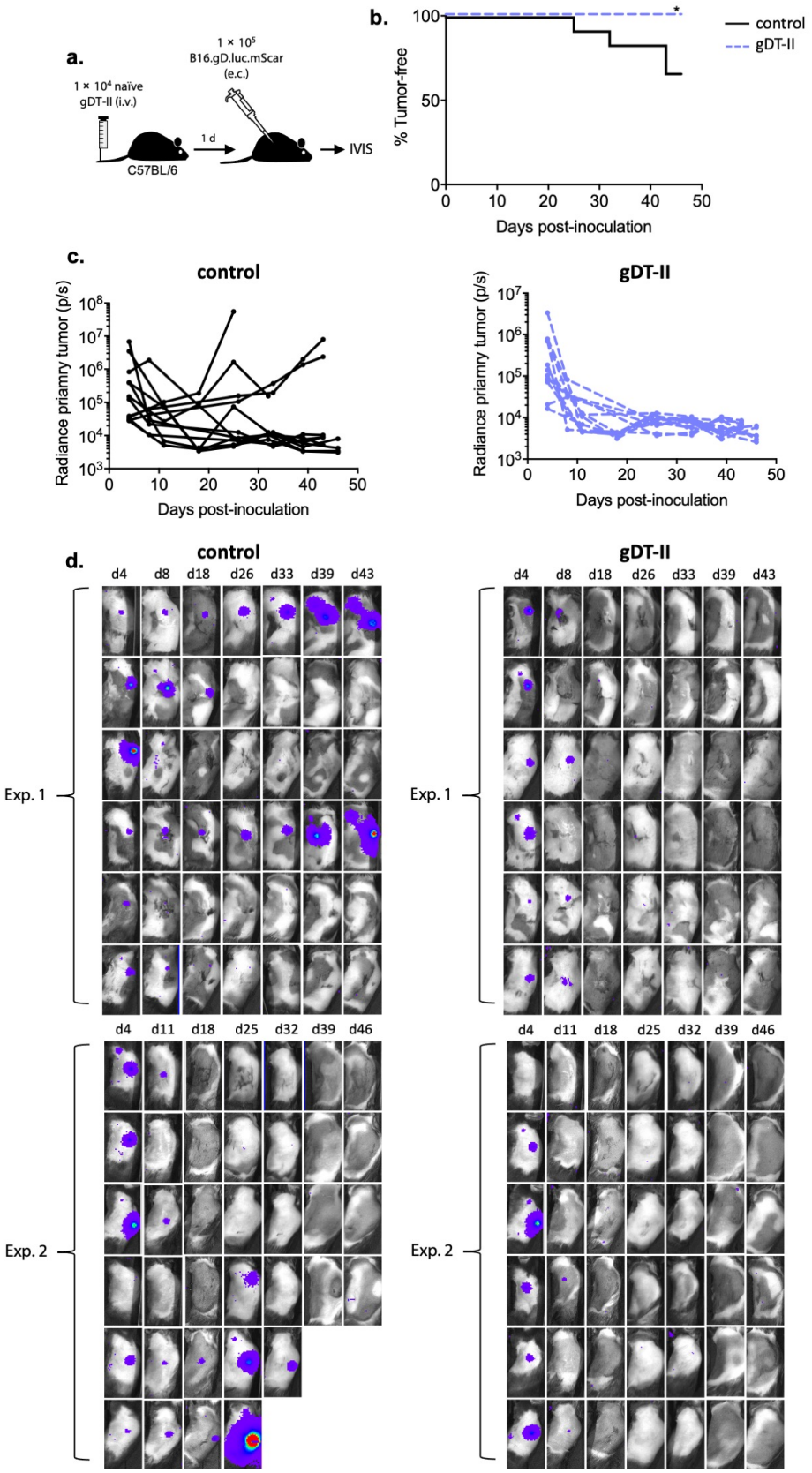
a.
1 × 10^4 naïve gDT-II (i.v.)
1 × 10^5 B16.gD.luc.mScar (e.c.)
1 d
C57BL/6
IVIS
b.
% Tumor-free
Days post-inoculation
control
gDT-II
*
c.
control
gDT-II
Radiance priamry tumor (p/s)
Days post-inoculation
d.
control
gDT-II
d4 d8 d18 d26 d33 d39 d43
d4 d11 d18 d25 d32 d39 d46
Exp. 1
Exp. 2

Figure 4.3. Longitudinal bioluminescence imaging to monitor protection mediated by gDT-II cells against B16.gD tumor development.
a. Schematic of experimental protocol; C57BL/6 mice received 1 × 10^4 naïve gDT-II cells i.v. (gDT-II) and were challenged the following day with B16.gD.Luc-mScar cells (1 × 10^5 e.c), in parallel to aged-matched, naïve C57BL/6 mice (control). **b.** Proportion of mice that resisted the development of progressing primary tumors. **c, d,** Bioluminescence was monitored longitudinally using an *in vivo* imaging system (IVIS) on day (d) p.i. indicated. **c,** Bioluminescence signals measured at the site of tumor inoculation and calculated as total flux (Radiance, photons/second, p/s). **b, c,** n=12 mice/group, data pooled from 2 biologically independent experiments (*p=0.0321). **d,** Photos from experiment one (Exp.1, top) and experiment two (Exp. 2, bottom). Statistics determined by log-rank Mantel Cox test. *IVIS imaging performed by David Freestone.*

4.2.3 Activated CD4$^+$ T cells can suppress tumor development in the absence of CD8$^+$ T cells and B cells.

The adoptive transfer of naïve gDT-II cells reduced tumor incidence in B16.gD-challenged wild-type mice. To further examine the anti-tumoral role of CD4$^+$ T cells, gDT-II cells were transferred into B16.gD-challenged recombination-activating gene (Rag)-deficient mouse strains; *Rag1*$^{-/-}$ and *Rag2*$^{-/-}$*;Il2rg*$^{-/-}$. The deletion of *Rag* genes, which are required for the generation of B and T cell receptors, results in the failure to produce mature adaptive immune cells. *Rag2*$^{-/-}$*;Il2rg*$^{-/-}$ mice are additionally deficient in NK cells and innate-like lymphocytes (ILCs) due to gene deletion of the common gamma chain which forms part of receptors for lymphocyte survival-promoting cytokines, such as IL-2, IL-7 and IL-15 and others. Rag-deficient mice were challenged epicutaneously with B16.gD melanoma and received 1 × 10^6 *in vitro* activated gDT-II cells the following week (**Figure 4.4a**). gDT-II cells were activated by gD peptide-pulsed splenocytes prior to transfer into Rag-deficient mice to circumvent the possibility that disrupted lymph node architecture and insufficient activating signals in an immunodeficient environment may prevent T cell priming. Indeed, it has been shown that gamma chain signalling is crucial for effective CD4$^+$ T cell priming in a model of B16 melanoma (Xie et al., 2010).

Rag-deficient mice have been shown to be highly susceptible to epicutaneous melanoma challenge with the cell line, B16.gB (Park et al., 2019), and as expected, Rag-deficient mice were also susceptible to B16.gD melanoma development in the absence of T cell transfer. However, Rag-deficient mice receiving gDT-II cells were uniformly protected against the development of B16.gD melanoma (**Figure 4.4b, d**). This striking level of protection observed upon transfer of activated gDT-II cells corroborates the observation that transfer of naïve gDT-II cells was protective against B16.gD melanoma in C57BL/6 mice. Furthermore, full protection mediated by gDT-II cells in *Rag2*$^{-/-}$*;Il2rg*$^{-/-}$ mice shows that CD4$^+$ T cells are able to control melanoma in the absence of endogenous T cells, B cells, NKT cells, NK cells and ILCs.

In the absence of gDT-II cell transfer, tumors developed in 95 % of the *Rag2*$^{-/-}$;*Il2rg*$^{-/-}$ mice compared to 55 % of the *Rag1*$^{-/-}$ mice suggesting that gamma-chain signalling and/or the presence of NK cells or ILCs plays a role in spontaneous immunosurveillance of B16.gD in the e.c melanoma model. The kinetics of tumor growth aligned with the disparity in tumor incidence between the Rag-deficient strains. The majority of tumors grew quickly and reached endpoint by day 20 p.i. in the *Rag2*$^{-/-}$;*Il2rg*$^{-/-}$ mice whereas tumors arose slightly later, with some not reaching endpoint until 35 days p.i., in the *Rag1*$^{-/-}$ mice (**Figure 4.4c, e**)**.** In two *Rag2*$^{-/-}$*;Il2rg*$^{-/-}$ mice, possible non-progressing lesions were observed at the inoculation site although these were very small and it was unclear whether they were bona fide melanomas, or alternatively pigment deposits remaining after inoculation (**Appendix Figure 9** and **Appendix Figure 10**). Heavily pigmented cells with a morphology similar to melanoma cells could be identified in sections stained with H&E, however further analysis would be required to confirm the identity of these cells as B16.gD or alternatively, as melanophages, the latter of which represent phagocytic cells that retain melanoma-derived pigments (Busam et al., 2001, Behrens et al., 2019).

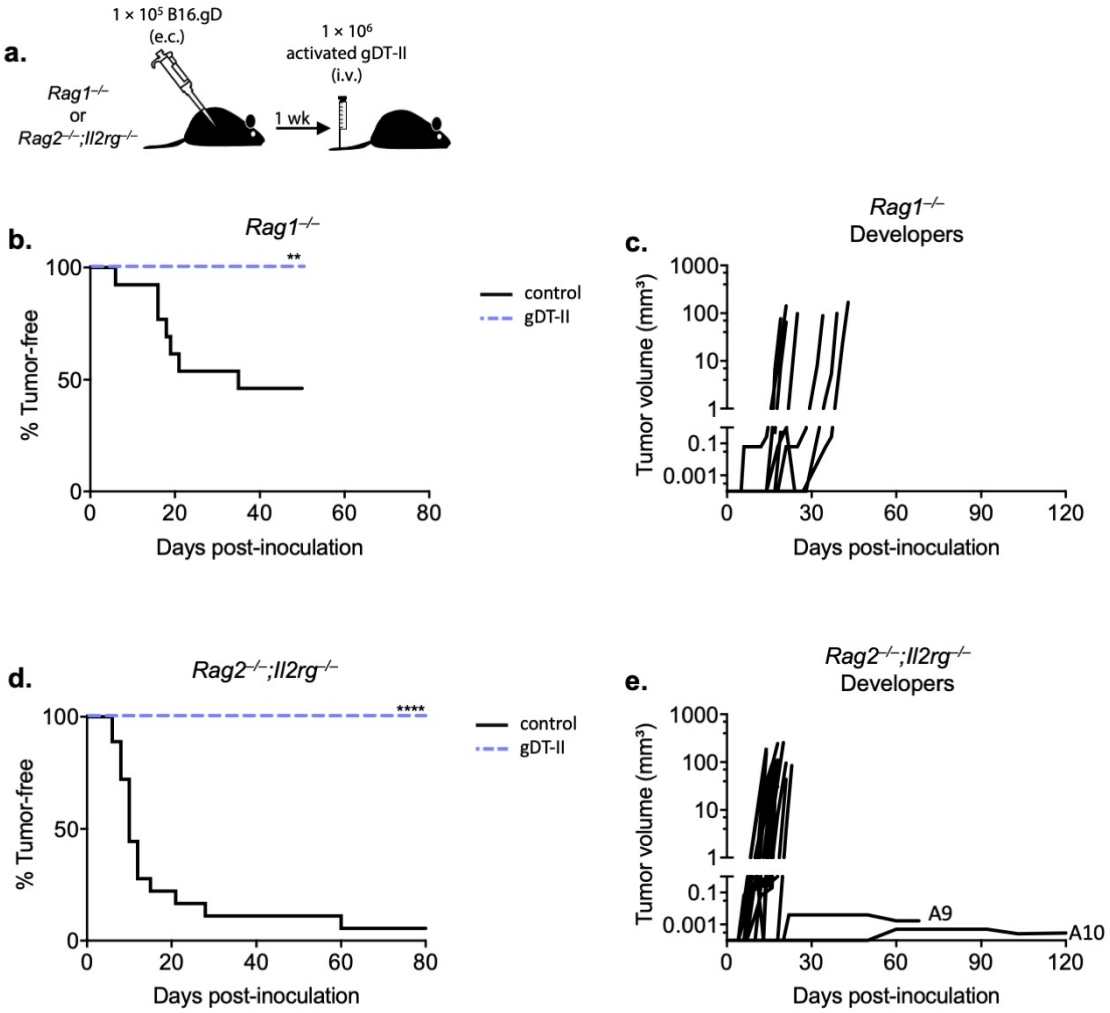

Figure 4.4. Activated gDT-II cells protect against development of B16.gD melanoma in *Rag1*$^{-/-}$ and *Rag2*$^{-/-}$;*Il2rg*$^{-/-}$ mice.
a, Schematic of experimental protocol; *Rag1*$^{-/-}$ and *Rag2*$^{-/-}$;*Il2rg*$^{-/-}$ mice were challenged with B16.gD cells (1 × 10^5 e.c.) and received *in vitro* activated gDT-II cells (1 × 10^6, i.v.) one-week p.i. (gDT-II), or did not receive gDT-II cells (control). **b,** Tumor incidence and **c,** tumor volumes in *Rag1*$^{-/-}$ mice. Data are pooled from 3 biologically independent experiments, n=13 mice/group. **P=0.0022. **d,** Tumor incidence and **e,** tumor volume in *Rag2*$^{-/-}$;*Il2rg*$^{-/-}$ mice. Data pooled from 5 biologically independent experiments, n=22 (gDT-II), n=18 (control), ****P<.0001. All statistics determined by log-rank Mantel Cox test. Photographical and histological evidence of lesions labelled A9 and A10 are provided in Appendix Figure 9 and Appendix Figure 10, respectively.

4.2.4 Characterising $CD4^+$ T cell priming in the epicutaneous melanoma model.

T cell priming initiates activation and proliferation of antigen-specific T cells. T cell priming generally takes place in the lymph node which drains the site of the source of antigen. Antigen may be delivered from the periphery by a migratory phagocyte or drain freely in the lymph (Haniffa et al., 2015). To test if $CD4^+$ T cell priming against melanoma antigens was indeed confined to the draining lymph node in the epicutaneous melanoma model, naïve gDT-II cells were stained with Cell Trace Violet (CTV) prior to transfer into C57BL/6 mice that were challenged with B16.gD. Cell proliferation that occurs during priming can be analysed by dilution of CTV which occurs with each successive cell division. As a positive control, mice were infected with HSV-1 on the left flank (at the same site where melanoma cells are transplanted in the epicutaneous melanoma model). Previous studies have shown that robust priming of gDT-II cells takes place in the ipsilateral brachial lymph node (ibLN) following HSV-1 challenge at this site (Hor et al., 2015, Bedoui et al., 2009). For a negative control, mice received CTV-labelled gDT-II cells but were neither challenged with HSV-1 nor B16.gD (**Figure 4.5a**). The pan-leukocyte marker, CD45, was used to track gDT-II cells by flow cytometry as gDT-II cells expressed the CD45.1 allele and were transferred into mice that expressed the CD45.2 allele. gDT-II cells were additionally identified by expression of CD4 and their TCR alpha chain, Vα3.2 (**Figure 4.5b**)**.** Of note, there was a small population of $CD45.1^+V\alpha3.2^-$ cells in brachial lymph nodes but these did not show upregulation of activation markers or dilution of CTV in mice challenged with B16.gD melanoma or HSV-1 (data not shown).

At 72 hours p.i., gDT-II cells that had diluted CTV were detected in the ibLN but not in the contralateral brachial lymph node (cbLN) nor the spleen in B16.gD-challenged and HSV-challenged mice (**Figure 4.5c**). This confirmed that $CD4^+$ T cells are primed at the ibLN, the lymph node draining the inoculation site in the epicutaneous melanoma model. The CTV profiles differed for gDT-II cells

primed in the context of infection and tumor challenge. In response to HSV-1 infection, the majority of gDT-II cells in the ibLN had divided at least once 72 hours p.i. and the entire population of gDT-II cells had divided upwards of eight times, the detection limit for CTV staining, 96 hours p.i.. Seventy-two hours following melanoma challenge there was considerable variation in the percentage of divided gDT-II cells, ranging from 16-35 % in one experiment and 38-74 % in a second experiment (**Figure 4.5d**)**.** An additional four mice from the second experiment were analysed at 96 hours following melanoma inoculation. At this later time point, gDT-II cells had divided a greater number of times than at 72 hours p.i. from the same experiment. It should be noted that the time point of 96 hours was only analysed in the second experiment which showed a greater proportion of divided cells at 72 hours compared to the first experiment. From these results we cannot determine whether the entire population would undergo cell division beyond 96 hours p.i. To better differentiate defective versus delayed priming, mice should also be analysed at later time points to see whether CTV is lost in all gDT-II cells in the ibLN. By 96 hours, but not 72 hours, following either melanoma or HSV challenge, CTV-negative gDT-II cells could be detected in the cbLN and in the spleen indicating primed gDT-II cells egress from the ipsilateral brachial lymph node into the periphery. However, at 96 hours following HSV infection the entire population of gDT-II cells were CTV-negative in the cbLN and spleen, whereas a population of undivided CTV-positive gDT-II cells were still observed in these organs 96 hours following melanoma challenge (**Figure 4.5c**).

Expression of activation markers, CD44, CD69 and CD25, was analysed by flow cytometry during the priming response at 72 hours p.i. (**Figure 4.5e**). As expected, in mice challenged with HSV and B16.gD, divided gDT-II cells universally expressed high levels of CD44, a marker of antigen-experienced T cells. When T cells encounter cognate antigen, they transiently upregulate CD69 which functions to prolong retention in the lymph node until priming is complete (Shiow et al., 2006). Accordingly, in HSV-challenged mice, CD69 was upregulated in undivided gDT-II cells (which were presumably activated based on their expression of CD44) and CD69 expression was progressively lost with

each successive cell division. The majority of undivided gDT-II cells in melanoma-challenged mice had not upregulated CD69 by 72 hours consistent with the proportion CD44-negative gDT-II cells that had not yet seen antigen at this time point. IL-2 signalling drives T cell proliferation, rendering CD25, the α-chain of the IL-2 receptor, a routinely used activation marker. Whilst there was robust CD25 upregulation by HSV-primed gDT-II cells that increased with each successive cell division, gDT-II cells which had divided in response to melanoma challenge showed very little CD25 expression.

Light-sheet fluorescence microscopy was used to visualise gDT-II cells in the lymph nodes of mice challenged epicutaneously with B16.gD melanoma one week p.i., the time at which priming is expected to have occurred based on results from CTV-labelling experiments (Figure 4.5). Lymph nodes were analysed from two mice that received naïve GFP-labelled gDT-II cells prior to inoculation with B16.gD. In the first mouse, gDT-II cells were abundant in the ibLN but interspersed at a lower cell density in ipsilateral axillary lymph node and contralateral inguinal lymph node. gDT-II cells in the ibLN were condensed in clusters reminiscent of T cell zones. The density and organisation of gDT-II cells in the ibLN corroborated that this was the location of gDT-II cell priming in the epicutaneous melanoma model (**Figure 4.6** and **Appendix: Video 1**). By comparison, in the second mouse only low numbers of gDT-II cells were observed in all analysed lymph nodes one week following inoculation. Additionally, gDT-II cells did not show clear clustering in the ibLN of the second mouse which may indicate a weaker priming response (**Figure 4.6 and Appendix: Video 2**).

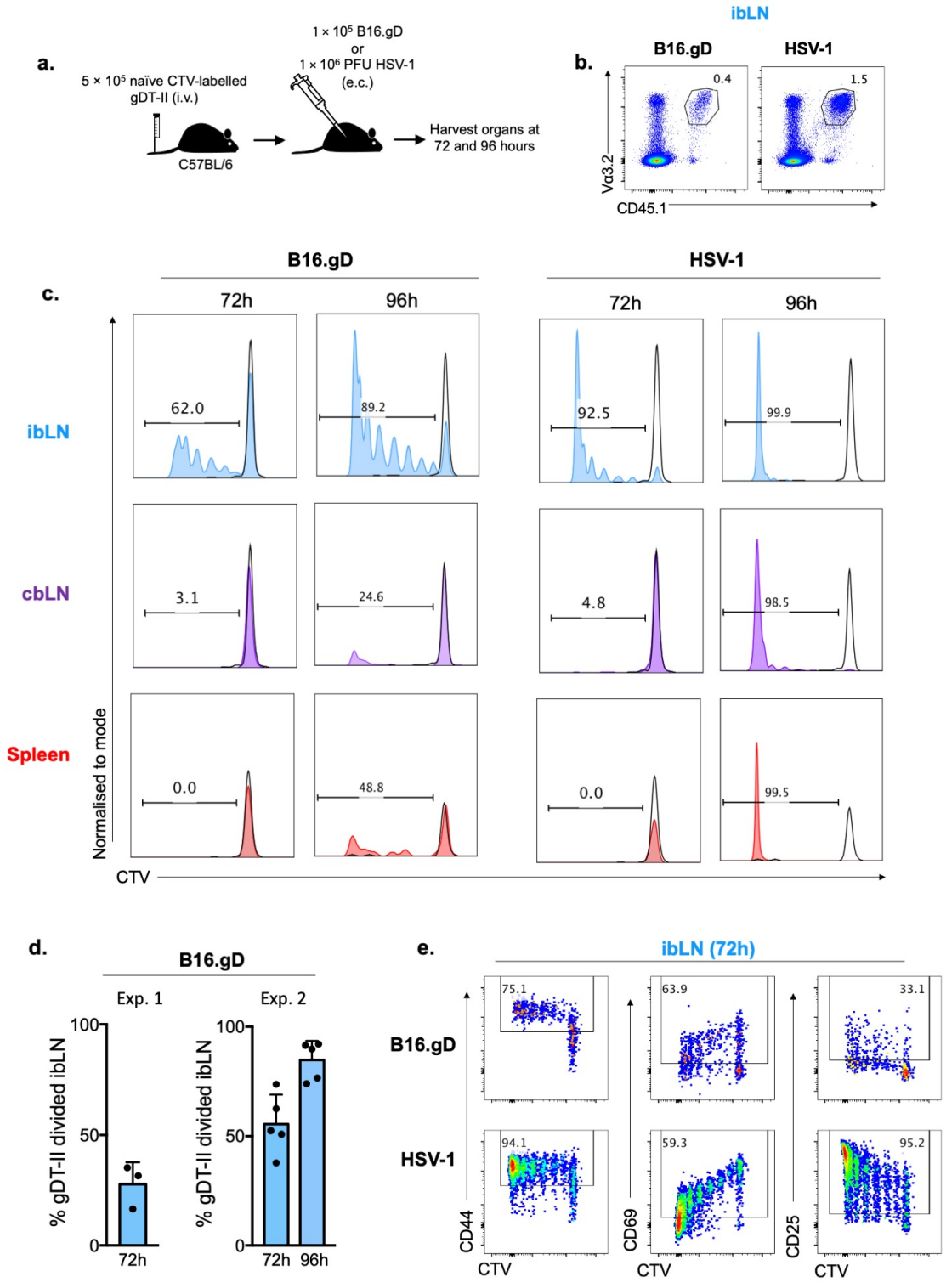

Figure 4.5. Priming of naïve gDT-II cells in the ipsilateral brachial lymph node in the epicutaneous melanoma model.

a, Schematic of experimental protocol; C57BL/6 mice received naïve, CTV-labelled gDT-II cells (5 × 10^5, i.v.) and were challenged with B16.gD cells (1 ×

10^5, e.c.) or HSV-1 (1×10^6 PFU, e.c.) the following day. The ipsilateral brachial lymph node (ibLN), contralateral brachial lymph node (cbLN) and spleen were harvested 72 and 96 hours p.i. and gDT-II cells were analysed by flow cytometry. **b,** Representative flow cytometry plots showing gating on gDT cells. Samples from ibLN of mouse inoculated with B16.gD (left) or mouse infected with HSV-1 (right). gDT-II cells ($V\alpha3.2^+CD45.1^+$) were pre-gated on DAPI-negative (live), single, $CD45.2^+$, $CD4^+$ cells. **c,** Representative flow cytometry histograms of CTV profiles of gDT-II cells. Control histogram (black) are CTV-labelled gDT-II cells harvested from unchallenged mice. Gates show percentage of cells that had diluted CTV, corresponding to % of divided cells. **d,** Percent gDT-II divided in ibLN of mice inoculated with B16.gD at 72 h or 96 h following melanoma challenge. Two separate experiments shown. Left; Experiment 1 (Exp. 1), n=3 mice at 72 h, Right; Experiment 2 (Exp. 2), n=5 at 72h and n=5 at 96h. Bars and error bars represent mean and standard deviation, respectively. **e,** Representative flow cytometry plots of gDT-II cells stained with activation markers, CD44, CD69 and CD25, plotted against CTV.

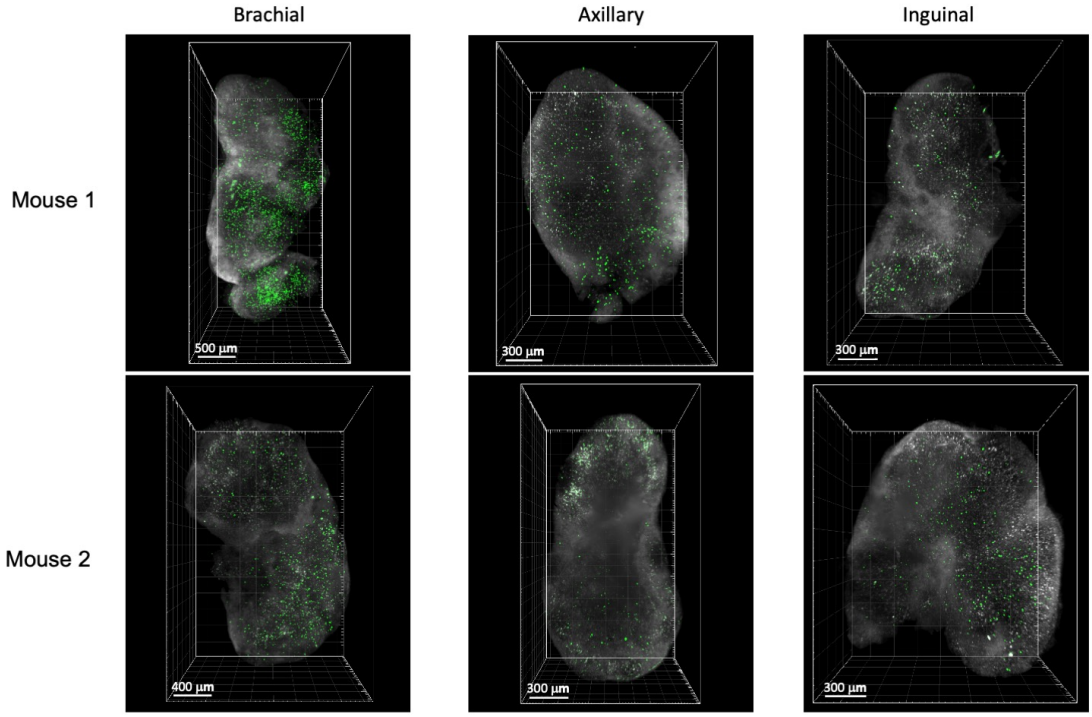

Figure 4.6. Visualisation of CD4⁺ T cells in the lymph nodes by light-sheet microscopy following epicutaneous melanoma challenge.
Two albino mice (Mouse 1; top images, and Mouse 2; bottom images) received 1×10^4 naïve gDT-II.GFP cells and were challenged with B16.gD.*Tyr*$^{-/-}$.mCherry cells (1×10^5 e.c.) the following day. Images from light-sheet microscopy of lymph nodes (ipsilateral brachial, ipsilateral auxiliary, contralateral inguinal) 8 days p.i.. Green; gDT-II.GFP, white; autofluorescence. *Light-sheet microscopy performed by Teagan Wagner.*

4.2.5 Migratory and phenotypic characteristics of CD4$^+$ T cells in the epicutaneous melanoma model.

To further characterise melanoma immunosurveillance by CD4$^+$ T cells, the phenotype and migratory patterns of gDT-II were analysed in C57BL/6 mice that remained macroscopically tumor-free (mTF) or that developed progressively growing melanoma (developer) following e.c. B16.gD melanoma challenge. To this end, gDT-II cells were analysed by flow cytometry in the ibLN, spleen and skin at the site of inoculation (mTF) or peritumoral skin and tumor (developer) at different time points p.i. (**Figure 4.7a, b**).

One week following melanoma challenge, which precedes the onset of tumor development in the e.c. melanoma model, gDT-II cells were detected in the spleen and ibLN in 6 out of 6 mice and in the skin in 5 out of 6 mice (**Figure 4.7c**). By three weeks p.i., gDT-II cells were detected in the ibLN of all mTF mice and developer mice but there were significantly more gDT-II cells in the lymph node of developer mice (**Figure 4.7d**)**.** At five and ten weeks p.i. gDT-II cells could no longer be detected in the ibLN of approximately half of the mTF mice (**Figure 4.7c**). Such waning of the memory pool of gDT-II cells was also observed in the spleen and skin. At 3 and 5 weeks p.i., the percentages of mTF mice in which gDT-II cells were detected in the spleen were 63 % and 13 %, respectively, and in the skin were 50 % and 6 %, respectively.

Enzymatic digestion for the release of T cells from skin and other nonlymphoid tissues has been shown to lead to poor isolation efficiencies when compared with microscopic assessment of T cell tissue content (Clark et al., 2006, Steinert et al., 2015, Collins et al., 2016). Accordingly, the numbers of gDT-II cells detected in the skin and tumor samples by flow cytometry are predicted to be gross underestimates but can still be informative for comparative analyses. There was no obvious difference between the number of gDT-II cells detected in the skin of mTF and peri-tumoral skin of developer mice (**Figure 4.7d**). Detection of gDT-II cells was variable and did not exceed 100 cells per 1 × 1 cm^2 skin. gDT-II cells

were detected in 74 % of tumors. There was variation in the number of intratumoral gDT-II cells detected but on average there were more gDT-II cells detected within the tumor than in the skin. Additionally, gDT-II cell numbers were higher in tumors analysed at week 3 p.i. compared to those analysed at week 5 p.i..

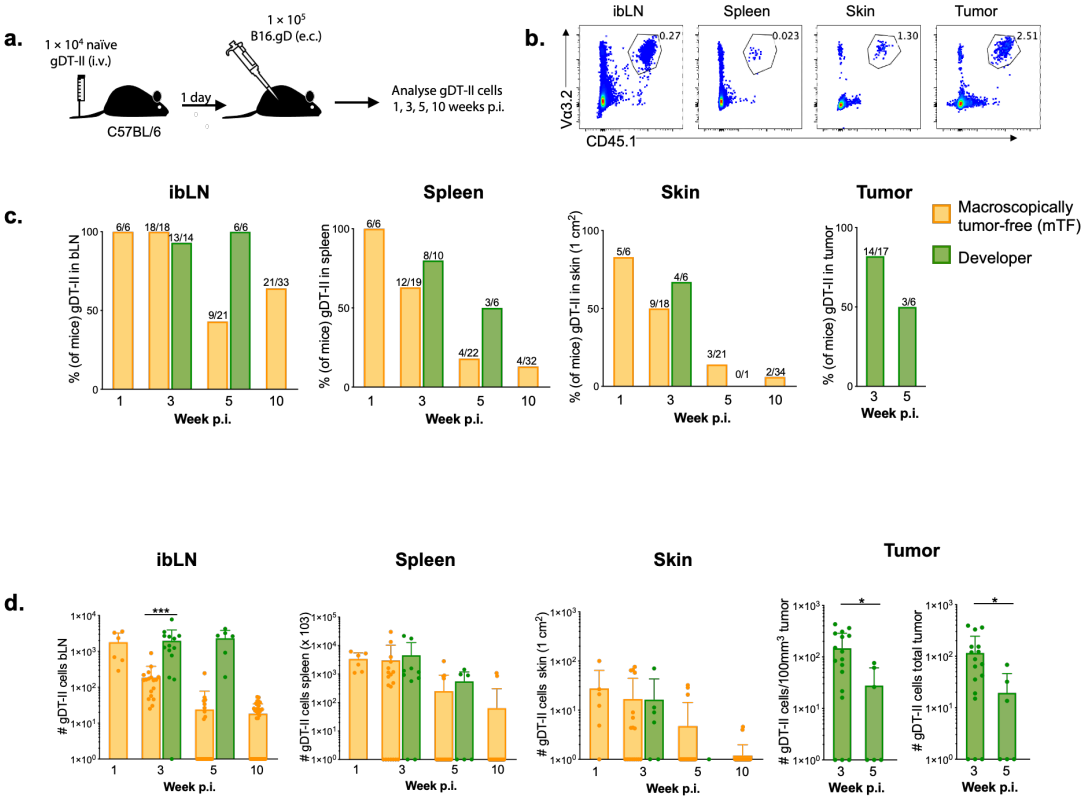

Figure 4.7. Enumeration of gDT-II cells in the e.c. melanoma model in C57BL/6 mice by flow cytometry.

a, Schematic of experimental protocol; C57BL/6 mice received naïve gDT-II cells (1×10^4 i.v.) and were challenged 1 day later with B16.gD cells (1×10^5 e.c.). Organs (spleen, ibLN, skin and tumor) were analyzed by flow cytometry 1, 3, 5 and 10 weeks p.i., from both macroscopically tumor free mice (mTF, yellow) or mice with progressively growing melanoma (developer, green). Skin was harvested as a 1×1 cm^2 section at inoculation site (mTF mice) or surrounding the tumor (developers). **b,** Representative flow cytometry plots of gating strategy for gDT-II cells (Vα3.2$^+$CD45.1$^+$) which were pre-gated on DAPI-negative, single, CD45.2$^+$, CD4$^+$ cells. **c,** Percentage (shown as bars) of mice in which gDT-II cells were detected by flow cytometry in indicated organs. Positive detection defined as ≥ 4 Vα3.2$^+$CD45.1$^+$ events in skin or tumor, ≥ 15 Vα3.2$^+$CD45.1$^+$ events in the ibLN and ≥ 12 Vα3.2$^+$CD45.1$^+$ events in 1/40 of the spleen (≥ 500 total spleen). Number of mice in each group shown above bars**. d,** Enumeration, by flow cytometry, of gDT-II cells in indicated organs. Each point represents data from a single mouse and bars and error bars depict mean and SD, respectively. Mice with gDT-II cell numbers below cut off values described in (c) are shown at 1×10^0. Data pooled from 6 biologically independent experiments. *p<0.05, ***p=0.0002, statistics determined by Mann-Whitney test.

Expression of CD44 and CD62L was analysed by flow cytometry to track T cell activation and discriminate naïve and effector/memory T cell subsets. CD44 is upregulated upon cognate antigen recognition and expression is sustained in both memory and effector T cell populations. The lymph node homing marker, CD62L, is expressed on naïve and central memory T cells, both of which recirculate between the secondary lymphoid organs (Sallusto et al., 1999). T_{EM} cells and a proportion of T_{EFF} cells lack expression of CD62L and instead upregulate a number of homing receptors that guide their migration into non-lymphoid tissue. A difference in the relative proportions of T_{CM} and T_{EFF}/T_{EM} gDT-II cell populations were observed between developer and mTF mice. In the ibLN of mTF mice at three weeks p.i., the majority of gDT-II cells displayed a $CD44^+CD62L^+$ T_{CM} cell phenotype whereas gDT-II cells were mostly $CD44^+CD62L^-$ in developer mice (**Figure 4.8a, b**). Similarly, T_{CM} cells were more prevalent than their T_{EFF}/T_{EM} counterparts in the spleen of mTF mice whereas there were approximately equal proportions of $CD44^+CD62L^+$ and $CD44^+CD62L^-$ gDT-II cells in the spleen of developers. As expected, all gDT-II cells in the skin expressed CD44, while CD62L expression could not be determined via FACS due to enzymatic cleavage of this molecule during skin preparation. In addition, phenotypic markers typically associated with $CD8^+$ T_{RM} cells in the skin, CD103 and CD69, were analysed by flow cytometry. These molecules are involved in tissue retention in peripheral organs. CD69 blocks signalling by tissue egress regulator, S1P1 (Shiow et al., 2006), whilst CD103 interacts with E-cadherin on epithelial cells (Cepek et al., 1994). CD69 could be detected on a proportion of gDT-II cells in the skin one week following melanoma challenge but CD103 was rarely detected (**Figure 4.8c, d**). At three weeks p.i. however, co-expression of CD69 and CD103 was detected on a substantial proportion of gDT-II cells in skin. This is consistent with previous reports of sequential upregulation of these molecules upon T cell entry and retention in skin (Mackay et al., 2013, Watanabe et al., 2015).

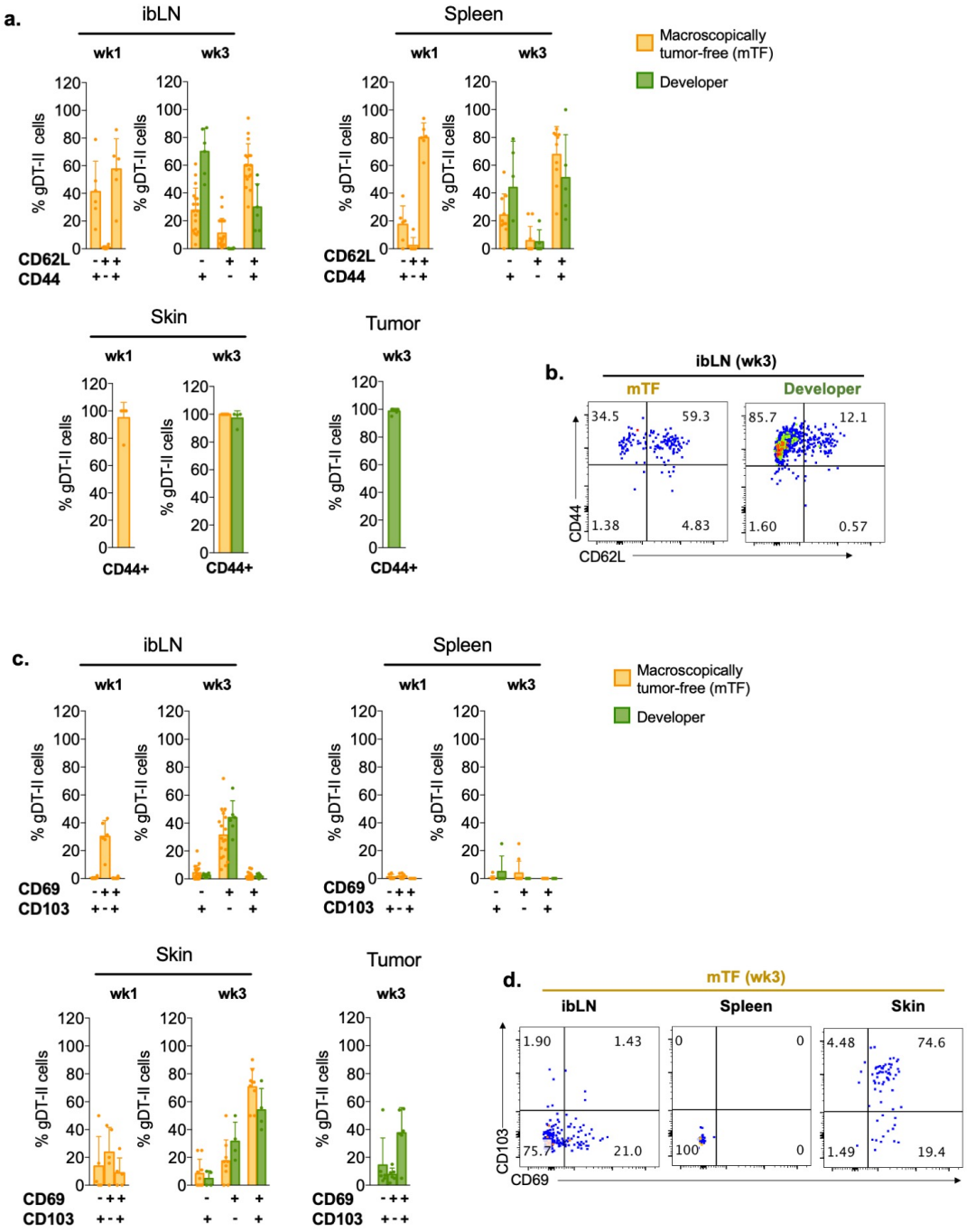

Figure 4.8. Phenotypic characterisation of gDT-II cells in the e.c. melanoma model in C57BL/6 mice by flow cytometry.
C57BL/6 mice received naïve gDT-II cells (1×10^4 i.v.) and were challenged 1 day later with B16.gD cells (1×10^5 e.c.), as in Figure 4.5. Organs (spleen, ibLN, skin and tumor) were analyzed by flow cytometry 1 and 3 weeks p.i. from both macroscopically tumor free mice (mTF, yellow) or mice with progressively growing melanoma (developer, green). Skin was harvested as a 1×1 cm^2 section at inoculation site (mTF mice) or surrounding the tumor (developers). **a, b,** Expression of CD44 and CD62L and **c, d,** CD103 and CD69 by gDT-II cells.

a, c, Each point represents data from a single mouse and bars and error bars depict mean and SD, respectively. Mice with gDT-II cell numbers below cut off values described in (Figure4.6.c) are shown at 10^0. Data pooled from 6 biologically independent experiments. *p<0.05, ***p=0.0002, statistics determined by Mann-Whitney test. **b,** Representative flow cytometry plots of CD44 and CD62L expression in ibLN of mTF mouse (left) and developer mouse (right) at wk 3 p.i. **d,** Representative flow cytometry plots of CD103 and CD69 expression in ibLN, spleen and skin of mTF mouse at wk 3 p.i..

The population of gDT-II cells contracted to very low or undetectable numbers by five weeks following inoculation in wild-type mice limiting the ability to perform phenotypic analysis of the memory pool by flow cytometry. In order to analyse gDT-II cells several weeks following inoculation by flow cytometry, *Rag1*$^{-/-}$ mice were inoculated with B16.gD melanoma subsequent to the transfer of gDT-II cells activated by peptide-pulsed splenocytes (**Figure 4.9a**). gDT-II cells could readily be detected in the ibLN, spleen and skin (inoculation site) of mTF *Rag1*$^{-/-}$ mice 10 weeks p.i. (**Figure 4.9b**)**.** Efficient cell recovery was likely due to a combination of transferring a high dose (1×10^6) of activated gDT-II cells and the open "T cell niche" in a lymphopenic environment, which enables homeostatic proliferation and facilitates survival of adoptively transferred T cells (Xie et al., 2010, Tchao and Turka, 2012). Although gDT-II cells were activated *in vitro* prior to transfer into *Rag1*$^{-/-}$ mice they exhibited a similar phenotype in terms of CD44, CD62L, CD103 and CD69 expression compared to the *in vivo* melanoma-primed gDT-II cells isolated 3 weeks p.i. from mTF wild-type mice. Uniform CD44 expression and mixed CD62L expression of gDT-II cells in the spleen and ibLN indicated the expected presence of both T_{CM} and T_{EM} or T_{EFF} subsets (**Figure 4.9c**). In the skin gDT-II cells expressed CD44 and often co-expressed CD103 and CD69 (**Figure 4.9d, e**). There were also $CD69^+$ $CD103^-$, $CD69^-$ $CD103^+$ and $CD69^-$ $CD103^-$ gDT-II cell populations present in the skin. However, in contrast to gDT-II cells analysed from wild-type mice (**Figure 4.9c**)**,** CD103 expression could be detected, and occasionally in combination with CD69, on a proportion of gDT-II cells in the ibLN and spleen (**Figure 4.9e**).

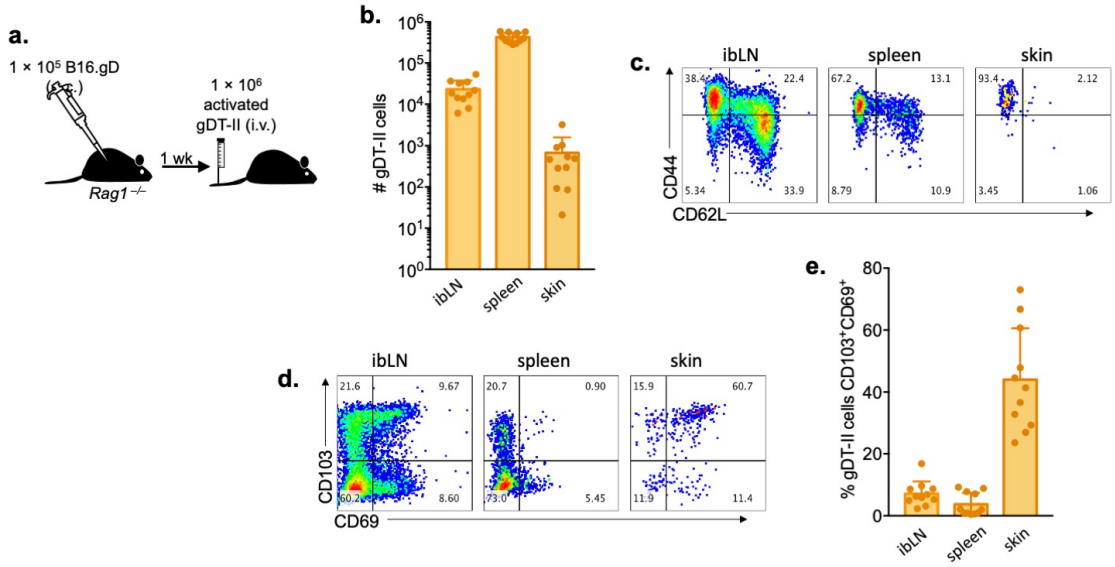

Figure 4.9. Phenotypic characterisation and enumeration of gDT-II cells in the e.c. melanoma model in *Rag1*$^{-/-}$ mice.
a, Schematic of experimental protocol; *Rag1*$^{-/-}$ mice were challenged with B16.gD cells (1 × 10^5 e.c.) and 6-7 days later received *in vitro* activated gDT-II cells (1 × 10^6 i.v.) as in Figure 4.3. The ibLN, spleen and 1 × 1 cm^2 skin from the inoculation site were harvested 10 weeks p.i. from macroscopically tumor-free mice and analyzed by flow cytometry. **b**, Total number of gDT-II cells detected in indicated organ. **c, d,** Representative flow cytometry plots of **(c)** CD44 and CD62L and **(d)** CD103 and CD69 surface expression by gDT-II cells. **e,** CD103 and CD69 surface expression by gDT-II cells indicated organs. **b, e** Data from n=11 mice, pooled from 3 biologically independent experiments. Bars and error bars depict mean and SD, respectively.

4.2.6 CD4$^+$ T cells colocalise with melanoma cells in the skin.

Two-photon microscopy was used to characterise the spatiotemporal dynamics of gDT-II cells in the skin of melanoma-challenged mice one week p.i. GFP-expressing gDT-II cells (gDT-II.GFP) were transferred into albino mice prior to inoculation with tyrosinase-deficient, mCherry-expressing B16.gD melanoma cells (B16.gD.*Tyr* $^{-/-}$.mCherry). Tyrosinase-deficient cells and albino mice both lack melanin pigment which is necessary to reduce quenching of fluorescence during imaging. The dermis was distinguished from the epidermis through visualisation of the second-harmonic generation (SHG) signal, which demarcates the collagenous dermis.

There was a degree of variability in the appearance of the inoculation site one week following melanoma challenge. In some cases, melanoma cells could not be observed in the skin. In the apparent absence of melanoma cells, gDT-II.GFP cells were also undetectable or detected at low cell numbers briefly traversing the dermis (data not shown). The inability to detect melanoma cells may result from a failure of grafting or locating low numbers of melanoma cells in flank skin, or alternatively, may reflect complete elimination of transplanted cells by the time of analysis. Conversely, in some mice, melanoma cells were clearly present at the inoculation site and were surrounded by gDT-II.GFP cells detected in the dermis and epidermis (**Figure 4.10a, b** and **Appendix video 3**). gDT-II cells in the epidermis appeared to move more slowly compared to their dermal counterparts, consistent with previous reports of reduced migratory velocities of epidermis-residing T cells, a phenomenon thought to be influenced by physical constraints of the epidermal niche (Gebhardt et al., 2011).

Whilst in some cases, melanoma cells were surrounded by gDT-II cells, the skin of one mouse harboured a defined melanoma lesion to which only 3 gDT-II cells colocalised very early after inoculation (**Figure 4.10c and Appendix video 4**). In this situation, the melanoma cells penetrated the epidermal and dermal layers whilst the gDT-II cells localised at the base of the lesion within the

dermis. The gDT-II cells adopted a rather stationary morphology and appeared to be surveilling the area around the lesion by extending and protracting cellular projections. These interactions between gDT-II.GFP cells and the melanoma lesion were sustained over the course of the three-hour analysis period. In most cases, as seen in both videos (**Appendix video 3** and **Appendix video 4**), physical distance space between the GFP and mCherry signals was observed. This suggested that the $CD4^+$ T cells and melanoma cells might not be directly in contact and other cell types, which are not fluorescently labelled, may be mediating indirect crosstalk.

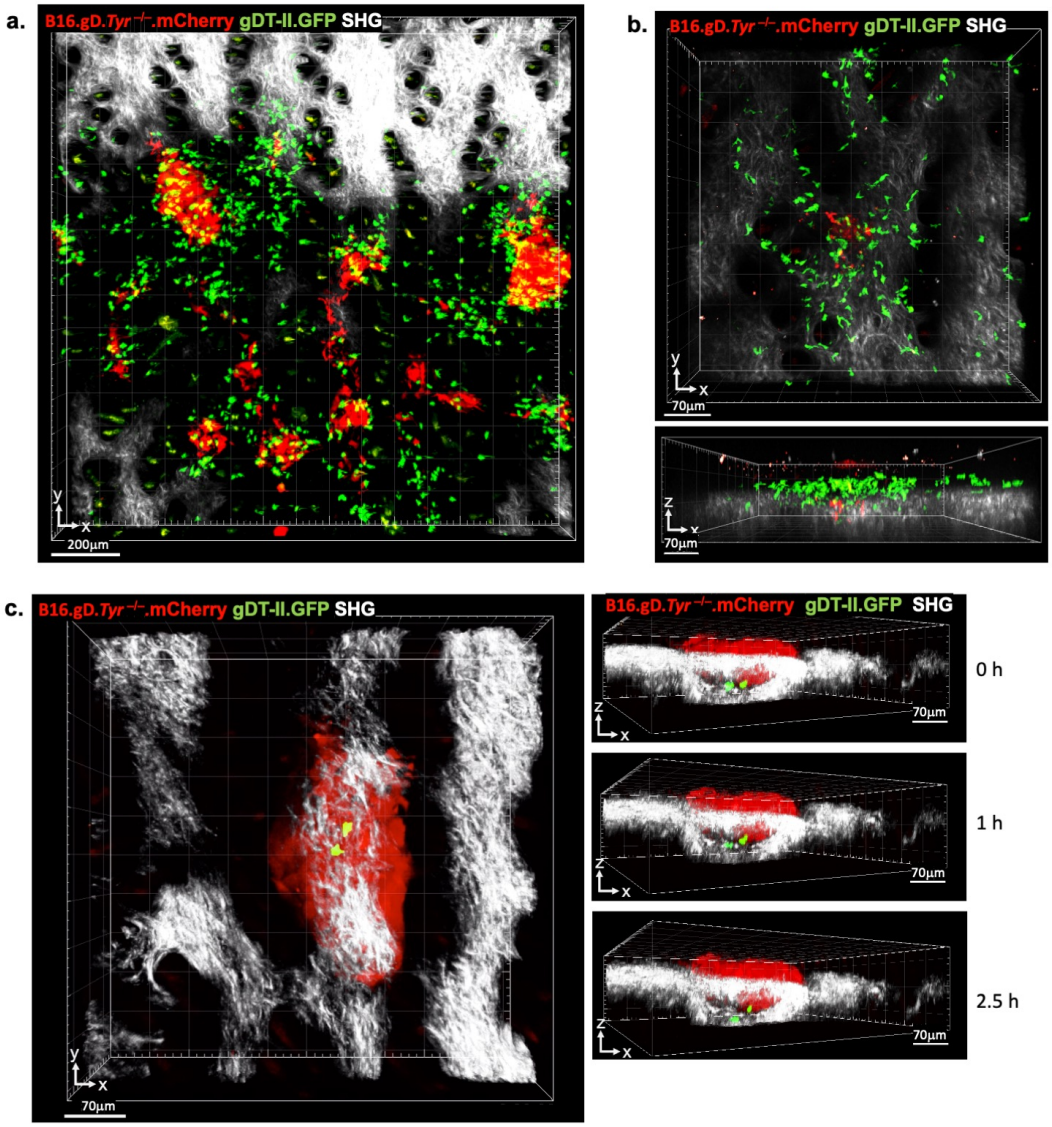

Figure 4.10. Visualisation of CD4⁺ T cells and melanoma cells in the skin in the epicutaneous melanoma model.
Two-photon microscopy images of the skin of C57BL/6 albino mice at the site of tumor inoculation 8 days p.i.. Mice received 1-4 × 10^4 naïve gDT-II.GFP cells (green) intravenously, one day prior to e.c. challenge with 1 × 10^5 B16.gD.Tyr$^{-/-}$.mCherry cells (red). Second harmonic generation signal (SHG) shown in white and autofluorescence of hair appears yellow/green. Images from three individual mice (**a, b and c**), representative of n=10 mice from four biologically independent experiments. **b,** Images from Appendix video 3 **c,** Images from Appendix video 4. Left; Time-lapse series at indicated hours from beginning of video acquisition. *Two-photon microscopy performed in collaboration with Teagan Wagner.*

4.2.7 CD4$^+$ T cells express T-bet in melanoma-challenged skin.

CD4$^+$ T cell subsets are largely defined by the expression of lineage-specific master transcription factors, which in turn drive their specific functions. The canonical master transcription factors associated with different CD4$^+$ T cell subsets were analysed using flow cytometry 8 days following e.c. melanoma challenge, a time-point that precedes development of tumors in the epicutaneous model. Prior to *ex vivo* transcription factor analysis, gDT-II cells were validated *in vitro* for their intrinsic capability to polarise into all T cell subset under established cytokine conditions (data not shown). As a control for transcription factor analysis of *in vivo*-primed gDT-II cells we used the cutaneous HSV-1 infection model in which gDT-II cells have been shown to form a population of Bcl6-expressing Tfh cells in the ibLN and a significant population of Tbet-expressing Th1 cells in the skin at the site of infection (Harpur et al., 2019, Stankovic et al., 2015). There was a similar trend of gDT-II cell polarisation in response to e.c. melanoma challenge (**Figure 4.11a, b**). Firstly, Bcl-6 was upregulated in a proportion of gDT-II cells in the ibLN but not the spleen and these cells expressed intermediate levels of PD-1, a characteristic marker of Tfh cells in germinal centres. Secondly, T-bet, was detected in a significant proportion of gDT-II cells in melanoma-challenged skin, suggesting that Th1 cells are the dominant anti-tumoral Th subset in pre-lesional skin. Interestingly, whilst the proportion of T-bet-positive gDT-II cells was similar in the skin of melanoma-challenged and HSV-challenged mice, proportions in the ibLN and spleen were appreciably lower in gDT-II cells primed in the context of melanoma. gDT-II cells with deletion of the gene encoding T-bet (gDT-II.*Tbx21*$^{-/-}$) were used as a negative control to define the gate for T-bet expression (**Figure 4.11c**). Pooled data from day 8 post-melanoma challenge showed a degree of variability in the proportion of T-bet-expressing gDT-II cells in the skin whilst T-bet expression was consistently low in the ibLN and spleen at this early timepoint (**Figure 4.11d**).

RORγt and GATA3, the transcription factors associated with Th17 and Th2

subsets, respectively, were detected in a small proportion (10-20 %) of gDT-II cells in the inoculation site skin but not within the spleen or ibLN, 8 days following melanoma challenge (**Figure 4.11a, b**). GATA3 expression has also been described for Th9 cells, however, to date there is no known lineage-specific transcription factor to define this subset (Malik and Awasthi, 2018). FoxP3, the transcription factor associated with suppressive Treg cells, was not detected in gDT-II cells in the skin, ibLN or spleen of melanoma-challenged mice. Except for the gDT-II.*Tbx21*$^{-/-}$ cells, gDT-II cells deficient in transcription factors were not available for use as negative controls. As such, gates for Bcl6, GATA3, RORγt and FoxP3 were selected based on staining of endogenous populations of lymphocytes in the respective organs (data not shown). Therefore, relative proportions of the less abundant transcription factors cannot be fully determined from flow cytometry alone. Results from transcription factor staining suggested that T-bet-expressing gDT-II cells are the dominant subset in pre-lesional melanoma-challenged skin although a smaller proportion of gDT-II cells express transcription factors associated with Th2, Th9 or Th17 subsets, but not with Treg cells. This heterogeneity was more apparent in the melanoma challenged skin compared to HSV-challenged skin.

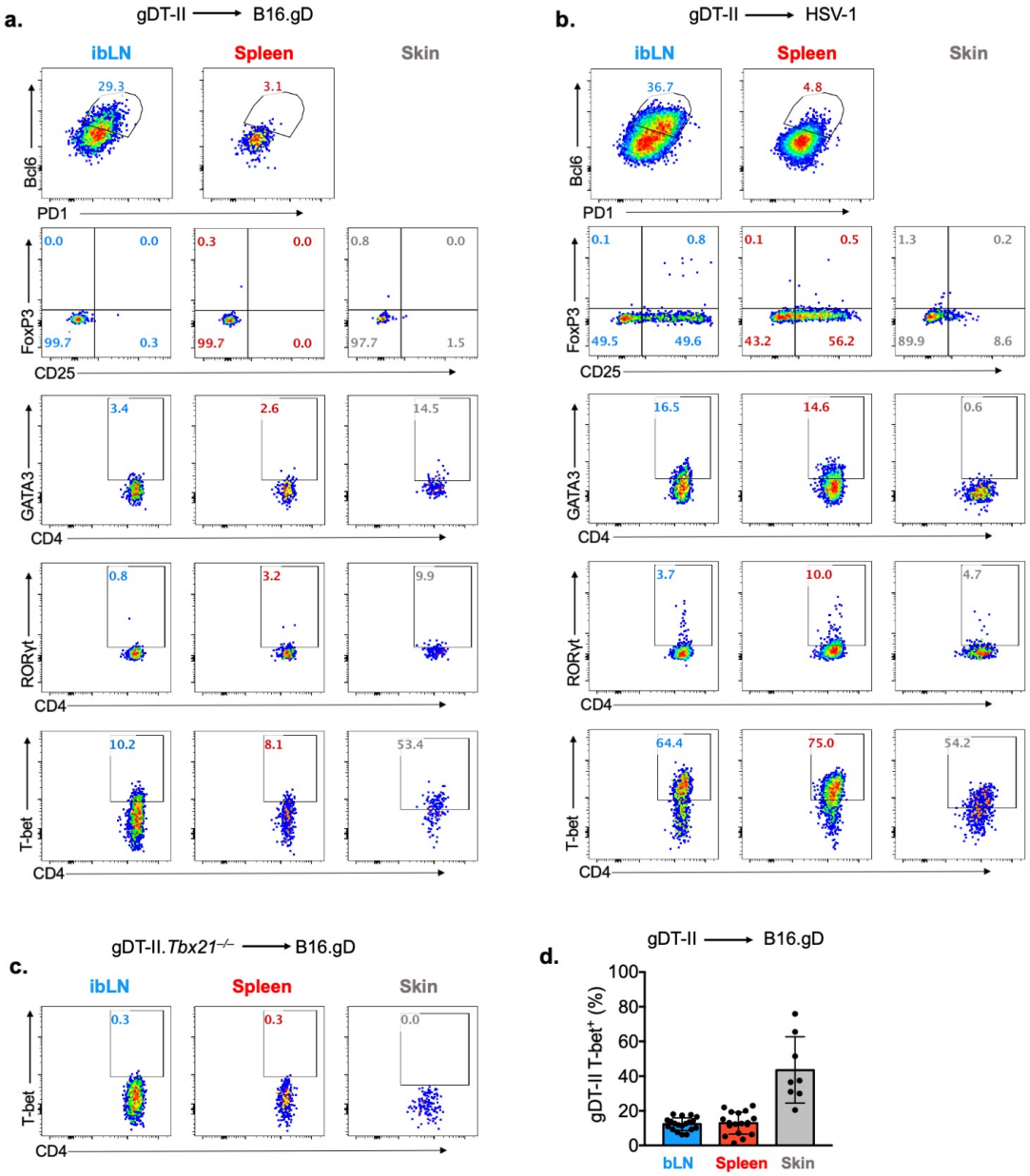

Figure 4.11. Transcription factor profile of gDT-II cells on day 8 following epicutaneous melanoma challenge.
Intracellular expression of transcription factors by gDT-II cells analysed by flow cytometry. C57BL/6 mice received wild-type gDT-II cells **(a, b, d)** or gDT-II.*Tbx21*$^{-/-}$ cells **(c),** (naïve, 1 × 10^4 i.v.), one day prior to challenge with B16.gD (1 × 10^5 e.c.) **(a, c, d)** or 1 × 10^6 PFU HSV-KOS **(b)**. Cells analysed on day 8 p.i. from ibLN, spleen and 1 × 1 cm^2 skin at inoculation site (skin). **a-c,** Representative flow cytometry plots. **d,** Percentage of gDT-II cells expressing T-bet in B16.gD-challenged mice from n=8 mice (skin), n=18 mice (spleen), n=19 mice (ibLN) pooled from 4 biologically independent experiments. Positive gate defined using *ex vivo*-derived gDT-II.*Tbx21*$^{-/-}$ cells from respective organs as a negative control **(c)**. Data in **(d)** includes mice with ≥ 10 gDT-II cells detected in skin, ≥ 50 gDT-II cells detected in the ibLN and ≥ 50 gDT-II cells detected in 1/40 of the spleen.

4.2.8 Investigating the role of T-bet expression by CD4$^+$ T cells in melanoma immunosurveillance.

Since gDT-II cells expressed T-bet at the site of melanoma challenge, we hypothesized that Th1 cells play a peripheral effector role to contribute to protection against melanoma development. To further investigate the role of T-bet in the antitumoral function of CD4$^+$ T cells, gDT-II cells with a deletion of the gene encoding T-bet (gDT-II.*Tbx21*$^{-/-}$) were adoptively transferred into wild-type mice prior to epicutaneous melanoma challenge with B16.gD (**Figure 4.12a**)**.** Mice that received gDT-II.*Tbx21*$^{-/-}$ cells exhibited a higher incidence of tumor development, compared to mice that received wild-type gDT-II cells, and an equivalent incidence to naïve control mice that did not receive gDT-II cells (**Figure 4.12b**)**.** However, 27 % (4/15) of the "developer" gDT-II.*Tbx21*$^{-/-}$-recipient mice presented with persistent lesions suspected to be "controlled" melanomas (**Appendix figure 1-4**). In contrast, there were no persistent lesions in the naïve control group and 22 % (2/9) of developer mice in the gDT-II-recipient group presented with suspected persistent melanoma (**Appendix figure 5, 6**)**.** As such, when comparing incidence of progressing lesions only, the difference between mice receiving gDT-II or gDT-II.*Tbx21*$^{-/-}$ cells was not statistically significant (**Figure 4.12c, d**)**.**

All gDT-II.*Tbx21*$^{-/-}$ recipient mice with progressing primary lesions presented with lymph node metastasis which were mostly overt or dominant in size. By contrast, only 57 % (4/7) of the gDT-II-recipient mice with progressively growing primary tumors had an observable brachial lymph node metastasis. None of the mice with non-progressing primary lesions had an observable lymph node metastasis (**Figure 4.12e**)**.** The absence of T-bet expression in gDT-II.*Tbx21*$^{-/-}$ cells was confirmed by flow cytometry (**Figure 4.12f**)**.** In addition, transcription factor analysis revealed that a larger proportion of gDT-II.*Tbx21*$^{-/-}$ cells in the skin expressed Th17-associated transcription factor RORγT compared to wild-type gDT-II cells.

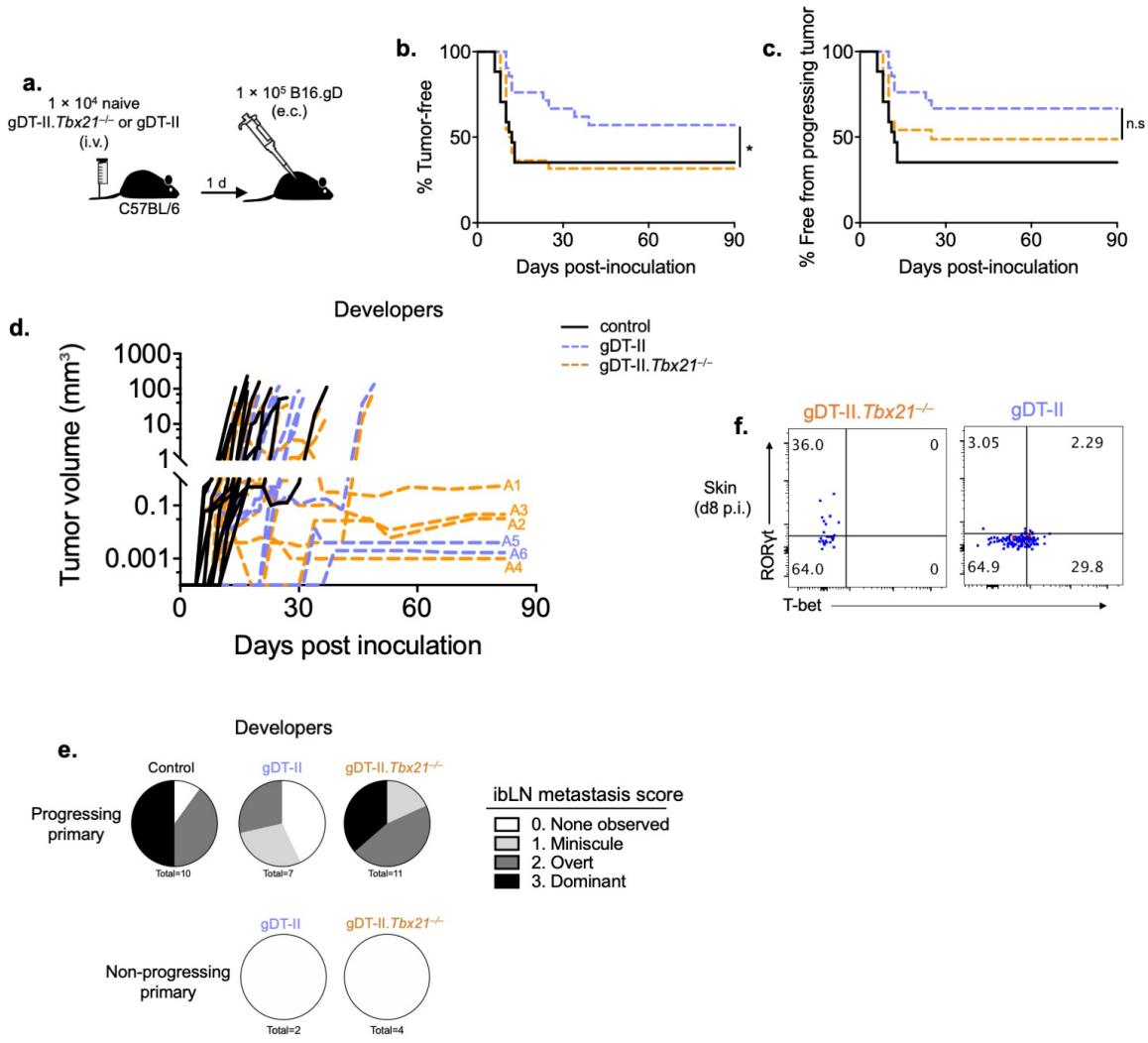

Figure 4.12. Investigating the role of T-bet expression by CD4⁺ T cells in melanoma immunosurveillance in C57BL/6 mice.

a, Schematic of experimental protocol; C57BL/6 mice received naïve gDT-II cells or gDT-II.*Tbx21*$^{-/-}$ cells (1 × 10^4 i.v.) and were challenged the following day with B16.gD cells (1 × 10^5 e.c), in parallel with naïve (control) mice. **b, c,** Primary tumor incidence; n=17 (control), n=21 (gDT-II), n=22 (gDT-II.*Tbx21*$^{-/-}$), data pooled from 3 biologically independent experiments. **b,** Incidence of mice that developed progressing tumors or showed signs of persistent melanoma. **c,** Incidence of mice that developed a progressing tumor. **d,** Primary tumor growth kinetics (progressing and non-progressing lesions). Photographical and histological evidence of persistent lesions labelled A1-A6 are provided in Appendix Figure 1-6, respectively. **e,** Incidence of brachial lymph node metastasis observed in mice with progressively growing primary tumors (top row), harvested when tumor volume >20 mm^3, or non-progressing lesions (bottom row). Metastases scored from 0-3 based on the surface area of black pigment observed; 0 corresponds to no observable pigment, 1 corresponds to pigment <0.5 mm^2, 2 corresponds to

pigment 0.5-1.5 mm^2, 3 corresponds to pigment >2.0 mm^2. Data pooled from 3 biologically independent experiments. **f,** FACS plots of RorγT and T-bet expression in gDT-II.*Tbx21*$^{-/-}$ cells (left) and gDT-II cells (right) from the skin 8 days p.i. Representative of n=3 mice (gDT-II.*Tbx21*$^{-/-}$) or n=8 (gDT-II).

The role of T-bet expression by $CD4^+$ T cells in control of melanoma was further investigated in an experiment with *Rag2*$^{-/-}$*;Il2rg*$^{-/-}$ mice (**Figure 4.13a**). Interestingly, 2/5 *Rag2*$^{-/-}$*;Il2rg*$^{-/-}$ mice that received activated gDT-II.*Tbx21*$^{-/-}$ cells presented with persistent lesions (**Appendix Figure 7, 8**), whilst the remainder remained macroscopically tumor-free (**Figure 4.13b-d**). As expected, neither progressing or non-progressing lesions were observed in the *Rag2*$^{-/-}$*;Il2rg*$^{-/-}$ mice receiving wild-type gDT-II cells. Three out of five naïve *Rag2*$^{-/-}$*;Il2rg*$^{-/-}$ mice developed progressing tumors and the remaining two presented with signs of persistent lesions **(Appendix Figure 9, 10**)**.** In all cases, the persistent lesions were miniscule and whether they contained bona fide live melanoma cells was not confirmed, although cells of a similar morphology to melanoma cells were identified by histology in all cases (**Appendix Figure 7-10**)**.**

Similar to gDT-II.*Tbx21*$^{-/-}$ cells in the skin 8 days p.i. in C57BL/6 mice (**Figure 4.12f**), gDT-II.*Tbx21*$^{-/-}$ cells expressed RORγT in the skin 64 days p.i. in non-developer *Rag2*$^{-/-}$*;Il2rg*$^{-/-}$ mice (**Figure 4.13e**)**.** Interestingly, a proportion of the wild-type gDT-II cells in the skin of *Rag2*$^{-/-}$*;Il2rg*$^{-/-}$ also expressed RORγT 64 days p.i., albeit a smaller proportion than the gDT-II.*Tbx21*$^{-/-}$ cells.

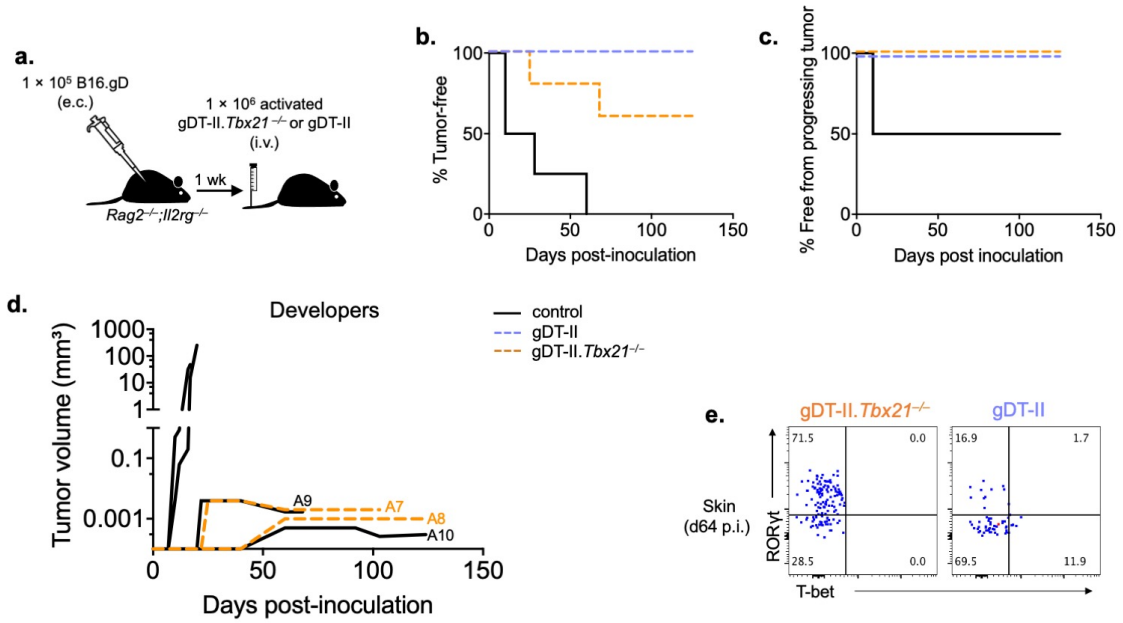

Figure 4.13. Investigating the role of T-bet expression by CD4⁺ T cells in melanoma immunosurveillance in *Rag2*$^{-/-}$*;Il2rg*$^{-/-}$ mice.
a, Schematic of experimental protocol*; Rag2*$^{-/-}$*;Il2rg*$^{-/-}$ mice were challenged with B16.gD cells (1 × 10^5 e.c.) and received either *in vitro* activated gDT-II cells, gDT-II.*Tbx21*$^{-/-}$ cells (1 × 10^6 i.v.) or did not receive T cells (control). **b, c,** Primary tumor incidence; n=4 (control), n=5 (gDT-II), n=5 (gDT-II.*Tbx21*$^{-/-}$), data from a single experiment. **d,** Incidence of mice that developed progressing tumors or showed signs of persistent melanoma. **c,** Incidence of mice that developed a progressing tumor. **e,** Primary tumor growth kinetics (progressing and non-progressing lesions). Photographical and histological evidence of persistent lesions labelled A7-A10 are provided in Appendix Figures 7-10, respectively. **,** FACS plots of RorγT and T-bet expression in gDT-II.*Tbx21*$^{-/-}$ cells (left) and gDT-II cells (right) from the skin 64 days p.i. in non-developer mice. Representative of n=2 mice/group.

4.2.9 A large proportion of tumor-infiltrating CD4$^+$ T cells express FoxP3.

Treg cells form a heterogeneous population of suppressive CD4$^+$ T cells that inhibit the functionality and survival of other cells via multiple mechanisms. Since Treg cells are frequently reported in tumors and can play a role in suppressing anti-tumoral immunity (Paluskievicz et al., 2019), markers routinely used to identify CD4$^+$ Treg cells, FoxP3 and CD25, were analysed in this study. FoxP3-expressing CD4$^+$ T cells that lack CD25 expression have also recently been identified in a number of studies but the functionality of these cells is not well defined (Yin et al., 2018, Ferreira et al., 2017).

Developer mice inoculated with B16.gD were analysed when tumor volume exceeded 50 mm^3 which generally transpired between 3 and 5 weeks p.i.. In contrast to analysis one-week p.i., at which time FoxP3 was not detected in any gDT-II cells from the ibLN, spleen or pre-lesional skin (**Figure 4.11b**), over half of the tumor-infiltrating gDT-II cells expressed FoxP3 (**Figure 4.14 a, b**). In developer mice, approximately 10 % of gDT-II cells in the ibLN expressed FoxP3 whilst the number of gDT-II cells recovered in the spleen was too low for phenotypic analysis. Both FoxP3$^+$CD25$^-$ and FoxP3$^+$CD25$^+$ gDT-II cell populations were identified in the ibLN and tumor.

FoxP3 was also detected in approximately half of the endogenous tumor-infiltrating CD4$^+$ T cells and both FoxP3$^+$CD25$^-$ and FoxP3$^+$CD25$^+$ populations were identified although relative proportions were biased towards the double-positive conventional Treg phenotype (**Figure 4.14 c, d**). In spleens and ibLNs of developer mice approximately 15 % of endogenous CD4$^+$ T cells were FoxP3$^+$ the majority of which co-expressed CD25$^+$.

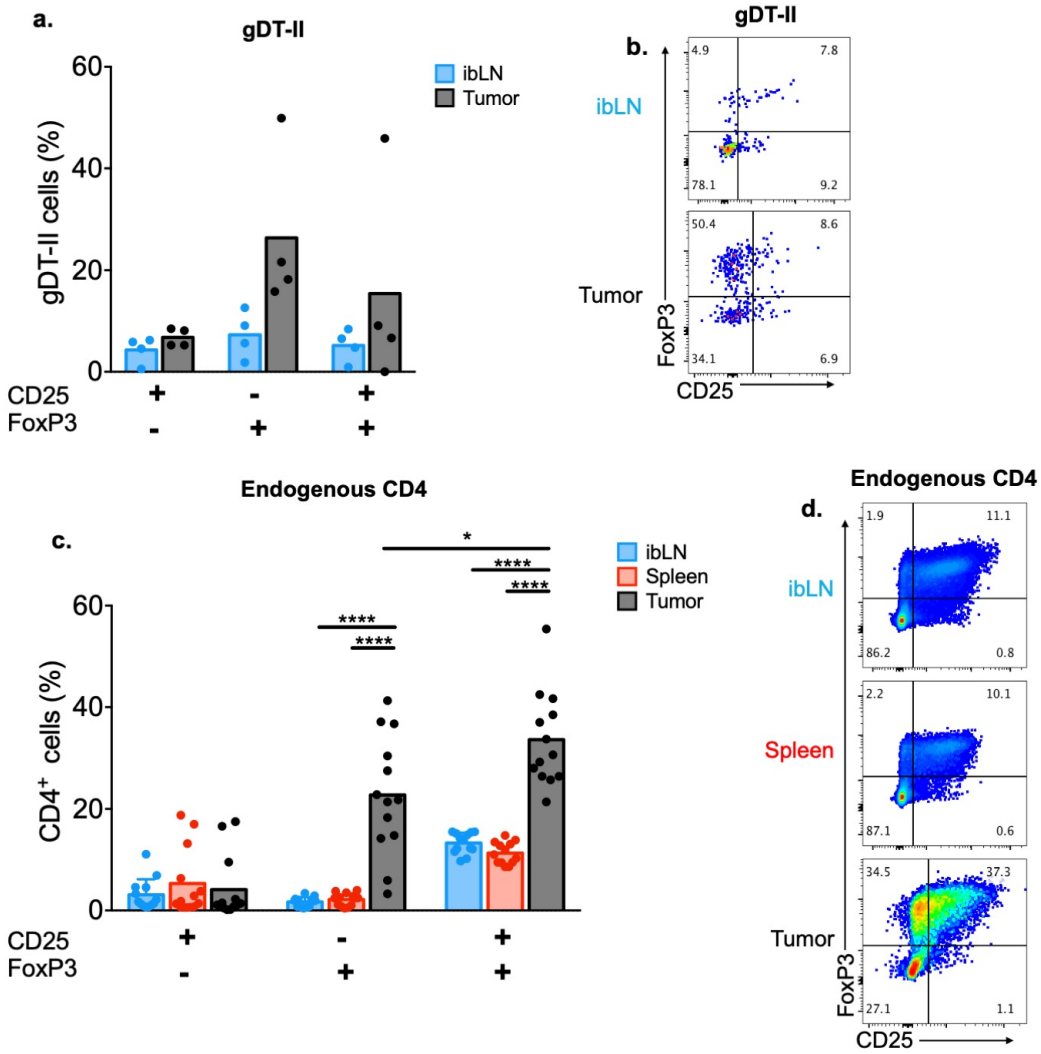

Figure 4.14. FoxP3 expressing CD4⁺ T cells are abundant in B16.gD tumors. Analysis of FoxP3 and CD25 expression by flow cytometry from C57BL/6 developer mice challenged with B16.gD cells (1×10^5 e.c.). Analysis performed when volume >50 mm^3 which occurred between 3-5 weeks p.i. **a,** Analysis of gDT-II cells in tumors and ibLN of developer mice that received naïve gDT-II cells (1×10^4 i.v.) prior to tumor challenge. Data includes tumors in which >19 gDT-II cells were detected and ibLNs in which >200 gDT-II cells were detected by flow cytometry; n=4 mice from two biologically independent experiments. Number of gDT-II cells in spleen was too low for phenotypic analysis. **b,** Representative flow cytometry plots of FoxP3 and CD25 expression in gDT-II cells from the ibLN and tumor. **c,** Analysis of endogenous CD4⁺ T cells (CD45.2⁺ CD4⁺) in the ibLN, spleen and tumor; n=13 mice from two biologically independent experiments. Data pooled from mice that received naïve gDT-II cells (1×10^4 i.v.) prior to inoculation and naïve mice (no gDT-II transfer). **d,** Representative flow cytometry plots of FoxP3 and CD25 expression in endogenous CD4⁺ T cells. *p<0.05, ****p<0.0001, ns=not significant, statistics determined by Mann-Whitney test. Statistics only performed for data in **(c)** due to small sample size for data in **(a)**.

4.2.10 Anti-tumoral CD4$^+$ T cells express several effector molecules and Th1 cytokines.

gDT-II cells were able to control B16.gD melanoma in the absence of CD8$^+$ T cells and B cells in Rag-deficient mice, indicating their role in melanoma immunosurveillance goes beyond the classical “helper” function. Furthermore, gDT-II cells were shown to infiltrate the skin following epicutaneous melanoma challenge and co-localise with melanoma cells suggesting they exert effector functions *in situ.* Possible effector mechanisms included both the direct induction of cell death in melanoma cells or the modulation of the tumor microenvironment which leads to killing of melanoma cells by other cell types. To gain insight into possible direct killing mechanisms, effector molecules involved in classical T cell killing pathways were analysed by flow cytometry.

Granzyme B and perforin are important effector molecules in the granule-mediated killing pathway (Chowdhury and Lieberman, 2008). Granzyme B was analysed by flow cytometry 8 days following epicutaneous B16.gD inoculation in C57BL/6 mice that had received naïve gDT-II cells (**Figure 4.15a, b**). Activated NK cells express high levels of granzyme B and were used as a positive control for granzyme B detection. Granzyme B was detected in 10-30 % of *in vivo* primed gDT-II cells and in a small proportion of endogenous CD4$^+$ T cells in the skin at the site of melanoma inoculation. Less than 2 % of gDT-II cells and endogenous CD4$^+$ T cells from ibLN and spleens stained positive for granzyme B. Interestingly, over 80 % of gDT-II cells in HSV-challenged skin expressed granzyme B, demonstrating another phenotypic disparity between CD4$^+$ T cells primed in the context of HSV and melanoma (**Figure 4.15b**). Expression of granzyme B by gDT-II cells in the cutaneous HSV-1 infection model has not been published although it is well-established that virus-specific CD4$^+$ T cells can express granzyme B (Johnson et al., 2008, van Leeuwen et al., 2004). Granzyme B was also highly expressed by *in vitro* activated gDT-II cells analysed directly from cell culture media (**Figure 4.15c**). Rested gDT-II cells removed from cell culture media for 10 hours showed an obvious decrease in granzyme B

expression, indicating that activated gDT-II cells may require sustained activating signals such as those in the conditioned cell culture media, to sustain production of granzyme B. There was a slight positive shift in perforin staining of *in vitro* activated gDT-II cells, compared to *in vitro* activated gDT-II.*Prf1*$^{-/-}$ cells suggesting that perforin is expressed, albeit at low levels, by *in vitro* activated gDT-II cells (**Figure 4.15d**).

Engagement with the cell death receptor Fas, by its ligand, FasL, leads to cell death, generally by initiation of Caspase-mediated apoptosis (Russell and Ley, 2002). To determine whether FasL was expressed on melanoma-specific CD4^{+} T cells, gDT-II cells were isolated from the spleens of B16.gD-challenged non-developer *Rag2*$^{-/-}$*;Il2rg*$^{-/-}$ mice and assessed for FasL expression via flow cytometry (**Figure 4.15e**). FasL expression was undetectable on the cell surface but was detectable in the intracellular compartment of splenic gDT-II cells analysed directly *ex vivo*. Following non-specific re-stimulation with PMA and ionomycin, and inhibition of vesicle secretion using BFA, there was a substantial increase in levels of extracellular and intracellular FasL. Since BFA inhibits vesicle transport from the Golgi network, newly synthesized FasL would be prevented from translocating to the cell membrane. Therefore, the increase in extracellular FasL of restimulated gDT-II cells is likely due to the translocation of preformed intracellular FasL stores that existed on the inner leaflet of the cell membrane prior to restimulation. This is supported by the fact that intracellular FasL expression on unstimulated gDT-II cells was similar to the levels of extracellular FasL expression on stimulated gDT-II cells. The increase in intracellular FasL expression on restimulated gDT-II cells suggests that de novo synthesis of FasL occurred during restimulation.

Production of classical Th1 cytokines, TNFα and IFNγ, by gDT-II cells isolated from the spleens of B16.gD-challenged mTF *Rag2*$^{-/-}$*;Il2rg*$^{-/-}$ mice was analysed by flow cytometry (**Figure 4.15f**). Approximately 95 % of gDT-II cells produced TNFα of which 40 % additionally produced IFNγ upon restimulation with PMA and Ionomycin. Of note, this bias towards TNFα production relative to IFNγ was also

observed when gDT-II cells were stimulated by B16.gD cells *in vitro* (**Figure 3.2c**)**.** In both experiments, gDT-II cells had been pre-activated *in vitro* using gD peptide-pulsed splenocytes and IL-2. This suggests that this *in vitro* activating method favours polarisation into a Th1-like phenotype, and this phenotype is preserved in gDT-II cells transferred into *Rag2*$^{-/-}$*;Il2rg*$^{-/-}$ mice*.* It is important to consider that this cytokine profile may differ from gDT-II cells primed *in vivo* in B16.gD-challenged wild-type mice.

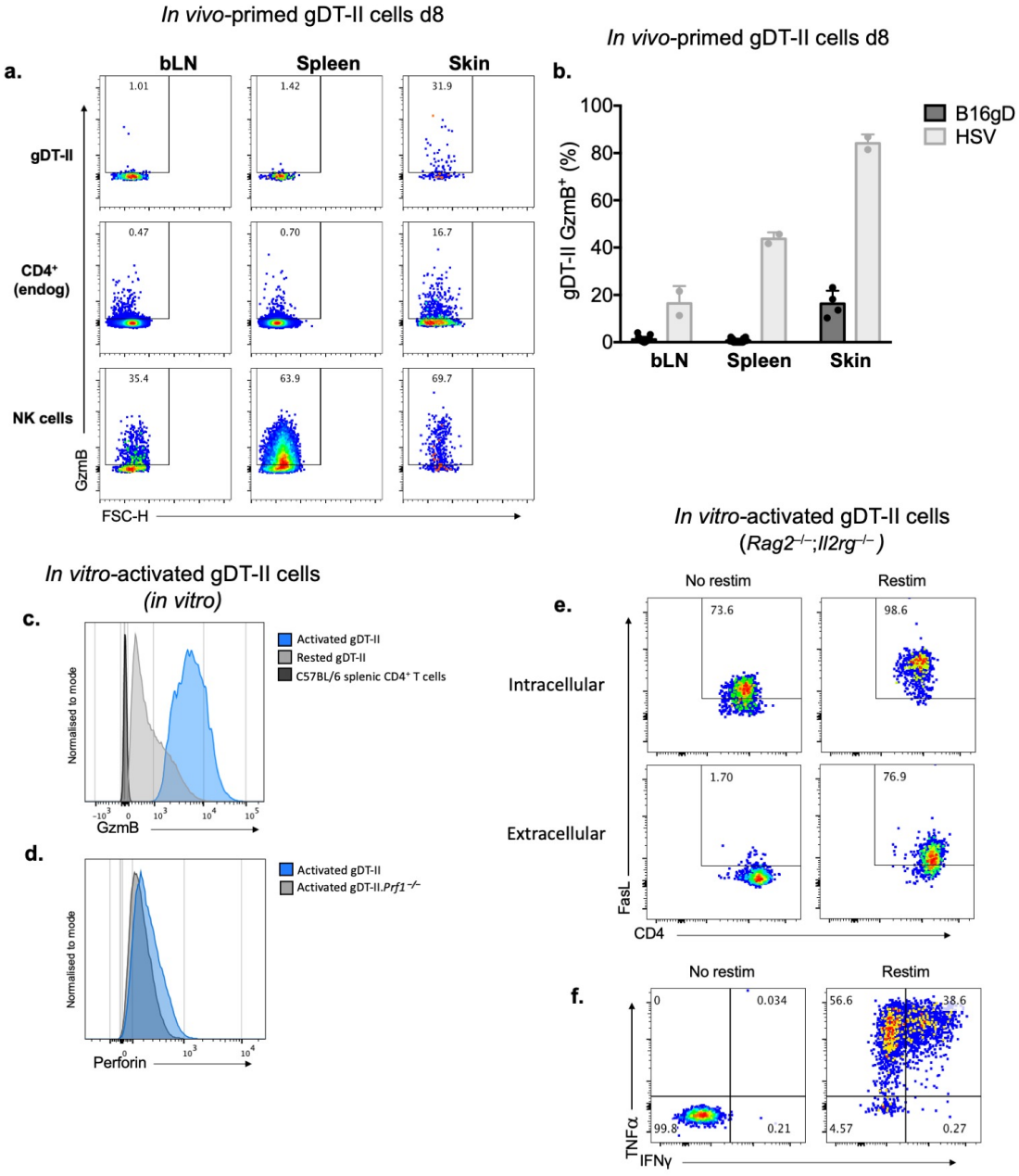

Figure 4.15. Analysis of effector molecules, Granzyme B, Perforin, FasL, TNFα and IFNγ expressed by gDT-II cells.

a-b, C57BL/6 mice received naïve gDT-II cells (1×10^4 i.v.) one day prior to challenge with B16.gD (1×10^5 e.c.) or HSV-KOS (1×10^6 PFU e.c.). Granzyme B (GzmB) expression was analysed by flow cytometry in the ibLN, spleen and 1×1 cm^2 skin at site of inoculation (skin) 8 days p.i.. **a,** Representative flow cytometry plots of GzmB expression in gDT-II cells (CD4$^+$ Vα3.2$^+$ CD45.1$^+$), endogenous (endog) CD4$^+$ T cells (CD45.2$^+$ CD4$^+$ CD3$^+$) and NK cells (NK1.1$^+$CD3$^-$) from mice challenged with B16.gD. **b,** Percentage of GzmB$^+$ gDT-II cells. Data pooled from two biologically independent experiments (for B16.gD challenge) with n=15 mice (ibLN, spleen), n=4 mice (skin). Data for HSV-infection

are from a single experiment with n=2 mice. Each point represents data from a single mouse. Bars and error bars depict mean and SD, respectively. **c,** Flow cytometric analysis of intracellular GzmB in *in vitro* activated gDT-II cells (blue), *in vitro* activated gDT-II cells removed from conditioned cell culture media for 10 hours and enriched by magnetic-activated cell sorting (briefly rested, grey), and endogenous $CD4^+CD8^-$ cells from spleens of C57BL/6 mice (black). **d,** Flow cytometric analysis of intracellular perforin in *in vitro* activated gDT-II (blue) and gDT-II.*Prf1*$^{-/-}$ cells (grey). **e-f** *Rag2*$^{-/-}$;*Il2rg*$^{-/-}$ mice were challenged with B16.gD (1×10^5 e.c) 6 days prior to receiving *in vitro* activated gDT-II cells (1×10^6 i.v.). Splenic cells were isolated on day 20 p.i. (macroscopically tumor-free mice) and re-stimulated with PMA/Ionomycin in the presence of BFA (restim), or left unstimulated (no restim) and analysed by flow cytometry; **e,** Flow cytometry plots of gDT-II cells stained with Fas-L either extracellularly (bottom panels) or intracellularly following permeabilization (top panels). **f,** Flow cytometry plots of gDT-II cells stained with TNFα and IFNγ intracellularly following permeabilization.

4.3 Discussion

In this study, adoptive transfer of gDT-II cells into Rag-deficient mice which lack an adaptive immune system provided complete protection against melanoma development. This finding provides direct evidence that $CD4^+$ T cells can control melanoma in the absence of $CD8^+$ T cells, B cells and NK cells. This suggests $CD4^+$ T cells mediate peripheral effector functions but does not preclude that $CD4^+$ cells play a “helper” role to endogenous $CD8^+$ T cells and B cells in wild-type mice in the e.c. melanoma model. In order to elicit anti-tumoral activity by $CD4^+$ T cells, many studies have used genetically immunocompromised or lymphodepleted mice to enhance proliferation and survival of adoptively transferred $CD4^+$ T cells (Shklovskaya et al., 2016, Hirschhorn-Cymerman et al., 2012, Quezada et al., 2010). In addition, administration of immunomodulatory drugs such as immune checkpoint inhibitor, CTLA-4, has been required to support $CD4^+$ T cell-mediated immunosurveillance in some melanoma models (Hirschhorn-Cymerman et al., 2012, Quezada et al., 2010). Furthermore, some studies required a high transfer dose of TCR-transgenic $CD4^+$ T cells to mediate tumor control (Malandro et al., 2016). By contrast, this study established a model in which the transfer of as few as 1×10^4 naïve antigen-specific $CD4^+$ T cells were capable of preventing melanoma development in a proportion of wild-type mice. Furthermore, it has been estimated that only 10 % of naïve T cells survive adoptive transfer, which would mean that the transfer dose of 1×10^4 gDT-II cells approximates a precursor number of 1×10^3 gDT-II cells in recipient mice (Blattman et al., 2002, Hataye et al., 2006). It has been shown that high precursor frequency of adoptively transferred TCR-transgenic T cells caused intraclonal competition leading to impaired differentiation and memory formation (Hataye et al., 2006, Foulds and Shen, 2006, Marzo et al., 2005). The low transfer dose of naïve gDT-II cells was thus used to prevent possible defects in maturation of the transferred cells that could be caused at higher precursor frequencies and therefore better model the formation of an endogenous $CD4^+$ T cell response to melanoma. The protection against melanoma development that occurred from the transfer of as few as 1×10^4 gDT-II cells in wild-type mice corroborates that

CD4$^+$ T cells play significant role in melanoma immunosurveillance.

The ability of CD4$^+$ T cells to potently induce protection in this system may be attributable, at least in part, to the epicutaneous route of tumor inoculation in contrast to models of subcutaneously or intradermally lodged melanoma cells. Tumors develop later in the e.c. model which may be due to poor survival or delayed proliferation of melanoma cells. The immune system is one important determinant for the delayed tumor development, evidenced by the fact that tumors grow rapidly in immunodeficient mice in the e.c model. In addition, tumor growth kinetics is likely contributed to by intrinsic properties of the melanoma cells. Regardless of the underlying mechanisms, the delay in tumor development may provide the immune system with additional time to mount an effective adaptive immune response before tumor growth outpaces melanoma cell elimination. It has previously been shown that the route of tumor inoculation has a direct impact on the immunogenicity of the tumor. Intradermal tumors elicit better CD4$^+$ and CD8$^+$ T cell priming than s.c. transplanted tumors due to more efficient drainage of migratory DCs to the lymph node from the dermis (Joncker et al., 2016). It is therefore possible that the epidermal route of transplantation too supports better CD4$^+$ T cell priming or peripheral CD4$^+$ T cell effector function. Melanoma cells transplanted in the e.c. model are in contact with the epidermis, unlike in i.d. and s.c. models, and also probably with the dermis, as the epidermis is very thin and even a light scarification prior to cell transfer may expose some dermal tissue. Whilst protection by the endogenous immune system was considerably more pronounced in the e.c. compared to the s.c. model (chapter 3), the ability of gDT-II cells to protect against B16.gD challenge had not been tested in either the s.c. or i.d. transplantable models. Many biological differences may exist between different transgenic CD4$^+$ T cells as well as between different melanoma cell lines. The combination of gDT-II cells and B16.gD cells may represent a particularly robust model for the anti-tumoral CD4$^+$ T cell response compared to other transgenic systems. It will therefore be important to use other transgenic CD4$^+$ T cells in the epicutaneous melanoma model to test how they compare with gDT-II cells. Similarly, gDT-II cells could be used in the i.d. and s.c.

model to determine how anatomical location of tumor formation affects melanoma immunosurveillance by $CD4^+$ T cells.

Many subsets of $CD4^+$ T cells have been identified to play a role in melanoma immunosurveillance in mouse models. In particular, an increasing number of studies have demonstrated an IFNγ-dependent protective role of Th1 cells in melanoma mouse models (Shklovskaya et al., 2016, Xie et al., 2010, Haabeth et al., 2018, Malandro et al., 2016). TRP-1 cells, transgenic $CD4^+$ T cells specific for melanoma antigen, TYRP1, differentiate into anti-tumoral Th1 cells when transferred into B16 melanoma-bearing hosts (Xie et al., 2010, Malandro et al., 2016, Haabeth et al., 2018). These cells have been differentiated into other subsets *in vitro* under specific cytokine polarising conditions which modulated their function when transferred *in vivo*. TRP-1 cells exhibited a more durable anti-tumoral response to B16 melanoma when polarised into Th17 cells, compared to Th1 cells prior to transfer (Muranski et al., 2008, Bowers et al., 2017). Other studies using TRP-1 cells or other TCR-transgenic $CD4^+$ T cells found that mice receiving adoptive transfer of Th9-polarised $CD4^+$ T cells, compared to Th1 or Th17-polarised cells, showed more robust resistance to melanoma growth (Lu et al., 2018, Purwar et al., 2012).

Similar to the Th1 polarisation seen by *in vivo* primed TRP-1 cells, gDT-II cells in the skin predominantly expressed T-bet suggesting that Th1 cells may be driving the anti-tumoral response. The transcription factors RORγT and GATA3 were detected on less abundant populations of gDT-II cells in the skin and thus a potential contribution of Th17, Th2 and Th9 cells to melanoma immunosurveillance in this model cannot be excluded. It is important to consider that subsetting Th cells based on transcription factors and cytokine expression profiles was developed from *in vitro* studies. The complexity of different tissue microenvironments *in vivo* may yield more heterogeneic and plastic populations of $CD4^+$ T cells compared to *in vitro* polarised cells. Indeed, a number of studies report heterogeneous populations of antitumoral $CD4^+$ T cells in the tumor microenvironment (Xie et al., 2010, Oh et al., 2020).

Heterogenous populations of CD4$^+$ T cells within the TME make it difficult to decipher specific roles of different subsets in antitumoral immunity. The use of T-bet-deficient gDT-II.*Tbx21*$^{-/-}$ cells enabled further investigation as to whether the Th1 subset was the sole driver of melanoma immunosurveillance by CD4$^+$ T cells or whether a level of redundancy existed amongst CD4$^+$ T cell subsets. In C57BL/6 mice, gDT-II.*Tbx21*$^{-/-}$ cells were less protective against development of progressing melanomas than wild-type gDT-II cells, highlighting the important role of Th1 cells in eliminating melanoma (or maintaining melanoma at levels below the detection limit). Interestingly, several melanomas in mice receiving gDT-II.*Tbx21*$^{-/-}$ cells persisted for the life-time of the mouse, whereas all the tumors arising in naïve controls were progressively growing. This difference in tumor growth kinetics suggested that CD4$^+$ T cell subsets other than Th1 cells may support long-term tumor control, particularly in cases where melanoma cells are not completely eliminated.

The notion that subsets other than conventional Th1 cells could mediate melanoma control was supported by an experiment where activated gDT-II.*Tbx21*$^{-/-}$ cells adoptively transferred into *Rag2*$^{-/-}$*;Il2rg*$^{-/-}$ mice were protective against progressively growing melanoma. A significant proportion the gDT-II.*Tbx21*$^{-/-}$ cells expressed RORγT in the skin which may be indicative of polarisation into Th17 cells, although further characterisation would be required to determine the phenotypic and functional characteristics of these cells. To further assess the role of different CD4$^+$ T cell subsets in the epicutaneous melanoma model, activated gDT-II cells will be differentiated into functionally distinct subsets prior to adoptive transfer. This may assist with disentangling the discrepant results observed when *in vitro*-differentiated transgenic TRP-1 T cells were transferred into B16 melanoma-bearing hosts (Muranski et al., 2008, Bowers et al., 2017, Lu et al., 2018, Purwar et al., 2012).

It is important to note that the experiment in which gDT-II.*Tbx21*$^{-/-}$ cells were transferred into *Rag2*$^{-/-}$*;Il2rg*$^{-/-}$ mice was only performed once and therefore

needs to be repeated to confirm that T-bet expression by activated gDT-II cells is dispensable for protection against progressing melanoma in *Rag2*$^{-/-}$*;Il2rg*$^{-/-}$ mice. Furthermore, the transfer dose of gDT-II cells should be titrated to lower numbers to elucidate possible different thresholds at which wild-type or T-bet-deficient gDT-II cells mediate protection. Characterisation of B16.gD in *Rag2*$^{-/-}$*;Il2rg*$^{-/-}$ demonstrated that tumor development is normally unrestrained therefore it was unexpected that two out of five naïve *Rag2*$^{-/-}$*;Il2rg*$^{-/-}$ mice did not develop progressing tumors and showed signs of persistent lesions which could be dormant melanoma cells. Long-term control of melanoma in *Rag2*$^{-/-}$*;Il2rg*$^{-/-}$ mice has not previously been reported in the epicutaneous model. If indeed long-term control of melanoma can occur in *Rag2*$^{-/-}$*;Il2rg*$^{-/-}$ mice a possible mechanisms of persistence could be cell-intrinsic tumor dormancy or extrinsic control by cells of the innate immune system, such as monocytes and granulocytes. Although CD8^{+} T_{RM} have been shown to maintain melanoma cells in a state of tumor dormancy (Park et al., 2019), other mechanisms of long-term melanoma persistence should be further investigated.

Experiments with gDT-II.*Tbx21*$^{-/-}$ cells reveal an important role of T-bet in the differentiation of antitumoral CD4^{+} T cells and also provide evidence that other subsets, potentially Th17 cells, may exert certain antitumoral functions by preventing outgrowth of melanoma cells. This highlights the potential redundancy in CD4^{+} T cell subsets that contribute to melanoma immunosurveillance and may provide rationale as to why heterogenous populations of CD4^{+} T cells exist in the TME.

In the lymph node draining the inoculation site, a population of gDT-II cells expressed Bcl-6, the master transcription factor associated with Tfh differentiation. Whether Bcl-6-expressing gDT-II cells perform the classical Tfh function in promoting the formation of geminal centres and B cell affinity maturation was not examined in this study. In the epicutaneous melanoma model, mice deficient in B cells were no more susceptible to tumor development than wild-type controls suggesting B cells may be dispensable for melanoma

immunosurveillance in this model (unpublished data, Gebhardt laboratory). Although deletion of the entire B cell repertoire may obfuscate the underlying roles of specific B cell subsets, which could include pro-tumoral and anti-tumoral B cells (Sharonov et al., 2020). Interestingly, evidence suggests that Tfh cells can exert peripheral effector functions in certain cancers. In breast and colorectal tumors the presence of Tfh within tumors promoted the organisation of TLS, enhanced CTL responses and was associated with better survival (Bindea et al., 2013, Gu-Trantien et al., 2013). The presence of B cells arranged in TLS within the TME also correlated with response to ICB in melanoma patients (Helmink et al., 2020). Further analysis of Bcl6 expression in $CD4^+$ T cells within the TME is warranted.

Transcription factor analysis is a useful tool to enable prediction the cytokine profiles expressed by a given $CD4^+$ T cell lineage. However, the complexity imparted by cellar plasticity and intrasubset heterogeneity *in vivo* neccessitates complementary cytokine analysis. *In vitro* activated gDT-II cells isolated from the skin of *Rag2*$^{-/-}$*;Il2rg*$^{-/-}$ non-developer mice produced TNFα and IFNγ when stimulated *ex vivo,* consistent with a Th1-polarised phenotype*,* however, a more in-depth analysis of cytokine production by *in vivo* polarised gDT-II cells should be carried out in future experiments. Using multiparametic flow cytometry to analyse the cytokine profiles of *in vivo* primed gDT-II cells from the skin would be useful although this technique would be challenging due to the low number of gDT-II cells that can be isolated from melanoma-challenged skin. An alternative approach would be to use single-cell transcriptomic or proteomic analysis. In-depth phenotypic analysis of $CD4^+$ T cells involved in the anti-tumoral response would help to elucidate the possible mechanisms of tumor control. Various studies demonstrate that a particular Th subset can mediate a multiplicity of functions in the context of tumor control. For example Th1 have been shown to mediate melanoma elimination by direct killing of MHC-II positive tumor cells (Quezada et al., 2010, Xie et al., 2010) and through indirect mechanisms requiring cytokine signalling and the involvement of other immune cell subtypes (Shklovskaya et al., 2016, Perez-Diez et al., 2007).

Whilst the transfer of naïve gDT-II cells was protective against tumor development, a small proportion of gDT-II-recipient mice developed progressively growing melanoma. The e.c. model is thus not only valuable for studying anti-tumoral $CD4^+$ T cell mechanisms that prevent tumor development in macroscopically tumor-free mice, but also for investigating factors which may hinder the anti-tumoral $CD4^+$ T cell response and promote immune escape in developer mice. Initial evidence that weak T cell priming and Treg accumulation within tumors may occur in the e.c. melanoma model were identified in this project. These are two processes which have been reported to thwart effector $CD4^+$ T cell responses. And whether they contribute to immune evasion in the e.c. melanoma model should be followed up in future studies.

T cell priming is a critical event in initiating and shaping adaptive immune responses. The strength of antigenic stimulation as well as the nature of co-stimulation and cytokine signalling during priming can impact the magnitude of T cell proliferation and the ability to form long-lived memory T cells (Kim et al., 2013, Gasper et al., 2014). Results from this study suggest that $CD4^+$ T cell priming in the e.c melanoma model was considerably weaker than $CD4^+$ T cell priming in the cutaneous HSV-1 infection model. Firstly, weaker priming was evidenced by the significantly lower expression of the IL-2 receptor alpha chain, CD25, by melanoma-primed gDT-II cells compared to HSV-primed gDT-II cells. Low CD25 expression suggests a reduced ability to respond to IL-2 which is important in regulating proliferation, responsiveness to other cytokines, and lineage-specific memory. A previous study showed that a $CD25^{low}$ effector phenotype after immunisation with UV-inactivated HSV-1 correlated with inefficient expansion and perturbed differentiation of gDT-II cells (Harpur et al., 2019). In addition, CD25-deficient mice have been shown to have reduced ability to form Th1 memory (Pepper et al., 2011). It is therefore likely that strongly reduced expression of CD25 during priming after melanoma challenge contributed to impaired memory formation and the poor recovery of gDT-II cells at late time points in macroscopically tumor-free mice. In addition, the number of gDT-II cells recovered in the skin early following melanoma challenge was 10-100 fold lower

than gDT-II accumulation in skin that occurs after HSV-1 infection (Gebhardt et al., 2011) which may result from poor proliferation due to low CD25 expression as a result of weak priming. The different microenvironments within the skin of B16.gD or HSV-challenged mice may also affect recruitment or retention of gDT-II cells *in situ*. Firstly, HSV-I establishes lytic infections in epithelial cells leading to rapid amplification of antigen load. It is thus likely that levels of glycoprotein D, and thus availability of antigen specific for gDT-II cells differs substantially in the context of B16.gD infection compared to HSV-I infection. In addition, the overt inflammation that occurs during acute infection is likely to result in more DAMPS and PAMPS compared melanoma challenge.

The magnitude of T-bet expression by gDT-II cells provided further evidence of weak priming in the e.c. melanoma model. In contrast to HSV-challenged mice in which gDT-II cells showed high levels of T-bet expression in the ibLN, spleen and skin, T-bet was only highly expressed in the skin, not the ibLNs nor spleens, of melanoma-challenged mice. No other lineage-specific transcription factors were observed in the gDT-II cells in the lymph node or spleen of melanoma challenged mice, so the lack of T-bet expression was not likely to be due to polarisation into a different subset. This suggests that gDT-II cells may not be fully differentiated into effector Th1 cells during priming in lymph nodes and that they received additional activation signals at the site of tumour inoculation. In line with this, expression of T-bet in Th1 cells has been found to require multiple encounters with antigen and sustained cytokine signalling (Bajenoff et al., 2002). The lack of T-bet expression by melanoma-primed gDT-II cells in the ibLN is reminiscent of the phenotype observed for gDT-II cells primed by UV-inactivated HSV-1 (Harpur et al., 2019). The defective priming that occurred in mice inoculated with inactivated HSV was due to insufficient antigen presentation by both LN-resident $CD8^+$ DC and $CD103^+$ dermal DC during priming. Impaired antigen presentation was not solely due to reduced antigen availability, leading the authors to hypothesise that the lack of additional DAMPs and PAMPs may prevent optimal priming. Future experiments should be performed to determine whether reduced antigen availability and/or the lack of signals to activate APCs are mechanisms

that prevent effective $CD4^+$ T cell priming in the e.c. melanoma model.

Experiments in which gDT-II cells were labelled with CTV were instrumental to determine the location of priming. In addition, characterisation of proliferation during priming can reveal information about kinetics and strength of T cell activation. Proliferation of gDT-II cells was observed in all melanoma-challenged mice but was delayed compared to HSV-1 infected mice. There appeared to be a level of variability in the kinetics of proliferation, although quantification is limited since the experiment was only performed twice. Additionally, imaging by light-sheet microscopy revealed expansion and clustering of gDT-II cells in the draining lymph node in only one out of two mice from the same experiment. Only two mice were analysed by Light-sheet microscopy and thus a larger sample size would be required to characterise the variability in priming responses. Light-sheet microscopy was used at an early time point to visualise priming, however future experiments will use Light-sheet microscopy to investigate the $CD4^+$ T cell response to melanoma challenge at other stages of the immune response. For example, by using fluorescently-labelled melanoma cells, we could determine whether $CD4^+$ T cells colocalise with metastasis deposits in the tumor-draining lymph node.

A possible mechanism underlying variability in priming in the epicutaneous melanoma model could be that, due the technical challenges of melanoma cell grafting, an inconsistent number of melanoma cells survive transplantation. Whilst the underlying mechanism remains to be determined, this variation offers an opportunity to dissect how variation in priming impacts the ensuing immune response. For instance, it would be interesting to determine whether there is a causative relationship between better priming and melanoma elimination. In support of this hypothesis, *in vivo* bioluminescence imaging revealed a correlation between the presence of melanoma cells in the priming lymph node, early following inoculation, and elimination or control of melanoma cells at the primary site (chapter 3). It could be speculated that an increase in antigen availability at the lymph node due to early metastasis may lead to better T cell

priming. Future studies should investigate what factors support or prevent effective T cell priming in the epicutaneous model.

Initial evidence that an immunosuppressive tumor microenvironment may contribute to tumor escape in the epicutaneous model was demonstrated by an abundance of FoxP3-expressing $CD4^+$ T cells (endogenous and gDT-II cells) within B16.gD tumors. Immunosuppressive Treg cells, which are characterised by the transcription factor FoxP3, are frequently reported within tumor microenvironments where they are generally considered to contribute to immune escape. On the other hand, Treg cells may actually play an anti-tumoral role in certain situations by controlling inflammation and preventing tissue damage which can contribute to cancer development. This dual role for Treg in cancer immunology is not well understood (Paluskievicz et al., 2019).

Interestingly, CD25 which is commonly expressed by Treg cells, was not detected in a large proportion of $FoxP3^+$ gDT-II cells. $FoxP3^+CD25^-$ $CD4^+$ T cells have been reported in a number of settings, including in human tumors (Oh et al., 2020), but their role is not well understood compared to their CD25-expressing counterparts. $FoxP3^+CD25^-$ $CD4^+$ T cells are present at elevated numbers in patients with various autoimmune diseases compared to healthy controls, suggesting they may have immunosuppressive functions (Yin et al., 2018, Ferreira et al., 2017). Unlike conventional $FoxP3^+CD25^+$ Treg, $FoxP3^+CD25^-$ $CD4^+$ T cells have been shown to display pro-inflammatory features, such as lower expression of CTLA-4 and higher levels of IFNγ production (Yin et al., 2018). However, these cells can also share phenotypic characteristics with conventional Treg such as the production of high levels of IL-10 and TGF-β, a lack of IL-2 production and the ability to suppress proliferation of conventional T cells (Liu et al., 2007). Whether $FoxP3^+CD25^+$ or $CD25^-FoxP3^+$ $CD4^+$ T cell populations that reside in tumors in the epicutaneous melanoma model exert suppressive activity and promote tumor development remains to be determined.

It would be interesting to examine the origin of FoxP3-expressing gDT-II cells

within the tumor microenvironment. One possibility is that these cells arise from classical peripheral Treg differentiation during activation in the lymph node and are subsequently recruited to the tumor. Alternatively, the FoxP3$^+$ phenotype may be induced within the tumor microenvironment itself. FoxP3 is not expressed by gDT-II cells in the skin one week following inoculation supporting the hypothesis that conventional effector Th subsets may be converted into suppressive Treg cells due to suppressive signals within the tumor microenvironment. Many factors including TGF-β, retinoic acids and short chain fatty acids found within tumor microenvironments have been shown to induce tumor associated Treg cell formation (Paluskievicz et al., 2019). Although FoxP3-expressing CD4$^+$ T cells require further characterisation their abundance in tumors suggests that the epicutaneous melanoma model may be useful to further study the role of Treg cells in cancer development.

To characterise migratory kinetics of melanoma-specific CD4$^+$ T cells in the epicutaneous melanoma model, the location and phenotype of gDT-II cells was analysed by flow cytometry over time. CD103 and CD69 play important roles in lodgement and retention of CD8$^+$ T_{RM} in the epidermis as CD103 binds to E-cadherin expressed on epithelial cells and CD69 interferes with S1P1 egress signals. Whether CD4$^+$ T cells form T_{RM} cells in the skin, and whether these markers are sufficient to define tissue residency for the CD4$^+$ T cell lineage has remained a subject of debate (Collins et al., 2016, Beura et al., 2019, Klicznik et al., 2019, Watanabe et al., 2015, Bromley et al., 2013). In this study gDT-II cells in the skin co-expressed CD69 and CD103 three weeks following melanoma challenge. However, since gDT-II cells were rarely detected by flow cytometry in the skin onwards of five weeks p.i., this suggests they may not form long-lived T_{RM} cells.

An important limitation to consider when enumerating cells in the skin by flow cytometry is that enzymatic digestion to prepare a single-cell suspension does not effectively release cells from the tissue and can also lead to a significant amount of cell death. Collagenase was the digestive enzyme selected to prepare

skin samples for flow cytometric analysis in this study, as it has been shown to be less harsh than other digestive enzymes in terms of cleavage of surface markers and cell viability (Botting et al., 2017). Yet it has been estimated, through quantitative microscopy, that skin digestion by collagenase recovers less than 10 % of the total cells (Clark et al., 2006, Steinert et al., 2015, Collins et al., 2016). In addition, collagenase digestion liberates cells within the dermis but shows poor extraction of cells from the epidermis (Botting et al., 2017). Two-photon microscopy revealed that gDT-II cells infiltrate the epidermis one week following melanoma inoculation. In the cutaneous HSV infection model, $CD4^+$ T cells infiltrated into both the epidermis and dermis at the site of infection at the peak of the response post-challenge, although at later time points memory $CD4^+$ T cells were largely confined to the dermis (Collins et al., 2017). Therefore, infiltration of $CD4^+$ T cells into the epidermis at the site of melanoma challenge may be specific to the early effector phase although the possibility that gDT-II cells may remain in the epidermis at later time points following melanoma challenge cannot be excluded. Indeed, the existence of $CD4^+$ T_{RM} cells in the epidermis has been reported in human skin (Watanabe et al., 2015). Hence, despite being unable to detect gDT-II cells by flow cytometry at late time points in the skin following melanoma inoculation, it is possible that cells were present but not liberated during collagenase digestion. Future studies should consider using an alternative skin digestion enzyme, for example, trypsin, dispase or liberase, which better extract cells from the epidermis, although caution should be made as different enzymes have different consequences on the viability and phenotype of the extracted cells (Li et al., 2018, Botting et al., 2017). Imaging can provide a more reliable quantification of cell number (Collins et al., 2016, Steinert et al., 2015, Clark et al., 2006) and microscopy will be used in future experiments to image the inoculation site at later timepoints following melanoma challenge.

Due to the limitation of cell enumeration by flow cytometry, and the lack of unequivocal markers that define residency, results of this study do not disprove the formation of $CD4^+$ T_{RM} cells, but rather support preferential recirculation and a limited longevity of $CD4^+$ T cells within the skin. Additionally, these results

challenge the use of co-expression of CD103 and CD69 to define permanent residency, at least for $CD4^+$ T cells in the context of cutaneous melanoma. These markers may better circumscribe skin tropism, and possibly prolonged retention, rather than formation of stable T_{RM} cells. These result are consistent with the murine model of cutaneous HSV infection whereby gDT-II cells expressed CD103 and CD69 in the skin but eventually re-entered the circulation after a prolonged period of time (Collins et al., 2017). Previous studies have shown that CD103 is upregulated on T cells after entry into skin (Mackay et al., 2013). In support of recirculation, $CD103^+$ gDT-II cells were observed in the ibLN and spleen 10 weeks p.i. in *Rag1*$^{-/-}$ mice, which may represent a population of cells that have egressed from the skin. Indeed, the formation of a memory $CD4^+$ T cell population that expresses $CD103^+$ and recirculates between the skin and lymphoid tissue has been identified in migration experiments using Kaede, a photoconvertible fluorescent protein that changes colour upon exposure to UV light, thus facilitating tracking of cells by flowcytometry (Bromley et al., 2013). In humans, a small population of $CD103^+CD4^+$ cells exist in the circulation and $CD103^+CD4^+$ T cells were observed re-entering the skin in a xenograft model (Klicznik et al., 2019). Migration experiments using parabiosis, skin transplants, or the photoconvertible fluorescent protein, Kaede, could be explored in the epicutaneous melanoma model to further characterise migratory kinetics of $CD4^+$ T cells in melanoma immunosurveillance. Furthermore, to investigate the migratory capacity of $CD4^+$ T cells, future experiments will be carried out to determine whether the observed protection against B16.gD challenge in the HSV memory mice (chapter 3) was due to local or systemic protection. This will involve epicutaneous tumor challenge at a site of the skin not previously infected by HSV. Since $CD8^+$ T cells and B cells may recognise epitopes of gD, to specifically investigate $CD4^+$ T cells in these experiments, CRISPitope-generated B16 cell lines that express the MHC-II restricted epitope of gD (rather than the full-length protein) will be used.

Results of this study suggest $CD4^+$ T cells do not readily form long-lived T_{RM} cells in the e.c. melanoma model yet $CD8^+$ T cells show a distinct $CD69^+$ $CD103^+$ T_{RM} phenotype in this same model (Park et al., 2019). The same disparity in $CD8^+$

and $CD4^+$ T cell retention in the skin has been demonstrated in the cutaneous HSV model (Gebhardt et al., 2011, Park et al., 2019) suggesting this dichotomy is cell-intrinsic and location-dependent rather than dependent on disease context. However, it should be noted that the same transgenic T cells (gDT-II cells) were used to study the migratory and phenotypic patterns of antigen-specific $CD4^+$ T cells in both models. The shared TCR may beget an inherent phenotypic bias as the affinity of a TCR for cognate peptide/MHC-II complex can influence the T cell differentiation program (Tubo et al., 2013). Indeed, the conflicting findings surrounding the ability of $CD4^+$ T cells to form T_{RM} in different studies could be partly due to the use of different transgenic $CD4^+$ T cells. Whether the antigen specificity of gDT-II cells or the Th1 polarisation that occurs in both HSV-1 infection and e.c. melanoma challenge affects the capacity for T_{RM} formation requires further investigation. Indeed, in a model of *Candida albicans* infection heterogeneous populations of $CD4^+$ T cells mediated effector functions within the skin but only the Th17-polarised $CD4^+$ T cells formed T_{RM} cells (Park et al., 2018). Further studies should investigate the impact of $CD4^+$ T cell subset polarisation on skin migratory patterns and T_{RM} potential. The reason for which $CD4^+$ T cells may less readily form a stable population of T_{RM} cells in the skin, compared to their $CD8^+$ T cell counterparts is largely unknown. From an evolutionary perspective, although we can only speculate, formation of $CD4^+$ T_{RM} cells in the skin may be detrimental to the host in the long-term. The reason being may relate to the phenotypic and functional plasticity exhibited by the $CD4^+$ T cell lineage. If these cells can easily adopt different functions in response to changes in their local environment, aberrant immune responses could transpire rendering permanent lodgement a risk.

The signals that drive $CD4^+$ T cell recruitment into the skin, modulate retention time and facilitate egress are not well understood. However, local antigen presentation in the periphery is an important factor in recruiting antigen-specific $CD4^+$ T cells (Reinhardt et al., 2003). To support that the recruitment of gDT-II cells to the inoculation site is antigen-specific, two-photon microscopy revealed that gDT-II cells colocalised with melanoma cells in the skin and gDT-II cells were

frequently detected within melanomas by flow cytometry. gDT-II cells were not detected at the inoculation site by two-photon microscopy in the absence of detectable melanoma cells suggesting that non-specific inflammation from the inoculation alone was not sufficient to drive antigen-specific T cell recruitment. Additionally, developer mice had a greater number of gDT-II cells in the ibLN, with a higher relative proportion of T_{EM}/T_{EFF} to T_{CM}, compared to mTF mice. One factor that contributes to an increase in the number of effector gDT-II cells in the ibLN in developer mice may be the presence of cognate antigen as a result of metastatic spread. Together these observations provide indications that gDT-II cells accumulate at sites of B16.gD deposits in an antigen-dependent manner. However, to confirm this finding, gDT-II-recipient mice could be inoculated with a combination of B16.gD cells and B16 melanoma cells lacking gD expression that could be distinguished by different fluorescence markers. Co-localisation with gDT-II cells could then be assessed via microscopy.

Whilst $CD8^+$ T_{RM} cells do not require persistence of antigen for maintenance in the skin (Park et al., 2019, Lauron et al., 2019), it is unclear whether this is true for $CD4^+$ T cells. If antigen is required for survival and retention of melanoma specific $CD4^+$ T cells in the skin, mTF mice in which gDT-II cells were not detected at the inoculation site by flow cytometry may represent a situation whereby melanoma cells had already been eliminated. Conversely, the presence of gDT-II cells in the skin of mTF mice may be indicative of residual surviving melanoma cells. Future experiments will combine bioluminescence imaging with two-photon microscopy to test this hypothesis. Bioluminescence imaging will be used to detect persistent melanoma cells in mTF skin and then two-photon and light-sheet microscopy will be used to image the inoculation site and determine whether antigen-specific $CD4^+$ T cells are retained within the skin in a situation of sustained antigen availability. As such, B16.gD cells that express the luciferase and mScarlet proteins will be generated on a tyrosinase-deficient background.

The major findings from this chapter are that in the e.c. melanoma model, $CD4^+$ T cells infiltrated into the skin at the inoculation site, colocalised with melanoma

cells and expressed the Th1-associated transcription factor T-bet. $CD4^+$ T cells were highly protective against melanoma development despite evidence for weak priming, modest proliferation and poor long-term survival of the memory pool. Overall, results of this study demonstrated that using transgenic gDT-II cells in the epicutaneous melanoma model is valuable for studying the anti-tumoral role of $CD4^+$ T cells in melanoma immunosurveillance.

Chapter 5:
Deciphering the mechanisms underlying melanoma immunosurveillance by $CD4^+$ T cells.

Chapter 5: Deciphering the mechanisms underlying melanoma immunosurveillance by CD4$^+$ T cells.

5.1 Background

Whilst a growing number of studies have established that CD4$^+$ T cells play an important role in cancer immunosurveillance, the underlying mechanisms remain equivocal. Several preclinical cancer models recently demonstrated the importance of CD4$^+$ T cell "help" in priming CD8$^+$ T cells against cancer antigens (Alspach et al., 2019, Zhu et al., 2015, Ferris et al., 2020). However, consistent with previous reports (Shklovskaya et al., 2016, Xie et al., 2010), this study showed that CD4$^+$ T cells are able to protect against melanoma development in the absence of CD8$^+$ T cells and B cells. This indicates that CD4$^+$ T cells mediate effector functions independent of classical T cell "help".

To exert effector function, CD4$^+$ T cells require TCR stimulation and thus the provision of cognate antigen on an MHC-II molecule (McLachlan et al., 2009, Macleod et al., 2014). Whilst MHC-II expression is largely restricted to professional APCs, some cancers express MHC-II and thus may present endogenously processed antigens directly to CD4$^+$ T cells (Axelrod et al., 2019). The frequency by which CD4$^+$ T cells directly bind MHC-II-positive cancer cells and the downstream consequence of direct stimulation, compared to stimulation by different subsets of professional APCs, are not well understood. Ergo, the first aim of this chapter was to determine the role of MHC-II expression by melanoma cells on immunosurveillance by CD4$^+$ T cells.

Once stimulated, CD4$^+$ T cells within the TME have been shown to promote antitumoral immunity by diverse mechanisms. This includes the recruitment and activation of other antitumoral immune cells (Wong et al., 2008, Bos and Sherman, 2010, Alspach et al., 2019, Huang et al., 2005, Martin-Orozco et al., 2009, Church et al., 2014, Corthay et al., 2005, Haabeth et al., 2018, Perez-Diez et al., 2007, Doorduijn et al., 2017) or direct killing of cancer cells (Quezada et

al., 2010). Cytotoxicity is only a recently appreciated characteristic of antitumoral $CD4^+$ T cells and has primarily been observed *in vitro.* Whether killing mechanisms of cytotoxic $CD4^+$ T cells *in vivo* are analogous to those mediated by cytotoxic $CD8^+$ T cells has not been determined. The second aim of this chapter was thus to investigate the potential mechanisms by which peripheral effector $CD4^+$ T cells may directly kill melanoma cells.

5.2 Results

5.2.1 Mice deficient in CD40/CD40L signalling are more susceptible to tumor development.

$CD4^+$ T cells can promote antitumoral $CD8^+$ T cell responses. The provision of help from $CD4^+$ T cells to $CD8^+$ T cells can be broadly divided into “licensing” or “post-licensing” roles. Licensing occurs in SLOs and involves engagement of CD40L expressed by an antigen-specific $CD4^+$ T cell with the costimulatory receptor, CD40, expressed by a cognate DC (Bennett et al., 1998). Licensing enhances the activation state of the DC, enabling it to more efficiently prime $CD8^+$ T cells which in turn augments the magnitude, quality and longevity of the $CD8^+$ T cell response (Ahrends et al., 2019, Ahrends et al., 2017).

To investigate whether $CD4^+$ T cell “help” via DC licensing is important for melanoma immunosurveillance in the epicutaneous melanoma model, the susceptibility of *Cd40*$^{-/-}$ and *Cd40l*$^{-/-}$ mice to tumor development was evaluated. Mice were inoculated with the cell line B16.gD.Luc-mScar for longitudinal monitoring of melanoma cells by bioluminescence. *Cd40*$^{-/-}$ mice had a significantly higher incidence of tumor development compared to wild-type mice (**Figure 5.1a**). The incidence of melanoma development for *Cd40l*$^{-/-}$ mice was higher than wild-type mice, and lower than *Cd40*$^{-/-}$ mice, however, neither difference was statistically significant. Recurring bioluminescent signals at the

inoculation site were observed for some *Cd40*$^{-/-}$ and *Cd40l*$^{-/-}$ mice (**Figure 5.1b**). One controlled lesion in a *Cd40*$^{-/-}$ mouse emitted a bioluminescence signal every week for up to 8 weeks and could be observed by eye (**Appendix Figure 11**), suggesting that that long-term control of macroscopic melanoma lesions can occur in absence of CD40/CD40L signalling. However, the increased tumor incidence of *Cd40*$^{-/-}$ mice suggests that the CD40/CD40L signalling pathway, and thus possibly CD4^{+} T cell help, is important in protection from progressively growing tumors in the epicutaneous model.

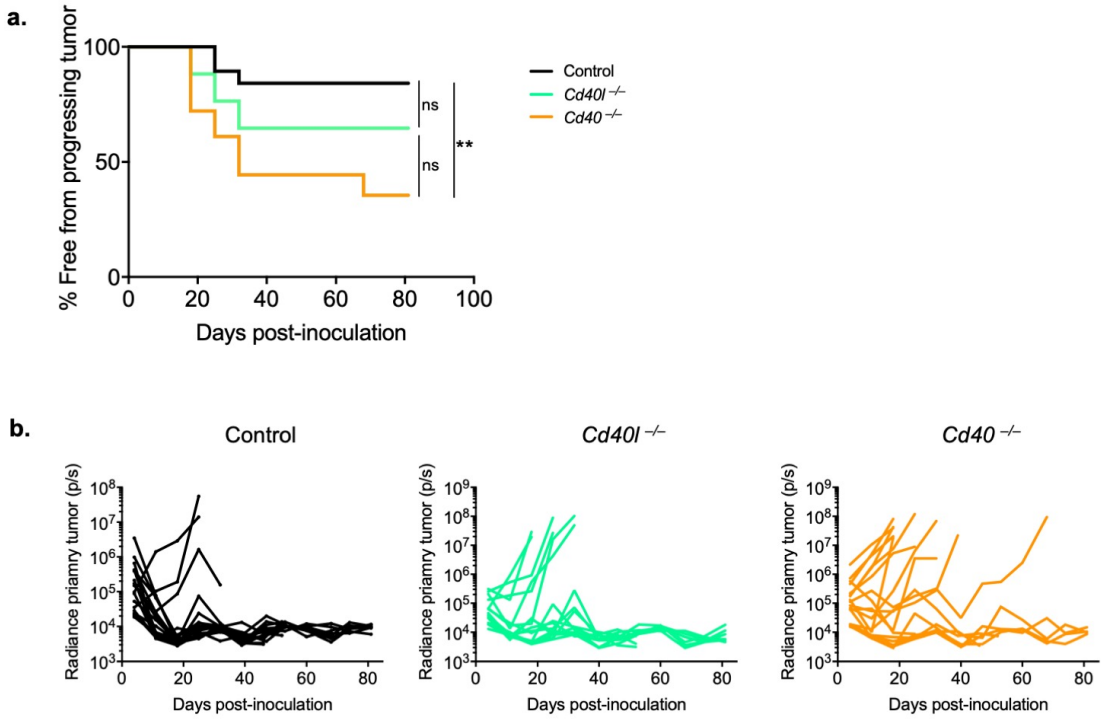

Figure 5.1. *Cd40*$^{-/-}$ mice are more susceptible to B16.gD melanoma development.
a, b, Wild-type C57BL/6 (control), *Cd40*$^{-/-}$ and *Cd40l*$^{-/-}$ mice were inoculated with 1 × 10^5 B16.gD.Luc-mScar (e.c.) and monitored longitudinally for bioluminescence signals using an In Vivo Imaging System (IVIS), n=17-19 mice/group, pooled from three biologically independent experiments. **a,** Incidence depicts the percentage of mice that did not develop a progressing primary tumor, **P=0.0058, ns; not significant, statistics determined by log-rank Mantel–Cox test. **b,** Bioluminescence signals measured at site of tumor inoculation and calculated as total flux (photons/second, p/s). *IVIS imaging performed by David Freestone*.

5.2.2 Characterisation of MHC-II expression by melanoma cells and tumor-infiltrating immune cells.

The frequency by which MHC-II-restricted antigens are presented directly by cancer cells to $CD4^+$ T cells is not known. Nor is it understood how antigen presentation by cancer cells compares with professional APCs in regulating the ensuing $CD4^+$ T cell response. In chapter 3, it was shown that the B16.gD cell line expressed MHC-II following exposure to IFNγ and that B16.gD cells directly stimulated gDT-II in an MHC-II-dependent manner *in vitro* (**Figure 3.2**). IFNγ-induced MHC-II expression is under the control of *Ciita*, the "master transactivator" of MHC-II genes (Steimle et al., 1994). As discussed in Chapter 3, B16.gD.*Ciita*$^{-/-}$ cells that are unable to upregulate MHC-II were generated to address the role of MHC-II expression by melanoma cells on immunosurveillance by $CD4^+$ T cells.

To determine whether transplanted B16.gD cells expressed MHC-II in the epicutaneous melanoma model, tumors were analysed by flow cytometry. As a control, tumors from mice inoculated with MHC-II-deficient B16.gD.*Ciita*$^{-/-}$ cells were also analysed. Melanoma cells were identified by flow cytometry by their characteristic large size and dense granularity, high expression of GFP and the absence of lymphopoietic marker CD45.2 (**Figure 5.2a**). In the majority of progressively growing tumors, MHC-II was not detected on B16.gD cells. However, in several smaller tumors, of which the tumor volume was less than 70 mm^3, MHC-II was expressed by a large proportion of B16.gD cells. As expected, the B16.gD.*Ciita*$^{-/-}$ cells did not express MHC-II in any tumors (**Figure 5.2b**). The number of infiltrating $CD4^+$ T cells was also analysed with respect to tumor volume and MHC-II expression. Smaller B16.gD tumors tended to have higher numbers of infiltrating $CD4^+$ T cells, however, this correlation was not observed in B16.gD.*Ciita*$^{-/-}$ tumors (**Figure 5.2c**). This suggested that the inverse correlation of intratumoral $CD4^+$ T cell number with tumor volume was dependent on the expression of *Ciita* in smaller B16.gD tumors. Consistent with this hypothesis, tumors in which B16.gD cells expressed MHC-II had a higher density

of infiltrating $CD4^+$ T cells. This was observed for both the endogenous $CD4^+$ T cell compartment and also gDT-II cells, albeit only two gDT-II-recipient mice with MHC-II-positive B16.gD tumors were analysed (**Figure 5.2d**).

MHC-II-expression on tumor-infiltrating immune cells was analysed by flow cytometry. In both B16.gD and B16.gD.*Ciita*$^{-/-}$ tumors, MHC-II was detected on approximately 75 % of all tumor-infiltrating immune ($CD45^+$) cells (**Figure 5.3a, b**). The majority of $CD45^+$MHC-II^+ cells expressed CD11b, a molecule expressed on the surface of many leukocytes. Approximately half of the $CD11b^+$ cells co-expressed CD11c, a well-established, but not exclusive, cDC marker (**Figure 5.3c**). Interestingly, an intermediate level of GFP was detected in a population of intratumoral $CD45^+$ cells (**Figure 5.3d**). These cells were thus suspected to be immune cells which phagocytosed GFP derived from B16.gD cells. The $CD45^+$GFP-intermediate (GFP^{int}) population were smaller and less granular compared to $CD45^-GFP^{high}$ melanoma cells as determined by flow cytometry (data not shown). Similar to the total $CD45^+$MHC-II^+ cells in B16.gD tumors (**Figure 5.3c**), the $CD45^+GFP^{int}$ cells uniformly expressed CD11b and exhibited a spectrum of CD11c expression (**Figure 5.3d**). As expected, the B16.gD cells ($CD45^-GFP^{high}$) were negative for the immune cell markers CD11b and CD11c. Importantly, $CD45^+GFP^{int}$ cells expressed MHC-II and the co-stimulatory molecules CD80 and CD86. A subpopulation additionally expressed co-stimulatory molecule CD83. The expression of these costimulatory molecules by B16.gD melanoma cells was low or undetectable by flow cytometry (**Figure 5.3e**).

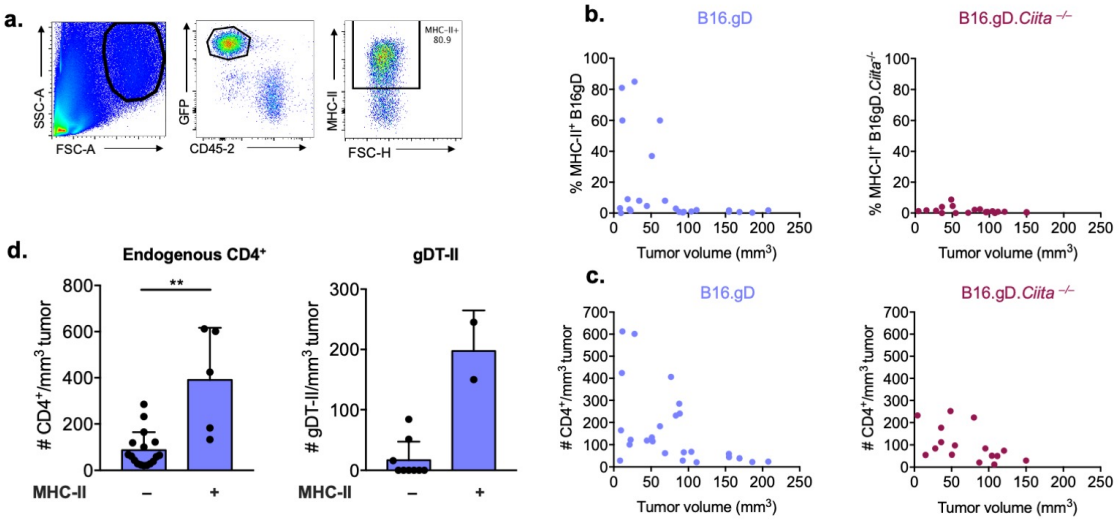

Figure 5.2. MHC-II expression by B16.gD cells inversely correlates with tumor volume and positively correlates with the number of CD4⁺ tumor-infiltrating lymphocytes.

Analysis of tumors from C57BL/6 mice challenged with B16.gD or B16.gD.*Ciita*$^{-/-}$ (1×10^5 cells e.c), with or without transfer of naïve gDT-II cells (1×10^4). **a,** Gating strategy for analysis of MHC-II expression by melanoma cells in primary tumors. **b,** Correlation between tumor volume and MHC-II expression of melanoma cells, determined by flow cytometry, n=24 B16.gD tumors (purple) and n=20 B16.gD.*Ciita*$^{-/-}$ tumors (red). **c,** Correlation between tumor volume and the number of intratumoral CD4⁺ T cells, determined by flow cytometry ($CD45.2^+CD4^+CD8^-$), in n=25 B16.gD tumors (purple) and n=16 B16.gD.*Ciita*$^{-/-}$ tumors (red). **d,** Number of endogenous CD4⁺ T cells ($CD45.2^+CD4^+CD8^-$, left), or gDT-II cells ($CD4^+V\alpha3.2^+CD45.1^+$, right) in primary B16.gD tumors stratified by MHC-II expression whereby MHC-II⁺ tumors are defined as >37 % MHC-II⁺ B16.gD cells and MHC-II^{neg} tumors are defined as <4 % MHC-II⁺ B16.gD cells. Bars and error bars depict mean and SD, respectively **c-d,** Data pooled from 5 biologically independent experiments. Each point represents an individual tumor. Statistical significance determined by Mann-Whitney test for panel **(d)**. **P= 0.0014

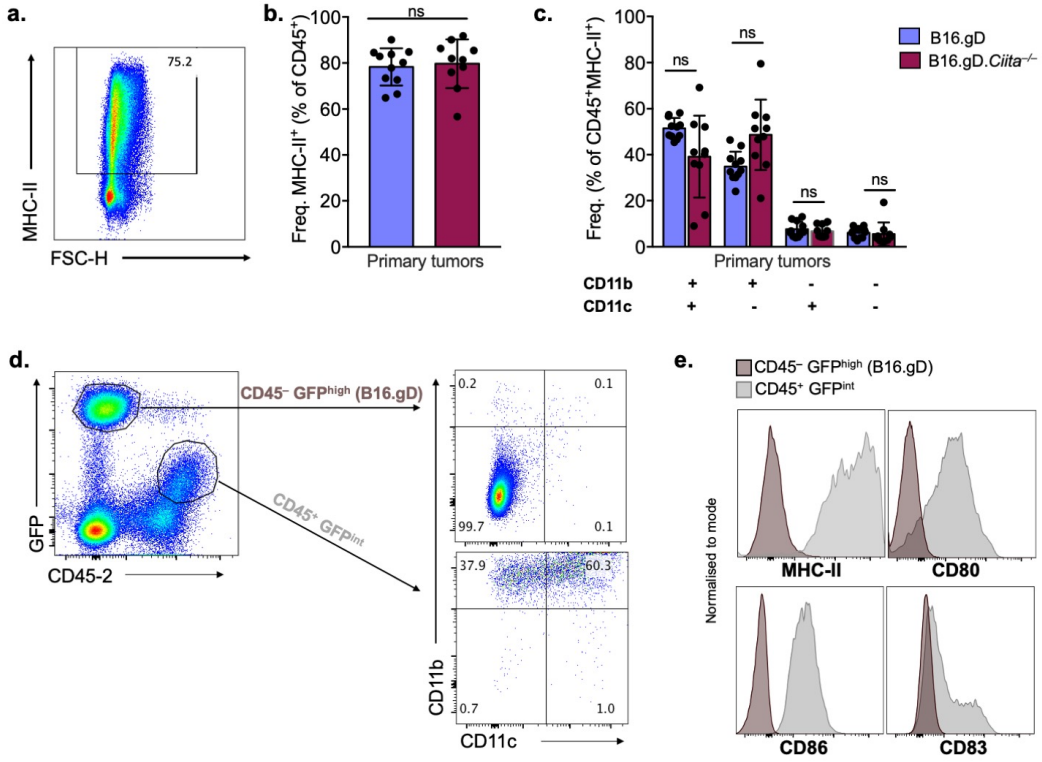

Figure 5.3. Characterisation of MHC-II⁺ tumor-infiltrating leukocytes.
Flow cytometric analysis of tumors from C57BL/6 mice challenged with B16.gD or B16.gD.*Ciita*$^{-/-}$ (1×10^5 cells e.c), with or without transfer of naïve gDT-II cells (1×10^4 i.v). **a, b,** MHC-II expression by intratumoral immune (CD45.2$^+$) cells. **a,** Representative flow cytometry plot from a B16.gD tumor and **b,** pooled data from B16.gD (purple) and B16.gD.*Ciita*$^{-/-}$ (red) tumors. **c,** CD11b and CD11c expression of intratumoral MHC-II$^+$CD45.2$^+$ cells. **b, c,** Each point represents a single tumor, bars and error bars depict mean and SD, respectively. Data pooled from three independent experiments. ns; not significant, statistical significance determined by Mann-Whitney test. **d, e,** Flow cytometric analysis of GFP-positive populations in a single B16.gD tumor, representative of n=8 tumors from 3 individual experiments. **d,** CD11b and CD11c expression in GFP-positive populations (CD45.2$^-$GFP^{high} and CD45.2$^+$GFP^{int}). **e,** Expression of costimulatory molecules (CD80, CD86 and CD83) and MHC-II in the two GFP-positive populations from **(d)**; CD45.2$^-$GFP^{high} (brown) and CD45.2$^+$GFP^{int} (grey).

5.2.3 Role of CIITA expression by melanoma cells in tumor development.

B16.gD.*Ciita*$^{-/-}$ cells were characterised in the epicutaneous melanoma model to investigate the role of MHC-II expression by melanoma cells on immunosurveillance. Tumor development was compared between C57BL/6 mice challenged with the B16.gD.*Ciita*$^{-/-}$ cell line or the control (B16.gD) cell line. In naïve mice, 90 % (20/22) of B16.gD.*Ciita*$^{-/-}$ tumors exceeded a volume greater than 20mm^3 within 20 days post-inoculation compared to 52 % (11/21) of B16.gD tumors (**Figure 5.4a, b**). However, there was no difference in the tumor incidence in mice inoculated with B16.gD.*Ciita*$^{-/-}$ or B16.gD cells (**Figure 5.4c**). Interestingly, naïve mice inoculated with B16.gD.*Ciita*$^{-/-}$ cells presented with less frequent and smaller metastatic lesions than naïve mice inoculated with B16.gD cells, suggesting a possible role of *Ciita* in metastasis (**Figure. 5.4d**).

To specifically investigate whether MHC-II expression was required for protection by CD4$^+$ T cells, gDT-II cells were transferred into mice prior to melanoma challenge with B16.gD.*Ciita*$^{-/-}$. Similar to the control B16.gD tumors, B16.gD.*Ciita*$^{-/-}$ tumors grew more slowly in gDT-II recipient mice than naïve mice (**Figure 5.4a, b**). Furthermore, gDT-II recipient mice had a significantly lower incidence of B16.gD.*Ciita*$^{-/-}$ tumor development compared to naïve mice (**Figure 5.4c**). This demonstrated that the absence of MHC-II expression by melanoma cells does not inhibit protection driven by CD4$^+$ T cells against primary tumor development. Whilst gDT-II-recipient mice presented with smaller, less frequent lymph node metastases than naïve mice when challenged with the B16.gD cell line, this difference was not observed between naïve and gDT-II recipent mice challenged with the B16.gD.*Ciita*$^{-/-}$ cell line (**Figure. 5.4d**).

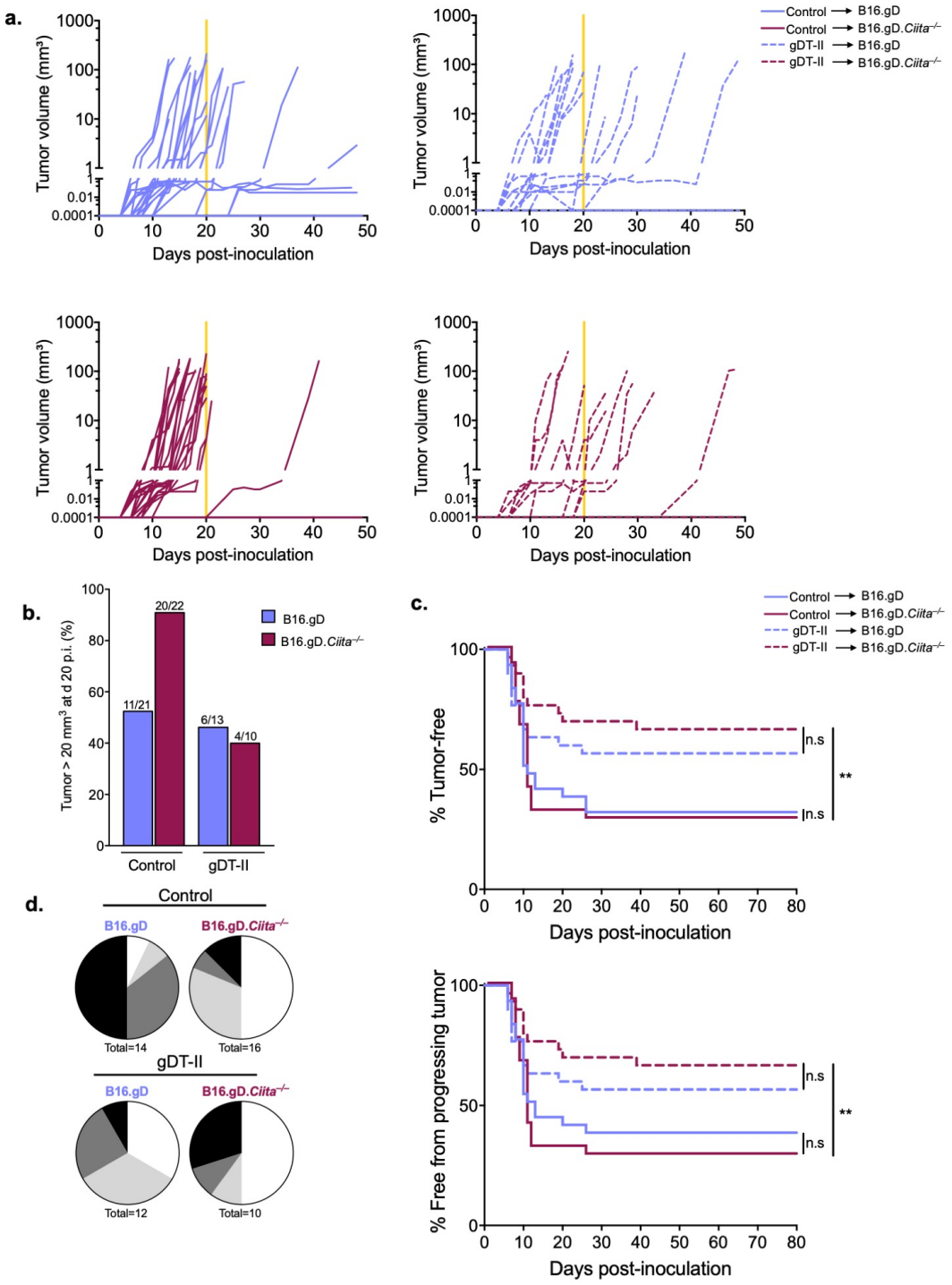

Figure 5.4. Effect of CIITA expression by melanoma cells on immunosurveillance.
C57BL/6 mice received naïve gDT-II cells (1×10^4, i.v.) and were challenged the following day with B16.gD or B16.gD.*Ciita*$^{-/-}$ (1×10^5 cells e.c), in parallel with naïve (Control) mice that did not receive gDT-II cells. **a,** Tumor growth kinetics of

primary tumors. Yellow line demarcates day 20 p.i. **b,** Percentage of tumor-developing mice in which the tumor volume exceeded 20 mm^3 by day 20 p.i. Number of developer mice presented as a fraction of total mice per group (displayed above bars). **c,** Tumor incidence. Incidence shown in top graph includes progressing tumors and lesions suspected to be persistent melanoma. Incidence shown in bottom graph includes only progressively growing tumors; n=30-31 mice/group, from 5 independent experiments, **P=0.0018. **d,** Incidence of ibLN metastasis observed by eye in mice with progressively growing primary tumors, ranging from 20-180 mm^3. Metastases scored from 0-3 based on the surface area of black pigment observed; 0 (none observed) corresponds to no observable pigment, 1 (miniscule) corresponds to pigment <0.5 mm^2, 2 (overt) corresponds to pigment 0.5-1.5 mm^2, 3 (dominant) corresponds to pigment >1.5 mm^2. Number of mice per group listed below pie chart, pooled from 5 biologically independent experiments.

5.2.4 CD4$^+$ T cells directly kill melanoma cells *in vitro*.

CD4$^+$ T cells contribute to cancer immunosurveillance by diverse mechanisms including direct killing of cancer cells. To determine whether gDT-II cells could directly kill B16.gD cells *in vitro,* B16 cell lines were co-cultured with gDT-II cells for 24 hours following treated with IFNγ to upregulate MHC-II. Cell death was analysed using two techniques. Firstly, Propidium iodide (PI), which permeates dying cells but does not stain healthy cells, was added to the cell culture media during co-culture and cell death was measured in real-time by PI uptake (fluorescence intensity). Secondly, melanoma cells were enumerated by flow cytometry subsequent to the 24-hour co-culture (**Figure 5.5a**).

Cell death, measured by PI uptake, increased in a dose-dependent manner when IFNγ-treated B16.gD cells were co-cultured with an increasing number of gDT-II cells (**Figure 5.5b**). In the absence of IFNγ treatment, only a modest increase in PI fluorescence intensity was observed. As expected, no PI uptake was observed in the absence of gDT-II cells during the assay, indicating that cell death was attributable to the presence of gDT-II cells. There was substantially less killing when gDT-II cells were co-cultured with IFNγ-stimulated B16.gD.*Ciita*$^{-/-}$ cells compared to IFNγ-stimulated B16.gD cells (**Figure 5.5c**). In fact, IFNγ-treated B16.gD.*Ciita*$^{-/-}$ cells showed equivalent cell death to unstimulated (not pre-treated with IFNγ) B16.gD and B16.gD.*Ciita*$^{-/-}$ cells. This confirmed that the requirement of IFNγ pre-treatment for killing by gDT-II cells was due to its function in upregulating *Ciita* required for MHC-II expression. Enumeration of B16.gD cells by flow cytometry following co-culture with gDT-II cells corroborated the results of the PI assay. There was 80 % less IFNγ-stimulated B16.gD cells following co-culture with gDT-II cells relative to the number of IFNγ-stimulated B16.gD cells cultured in media alone. In the absence of IFNγ pre-stimulation, the addition of gDT-II cells did not affect B16.gD cell number relative to the media only control. As expected, in the presence of gDT-II cells, there was no significant difference in the relative percentage of surviving B16.gD.*Ciita*$^{-/-}$ cells or B16.Ova cells

between IFNγ-treated and untreated conditions (**Figure 5.5d**). This demonstrated that the reduction in cell number of IFNγ-treated B16.gD cells is antigen-specific and MHC-II dependent. A limitation of enumerating cells subsequent to co-culture is that changes in the rate of proliferation may obfuscate the calculation of cell death. However, the combined results from flow cytometry and the PI assay, which directly measures cell death in real-time, definitively demonstrate that gDT-II cells can directly kill B16.gD cells *in vitro.*

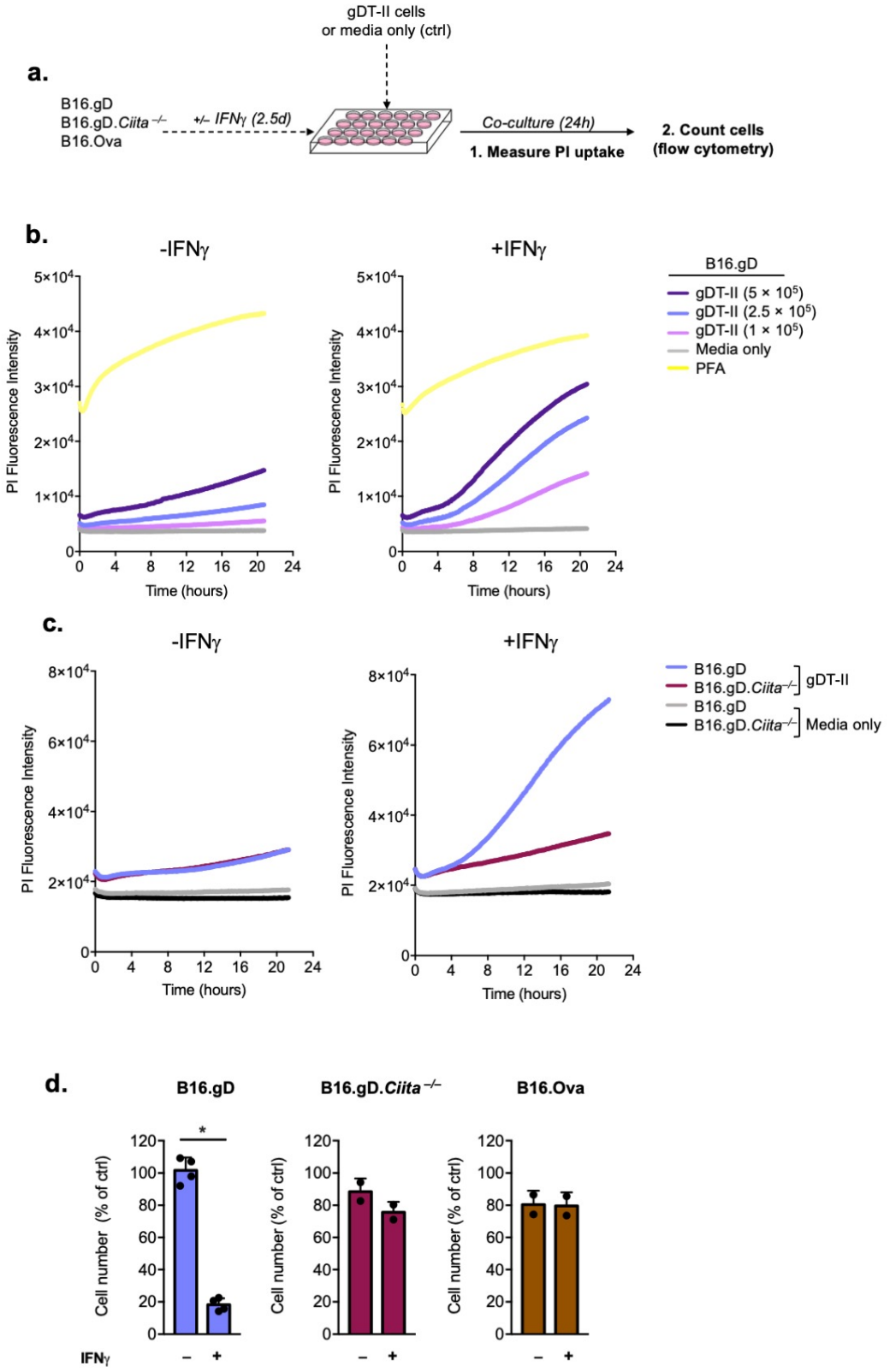

Figure 5.5. gDT-II cells specifically kill B16.gD cells in an MHC-II-dependent manner.

a, Experimental schematic of *in vitro* killing assay; B16 cell lines were plated (1 ×

10^4 cells) in the absence or presence of IFNγ (500 U/mL). Two and a half days later cell lines were co-cultured with *in vitro* activated gDT-II cells (2.5×10^4 cells or as otherwise indicated in (**b**)) or with cell-culture media alone for 24 hours. PI fluorescence intensity was measured during the 24 hours and B16 cells were enumerated by flow cytometry ($DAPI^{-}CD45.1^{-}V\alpha3.2^{-}CD4^{-}GFP^{+}$) following co-culture. **b,** PI Fluorescence intensity measured during co-culture of B16.gD cells (left; without IFNγ pre-stimulation, or right; with IFNγ stimulation) with different numbers of gDT-II cells as indicated in key. PFA; B16.gD cells treated with 4 % paraformaldehyde (in media without gDT-II cells) immediately prior to 24-hour assay. Data from one experiment, representative of 3 biologically independent experiments. **c,** PI fluorescence intensity measured during co-culture of B16.gD or B16.gD.*Ciita*$^{-/-}$ cells with 2.5×10^5 gDT-II cells, data from one experiment, representative of two biologically independent experiments. **d,** Number of surviving melanoma cells (+/- IFNγ pre-stimulation) determined by flow cytometry after co-culture with 2.5×10^5 gDT-II cells, relative to the number of surviving melanoma cells cultured with media alone (ctrl). Data pooled from 4 (B16.gD), or 2 (B16.gD.*Ciita*$^{-/-}$, B16.Ova) biologically independent experiments, where each data point represents a different experiment, bars and error bars show mean and standard deviation, respectively.*P=0.029, Statistical significance determined by Mann-Whitney test.

5.2.5 CD4$^+$ T cells execute melanoma killing via multiple mechanisms *in vitro.*

Direct killing of melanoma cells by cytotoxic CD8$^+$ T cells can occur via different pathways involving perforin-granzyme, Fas-FasL engagement or cytokines such as TNFα or IFNγ. Less is known surrounding the mechanisms by which cytotoxic CD4$^+$ T cells kill target cells. In chapter 4, gDT-II cells were characterised for expression of cytotoxic molecules and cytokine production via flow cytometry. gDT-II cells activated *in vitro* by peptide pulsed splenocytes produced TNFα (some of which co-produced IFNγ), and co-expressed Granzyme B and FasL (**Figure. 4.15c-f**). To further investigate whether these molecules contributed to the cytotoxicity of gDT-II cells, killing assays were performed using a range of tools to block the associated killing pathways. Two methods were used to investigate the role of TNFα produced by CD4$^+$ T cells in melanoma cell killing. Firstly, the receptor to which TNFα binds (TNFR1) was genetically disrupted in B16.gD melanoma cells (as described in Chapter 3). Secondly, an antagonistic TNFα antibody was used during co-culture with gDT-II cells. Antagonistic antibodies for IFNγ and FasL were also used to investigate the potential role of these molecules in induction of melanoma cell death. Finally, perforin-deficient gDT-II.*Prf1*$^{-/-}$ cells were used to block killing via perforin-dependent cytolysis (**Figure 5.6a**).

As previously described, melanoma cells were pre-treated with IFNγ prior to co-culture to upregulate MHC-II required for *in vitro* killing by gDT-II cells. Cell death was measured during co-culture by PI uptake (PI fluorescence intensity) and subsequent to co-culture by enumeration of surviving melanoma cells using flow cytometry **(Figure 5.6a)**. Following co-culture, there was slightly more surviving B16.gD.*Tnfr1*$^{-/-}$ cells compared to wild type B16.gD cells (**Figure 5.6b**). Similarly, in the presence of a TNFα blocking antibody there were slightly more surviving B16.gD cells following co-culture (**Figure 5.6c**). The use of IFNγ blocking antibody had no effect on the number of surviving melanoma cells when used

alone or in combination with TNFα blockade (**Figure. 5.6b, c**). Flow cytometric analysis was only performed twice and thus statistical significance was not evaluated.

Measurement of cell death in real-time by PI uptake provided information on the kinetics of $CD4^+$ T cell killing mechanisms. During the first 15 hours of co-culture with gDT-II cells, the same level of cell death occurred for B16.gD.*Tnfr1*$^{-/-}$ and B16.gD cells (no block). However, onwards of 15 hours, PI uptake was slightly reduced in B16.gD.*Tnfr1*$^{-/-}$ cells suggesting that prolonged exposure to TNFα may contribute to cell death (**Figure 5.6d**). This mild reduction in killing of B16.gD.*Tnfr1*$^{-/-}$ cells after 15 hours co-culture compared to the control (no block) aligns with the mild reduction in cell number following 24 hours co-culture calculated by flow cytometry (**Figure 5.6b, c**). Blocking perforin through the use of gDT-II.*Prf1*$^{-/-}$ cells resulted in delayed killing of B16.gD cells (**Figure 5.6d**). However, perforin blockade alone only mildly reduced the final amount of PI uptake by melanoma cells compared to the control (no block). Blocking FasL, by use of an antagonistic antibody, had a pronounced effect on inhibition of cell death. FasL blockade mediated a substantial delay in killing and by the end of the 24-hour co-culture the level of PI uptake was approximately 50 % of the control (no block). Combination blocking of TNFα and Perforin together or FasL and Perforin together showed an additive effect in preventing death of melanoma cells. Strikingly, simultaneous blockade of all three pathways rendered the melanoma cells almost entirely resistant to PI uptake.

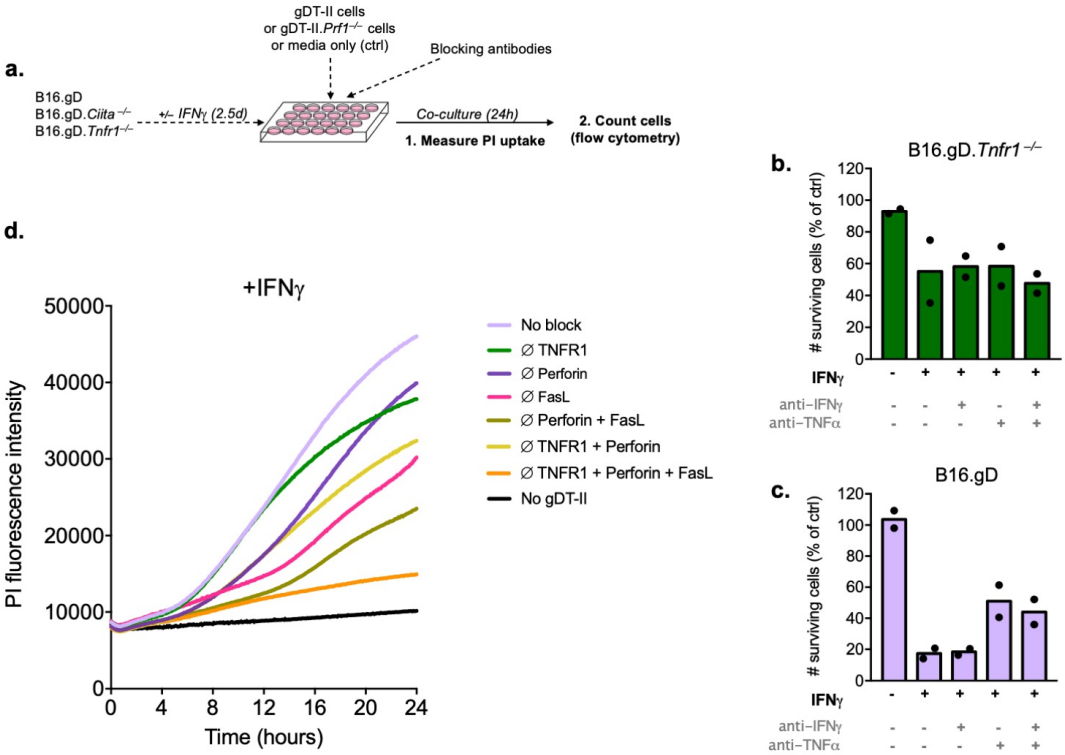

Figure 5.6. gDT-II cells specifically kill B16.gD cells by multiple mechanisms *in vitro.*

a, Experimental schematic of *in vitro* killing assay; B16 cell lines were plated (1 × 10^4 cells) in the absence or presence of IFNγ (500 U/mL). Two and a half days later cell lines were co-cultured with *in vitro* activated gDT-II or gDT-II.*Prf1*$^{-/-}$ cells (2.5 × 10^4) or with cell-culture media alone for 24 hours. PI absorbance was measured during the 24 hours and B16 cells were enumerated by flow cytometry ($DAPI^-CD45.1^-$ $V\alpha3.2^-$ $CD4^-$ GFP^+) following co-culture. **b, c,** Number of surviving B16.gD.*Tnf1*$^{-/-}$ cells **(b)** or B16.gD cells **(c)** determined by flow cytometry after co-culture with gDT-II cells, relative to the number of surviving melanoma cells cultured with media alone (ctrl). Melanoma cells were pretreated with IFNγ where indicated. Neutralizing antibodies (αIFNγ, αTNF) were added during co-culture (10 μg/mL) where indicated. Data pooled from 2 biologically independent experiments, where each data point represents an individual experiment, bars show mean. **d,** PI Fluorescence intensity measured during co-culture of; B16.gD cells with gDT-II cells (no block, light pink), B16.gD.*Tnf1*$^{-/-}$ cells with gDT-II cells (ØTNFR1, green), B16.gD cells with gDT-II.*Pfr1*$^{-/-}$ cells (Ø Perforin, purple), B16.gD cells with gDT-II cells and FasL blocking antibody (ØFasL, dark pink), B16.gD cells with gDT-II.*Pfr1*$^{-/-}$ cells and FasL blocking antibody (Ø Perforin + FasL, brown), B16.gD.*Tnf1*$^{-/-}$ cells with gDT-II.*Pfr1*$^{-/-}$ cells (Ø Perforin + TNFR1, yellow), B16.gD.*Tnf1*$^{-/-}$ cells with gDT-II.*Pfr1*$^{-/-}$ cells and FasL blocking antibody (Ø Perforin + TNFR1 + FasL, orange), B16.gD cells with media only (No gDT-II, black). Melanoma cells had been pre-treated with IFNγ prior to co-culture for all conditions. FasL antibody used at 2 μg/mL. Data from one experiment, representative of 3 experiments.

5.2.6 Loss of Perforin or TNFR1 does not prevent control of melanoma by CD4$^+$ T cells.

To determine whether production of TNFα by CD4$^+$ T cells is required to directly kill melanoma cells *in vivo*, B16.gD.*Tnfr1*$^{-/-}$ cells were transplanted epicutaneously into *Rag2*$^{-/-}$*;Il2rg*$^{-/-}$ mice that received *in vitro* activated gDT-II cells, or did not receive gDT-II cells (control) (**Figure 5.7a**). gDT-II cells afforded complete protection against development of B16.gD.*Tnfr1*$^{-/-}$ tumors whilst 100 % of control mice succumbed to tumor development (**Figure 5.7b, c**).

Perforin-deficient gDT-II cells were used to investigate whether perforin-dependent cytolysis was required for killing of melanoma cells by CD4$^+$ T cells *in vivo*. B16.gD cells were transplanted epicutaneously into *Rag2*$^{-/-}$*;Il2rg*$^{-/-}$ mice that received *in vitro* activated gDT-II.*Prf1*$^{-/-}$ cells, wild-type gDT-II cells or did not receive gDT-II cells (control) (**Figure 5.7d**). Both the wild-type gDT-II cells and gDT-II.*Prf1*$^{-/-}$ cells mediated full protection against the development of tumors, whilst there was a high incidence of tumors in the control cohort that did not receive gDT-II cells (**Figure 5.7e, f**). These experiments suggest that CD4$^+$ T cells can mediate melanoma control independently of TNFα or Perforin-mediated killing pathways.

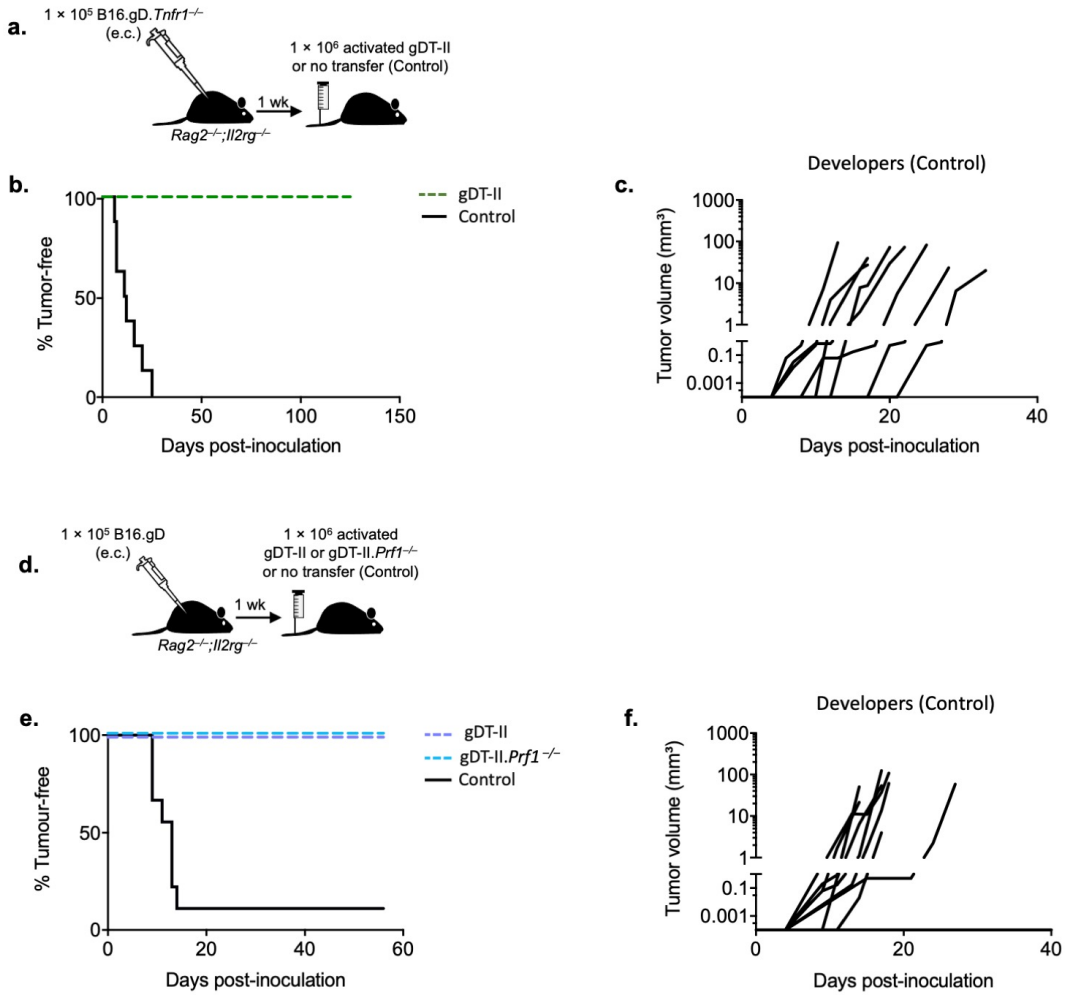

Figure 5.7. TNFR1 expression by B16.gD cells and perforin expression by gDT-II cells are dispensable for melanoma control.

a, Schematic of experimental protocol for **b,c**; *Rag2*$^{-/-}$*;Il2rg*$^{-/-}$ mice were challenged with B16.gD.*Tnfr1*$^{-/-}$ cells (1 × 10^5 e.c.) and received *in vitro* activated gDT-II cells (1 × 10^6, i.v.) 1 week p.i., or did not receive gDT-II cells (Control). **b,** Primary tumor incidence and **c,** primary tumor growth kinetics, n=8 (Control), n=11 (gDT-II), data pooled from 2 biologically independent experiments. **d,** Schematic of experimental protocol for **e,f**; *Rag2*$^{-/-}$*;Il2rg*$^{-/-}$ mice were challenged with B16.gD cells (1 × 10^5 e.c.) and received either *in vitro* activated gDT-II cells or gDT-II.*Prf1*$^{-/-}$ cells (1 × 10^6, i.v.) 1 week p.i, or did not receive gDT-II cells (Control). **e,** Primary tumor incidence and **f,** primary tumor growth kinetics, n=9 (Control), n=9 gDT-II or n=13 (gDT-II.*Prf1*$^{-/-}$), data pooled from 2 biologically independent experiments.

5.2.7 Blocking TNFR1 signalling may confer a selective advantage for melanoma cells.

Next Generation Sequencing (NGS) was used to analyse the *Tnfr1* indel allele frequencies in tumors from *Rag2*$^{-/-}$*;Il2rg*$^{-/-}$ and C57BL/6 mice inoculated with the B16.gD*.Tnfr1*$^{-/-}$ cell line (**Figure 5.8a, b**). Distinct mutations, represented in pie charts, enable visualisation of the overall indel distribution within a particular sample (**Figure 5.8a**). Restriction in indel distribution are likely to result from outgrowth of fitter clones (Glodde et al., 2019). Prior to inoculation, the polyclonal B16.gD*.Tnfr1*$^{-/-}$ cell line consisted of heterogenous clones harbouring distinct mutations (indels) in the *Tnfr1* gene. 6.2 % of *Tnfr1* sequences contained no indel, suggesting that this would be the approximate frequency of cells within the culture that expressed functional (wild-type) TNFR1. In all tumors, the frequency of wild-type *Tnfr1* sequences were lower than in the initially transplanted culture (0.3-4.6 % compared to 6.2 %). This suggests that deletion of *Tnfr1* may provide melanoma cells with a survival advantage *in vivo* however, only five mice were analysed (three from *Rag2*$^{-/-}$*;Il2rg*$^{-/-}$ and two from C57BL/6 mice) and a larger sample size would be required to validate this finding.

NGS sequencing enabled lineage tracing due to the unique mutations that were harboured by B16.gD*.Tnfr1*$^{-/-}$ clones. This technique could therefore be used to investigate the dynamics of clonal diversity within tumors. In the *Rag2*$^{-/-}$*;Il2rg*$^{-/-}$ mice the rate of tumor growth corresponded with the level of clonal diversity. That is, the tumor which developed rapidly (sample #2), exceeding a volume of 20 mm^3 within 13 days p.i., had a similar indel distribution to the cells which were initially transplanted. The tumor which exceeded a volume of 20 mm^3 on day 25 p.i. (sample #3) showed restriction in the indel composition suggesting that the tumor was oligoclonal. The slowest-growing tumor, which exceeded a volume of 20 mm^3 on day 33 p.i. (sample #4), showed profound clonal restriction as the indel distribution was comprised almost entirely of one indel. All tumors from C57BL/6 mice (which exceeded a volume of 20 mm^3 by day 25 p.i.) also showed a restriction of the indel distribution compared to the transplanted cell line.

Interestingly, the lymph node metastasis and primary tumor from the same mouse (samples #6,7) comprised a similar degree of clonality.

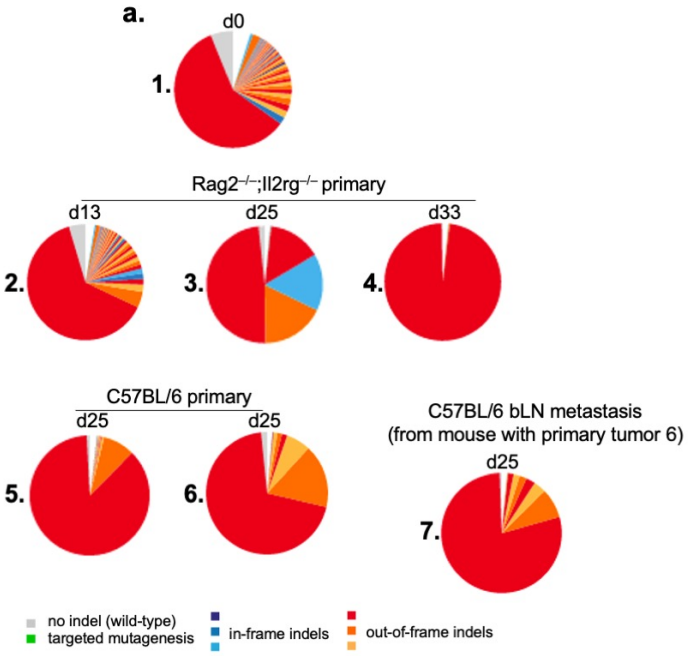

b.

Sample #	% Wild-type reads
1	6.2
2	1.7
3	4.6
4	0.3
5	0.8
6	1.6
7	0.5

Figure 5.8. Analysis of *Tnfr1* indel distribution in B16.gD.*Tnfr1*$^{-/-}$ tumors by Next Generation Sequencing.
Melanoma cells from tumors of mice inoculated with B16.gD.*Tnfr1*$^{-/-}$ cells (1 × 10^5 e.c.) were expanded *ex vivo* and genomic DNA was sequenced by NGS using the Illumina MiSeq platform. NGS data was aligned against the region of *Tnfr1* gene targeted by Px459-*Tnfr1(b)* using the web tool Outknocker 3.0 alignment tool. Analysis includes the B16.gD.*Tnfr1*$^{-/-}$ cell line prior to inoculation (#1), three primary tumors from *Rag2*$^{-/-}$*;Il2rg*$^{-/-}$ mice (#2-4), two primary tumors from C57BL/6 mice (#5,6), and one lymph node metastasis from C57BL/6 mouse with primary tumor #6 (#7). Tumors harvested, when tumor volume >20 mm^3, at day (d) indicated. **a,** *Tnfr1* indel distribution from samples 1-7 represented in pie charts with different types of indels categorized by color as indicated in key. **b,** Table listing the percentage of wild-type sequence reads (no indel) from samples 1-7.

5.3 Discussion

It is increasingly recognised that $CD4^+$ T cells play a crucial role in cancer immunosurveillance however the underlying mechanisms are not well understood. Both $CD4^+$ and $CD8^+$ T cells play a role in the formation of spontaneous immunity in the epicutaneous model evidenced by the increase in tumor incidence triggered by depletion of either $CD4^+$ or $CD8^+$ T cells prior to inoculation (unpublished data, Gebhardt laboratory). Several studies have shown that $CD4^+$ T cells cooperate with $CD8^+$ T cells to mediate antitumoral immunity. Adoptive transfer of both $CD4^+$ and $CD8^+$ T cells together, compared to either cell type alone, can elicit exceptionally better antitumoral responses in murine models (Ossendorp et al., 1998, Huang et al., 2005, Marzo et al., 2000, Bohm et al., 1998). Recently, it has been demonstrated that $CD4^+$ T cell "help" via DC licensing is important for cancer elimination by $CD8^+$ T cells (Alspach et al., 2019, Zhu et al., 2015, Ferris et al., 2020). It has also been shown that $CD4^+$ T cells potentiate antitumoral $CD8^+$ T cell responses through "post-licensing" mechanisms such as augmenting $CD8^+$ T cell recruitment or cytotoxic function within the TME (Bos and Sherman, 2010, Wong et al., 2008, Schietinger et al., 2010, Huang et al., 2005).

The present study revealed that *Cd40*$^{-/-}$ mice were more susceptible to tumor development suggesting that $CD4^+$ T cell "help" through DC licensing may be important for spontaneous immune control in the epicutaneous melanoma model. However, since the genetic ablation of CD40 was not cell-type specific, it is important to consider that other processes may contribute to the loss of tumor control in *Cd40*$^{-/-}$ mice. Indeed, CD40 can be expressed by several cell types and may be involved in other biological processes. For example, it is well established that CD40/CD40L signalling is required for transducing "helper" signals from Tfh cells to B cells. However, previous characterisation of the epicutaneous melanoma model found that μMT mice, which are deficient in B cells, were no more susceptible to melanoma development than wild-type mice (unpublished data, Gebhardt laboratory). This suggests that B cells are

dispensable for spontaneous immune control in the epicutaneous melanoma model and that the lack of spontaneous tumor control in *Cd40*$^{-/-}$ mice is unlikely due to impaired humoral immunity. A recent study demonstrated that deletion of CD40 specifically in cDC1, a subset of DCs that primes CD8^{+} T cells, abrogated CD4^{+} T cell licensing resulting in impaired antitumoral immunity (Ferris et al., 2020). In addition, administration of CD40 antibody to mimic T cell "help," in combination with ICB therapy, protected mice against pancreas tumor development by enhancing T cell priming (Morrison et al., 2020). These data further substantiate that impaired tumor control due to the loss of CD40 observed in the epicutaneous melanoma model may be due to loss of DC licensing and poor T cell priming. The impaired ability of *Cd40*$^{-/-}$ mice to control tumors encourages use of the epicutaneous melanoma model to further investigate CD4^{+} T cell "help" in priming CD8^{+} T cell responses against melanoma antigens.

The current data, although not statistically significant, suggests that *Cd40l*$^{-/-}$ mice show a less pronounced defect in tumor control compared to *Cd40*$^{-/-}$ mice. This could be explained by other possible ligands that may bind CD40 and thereby may compensate for lack of CD40L. Indeed, promiscuity of receptor-ligand interactions is a common biological phenomenon that can provide the host with a level of flexibility to adapt to diverse microenvironments. To our knowledge, the identity and origin of alternative ligands for CD40 have not been described.

Whilst CD4^{+} T cell "help" may contribute to melanoma immunosurveillance in the epicutaneous model, the transfer of *in vitro* activated gDT-II cells protected against B16.gD tumor development in *Rag2*$^{-/-}$*;Il2rg*$^{-/-}$ mice deficient in endogenous T cells, B cells, and NK cells. In addition, *in vivo* primed gDT-II cells colocalised with B16.gD melanoma cells at the inoculation site in wild-type mice. These data provide evidence that CD4^{+} T cells can play a direct peripheral effector role in eliminating or controlling the outgrowth of melanoma.

Since T cells require TCR engagement to elicit effector activity, we sought to determine the mechanism by which cognate antigen is presented to CD4^{+} T cells

in the TME. That is, whether the provision of MHC-II-restricted antigens to $CD4^+$ T cells is carried out indirectly by professional APCs or directly by MHC-II-positive melanoma cells. Expression of MHC-II by B16.gD cells inversely correlated with tumor volume. IFNγ induced MHC-II expression by B16.gD cells *in vitro* and thus is likely to regulate MHC-II upregulation *in vivo*. In general, smaller tumors are more permissive to immune cell infiltration, in contrast to larger tumors which are associated with pathological hypoxia, a condition that can inhibit immune cell infiltration, survival and function (Taylor and Colgan, 2017). Therefore, smaller tumors that expressed MHC-II may represent "immunologically hot" tumors in which higher numbers of immune cell infiltrates produced sufficient IFNγ in the TME to upregulate MHC-II. Conversely, the lack of MHC-II expression on larger tumors may result from low concentrations of IFNγ in the TME. It is also possible that other mechanisms may downregulate MHC-II expression, such as epigenetic silencing or loss of function mutations in the genes involved in the MHC-II regulatory pathway.

$CD4^+$ T cells were present at higher densities in tumors in which B16.gD cells expressed MHC-II. Evidence that MHC-II expression was responsible for higher $CD4^+$ T cell number, comes from the inverse correlation between $CD4^+$ T cell infiltration and tumor volume in wild-type B16.gD tumors, but not in B16.gD.*Ciita*$^{-/-}$ tumors. Dependency of intratumoral $CD4^+$ T cell number on MHC-II expression by melanoma suggests melanoma cells can directly present antigen to $CD4^+$ T cells. A positive correlation between expression of MHC-II on cancer cells and the number of intratumoral $CD4^+$ T cells has been observed in human patients and these parameters are often associated with a good prognosis and positive response to immunotherapy (Johnson et al., 2016, Park et al., 2017, Matsuzaki et al., 2014). To further investigate the relevance of MHC-II expression by melanoma cells in immunosurveillance, tumor incidence and tumor growth kinetics were assessed in mice inoculated with B16.gD.*Ciita*$^{-/-}$. The deletion of *Ciita* from melanoma cells did not impact the incidence of primary tumor development although B16.gD.*Ciita*$^{-/-}$ tumors did grow slightly faster compared to wild-type B16.gD tumors. From this observation, one could speculate that

MHC-II expression by melanoma cells initially hinders tumor growth, potentially through early recruitment of $CD4^+$ T cells into the TME, although additional experiments would be required to test this prediction.

Whilst melanoma cells may directly stimulate $CD4^+$ T cells in this model, the transfer of gDT-II cells was protective against primary tumor development in mice challenged with B16.gD.*Ciita*$^{-/-}$ cells. In line with several other studies, this finding demonstrates that MHC-II expression by melanoma cells is dispensable for immunosurveillance by $CD4^+$ T cells (Shklovskaya et al., 2016, Perez-Diez et al., 2007, Haabeth et al., 2018, Mumberg et al., 1999). Studies that showed direct engagement of $CD4^+$ T cells with MHC-II-positive melanoma cells did not address whether this interaction is necessary or represents a redundant process that can be overcome by indirect antigen presentation by professional APCs (Quezada et al., 2010, Malandro et al., 2016). Additional signals delivered to $CD4^+$ T cells during TCR engagement are likely to differ between professional APCs and cancer cells. For instance, we observed that B16.gD cells expressed low levels of costimulatory molecules compared to professional antigen-presenting cells in the TME and it is a well-established phenomenon that TCR engagement in the absence of costimulation can lead to T cell exhaustion or tolerance (Driessens et al., 2009).

Experiments using B16.gD.*Ciita*$^{-/-}$ revealed that *Ciita* may play context-specific roles in control of primary tumors and lymph node metastasis. This finding is highly important considering that metastasis is the primary cause of death in melanoma. Deletion of *Ciita* in melanoma cells led to a decrease in size and incidence of lymph node metastasis although the underlying mechanism was not further investigated. Whether *Ciita* impacts metastatic dissemination from the primary lesion or immune control at the lymph node remains to be determined. A possible mechanism by which *Ciita* could promote metastatic dissemination is through regulation of MHC-II and the resultant increase in $CD4^+$ T cell number in the TME. Although $CD4^+$ T cells can protect against primary tumor development, the increase in immune pressure from high numbers of intratumoral $CD4^+$ T cells

may favour intravasation of escape variants into the vasculature. Another hypothesis is that *Ciita* expression could impair immune control in the lymph node as MHC-II expression by melanoma cells may tolerise $CD4^+$ T cells due to lack of costimulation as previously discussed. This would imply that MHC-II negative melanoma cells that seed in the lymph node may be better controlled or eliminated due to more efficient antigen presentation by the abundance of professional APCs. Furthermore, MHC-II is a known ligand for Lag-3, an inhibitory receptor expressed by $CD4^+$ T cells. MHC-II expressed by melanoma cell in the lymph node may thus induce CD4+ T cell exhaustion and escape immune control in the lymph node. Lag-3 expression within tumors has been associated with poor prognoses and negative responses to immunotherapy. Lag-3 is currently being explored as a target for cancer immunotherapy (He et al., 2016) which is supported by animal models in which tumor growth was delayed when blocking Lag-3 (Huang et al., 2015).

It is also important to consider that *Ciita* is the master transcriptional activator for several genes involved in the MHC-II presentation pathway which include not only MHC-II molecules but chaperone proteins such as the invariant chain (CD74) (Harton and Ting, 2000). CD74 has been shown to play diverse functions beyond the assembly and trafficking of MHC-II molecules. Such functions include endosomal trafficking and cell migration (Faure-Andre et al., 2008). Through modulating motility and migration, CD74 may play a cell-intrinsic role in enhancing metastatic potential of melanoma cells, independent of the immune system. In addition, CD74 can interact with MHC-I and play a role in regulating presentation of MHC-I restricted antigens (Basha et al., 2012). MHC-I is a ligand for Ly49, which acts as an inhibitory receptor on NK cells. This renders cells with low expression of MHC-I more susceptible to killing by NK cells (Paul and Lal, 2017). NK cells play an important role in controlling metastasis in the epicutaneous melanoma model (unpublished data, Gebhardt laboratory) and therefore we postulated that a possible link between *Ciita* deletion and improved control of metastasis could be increased NK cell-mediated killing of melanoma cells with reduced MHC-I expression as a result of loss of CD74. However,

incongruous with this hypothesis, the genetic deletion of *Ciita* did not prevent IFNγ-induced upregulation of MHC-I in B16.gD.*Ciita*$^{-/-}$ cells *in vitro* (chapter 3). Nevertheless, expression of MHC-I on B16.gD.*Ciita*$^{-/-}$ melanoma cells should be characterised within tumors because using high concentrations of exogenous IFNγ may not truly reflect the complexity of MHC-I regulation that occurs *in vivo.* Whilst the most commonly recognised function of *Ciita* is regulation of MHC-II and hence CD4$^+$ T cell responses, it is evident that other potential roles of *Ciita* in metastasis should be further investigated. For instance, to specifically disentangle potential roles of MHC-II or CD74 in metastasis, these genes could be specifically targeted for genetic deletion in melanoma cells. Alternatively, these genes could be reintroduced using viral overexpression plasmids into the B16.gD.*Ciita*$^{-/-}$ cell line.

The protection driven by CD4$^+$ T cells in the absence of MHC-II expression by melanoma cells highlights the importance of APCs in presenting MHC-II restricted antigens to antitumoral CD4$^+$ T cells in the TME. This finding is consistent with the results of two-photon microscopy which suggested that CD4$^+$ T cells and melanoma cells interact indirectly presumably through intermediate cells such as professional APCs (**Appendix video 3, 4**). Within B16.gD tumors, a GFP signal was detected in a population of CD45$^+$CD11b$^+$ cells by flow cytometry. We speculate that this population constituted phagocytic cells that had engulfed GFP derived from B16.gD melanoma cells. The phenomenon whereby APCs acquire fluorescence derived from fluorescently labelled melanoma cells has been previously shown using flow cytometry in combination with intravital two-photon microscopy (Headley et al., 2016). In this study, two-photon microscopy revealed that tumor “microblebs” from fluorescently labelled B16 melanoma cells were engulfed by CD11b$^+$ myeloid cells. Other possible sources of melanoma fragments phagocytosed by immune cells include secreted extracellular vesicles, or the release of intracellular contents by dying melanoma cells. Expression of MHC-II and costimulatory molecules by the CD45$^+$GFP^{int} population supports their possible involvement in presenting tumor antigens to CD4$^+$ T cells. The CD45$^+$GFP^{int} population could comprise several different subsets of DCs and

markers additional to CD11b and CD11c would be instrumental in differentiating them (Macleod et al., 2014, Tamoutounour et al., 2013). It should also be noted that GFP and gD are independently expressed by B16.gD cells and therefore it is possible that GFP^{int} cells in the TME may have internalised GFP but not gD. The CRISPitope cell lines that were generated to harbour fusion proteins between the gD epitope, a target protein and a fluorescent molecule (Chapter 3) could be used to more specifically investigate the uptake and spread of gD with in the TME and characterise the APC subsets that present melanoma-derived antigens to $CD4^+$ T cells.

Due to the phenotypic and functional heterogeneity of $CD4^+$ T cells, mechanisms orchestrating tumor control in the TME remain equivocal and are likely to be context dependent. It has been shown that $CD4^+$ T cells drive antitumoral immunity indirectly by regulating other antitumoral immune cells in the TME, such as cytotoxic $CD8^+$ T cells and M1 macrophages. In addition, $CD4^+$ T cells directly lyse cancer cells *in vitro* (Quezada et al., 2010, Sashchenko et al., 2007, Lundin et al., 2004), and express cytotoxic transcriptional profiles in cancer patients (Oh et al., 2020, Kitano et al., 2013). Mechanisms by which cytotoxic $CD4^+$ T cells kill cancer cells are poorly understood. In contrast, killing pathways of $CD8^+$ T cells are more well characterised and include perforin/granzyme-mediated cytolysis or signalling through TNF superfamily proteins such as FasL and TNFα. As such, these signalling pathways were investigated as potential mechanisms by which $CD4^+$ T cells targeted melanoma cells. *In vitro,* gDT-II cells killed B16.gD melanoma cells directly in an MHC-II-dependent, antigen-specific manner. Since professional APCs were absent in the *in vitro* killing assay, IFNγ was used to pre-stimulate the melanoma cells to express MHC-II*,* however blockade of IFNγ during co-culture had no impact on killing by $CD4^+$ T cells. The role of IFNγ in the antitumoral $CD4^+$ T cell response has not yet been investigated in the epicutaneous melanoma model. However, several studies showed that elimination of cancer cells by $CD4^+$ T cells was abrogated upon neuralisation of IFNγ with an antagonistic antibody (Haabeth et al., 2018, Mumberg et al., 1999, Shklovskaya et al., 2016, Muranski et al., 2008, Malandro et al., 2016, Quezada

et al., 2010). IFNγ can regulate many processes and the underlying mechanism by which IFNγ is required for cancer immunosurveillance by $CD4^+$ T cells remains enigmatic. Results of the *in vitro* killing assay thus provide evidence that IFNγ is not involved in killing of melanoma cells. As previously discussed, IFNγ has a role in regulating MHC molecules, however, it has been shown that IFNγ is required for the antitumoral $CD4^+$ T cell response against MHC-II deficient cancer cells (Haabeth et al., 2018, Mumberg et al., 1999, Shklovskaya et al., 2016). IFNγ can regulate other processes which may pre-sensitise melanoma cells to killing. For example, B16F10 cells have been shown to upregulate Fas upon treatment with IFNγ (Bohm et al., 1998) and the killing assay revealed that FasL was a major pathway by which $CD4^+$ T cells can kill melanoma cells *in vitro*.

Increasing evidence suggests that the role of IFNγ in cancer immunosurveillance involving $CD4^+$ T cells is due to effects on the host cells rather than directly on melanoma cells. One study showed that genetic disruption of the IFNγ receptor in melanoma cells did not inhibit their elimination by $CD4^+$ T cells *in vivo* (Mumberg et al., 1999). In addition, adoptively transferred $CD4^+$ T cells have been shown to eliminate established B16 melanomas in mice with genetic disruption of IFNγ but not in mice with genetic disruption of the IFNγ receptor (Muranski et al., 2008, Quezada et al., 2010). This suggests that IFNγ produced by $CD4^+$ T cells signals through host cells to eliminate melanoma.

The *in vitro* killing assay was instrumental in demonstrating the multiple pathways by which $CD4^+$ T cell kill melanoma cells. Killing was slightly reduced by blocking TNFα or Perforin. Reduction in killing was even more pronounced by blocking FasL. Importantly, simultaneous blockade of FasL, Perforin and TNFR1 *in vitro* abolished the killing of melanoma cells. This experiment thus revealed that direct killing by $CD4^+$ T occurs through FasL, Perforin or TNFα. $CD4^+$ T cell-mediated killing of cancer cells via the effector molecule TRAIL has been reported (Wang et al., 2003). Since blocking FASL, Perforin and TNFα was sufficient to abrogate killing, it is unlikely that any other cytolytic pathways, such as that induced by

TRAIL, play a substantial role in the melanoma cell killing. Whilst *in vitro* killing assays are valuable for investigating intrinsic molecular killing pathways, results are not always translatable to *in vivo* observations. For instance, one study found that $CD4^+$ T cells killed lymphoma cells through FasL *in vitro* but FasL blockade or genetic deletion of *FasL* had no effect on the ability of $CD4^+$ T cells to protect against tumor challenge *in vivo* (Lundin et al., 2004). This provided evidence that $CD4^+$ T cells can mediate tumor control through redundant mechanisms. Results from the current study also support that multiple pathways may provide a level of redundancy for $CD4^+$ T cell-driven antitumoral immunity. In *Rag2*$^{-/-}$*;Il2rg*$^{-/-}$ mice, perforin expression by $CD4^+$ T cells and TNFR1 expression by melanoma cells were dispensable for control of melanoma by $CD4^+$ T cells. It is possible that the high adoptive T cell transfer dose may obfuscate effects of blocking TNFR1 or perforin that could potentially pose a survival disadvantage to melanoma cells. As such, lower transfer doses will be titrated in future experiments to determine if processes are truly redundant or if there is a threshold at which the number of T cells are able to compensate for the loss of certain killing pathways. In addition, future adoptive transfer experiments will utilise a similar approach to the *in vitro* killing assay to simultaneously block TNFα, FasL and Perforin. This will serve to further elucidate the relative contributions of these pathways, and the possible level of redundancy, to control melanoma cells *in vivo*. Potential indirect effector roles of $CD4^+$ T cells within the TME, such as cross-talk with intratumoral M1 macrophages and antitumoral $CD8^+$ T cells, should also be explored in the epicutaneous melanoma model.

Although deletion of *Tnfr1* in melanoma cells was redundant for killing by $CD4^+$ T cells in *Rag2*$^{-/-}$*;Il2rg*$^{-/-}$ mice, *Tnfa*$^{-/-}$ mice are more susceptible to tumor development in the epicutaneous melanoma model (Park et al., 2019). TNFα regulates many biological processes and the mechanism by which TNFα promotes tumor control in the epicutaneous melanoma model has not been determined. Data from NGS sequencing revealed that deletion of *Tnfr1* in melanoma cells may provide a survival advantage *in vivo*. This was demonstrated by an increase in the frequency of out-of-frame indels relative to wild-type *Tnfr1*

sequences (no indels), in progressing tumors compared to the relative proportions that were initially transplanted. However, the starting frequency of wild-type clones was only 6.2 % and thus it would be advantageous to repeat the experiment with the transfer of an equal ratio of gene-deficient and wild-type clones. Furthermore, data is from a limited number of mice (n=5) so caution should be heeded in the interpretation of the results. It is also important to consider that changes in clonal frequencies may represent differential rates of proliferation and cell death and to disentangle the two processes requires further investigation. If the B16.gD*.Tnfr1*$^{-/-}$ cells are indeed more fit to survive *in vivo* than their wild-type counterparts, this provides evidence that TNFα produced by the host may play an antitumoral role by directly targeting melanoma cells to inhibit their proliferation or survival. To confirm that TNFα directly targets melanoma cells, survival of B16.gD*.Tnfr1*$^{-/-}$ cells compared to their wild-type counterparts should be examined in *Tnfa*$^{-/-}$ mice.

Finally, NGS revealed a correlation between clonal diversity and the rate of tumor growth in the epicutaneous model. Melanoma cells from a rapidly-growing tumor in a *Rag2*$^{-/-}$*;Il2rg*$^{-/-}$ mouse maintained a similar indel distribution to the initial culture of transplanted cells. This is consistent with an expected lack of “immunoediting” in an immunodeficient host. The tumors that developed later had a more restricted indel distribution suggesting that the rate of tumor growth depended largely on the number of surviving clones. Survival of melanoma cells could be influenced by engrafting efficiency or by host pressure favouring survival of particular clones. Of note, a similar clonal composition was observed between a primary tumor and lymph node metastasis from the same C57BL/6 mouse. This provides evidence that multiple metastatic seeding events occurred in contrast to a metastatic lesion developing from only a few clones. It should be noted that clonal composition was analysed using *Tnfr1*-deficient cells and kinetics of metastatic seeding may differ from that of the wild-type B16.gD cells. However, these preliminary experiments using NGS sequencing to trace clonal diversity provide initial insights into dynamics of tumor growth in the epicutaneous model.

Chapter 6:
Final Discussion

Chapter 6: Final discussion

6.1 Key findings

Despite growing recognition that $CD4^+$ T cells play an important role in cancer immunosurveillance the underlying mechanisms remain ambiguous. $CD4^+$ T cells are heterogeneous in nature and exert diverse functions driven by local environmental cues. Discrepant findings amongst studies that have characterised antitumoral $CD4^+$ T cell responses are thus likely to result from the use of different tumor models which foster different tumor microenvironments. Indeed, antitumoral mechanisms of $CD4^+$ T cells may differ depending on various factors such as cancer types, stage and location. This highlights the importance of preclinical models that closely recapitulate human cancer to study immunosurveillance mechanisms. As such, this study sought to characterise the $CD4^+$ T cell response using the recently developed epicutaneous melanoma model. This model has the advantage that tumor growth closely recapitulates both the location and progression of human melanoma. Furthermore, being a transplantable model enables the flexibility to use different melanoma cell lines. Thus, one aim of this project was to generate a series of genetically modified melanoma cell lines to use in the epicutaneous melanoma model. Melanoma cells were engineered to express molecules which enabled their tracking *in vivo* by microscopy or bioluminescence imaging. In addition, CRISPR/Cas9 technology was used to delete specific genes to investigate their importance in cancer immunosurveillance. Finally, the newly described CRISPitope platform (Effern et al., 2020) was used to generate melanoma cell lines that express $CD4^+$ T cell epitopes under different promotors in order to investigate how variation in antigen biology impacts the $CD4^+$ T cell response.

The epicutaneous melanoma model demonstrated to be of considerable value for investigating antitumoral responses of $CD4^+$ T cells. The transfer of naïve or activated melanoma-specific $CD4^+$ T cells into wild-type or RAG-deficient mice, respectively, mediated protection from development of tumors. Evidence

that CD4$^+$ T cells played a conventional “helper” role through licencing of DCs was provided by the increased susceptibility of mice deficient in CD40 signalling to tumor development. Additionally, we identified that CD4$^+$ T cells played a peripheral effector role at the site of melanoma challenge. Live cell imaging using two-photon microscopy was instrumental in visualising interactions between CD4$^+$ T cells and melanoma cells within the skin. Melanoma-specific CD4$^+$ T cells predominantly expressed T-bet in melanoma challenged skin, however, established tumors promoted Treg polarisation. The level of protection mediated by the transfer of naïve CD4$^+$ T cells was particularly striking considering we found evidence for weak priming. Compared to CD4$^+$ T cells primed against viral infection, CD4$^+$ T cells primed in the context of melanoma failed to upregulate IL-2 receptor alpha chain, exhibited reduced proliferation and showed less pronounced or delayed upregulation of T-bet.

To understand how peripheral CD4$^+$ T cells suppressed tumor outgrowth we sought to address two principal questions. Firstly, which cell types present antigen on MHC-II to CD4$^+$ T cells in the TME, and how does the nature of stimulation effect the ensuing CD4$^+$ T cell response? Secondly, what are the underlying effector mechanisms by which CD4$^+$ T cells promote melanoma cell death or senescence?

Whether antigen is taken up by profession APCs in the TME and indirectly presented to CD4$^+$ T cells, or whether cancer cells directly present endogenously processed antigens to CD4$^+$ T cells is not well understood. We found evidence that CD4$^+$ T cells could recognise melanoma-derived antigen both directly and indirectly. Melanoma cells were able to upregulate MHC-II and directly stimulate CD4$^+$ T cell *in vitro*, and expression of MHC-II by melanoma cells *in vivo* correlated with higher numbers of intratumoral CD4$^+$ T cells. However, CD4$^+$ T cells were able to protect against tumor outgrowth in mice challenged with an MHC-II-deficient melanoma cell line demonstrating the important role of indirect presentation within the TME. MHC-II-positive immune cells were abundant in tumors and, as expected, expressed higher levels of canonical costimulatory

molecules compared to melanoma cells. Interestingly, metastasis in the brachial lymph node was observed less frequently in mice inoculated with MHC-II-deficient melanoma cells suggesting that MHC-II expression by melanoma cells may negatively impact immunosurveillance at metastatic sites.

Finally, using a sensitive *in vitro* assay to measure cell death in real-time, we identified that $CD4^+$ T cells could directly kill melanoma through mechanisms involving the effector molecules FasL, perforin and TNFα. This finding reveals a potential redundancy in mechanisms by which $CD4^+$ T cells kill melanoma cells, a phenomenon which may reconcile discrepancies between studies attempting to characterise cytotoxicity of $CD4^+$ T cells.

6.2 Outlook

This study has provided valuable insight into understanding aspects of melanoma immunosurveillance by $CD4^+$ T cells. These findings, however, beget several further questions. Initial evidence that $CD4^+$ T cell help is important in spontaneous immune control in the epicutaneous melanoma model was shown by the increased susceptibility of CD40-deficient mice to tumor development. Experiments will be designed to further characterise the role of $CD4^+$ T cell help to $CD8^+$ T cells, not only in the initial priming phase, but also the potential synergism within the TME that has been previously recognised (Alspach et al., 2019, Bos and Sherman, 2010). To characterise both the $CD4^+$ and $CD8^+$ responses simultaneously, melanoma cells which harbour model epitopes for transgenic $CD4^+$ T cells (gD for gDT-II cells) and $CD8^+$ T cells (gB for gBT-I cells) will be generated. Melanoma-specific $CD8^+$ T cell responses can then be tracked using gBT-I cells in the presence of absence of adoptively transferred naïve gDT-II cells to investigate the potential licensing and post-licensing helper functions of $CD4^+$ T cells.

In this study, $CD4^+$ T cells were able to suppress tumor outgrowth in the

absence of MHC-II expression by melanoma cells. However, the potential contribution of MHC-II expression by melanoma cells to directly stimulate $CD4^+$ T cells in the TME requires further investigation. To elucidate whether direct stimulation of $CD4^+$ T cells is sufficient to elicit antitumoral immunity, $CD4^+$ T cells will be adoptively transferred into MHC-II deficient mice (*IAE*$^{-/-}$) inoculated with either MHC-II-expressing or MHC-II-deficient melanoma cells.

Experiments will also be designed to follow up on the finding that mice inoculated with MHC-II deficient melanoma cells presented with a lower incidence of lymph node metastases. We speculate that MHC-II positive melanoma cells that bind to $CD4^+$ T cells in the lymph node may induce T cell dysfunction or misguided $CD4^+$ T cell effector differentiation. This could be due to a lack of costimulatory signals provided by presenting melanoma cells or through direct ligation of the inhibitory receptor Lag-3 expressed on $CD4^+$ T cells by its ligand, MHC-II, expressed on melanoma cells. Future experiments in the epicutaneous melanoma model will use Lag-3 blocking antibodies to investigate its potential role in immune escape. Furthermore, the Gebhardt laboratory has developed a model in which incipient primary melanomas, which spontaneously metastasise, are resected from mice to enable investigation of immunosurveillance mechanisms of metastases. This model will be instrumental in investigating the possible role of MHC-II expression by melanoma cells in immune escape at metastatic sites. Furthermore light-sheet microscopy will be used to investigate possible interactions between melanoma cells and $CD4^+$ T cells in the lymph node in the context of metastasis.

Consistent with the finding that antigen presentation to $CD4^+$ T cells can be indirectly mediated by APCs, live cell imaging of melanoma challenged skin using two-photon microscopy revealed a physical distance between co-localised $CD4^+$ T cells and melanoma cells in the skin. This suggested that these cells may not be in direct contact with one another and future experiments will utilise mice in which subsets of professional APCs are fluorescently labelled in an attempt to visualise APCs interacting with $CD4^+$ T cells in the TME by two-photon

microscopy.

The transfer of naïve $CD4^+$ T cells greatly reduced the incidence of tumor development, however, a proportion of mice still developed progressively growing tumors. We found evidence for possible mechanisms which may impede antitumoral responses of $CD4^+$ T cells. Firstly, we identified weak priming of adoptively transferred $CD4^+$ T cells. Therefore, future experiments aim to investigate what factors support or prevent effective T cell priming in the epicutaneous model. Further investigation into strategies to improve T cell priming would be highly advantageous to develop adjuvant therapy for combined use with adoptive T cell therapy. Secondly, the abundance of Treg cells observed within established tumors demonstrated that the epicutaneous melanoma model would be useful to investigate mechanisms of Treg cells in cancer immune escape. Future experiments will investigate the effect of Treg depletion on immunosurveillance not only at the primary tumor but also in lymph node metastasis. Furthermore, the ontology of induced Treg cells, that is whether they are differentiated in the lymph node or locally within tumors, will be investigated. Understanding the mechanisms driving reprogramming of Th1 cells into Treg cells would be highly beneficial for designing therapeutics to inhibit immunosuppression in the tumor microenvironment and optimising current T cell-based immunotherapies.

The bias for antitumoral $CD4^+$ T cells to express Th1-associated transcription factor T-bet in this model does not preclude the possibility that other Th subsets also mediate antitumoral immunity. Indeed, the transfer of $CD4^+$ T cells in which the gene encoding T-bet was genetically ablated provided some level of protection against tumor outgrowth, albeit to a lesser extent than T-bet-expressing $CD4^+$ T cells. Some studies have found that differentiating $CD4^+$ T cells into Th17 or Th9 prior to adoptive transfer have yielded better results than transferring Th1 polarised $CD4^+$ T cells (Muranski et al., 2008, Bowers et al., 2017, Lu et al., 2018, Purwar et al., 2012). This approach of differentiating $CD4^+$ T cells prior to transfer into melanoma challenged mice will be explored in the

epicutaneous model in attempt to reconcile debate surrounding the role of different Th subsets in cancer immunity. Furthermore, single-cell transcriptomic analysis will be employed to provide a more comprehensive phenotypic characterisation of melanoma-specific $CD4^+$ T cells.

Finally, this project elucidated the mechanisms by which $CD4^+$ T cells kill melanoma cells *in vitro* but whether these translate *in vivo* remains to be determined. It is important to consider that killing mechanisms *in vivo* may be subject to many variables. For one, the status of MHC-II expression by melanoma cells may impact the killing mechanism. Using a similar approach to the *in vitro* killing assay, combinations of all known cytotoxic killing pathways of $CD4^+$ T cells will be simultaneously blocked. This will enable the relative contribution of each killing pathway to melanoma control by $CD4^+$ T cells to be assessed. In addition, it is possible that peripheral effector $CD4^+$ T cells contribute to local tumor suppression *in vivo* by mechanisms other than, or in addition to, direct killing. For instance, $CD4^+$ T cells that have been described to regulate the function and recruitment of macrophages and antitumoral $CD8^+$ T have within the TME (Corthay et al., 2005, Alspach et al., 2019, Bos and Sherman, 2010). Cross-talk between $CD4^+$ T cells and other cells types in the TME should be explored in the epicutaneous melanoma model.

This study demonstrated that $CD4^+$ T cells induce robust antitumoral immunity, in line with several models of murine cancer (Ferris et al., 2020, Alspach et al., 2019, Haabeth et al., 2018). Whilst attempts to target $CD8^+$ T cells in immunotherapy for melanoma have demonstrated remarkable success, there is still a significant proportion of patients that do not respond or relapse from therapies. This study strongly supports that targeting the $CD4^+$ T cell arm of the immune system holds promising therapeutic potential for the treatment of melanoma patients. Studies in humans also support this notion since $CD4^+$ TILs are frequently observed in melanoma lesions (Friedman et al., 2012) and melanoma-derived neoantigens are frequently recognised by $CD4^+$ T cells (Linnemann et al., 2015). This is consistent with the observation in mice that

immunogenic epitopes are more frequently recognised by $CD4^+$ T cells than $CD8^+$ T cells (Kreiter et al., 2015). Furthermore, evidence suggests that mobilised $CD4^+$ T cell responses play an important antitumoral role in the success of checkpoint blockade therapy (Kitano et al., 2013, Oh et al., 2020). Finally, this study provided valuable insight into underlying antitumoral mechanisms by which $CD4^+$ T cells drive melanoma immunosurveillance and this knowledge could assist in designing novel therapeutics to target different aspects of the antitumoral $CD4^+$ T cell response, such as priming, differentiation, cross-talk with other immune cells or killing pathways.

Chapter 7: References

AGARWAL, S. & RAO, A. 1998. Modulation of chromatin structure regulates cytokine gene expression during T cell differentiation. *Immunity,* 9**,** 765-75.

AHRENDS, T., BUSSELAAR, J., SEVERSON, T. M., BABALA, N., DE VRIES, E., BOVENS, A., WESSELS, L., VAN LEEUWEN, F. & BORST, J. 2019. CD4(+) T cell help creates memory CD8(+) T cells with innate and help-independent recall capacities. *Nat Commun,* 10**,** 5531.

AHRENDS, T., SPANJAARD, A., PILZECKER, B., BABALA, N., BOVENS, A., XIAO, Y., JACOBS, H. & BORST, J. 2017. CD4(+) T Cell Help Confers a Cytotoxic T Cell Effector Program Including Coinhibitory Receptor Downregulation and Increased Tissue Invasiveness. *Immunity,* 47**,** 848-861 e5.

ALEXANDROV, L. B., NIK-ZAINAL, S., WEDGE, D. C., APARICIO, S. A., BEHJATI, S., BIANKIN, A. V., BIGNELL, G. R., BOLLI, N., BORG, A., BORRESEN-DALE, A. L., BOYAULT, S., BURKHARDT, B., BUTLER, A. P., CALDAS, C., DAVIES, H. R., DESMEDT, C., EILS, R., EYFJORD, J. E., FOEKENS, J. A., GREAVES, M., HOSODA, F., HUTTER, B., ILICIC, T., IMBEAUD, S., IMIELINSKI, M., JAGER, N., JONES, D. T., JONES, D., KNAPPSKOG, S., KOOL, M., LAKHANI, S. R., LOPEZ-OTIN, C., MARTIN, S., MUNSHI, N. C., NAKAMURA, H., NORTHCOTT, P. A., PAJIC, M., PAPAEMMANUIL, E., PARADISO, A., PEARSON, J. V., PUENTE, X. S., RAINE, K., RAMAKRISHNA, M., RICHARDSON, A. L., RICHTER, J., ROSENSTIEL, P., SCHLESNER, M., SCHUMACHER, T. N., SPAN, P. N., TEAGUE, J. W., TOTOKI, Y., TUTT, A. N., VALDES-MAS, R., VAN BUUREN, M. M., VAN 'T VEER, L., VINCENT-SALOMON, A., WADDELL, N., YATES, L. R., AUSTRALIAN PANCREATIC CANCER GENOME, I., CONSORTIUM, I. B. C., CONSORTIUM, I. M.-S., PEDBRAIN, I., ZUCMAN-ROSSI, J., FUTREAL, P. A., MCDERMOTT, U., LICHTER, P., MEYERSON, M., GRIMMOND, S. M., SIEBERT, R., CAMPO, E., SHIBATA, T., PFISTER, S. M., CAMPBELL, P. J. & STRATTON, M. R. 2013. Signatures of mutational processes in human cancer. *Nature,* 500**,** 415-21.

ALSPACH, E., LUSSIER, D. M., MICELI, A. P., KIZHVATOV, I., DUPAGE, M., LUOMA, A. M., MENG, W., LICHTI, C. F., ESAULOVA, E., VOMUND, A. N., RUNCI, D., WARD, J. P., GUBIN, M. M., MEDRANO, R. F. V., ARTHUR, C. D., WHITE, J. M., SHEEHAN, K. C. F., CHEN, A., WUCHERPFENNIG, K. W., JACKS, T., UNANUE, E. R., ARTYOMOV, M. N. & SCHREIBER, R. D. 2019. MHC-II neoantigens shape tumour immunity and response to immunotherapy. *Nature,* 574**,** 696-701.

AXELROD, M. L., COOK, R. S., JOHNSON, D. B. & BALKO, J. M. 2019. Biological Consequences of MHC-II Expression by Tumor Cells in Cancer. *Clin Cancer Res,* 25**,** 2392-2402.

BAJENOFF, M., WURTZ, O. & GUERDER, S. 2002. Repeated antigen exposure is necessary for the differentiation, but not the initial proliferation, of naive CD4(+) T cells. *J Immunol,* 168**,** 1723-9.

BANGERT, C., BRUNNER, P. M. & STINGL, G. 2011. Immune functions of the skin. *Clin Dermatol,* 29**,** 360-76.

BARRETT, D. M., SINGH, N., PORTER, D. L., GRUPP, S. A. & JUNE, C. H. 2014. Chimeric antigen receptor therapy for cancer. *Annu Rev Med,* 65**,** 333-47.

BASHA, G., OMILUSIK, K., CHAVEZ-STEENBOCK, A., REINICKE, A. T., LACK, N., CHOI, K. B. & JEFFERIES, W. A. 2012. A CD74-dependent MHC class I endolysosomal cross-presentation pathway. *Nat Immunol,* 13**,** 237-45.

BECATTINI, S., LATORRE, D., MELE, F., FOGLIERINI, M., DE GREGORIO, C., CASSOTTA, A., FERNANDEZ, B., KELDERMAN, S., SCHUMACHER, T. N., CORTI, D., LANZAVECCHIA, A. & SALLUSTO, F. 2015. T cell immunity. Functional heterogeneity of human memory CD4(+) T cell clones primed by pathogens or vaccines. *Science,* 347**,** 400-6.

BEDOUI, S. & GEBHARDT, T. 2011. Interaction between dendritic cells and T cells during peripheral virus infections: a role for antigen presentation beyond lymphoid organs? *Curr Opin Immunol,* 23**,** 124-30.

BEDOUI, S., WHITNEY, P. G., WAITHMAN, J., EIDSMO, L., WAKIM, L., CAMINSCHI, I., ALLAN, R. S., WOJTASIAK, M., SHORTMAN, K., CARBONE, F. R., BROOKS, A. G. & HEATH, W. R. 2009. Cross-presentation of viral and self antigens by skin-derived CD103+ dendritic cells. *Nat Immunol,* 10**,** 488-95.

BEHRENS, E. L., BOOTHE, W., D'SILVA, N., WALTERSCHEID, B., WATKINS, P. & TARBOX, M. 2019. SOX-10 staining in dermal scars. *J Cutan Pathol,* 46**,** 579-585.

BENMOHAMED, L., BERTRAND, G., MCNAMARA, C. D., GRAS-MASSE, H., HAMMER, J., WECHSLER, S. L. & NESBURN, A. B. 2003. Identification of novel immunodominant CD4+ Th1-type T-cell peptide epitopes from herpes simplex virus glycoprotein D that confer protective immunity. *J Virol,* 77**,** 9463-73.

BENNETT, S. R., CARBONE, F. R., KARAMALIS, F., FLAVELL, R. A., MILLER, J. F. & HEATH, W. R. 1998. Help for cytotoxic-T-cell responses is mediated by CD40 signalling. *Nature,* 393**,** 478-80.

BEURA, L. K., FARES-FREDERICKSON, N. J., STEINERT, E. M., SCOTT, M. C., THOMPSON, E. A., FRASER, K. A., SCHENKEL, J. M., VEZYS, V. & MASOPUST, D. 2019. CD4(+) resident memory T cells dominate immunosurveillance and orchestrate local recall responses. *J Exp Med,* 216**,** 1214-1229.

BEURA, L. K., HAMILTON, S. E., BI, K., SCHENKEL, J. M., ODUMADE, O. A., CASEY, K. A., THOMPSON, E. A., FRASER, K. A., ROSATO, P. C., FILALI-MOUHIM, A., SEKALY, R. P., JENKINS, M. K., VEZYS, V., HAINING, W. N., JAMESON, S. C. & MASOPUST, D. 2016. Normalizing the environment recapitulates adult human immune traits in laboratory mice. *Nature,* 532**,** 512-6.

BINDEA, G., MLECNIK, B., TOSOLINI, M., KIRILOVSKY, A., WALDNER, M., OBENAUF, A. C., ANGELL, H., FREDRIKSEN, T., LAFONTAINE, L., BERGER, A., BRUNEVAL, P., FRIDMAN, W. H., BECKER, C., PAGES, F., SPEICHER, M. R., TRAJANOSKI, Z. & GALON, J. 2013. Spatiotemporal dynamics of intratumoral immune cells reveal the immune landscape in human cancer. *Immunity,* 39**,** 782-95.

BINNEWIES, M., MUJAL, A. M., POLLACK, J. L., COMBES, A. J., HARDISON, E. A., BARRY, K. C., TSUI, J., RUHLAND, M. K., KERSTEN, K., ABUSHAWISH, M. A., SPASIC, M., GIURINTANO, J. P., CHAN, V., DAUD, A. I., HA, P., YE, C. J., ROBERTS, E. W. & KRUMMEL, M. F. 2019. Unleashing Type-2 Dendritic Cells to Drive Protective Antitumor CD4(+) T Cell Immunity. *Cell,* 177**,** 556-571 e16.

BLATTMAN, J. N., ANTIA, R., SOURDIVE, D. J., WANG, X., KAECH, S. M., MURALI-KRISHNA, K., ALTMAN, J. D. & AHMED, R. 2002. Estimating the precursor frequency of naive antigen-specific CD8 T cells. *J Exp Med,* 195**,** 657-64.

BOECKE, A., CARSTENS, A. C., NEACSU, C. D., BASCHUK, N., HAUBERT, D., KASHKAR, H., UTERMOHLEN, O., PONGRATZ, C. & KRONKE, M. 2013. TNF-receptor-1 adaptor protein FAN mediates TNF-induced B16 melanoma motility and invasion. *Br J Cancer,* 109**,** 422-32.

BOHM, W., THOMA, S., LEITHAUSER, F., MOLLER, P., SCHIRMBECK, R. & REIMANN, J. 1998. T cell-mediated, IFN-gamma-facilitated rejection of murine B16 melanomas. *J Immunol,* 161**,** 897-908.

BOS, R. & SHERMAN, L. A. 2010. CD4+ T-cell help in the tumor milieu is required for recruitment and cytolytic function of CD8+ T lymphocytes. *Cancer Res,* 70**,** 8368-77.

BOTTING, R. A., BERTRAM, K. M., BAHARLOU, H., SANDGREN, K. J., FLETCHER, J., RHODES, J. W., RANA, H., PLASTO, T. M., WANG, X. M., LIM, J. J. K., BARNOUTI, L., KOHOUT, M. P., PAPADOPOULOS, T., MERTEN, S., OLBOURNE, N., CUNNINGHAM, A. L., HANIFFA, M. & HARMAN, A. N. 2017. Phenotypic and functional consequences of different isolation protocols on skin mononuclear phagocytes. *J Leukoc Biol,* 101**,** 1393-1403.

BOUDEWIJNS, S., BLOEMENDAL, M., GERRITSEN, W. R., DE VRIES, I. J. & SCHREIBELT, G. 2016. Dendritic cell vaccination in melanoma patients: From promising results to future perspectives. *Hum Vaccin Immunother,* 12**,** 2523-2528.

BOWERS, J. S., NELSON, M. H., MAJCHRZAK, K., BAILEY, S. R., ROHRER, B., KAISER, A. D., ATKINSON, C., GATTINONI, L. & PAULOS, C. M. 2017. Th17 cells are refractory to senescence and retain robust antitumor activity after long-term ex vivo expansion. *JCI Insight,* 2**,** e90772.

BRAUMULLER, H., WIEDER, T., BRENNER, E., ASSMANN, S., HAHN, M., ALKHALED, M., SCHILBACH, K., ESSMANN, F., KNEILLING, M., GRIESSINGER, C., RANTA, F., ULLRICH, S., MOCIKAT, R., BRAUNGART, K., MEHRA, T., FEHRENBACHER, B., BERDEL, J., NIESSNER, H., MEIER, F., VAN DEN BROEK, M., HARING, H. U., HANDGRETINGER, R., QUINTANILLA-MARTINEZ, L., FEND, F., PESIC, M., BAUER, J., ZENDER, L., SCHALLER, M., SCHULZE-OSTHOFF, K. & ROCKEN, M. 2013. T-helper-1-cell cytokines drive cancer into senescence. *Nature,* 494**,** 361-5.

BROGNA, S. & WEN, J. 2009. Nonsense-mediated mRNA decay (NMD) mechanisms. *Nat Struct Mol Biol,* 16**,** 107-13.

BROMLEY, S. K., YAN, S., TOMURA, M., KANAGAWA, O. & LUSTER, A. D. 2013. Recirculating memory T cells are a unique subset of CD4+ T cells with a distinct phenotype and migratory pattern. *J Immunol,* 190**,** 970-6.

BROWN, C. C., GUDJONSON, H., PRITYKIN, Y., DEEP, D., LAVALLEE, V. P., MENDOZA, A., FROMME, R., MAZUTIS, L., ARIYAN, C., LESLIE, C., PE'ER, D. & RUDENSKY, A. Y. 2019. Transcriptional Basis of Mouse and Human Dendritic Cell Heterogeneity. *Cell,* 179**,** 846-863 e24.

BULLANI, R. R., WEHRLI, P., VIARD-LEVEUGLE, I., RIMOLDI, D., CEROTTINI, J. C., SAURAT, J. H., TSCHOPP, J. & FRENCH, L. E. 2002. Frequent downregulation of Fas (CD95) expression and function in melanoma. *Melanoma Res,* 12**,** 263-70.

BUSAM, K. J., CHARLES, C., LEE, G. & HALPERN, A. C. 2001. Morphologic features of melanocytes, pigmented keratinocytes, and melanophages by in vivo confocal scanning laser microscopy. *Mod Pathol,* 14**,** 862-8.
CALLAHAN, M. K., FLAHERTY, C. R. & POSTOW, M. A. 2016. Checkpoint Blockade for the Treatment of Advanced Melanoma. *Cancer Treat Res,* 167**,** 231-50.
CAMPBELL, D. J. & BUTCHER, E. C. 2002. Rapid acquisition of tissue-specific homing phenotypes by CD4(+) T cells activated in cutaneous or mucosal lymphoid tissues. *J Exp Med,* 195**,** 135-41.
CARPENTIER, I., COORNAERT, B. & BEYAERT, R. 2004. Function and regulation of tumor necrosis factor receptor type 2. *Curr Med Chem,* 11**,** 2205-12.
CASEY, K. A., FRASER, K. A., SCHENKEL, J. M., MORAN, A., ABT, M. C., BEURA, L. K., LUCAS, P. J., ARTIS, D., WHERRY, E. J., HOGQUIST, K., VEZYS, V. & MASOPUST, D. 2012. Antigen-independent differentiation and maintenance of effector-like resident memory T cells in tissues. *J Immunol,* 188**,** 4866-75.
CAZA, T. & LANDAS, S. 2015. Functional and Phenotypic Plasticity of CD4(+) T Cell Subsets. *Biomed Res Int,* 2015**,** 521957.
CEBON, J. S., GORE, M., THOMPSON, J. F., DAVIS, I. D., MCARTHUR, G. A., WALPOLE, E., SMITHERS, M., CERUNDOLO, V., DUNBAR, P. R., MACGREGOR, D., FISHER, C., MILLWARD, M., NATHAN, P., FINDLAY, M. P. N., HERSEY, P., EVANS, T. R. J., OTTENSMEIER, C. H., MARSDEN, J., DALGLEISH, A. G., CORRIE, P. G., MARIA, M., BRIMBLE, M., WILLIAMS, G., WINKLER, S., JACKSON, H. M., ENDO-MUNOZ, L., TUTUKA, C. S. A., VENHAUS, R., OLD, L. J., HAACK, D., MARASKOVSKY, E., BEHREN, A. & CHEN, W. 2020. Results of a randomized, double-blind phase II clinical trial of NY-ESO-1 vaccine with ISCOMATRIX adjuvant versus ISCOMATRIX alone in participants with high-risk resected melanoma. *J Immunother Cancer,* 8.
CEPEK, K. L., SHAW, S. K., PARKER, C. M., RUSSELL, G. J., MORROW, J. S., RIMM, D. L. & BRENNER, M. B. 1994. Adhesion between epithelial cells and T lymphocytes mediated by E-cadherin and the alpha E beta 7 integrin. *Nature,* 372**,** 190-3.
CHAN, D. V., GIBSON, H. M., AUFIERO, B. M., WILSON, A. J., HAFNER, M. S., MI, Q. S. & WONG, H. K. 2014. Differential CTLA-4 expression in human CD4+ versus CD8+ T cells is associated with increased NFAT1 and inhibition of CD4+ proliferation. *Genes Immun,* 15**,** 25-32.
CHEN, H., FU, T., SUH, W. K., TSAVACHIDOU, D., WEN, S., GAO, J., NG TANG, D., HE, Q., SUN, J. & SHARMA, P. 2014. CD4 T cells require ICOS-mediated PI3K signaling to increase T-Bet expression in the setting of anti-CTLA-4 therapy. *Cancer Immunol Res,* 2**,** 167-76.
CHEN, Y. L., WANG, J. Y., CHEN, S. H. & YANG, B. C. 2002. Granulocytes mediates the Fas-L-associated apoptosis during lung metastasis of melanoma that determines the metastatic behaviour. *Br J Cancer,* 87**,** 359-65.
CHENG, W. F., LEE, C. N., CHANG, M. C., SU, Y. N., CHEN, C. A. & HSIEH, C. Y. 2005. Antigen-specific CD8+ T lymphocytes generated from a DNA vaccine control tumors through the Fas-FasL pathway. *Mol Ther,* 12**,** 960-8.
CHIN, L., GARRAWAY, L. A. & FISHER, D. E. 2006. Malignant melanoma: genetics and therapeutics in the genomic era. *Genes Dev,* 20**,** 2149-82.
CHOWDHURY, D. & LIEBERMAN, J. 2008. Death by a thousand cuts: granzyme pathways of programmed cell death. *Annu Rev Immunol,* 26**,** 389-420.
CHURCH, S. E., JENSEN, S. M., ANTONY, P. A., RESTIFO, N. P. & FOX, B. A. 2014. Tumor-specific CD4+ T cells maintain effector and memory tumor-specific CD8+ T cells. *Eur J Immunol,* 44**,** 69-79.
CLARK, R. A., CHONG, B., MIRCHANDANI, N., BRINSTER, N. K., YAMANAKA, K., DOWGIERT, R. K. & KUPPER, T. S. 2006. The vast majority of CLA+ T cells are resident in normal skin. *J Immunol,* 176**,** 4431-9.
CLARK, R. A., WATANABE, R., TEAGUE, J. E., SCHLAPBACH, C., TAWA, M. C., ADAMS, N., DOROSARIO, A. A., CHANEY, K. S., CUTLER, C. S., LEBOEUF, N. R., CARTER, J. B., FISHER, D. C. & KUPPER, T. S. 2012. Skin effector memory T cells do not recirculate and provide immune protection in alemtuzumab-treated CTCL patients. *Sci Transl Med,* 4**,** 117ra7.
CLAUSEN, B. E. & STOITZNER, P. 2015. Functional Specialization of Skin Dendritic Cell Subsets in Regulating T Cell Responses. *Front Immunol,* 6**,** 534.
COLLINS, N., HOCHHEISER, K., CARBONE, F. R. & GEBHARDT, T. 2017. Sustained accumulation of antigen-presenting cells after infection promotes local T-cell immunity. *Immunol Cell Biol,* 95**,** 878-883.
COLLINS, N., JIANG, X., ZAID, A., MACLEOD, B. L., LI, J., PARK, C. O., HAQUE, A., BEDOUI, S., HEATH, W. R., MUELLER, S. N., KUPPER, T. S., GEBHARDT, T. & CARBONE, F. R. 2016. Skin CD4(+) memory T cells exhibit combined cluster-mediated retention and equilibration with the circulation. *Nat Commun,* 7**,** 11514.
CORTHAY, A., LUNDIN, K. U., LORVIK, K. B., HOFGAARD, P. O. & BOGEN, B. 2009. Secretion of tumor-specific antigen by myeloma cells is required for cancer immunosurveillance by CD4+ T cells. *Cancer Res,* 69**,** 5901-7.
CORTHAY, A., SKOVSETH, D. K., LUNDIN, K. U., ROSJO, E., OMHOLT, H., HOFGAARD, P. O., HARALDSEN, G. & BOGEN, B. 2005. Primary antitumor immune response mediated by CD4+ T cells. *Immunity,* 22**,** 371-83.
CRETNEY, E., TAKEDA, K., YAGITA, H., GLACCUM, M., PESCHON, J. J. & SMYTH, M. J. 2002. Increased susceptibility to tumor initiation and metastasis in TNF-related apoptosis-inducing ligand-deficient mice. *J Immunol,* 168**,** 1356-61.
CULLEN, S. P., BRUNET, M. & MARTIN, S. J. 2010. Granzymes in cancer and immunity. *Cell Death Differ,* 17**,** 616-23.
DARDALHON, V., AWASTHI, A., KWON, H., GALILEOS, G., GAO, W., SOBEL, R. A., MITSDOERFFER, M., STROM, T. B., ELYAMAN, W., HO, I. C., KHOURY, S., OUKKA, M. & KUCHROO, V. K. 2008. IL-4 inhibits TGF-beta-induced Foxp3+ T cells and, together with TGF-beta, generates IL-9+ IL-10+ Foxp3(-) effector T cells. *Nat Immunol,* 9**,** 1347-55.
DAVIES, H., BIGNELL, G. R., COX, C., STEPHENS, P., EDKINS, S., CLEGG, S., TEAGUE, J., WOFFENDIN, H., GARNETT, M. J., BOTTOMLEY, W., DAVIS, N., DICKS, E., EWING, R., FLOYD, Y., GRAY, K., HALL, S.,

HAWES, R., HUGHES, J., KOSMIDOU, V., MENZIES, A., MOULD, C., PARKER, A., STEVENS, C., WATT, S., HOOPER, S., WILSON, R., JAYATILAKE, H., GUSTERSON, B. A., COOPER, C., SHIPLEY, J., HARGRAVE, D., PRITCHARD-JONES, K., MAITLAND, N., CHENEVIX-TRENCH, G., RIGGINS, G. J., BIGNER, D. D., PALMIERI, G., COSSU, A., FLANAGAN, A., NICHOLSON, A., HO, J. W., LEUNG, S. Y., YUEN, S. T., WEBER, B. L., SEIGLER, H. F., DARROW, T. L., PATERSON, H., MARAIS, R., MARSHALL, C. J., WOOSTER, R., STRATTON, M. R. & FUTREAL, P. A. 2002. Mutations of the BRAF gene in human cancer. *Nature,* 417**,** 949-54.

DE LA FUENTE-NUNEZ, C. & LU, T. K. 2017. CRISPR-Cas9 technology: applications in genome engineering, development of sequence-specific antimicrobials, and future prospects. *Integr Biol (Camb),* 9**,** 109-122.

DOORDUIJN, E. M., SLUIJTER, M., SALVATORI, D. C., SILVESTRI, S., MAAS, S., ARENS, R., OSSENDORP, F., VAN DER BURG, S. H. & VAN HALL, T. 2017. CD4(+) T Cell and NK Cell Interplay Key to Regression of MHC Class I(low) Tumors upon TLR7/8 Agonist Therapy. *Cancer Immunol Res,* 5**,** 642-653.

DRIESSENS, G., KLINE, J. & GAJEWSKI, T. F. 2009. Costimulatory and coinhibitory receptors in anti-tumor immunity. *Immunol Rev,* 229**,** 126-44.

DUDLEY, M. E., WUNDERLICH, J. R., ROBBINS, P. F., YANG, J. C., HWU, P., SCHWARTZENTRUBER, D. J., TOPALIAN, S. L., SHERRY, R., RESTIFO, N. P., HUBICKI, A. M., ROBINSON, M. R., RAFFELD, M., DURAY, P., SEIPP, C. A., ROGERS-FREEZER, L., MORTON, K. E., MAVROUKAKIS, S. A., WHITE, D. E. & ROSENBERG, S. A. 2002. Cancer regression and autoimmunity in patients after clonal repopulation with antitumor lymphocytes. *Science,* 298**,** 850-4.

DUNN, G. P., BRUCE, A. T., IKEDA, H., OLD, L. J. & SCHREIBER, R. D. 2002. Cancer immunoediting: from immunosurveillance to tumor escape. *Nat Immunol,* 3**,** 991-8.

DUPAGE, M., MAZUMDAR, C., SCHMIDT, L. M., CHEUNG, A. F. & JACKS, T. 2012. Expression of tumour-specific antigens underlies cancer immunoediting. *Nature,* 482**,** 405-9.

EFFERN, M., GLODDE, N., BRAUN, M., LIEBING, J., BOLL, H. N., YONG, M., BAWDEN, E., HINZE, D., VAN DEN BOORN-KONIJNENBERG, D., DAOUD, M., AYMANS, P., LANDSBERG, J., SMYTH, M. J., FLATZ, L., TUTING, T., BALD, T., GEBHARDT, T. & HOLZEL, M. 2020. Adoptive T Cell Therapy Targeting Different Gene Products Reveals Diverse and Context-Dependent Immune Evasion in Melanoma. *Immunity*.

EIZENBERG-MAGAR, I., RIMER, J., ZARETSKY, I., LARA-ASTIASO, D., REICH-ZELIGER, S. & FRIEDMAN, N. 2017. Diverse continuum of CD4(+) T-cell states is determined by hierarchical additive integration of cytokine signals. *Proc Natl Acad Sci U S A,* 114**,** E6447-E6456.

FAURE-ANDRE, G., VARGAS, P., YUSEFF, M. I., HEUZE, M., DIAZ, J., LANKAR, D., STERI, V., MANRY, J., HUGUES, S., VASCOTTO, F., BOULANGER, J., RAPOSO, G., BONO, M. R., ROSEMBLATT, M., PIEL, M. & LENNON-DUMENIL, A. M. 2008. Regulation of dendritic cell migration by CD74, the MHC class II-associated invariant chain. *Science,* 322**,** 1705-10.

FAUSKANGER, M., HAABETH, O. A. W., SKJELDAL, F. M., BOGEN, B. & TVEITA, A. A. 2018. Tumor Killing by CD4(+) T Cells Is Mediated via Induction of Inducible Nitric Oxide Synthase-Dependent Macrophage Cytotoxicity. *Front Immunol,* 9**,** 1684.

FERREIRA, R. C., SIMONS, H. Z., THOMPSON, W. S., RAINBOW, D. B., YANG, X., CUTLER, A. J., OLIVEIRA, J., CASTRO DOPICO, X., SMYTH, D. J., SAVINYKH, N., MASHAR, M., VYSE, T. J., DUNGER, D. B., BAXENDALE, H., CHANDRA, A., WALLACE, C., TODD, J. A., WICKER, L. S. & PEKALSKI, M. L. 2017. Cells with Treg-specific FOXP3 demethylation but low CD25 are prevalent in autoimmunity. *J Autoimmun,* 84**,** 75-86.

FERRIS, S. T., DURAI, V., WU, R., THEISEN, D. J., WARD, J. P., BERN, M. D., DAVIDSON, J. T. T., BAGADIA, P., LIU, T., BRISENO, C. G., LI, L., GILLANDERS, W. E., WU, G. F., YOKOYAMA, W. M., MURPHY, T. L., SCHREIBER, R. D. & MURPHY, K. M. 2020. cDC1 prime and are licensed by CD4(+) T cells to induce anti-tumour immunity. *Nature*.

FIDLER, I. J. 1973. Selection of successive tumour lines for metastasis. *Nat New Biol,* 242**,** 148-9.

FONTAINE, V., MOHAND-SAID, S., HANOTEAU, N., FUCHS, C., PFIZENMAIER, K. & EISEL, U. 2002. Neurodegenerative and neuroprotective effects of tumor Necrosis factor (TNF) in retinal ischemia: opposite roles of TNF receptor 1 and TNF receptor 2. *J Neurosci,* 22**,** RC216.

FOULDS, K. E. & SHEN, H. 2006. Clonal competition inhibits the proliferation and differentiation of adoptively transferred TCR transgenic CD4 T cells in response to infection. *J Immunol,* 176**,** 3037-43.

FRIEDMAN, K. M., PRIETO, P. A., DEVILLIER, L. E., GROSS, C. A., YANG, J. C., WUNDERLICH, J. R., ROSENBERG, S. A. & DUDLEY, M. E. 2012. Tumor-specific CD4+ melanoma tumor-infiltrating lymphocytes. *J Immunother,* 35**,** 400-8.

FURNESS, A. J., VARGAS, F. A., PEGGS, K. S. & QUEZADA, S. A. 2014. Impact of tumour microenvironment and Fc receptors on the activity of immunomodulatory antibodies. *Trends Immunol,* 35**,** 290-8.

GABRILOVICH, D. 2004. Mechanisms and functional significance of tumour-induced dendritic-cell defects. *Nat Rev Immunol,* 4**,** 941-52.

GAO, Y., NISH, S. A., JIANG, R., HOU, L., LICONA-LIMON, P., WEINSTEIN, J. S., ZHAO, H. & MEDZHITOV, R. 2013. Control of T helper 2 responses by transcription factor IRF4-dependent dendritic cells. *Immunity,* 39**,** 722-32.

GASPER, D. J., TEJERA, M. M. & SURESH, M. 2014. CD4 T-cell memory generation and maintenance. *Crit Rev Immunol,* 34**,** 121-46.

GEBHARDT, T., WAKIM, L. M., EIDSMO, L., READING, P. C., HEATH, W. R. & CARBONE, F. R. 2009. Memory T cells in nonlymphoid tissue that provide enhanced local immunity during infection with herpes simplex virus. *Nat Immunol,* 10**,** 524-30.

GEBHARDT, T., WHITNEY, P. G., ZAID, A., MACKAY, L. K., BROOKS, A. G., HEATH, W. R., CARBONE, F. R. & MUELLER, S. N. 2011. Different patterns of peripheral migration by memory CD4+ and CD8+ T cells. *Nature,* 477**,** 216-9.

GLENNIE, N. D., YERAMILLI, V. A., BEITING, D. P., VOLK, S. W., WEAVER, C. T. & SCOTT, P. 2015. Skin-resident memory CD4+ T cells enhance protection against Leishmania major infection. *J Exp Med,* 212**,** 1405-14.

GLODDE, N., KRAUT, A., VAN DEN BOORN-KONIJNENBERG, D., VADDER, S., KRETEN, F., SCHMID-BURGK, J., AYMANS, P., ECHELMEYER, K., RUMPF, M., LANDSBERG, J., BALD, T., TŰTING, T., BOVIER, A. & HOLZEL, M. 2019. Experimental and stochastic models of melanoma T-cell therapy define impact of subclone fitness on selection of antigen loss variants. *bioRxiv preprint*.

GODFREY, D. I., ULDRICH, A. P., MCCLUSKEY, J., ROSSJOHN, J. & MOODY, D. B. 2016. Corrigendum: The burgeoning family of unconventional T cells. *Nat Immunol,* 17**,** 469.

GONDEK, D. C., LU, L. F., QUEZADA, S. A., SAKAGUCHI, S. & NOELLE, R. J. 2005. Cutting edge: contact-mediated suppression by CD4+CD25+ regulatory cells involves a granzyme B-dependent, perforin-independent mechanism. *J Immunol,* 174**,** 1783-6.

GREEN, D. R., DROIN, N. & PINKOSKI, M. 2003. Activation-induced cell death in T cells. *Immunol Rev,* 193**,** 70-81.

GRETEN, F. R. & GRIVENNIKOV, S. I. 2019. Inflammation and Cancer: Triggers, Mechanisms, and Consequences. *Immunity,* 51**,** 27-41.

GREYER, M., WHITNEY, P. G., STOCK, A. T., DAVEY, G. M., TEBARTZ, C., BACHEM, A., MINTERN, J. D., STRUGNELL, R. A., TURNER, S. J., GEBHARDT, T., O'KEEFFE, M., HEATH, W. R. & BEDOUI, S. 2016. T Cell Help Amplifies Innate Signals in CD8(+) DCs for Optimal CD8(+) T Cell Priming. *Cell Rep,* 14**,** 586-597.

GRIFFITH, T. S., WILEY, S. R., KUBIN, M. Z., SEDGER, L. M., MALISZEWSKI, C. R. & FANGER, N. A. 1999. Monocyte-mediated tumoricidal activity via the tumor necrosis factor-related cytokine, TRAIL. *J Exp Med,* 189**,** 1343-54.

GU-TRANTIEN, C., LOI, S., GARAUD, S., EQUETER, C., LIBIN, M., DE WIND, A., RAVOET, M., LE BUANEC, H., SIBILLE, C., MANFOUO-FOUTSOP, G., VEYS, I., HAIBE-KAINS, B., SINGHAL, S. K., MICHIELS, S., ROTHE, F., SALGADO, R., DUVILLIER, H., IGNATIADIS, M., DESMEDT, C., BRON, D., LARSIMONT, D., PICCART, M., SOTIRIOU, C. & WILLARD-GALLO, K. 2013. CD4(+) follicular helper T cell infiltration predicts breast cancer survival. *J Clin Invest,* 123**,** 2873-92.

GUERY, L. & HUGUES, S. 2015. Th17 Cell Plasticity and Functions in Cancer Immunity. *Biomed Res Int,* 2015**,** 314620.

HAABETH, O. A. W., FAUSKANGER, M., MANZKE, M., LUNDIN, K. U., CORTHAY, A., BOGEN, B. & TVEITA, A. A. 2018. CD4(+) T-cell-Mediated Rejection of MHC Class II-Positive Tumor Cells Is Dependent on Antigen Secretion and Indirect Presentation on Host APCs. *Cancer Res,* 78**,** 4573-4585.

HABTETSION, T., DING, Z. C., PI, W., LI, T., LU, C., CHEN, T., XI, C., SPARTZ, H., LIU, K., HAO, Z., MIVECHI, N., HUO, Y., BLAZAR, B. R., MUNN, D. H. & ZHOU, G. 2018. Alteration of Tumor Metabolism by CD4+ T Cells Leads to TNF-alpha-Dependent Intensification of Oxidative Stress and Tumor Cell Death. *Cell Metab,* 28**,** 228-242 e6.

HANIFFA, M., GUNAWAN, M. & JARDINE, L. 2015. Human skin dendritic cells in health and disease. *J Dermatol Sci,* 77**,** 85-92.

HARPUR, C. M., KATO, Y., DEWI, S. T., STANKOVIC, S., JOHNSON, D. N., BEDOUI, S., WHITNEY, P. G., LAHOUD, M. H., CAMINSCHI, I., HEATH, W. R., BROOKS, A. G. & GEBHARDT, T. 2019. Classical Type 1 Dendritic Cells Dominate Priming of Th1 Responses to Herpes Simplex Virus Type 1 Skin Infection. *J Immunol,* 202**,** 653-663.

HARTON, J. A. & TING, J. P. 2000. Class II transactivator: mastering the art of major histocompatibility complex expression. *Mol Cell Biol,* 20**,** 6185-94.

HATAYE, J., MOON, J. J., KHORUTS, A., REILLY, C. & JENKINS, M. K. 2006. Naive and memory CD4+ T cell survival controlled by clonal abundance. *Science,* 312**,** 114-6.

HE, D., LI, H., YUSUF, N., ELMETS, C. A., ATHAR, M., KATIYAR, S. K. & XU, H. 2012. IL-17 mediated inflammation promotes tumor growth and progression in the skin. *PLoS One,* 7**,** e32126.

HE, Y., RIVARD, C. J., ROZEBOOM, L., YU, H., ELLISON, K., KOWALEWSKI, A., ZHOU, C. & HIRSCH, F. R. 2016. Lymphocyte-activation gene-3, an important immune checkpoint in cancer. *Cancer Sci,* 107**,** 1193-7.

HEADLEY, M. B., BINS, A., NIP, A., ROBERTS, E. W., LOONEY, M. R., GERARD, A. & KRUMMEL, M. F. 2016. Visualization of immediate immune responses to pioneer metastatic cells in the lung. *Nature,* 531**,** 513-7.

HELMINK, B. A., REDDY, S. M., GAO, J., ZHANG, S., BASAR, R., THAKUR, R., YIZHAK, K., SADE-FELDMAN, M., BLANDO, J., HAN, G., GOPALAKRISHNAN, V., XI, Y., ZHAO, H., AMARIA, R. N., TAWBI, H. A., COGDILL, A. P., LIU, W., LEBLEU, V. S., KUGERATSKI, F. G., PATEL, S., DAVIES, M. A., HWU, P., LEE, J. E., GERSHENWALD, J. E., LUCCI, A., ARORA, R., WOODMAN, S., KEUNG, E. Z., GAUDREAU, P. O., REUBEN, A., SPENCER, C. N., BURTON, E. M., HAYDU, L. E., LAZAR, A. J., ZAPASSODI, R., HUDGENS, C. W., LEDESMA, D. A., ONG, S., BAILEY, M., WARREN, S., RAO, D., KRIJGSMAN, O., ROZEMAN, E. A., PEEPER, D., BLANK, C. U., SCHUMACHER, T. N., BUTTERFIELD, L. H., ZELAZOWSKA, M. A., MCBRIDE, K. M., KALLURI, R., ALLISON, J., PETITPREZ, F., FRIDMAN, W. H., SAUTES-FRIDMAN, C., HACOHEN, N., REZVANI, K., SHARMA, P., TETZLAFF, M. T., WANG, L. & WARGO, J. A. 2020. B cells and tertiary lymphoid structures promote immunotherapy response. *Nature,* 577**,** 549-555.

HICKLIN, D. J., MARINCOLA, F. M. & FERRONE, S. 1999. HLA class I antigen downregulation in human cancers: T-cell immunotherapy revives an old story. *Mol Med Today,* 5**,** 178-86.

HILDNER, K., EDELSON, B. T., PURTHA, W. E., DIAMOND, M., MATSUSHITA, H., KOHYAMA, M., CALDERON, B., SCHRAML, B. U., UNANUE, E. R., DIAMOND, M. S., SCHREIBER, R. D., MURPHY, T. L. & MURPHY, K. M. 2008. Batf3 deficiency reveals a critical role for CD8alpha+ dendritic cells in cytotoxic T cell immunity. *Science,* 322**,** 1097-100.

HILLIGAN, K. L. & RONCHESE, F. 2020. Antigen presentation by dendritic cells and their instruction of CD4+ T helper cell responses. *Cell Mol Immunol,* 17**,** 587-599.

HIRSCHHORN-CYMERMAN, D., BUDHU, S., KITANO, S., LIU, C., ZHAO, F., ZHONG, H., LESOKHIN, A. M., AVOGADRI-CONNORS, F., YUAN, J., LI, Y., HOUGHTON, A. N., MERGHOUB, T. & WOLCHOK, J. D. 2012. Induction of tumoricidal function in CD4+ T cells is associated with concomitant memory and terminally differentiated phenotype. *J Exp Med,* 209**,** 2113-26.

HO, A. W. & KUPPER, T. S. 2019. T cells and the skin: from protective immunity to inflammatory skin disorders. *Nat Rev Immunol,* 19**,** 490-502.

HODIS, E., WATSON, I. R., KRYUKOV, G. V., AROLD, S. T., IMIELINSKI, M., THEURILLAT, J. P., NICKERSON, E., AUCLAIR, D., LI, L., PLACE, C., DICARA, D., RAMOS, A. H., LAWRENCE, M. S., CIBULSKIS, K., SIVACHENKO, A., VOET, D., SAKSENA, G., STRANSKY, N., ONOFRIO, R. C., WINCKLER, W., ARDLIE, K., WAGLE, N., WARGO, J., CHONG, K., MORTON, D. L., STEMKE-HALE, K., CHEN, G., NOBLE, M., MEYERSON, M., LADBURY, J. E., DAVIES, M. A., GERSHENWALD, J. E., WAGNER, S. N., HOON, D. S., SCHADENDORF, D., LANDER, E. S., GABRIEL, S. B., GETZ, G., GARRAWAY, L. A. & CHIN, L. 2012. A landscape of driver mutations in melanoma. *Cell,* 150**,** 251-63.

HOHLBAUM, A. M., MOE, S. & MARSHAK-ROTHSTEIN, A. 2000. Opposing effects of transmembrane and soluble Fas ligand expression on inflammation and tumor cell survival. *J Exp Med,* 191**,** 1209-20.

HOLLER, N., ZARU, R., MICHEAU, O., THOME, M., ATTINGER, A., VALITUTTI, S., BODMER, J. L., SCHNEIDER, P., SEED, B. & TSCHOPP, J. 2000. Fas triggers an alternative, caspase-8-independent cell death pathway using the kinase RIP as effector molecule. *Nat Immunol,* 1**,** 489-95.

HOLMGREN, L., O'REILLY, M. S. & FOLKMAN, J. 1995. Dormancy of micrometastases: balanced proliferation and apoptosis in the presence of angiogenesis suppression. *Nat Med,* 1**,** 149-53.

HONG, J. J., ROSENBERG, S. A., DUDLEY, M. E., YANG, J. C., WHITE, D. E., BUTMAN, J. A. & SHERRY, R. M. 2010. Successful treatment of melanoma brain metastases with adoptive cell therapy. *Clin Cancer Res,* 16**,** 4892-8.

HONG, S., QIAN, J., YANG, J., LI, H., KWAK, L. W. & YI, Q. 2008. Roles of idiotype-specific t cells in myeloma cell growth and survival: Th1 and CTL cells are tumoricidal while Th2 cells promote tumor growth. *Cancer Res,* 68**,** 8456-64.

HOR, J. L., WHITNEY, P. G., ZAID, A., BROOKS, A. G., HEATH, W. R. & MUELLER, S. N. 2015. Spatiotemporally Distinct Interactions with Dendritic Cell Subsets Facilitates CD4+ and CD8+ T Cell Activation to Localized Viral Infection. *Immunity,* 43**,** 554-65.

HORII, M. & MATSUSHITA, T. 2020. Regulatory B cells and T cell Regulation in Cancer. *J Mol Biol***,** 166685.

HUANG, H., BI, X. G., YUAN, J. Y., XU, S. L., GUO, X. L. & XIANG, J. 2005. Combined CD4+ Th1 effect and lymphotactin transgene expression enhance CD8+ Tc1 tumor localization and therapy. *Gene Ther,* 12**,** 999-1010.

HUANG, R. Y., EPPOLITO, C., LELE, S., SHRIKANT, P., MATSUZAKI, J. & ODUNSI, K. 2015. LAG3 and PD1 co-inhibitory molecules collaborate to limit CD8+ T cell signaling and dampen antitumor immunity in a murine ovarian cancer model. *Oncotarget,* 6**,** 27359-77.

HUNDER, N. N., WALLEN, H., CAO, J., HENDRICKS, D. W., REILLY, J. Z., RODMYRE, R., JUNGBLUTH, A., GNJATIC, S., THOMPSON, J. A. & YEE, C. 2008. Treatment of metastatic melanoma with autologous CD4+ T cells against NY-ESO-1. *N Engl J Med,* 358**,** 2698-703.

HURRELL, B. P., GALLE-TREGER, L., JAHANI, P. S., HOWARD, E., HELOU, D. G., BANIE, H., SOROOSH, P. & AKBARI, O. 2019. TNFR2 Signaling Enhances ILC2 Survival, Function, and Induction of Airway Hyperreactivity. *Cell Rep,* 29**,** 4509-4524 e5.

IGYARTO, B. Z., HALEY, K., ORTNER, D., BOBR, A., GERAMI-NEJAD, M., EDELSON, B. T., ZURAWSKI, S. M., MALISSEN, B., ZURAWSKI, G., BERMAN, J. & KAPLAN, D. H. 2011. Skin-resident murine dendritic cell subsets promote distinct and opposing antigen-specific T helper cell responses. *Immunity,* 35**,** 260-72.

IIJIMA, N. & IWASAKI, A. 2014. T cell memory. A local macrophage chemokine network sustains protective tissue-resident memory CD4 T cells. *Science,* 346**,** 93-8.

IVANOVA, E. A. & OREKHOV, A. N. 2015. T Helper Lymphocyte Subsets and Plasticity in Autoimmunity and Cancer: An Overview. *Biomed Res Int,* 2015**,** 327470.

IVANOVA, O. K., SHARAPOVA, T. N., ROMANOVA, E. A., SOSHNIKOVA, N. V., SASHCHENKO, L. P. & YASHIN, D. V. 2017. CD3(+) CD8(+) NKG2D(+) T Lymphocytes Induce Apoptosis and Necroptosis in HLA-Negative Cells via FasL-Fas Interaction. *J Cell Biochem,* 118**,** 3359-3366.

JACOBS, J. F., NIERKENS, S., FIGDOR, C. G., DE VRIES, I. J. & ADEMA, G. J. 2012. Regulatory T cells in melanoma: the final hurdle towards effective immunotherapy? *Lancet Oncol,* 13**,** e32-42.

JIANG, X., CLARK, R. A., LIU, L., WAGERS, A. J., FUHLBRIGGE, R. C. & KUPPER, T. S. 2012. Skin infection generates non-migratory memory CD8+ T(RM) cells providing global skin immunity. *Nature,* 483**,** 227-31.

JOHNSON, A. J., CHU, C. F. & MILLIGAN, G. N. 2008. Effector CD4+ T-cell involvement in clearance of infectious herpes simplex virus type 1 from sensory ganglia and spinal cords. *J Virol,* 82**,** 9678-88.

JOHNSON, D. B., ESTRADA, M. V., SALGADO, R., SANCHEZ, V., DOXIE, D. B., OPALENIK, S. R., VILGELM, A. E., FELD, E., JOHNSON, A. S., GREENPLATE, A. R., SANDERS, M. E., LOVLY, C. M., FREDERICK, D. T., KELLEY, M. C., RICHMOND, A., IRISH, J. M., SHYR, Y., SULLIVAN, R. J., PUZANOV, I., SOSMAN, J. A. & BALKO, J. M. 2016. Melanoma-specific MHC-II expression represents a tumour-autonomous phenotype and predicts response to anti-PD-1/PD-L1 therapy. *Nat Commun,* 7**,** 10582.

JONCKER, N. T., BETTINI, S., BOULET, D., GUIRAUD, M. & GUERDER, S. 2016. The site of tumor development determines immunogenicity via temporal mobilization of antigen-laden dendritic cells in draining lymph nodes. *Eur J Immunol,* 46**,** 609-18.

JORDAN, K. R., KAPOOR, P., SPONGBERG, E., TOBIN, R. P., GAO, D., BORGES, V. F. & MCCARTER, M. D. 2017. Immunosuppressive myeloid-derived suppressor cells are increased in splenocytes from cancer patients. *Cancer Immunol Immunother,* 66**,** 503-513.

JU, S. T., CUI, H., PANKA, D. J., ETTINGER, R. & MARSHAK-ROTHSTEIN, A. 1994. Participation of target Fas protein in apoptosis pathway induced by CD4+ Th1 and CD8+ cytotoxic T cells. *Proc Natl Acad Sci U S A,* 91**,** 4185-9.

KALLIOLIAS, G. D. & IVASHKIV, L. B. 2016. TNF biology, pathogenic mechanisms and emerging therapeutic strategies. *Nat Rev Rheumatol,* 12**,** 49-62.

KAUFMANN, W. K., CARSON, C. C., OMOLO, B., FILGO, A. J., SAMBADE, M. J., SIMPSON, D. A., SHIELDS, J. M., IBRAHIM, J. G. & THOMAS, N. E. 2014. Mechanisms of chromosomal instability in melanoma. *Environ Mol Mutagen,* 55**,** 457-71.

KAYAGAKI, N., YAMAGUCHI, N., NAKAYAMA, M., KAWASAKI, A., AKIBA, H., OKUMURA, K. & YAGITA, H. 1999. Involvement of TNF-related apoptosis-inducing ligand in human CD4+ T cell-mediated cytotoxicity. *J Immunol,* 162**,** 2639-47.

KEARNEY, C. J., VERVOORT, S. J., HOGG, S. J., RAMSBOTTOM, K. M., FREEMAN, A. J., LALAOUI, N., PIJPERS, L., MICHIE, J., BROWN, K. K., KNIGHT, D. A., SUTTON, V., BEAVIS, P. A., VOSKOBOINIK, I., DARCY, P. K., SILKE, J., TRAPANI, J. A., JOHNSTONE, R. W. & OLIARO, J. 2018. Tumor immune evasion arises through loss of TNF sensitivity. *Sci Immunol,* 3.

KIM, C., WILSON, T., FISCHER, K. F. & WILLIAMS, M. A. 2013. Sustained interactions between T cell receptors and antigens promote the differentiation of CD4(+) memory T cells. *Immunity,* 39**,** 508-20.

KIM, H. S., KIM, S. & LEE, M. S. 2005a. IFN-gamma sensitizes MIN6N8 insulinoma cells to TNF-alpha-induced apoptosis by inhibiting NF-kappaB-mediated XIAP upregulation. *Biochem Biophys Res Commun,* 336**,** 847-53.

KIM, W. H., LEE, J. W., GAO, B. & JUNG, M. H. 2005b. Synergistic activation of JNK/SAPK induced by TNF-alpha and IFN-gamma: apoptosis of pancreatic beta-cells via the p53 and ROS pathway. *Cell Signal,* 17**,** 1516-32.

KIMURA, M., HAISA, M., UETSUKA, H., TAKAOKA, M., OHKAWA, T., KAWASHIMA, R., YAMATSUJI, T., GUNDUZ, M., KANEDA, Y., TANAKA, N. & NAOMOTO, Y. 2003. TNF combined with IFN-alpha accelerates NF-kappaB-mediated apoptosis through enhancement of Fas expression in colon cancer cells. *Cell Death Differ,* 10**,** 718-28.

KITANO, S., TSUJI, T., LIU, C., HIRSCHHORN-CYMERMAN, D., KYI, C., MU, Z., ALLISON, J. P., GNJATIC, S., YUAN, J. D. & WOLCHOK, J. D. 2013. Enhancement of tumor-reactive cytotoxic CD4+ T cell responses after ipilimumab treatment in four advanced melanoma patients. *Cancer Immunol Res,* 1**,** 235-44.

KLICZNIK, M. M., MORAWSKI, P. A., HOLLBACHER, B., VARKHANDE, S. R., MOTLEY, S. J., KURI-CERVANTES, L., GOODWIN, E., ROSENBLUM, M. D., LONG, S. A., BRACHTL, G., DUHEN, T., BETTS, M. R., CAMPBELL, D. J. & GRATZ, I. K. 2019. Human CD4(+)CD103(+) cutaneous resident memory T cells are found in the circulation of healthy individuals. *Sci Immunol,* 4.

KLINE, J., ZHANG, L., BATTAGLIA, L., COHEN, K. S. & GAJEWSKI, T. F. 2012. Cellular and molecular requirements for rejection of B16 melanoma in the setting of regulatory T cell depletion and homeostatic proliferation. *J Immunol,* 188**,** 2630-42.

KOEBEL, C. M., VERMI, W., SWANN, J. B., ZERAFA, N., RODIG, S. J., OLD, L. J., SMYTH, M. J. & SCHREIBER, R. D. 2007. Adaptive immunity maintains occult cancer in an equilibrium state. *Nature,* 450**,** 903-7.

KOELLE, D. M., LIU, Z., MCCLURKAN, C. L., CEVALLOS, R. C., VIEIRA, J., HOSKEN, N. A., MESEDA, C. A., SNOW, D. C., WALD, A. & COREY, L. 2003. Immunodominance among herpes simplex virus-specific CD8 T cells expressing a tissue-specific homing receptor. *Proc Natl Acad Sci U S A,* 100**,** 12899-904.

KOGA, Y., MATSUZAKI, A., SUMINOE, A., HATTORI, H. & HARA, T. 2004. Neutrophil-derived TNF-related apoptosis-inducing ligand (TRAIL): a novel mechanism of antitumor effect by neutrophils. *Cancer Res,* 64**,** 1037-43.

KREITER, S., VORMEHR, M., VAN DE ROEMER, N., DIKEN, M., LOWER, M., DIEKMANN, J., BOEGEL, S., SCHRORS, B., VASCOTTO, F., CASTLE, J. C., TADMOR, A. D., SCHOENBERGER, S. P., HUBER, C., TURECI, O. & SAHIN, U. 2015. Mutant MHC class II epitopes drive therapeutic immune responses to cancer. *Nature,* 520**,** 692-6.

KUMAR, V., PATEL, S., TCYGANOV, E. & GABRILOVICH, D. I. 2016. The Nature of Myeloid-Derived Suppressor Cells in the Tumor Microenvironment. *Trends Immunol,* 37**,** 208-220.

LA, O. R., TAI, L., LEE, L., KRUSE, E. A., GRABOW, S., FAIRLIE, W. D., HAYNES, N. M., TARLINTON, D. M., ZHANG, J. G., BELZ, G. T., SMYTH, M. J., BOUILLET, P., ROBB, L. & STRASSER, A. 2009. Membrane-bound Fas ligand only is essential for Fas-induced apoptosis. *Nature,* 461**,** 659-63.

LANDSBERG, J., KOHLMEYER, J., RENN, M., BALD, T., ROGAVA, M., CRON, M., FATHO, M., LENNERZ, V., WOLFEL, T., HOLZEL, M. & TUTING, T. 2012. Melanomas resist T-cell therapy through inflammation-induced reversible dedifferentiation. *Nature,* 490**,** 412-6.

LARKIN, J., CHIARION-SILENI, V., GONZALEZ, R., GROB, J. J., COWEY, C. L., LAO, C. D., SCHADENDORF, D., DUMMER, R., SMYLIE, M., RUTKOWSKI, P., FERRUCCI, P. F., HILL, A., WAGSTAFF, J., CARLINO, M. S., HAANEN, J. B., MAIO, M., MARQUEZ-RODAS, I., MCARTHUR, G. A., ASCIERTO, P. A., LONG, G. V., CALLAHAN, M. K., POSTOW, M. A., GROSSMANN, K., SZNOL, M., DRENO, B., BASTHOLT, L., YANG, A., ROLLIN, L. M., HORAK, C., HODI, F. S. & WOLCHOK, J. D. 2015. Combined Nivolumab and Ipilimumab or Monotherapy in Untreated Melanoma. *N Engl J Med,* 373**,** 23-34.

LAURON, E. J., YANG, L., HARVEY, I. B., SOJKA, D. K., WILLIAMS, G. D., PALEY, M. A., BERN, M. D., PARK, E., VICTORINO, F., BOON, A. C. M. & YOKOYAMA, W. M. 2019. Viral MHCI inhibition evades tissue-resident memory T cell formation and responses. *J Exp Med,* 216**,** 117-132.

LEE, W. & LEE, G. R. 2018. Transcriptional regulation and development of regulatory T cells. *Exp Mol Med,* 50**,** e456.

LEE, Y. K., TURNER, H., MAYNARD, C. L., OLIVER, J. R., CHEN, D., ELSON, C. O. & WEAVER, C. T. 2009. Late developmental plasticity in the T helper 17 lineage. *Immunity,* 30**,** 92-107.

LI, J. H., ROSEN, D., SONDEL, P. & BERKE, G. 2002. Immune privilege and FasL: two ways to inactivate effector cytotoxic T lymphocytes by FasL-expressing cells. *Immunology,* 105**,** 267-77.

LI, W., GERMAIN, R. N. & GERNER, M. Y. 2017. Multiplex, quantitative cellular analysis in large tissue volumes with clearing-enhanced 3D microscopy (Ce3D). *Proc Natl Acad Sci U S A,* 114**,** E7321-E7330.

LI, X., KOSTARELI, E., SUFFNER, J., GARBI, N. & HAMMERLING, G. J. 2010. Efficient Treg depletion induces T-cell infiltration and rejection of large tumors. *Eur J Immunol,* 40**,** 3325-35.

LI, Z., GOTHARD, E., COLES, M. C. & AMBLER, C. A. 2018. Quantitative Methods for Measuring Repair Rates and Innate-Immune Cell Responses in Wounded Mouse Skin. *Front Immunol,* 9**,** 347.

LIAKOU, C. I., KAMAT, A., TANG, D. N., CHEN, H., SUN, J., TRONCOSO, P., LOGOTHETIS, C. & SHARMA, P. 2008. CTLA-4 blockade increases IFNgamma-producing CD4+ICOShi cells to shift the ratio of effector to regulatory T cells in cancer patients. *Proc Natl Acad Sci U S A,* 105**,** 14987-92.

LINNEMANN, C., VAN BUUREN, M. M., BIES, L., VERDEGAAL, E. M., SCHOTTE, R., CALIS, J. J., BEHJATI, S., VELDS, A., HILKMANN, H., ATMIOUI, D. E., VISSER, M., STRATTON, M. R., HAANEN, J. B., SPITS, H., VAN DER BURG, S. H. & SCHUMACHER, T. N. 2015. High-throughput epitope discovery reveals frequent recognition of neo-antigens by CD4+ T cells in human melanoma. *Nat Med,* 21**,** 81-5.

LIU, V. C., WONG, L. Y., JANG, T., SHAH, A. H., PARK, I., YANG, X., ZHANG, Q., LONNING, S., TEICHER, B. A. & LEE, C. 2007. Tumor evasion of the immune system by converting CD4+CD25- T cells into CD4+CD25+ T regulatory cells: role of tumor-derived TGF-beta. *J Immunol,* 178**,** 2883-92.

LOCKSLEY, R. M., KILLEEN, N. & LENARDO, M. J. 2001. The TNF and TNF receptor superfamilies: integrating mammalian biology. *Cell,* 104**,** 487-501.

LU, Y., HONG, S., LI, H., PARK, J., HONG, B., WANG, L., ZHENG, Y., LIU, Z., XU, J., HE, J., YANG, J., QIAN, J. & YI, Q. 2012. Th9 cells promote antitumor immune responses in vivo. *J Clin Invest,* 122**,** 4160-71.

LU, Y., WANG, Q., XUE, G., BI, E., MA, X., WANG, A., QIAN, J., DONG, C. & YI, Q. 2018. Th9 Cells Represent a Unique Subset of CD4(+) T Cells Endowed with the Ability to Eradicate Advanced Tumors. *Cancer Cell,* 33**,** 1048-1060 e7.

LUNDIN, K. U., SCREPANTI, V., OMHOLT, H., HOFGAARD, P. O., YAGITA, H., GRANDIEN, A. & BOGEN, B. 2004. CD4+ T cells kill Id+ B-lymphoma cells: FasLigand-Fas interaction is dominant in vitro but is redundant in vivo. *Cancer Immunol Immunother,* 53**,** 1135-45.

MA, C. S., DEENICK, E. K., BATTEN, M. & TANGYE, S. G. 2012. The origins, function, and regulation of T follicular helper cells. *J Exp Med,* 209**,** 1241-53.

MA, R., JI, T., CHEN, D., DONG, W., ZHANG, H., YIN, X., MA, J., LIANG, X., ZHANG, Y., SHEN, G., QIN, X. & HUANG, B. 2016. Tumor cell-derived microparticles polarize M2 tumor-associated macrophages for tumor progression. *Oncoimmunology,* 5**,** e1118599.

MACKAY, L. K. & KALLIES, A. 2017. Transcriptional Regulation of Tissue-Resident Lymphocytes. *Trends Immunol,* 38**,** 94-103.

MACKAY, L. K., RAHIMPOUR, A., MA, J. Z., COLLINS, N., STOCK, A. T., HAFON, M. L., VEGA-RAMOS, J., LAUZURICA, P., MUELLER, S. N., STEFANOVIC, T., TSCHARKE, D. C., HEATH, W. R., INOUYE, M., CARBONE, F. R. & GEBHARDT, T. 2013. The developmental pathway for CD103(+)CD8+ tissue-resident memory T cells of skin. *Nat Immunol,* 14**,** 1294-301.

MACLEOD, B. L., BEDOUI, S., HOR, J. L., MUELLER, S. N., RUSSELL, T. A., HOLLETT, N. A., HEATH, W. R., TSCHARKE, D. C., BROOKS, A. G. & GEBHARDT, T. 2014. Distinct APC subtypes drive spatially segregated CD4+ and CD8+ T-cell effector activity during skin infection with HSV-1. *PLoS Pathog,* 10**,** e1004303.

MALANDRO, N., BUDHU, S., KUHN, N. F., LIU, C., MURPHY, J. T., CORTEZ, C., ZHONG, H., YANG, X., RIZZUTO, G., ALTAN-BONNET, G., MERGHOUB, T. & WOLCHOK, J. D. 2016. Clonal Abundance of Tumor-Specific CD4(+) T Cells Potentiates Efficacy and Alters Susceptibility to Exhaustion. *Immunity,* 44**,** 179-193.

MALIK, B. T., BYRNE, K. T., VELLA, J. L., ZHANG, P., SHABANEH, T. B., STEINBERG, S. M., MOLODTSOV, A. K., BOWERS, J. S., ANGELES, C. V., PAULOS, C. M., HUANG, Y. H. & TURK, M. J. 2017. Resident memory T cells in the skin mediate durable immunity to melanoma. *Sci Immunol,* 2.

MALIK, S. & AWASTHI, A. 2018. Transcriptional Control of Th9 Cells: Role of Foxo1 in Interleukin-9 Induction. *Front Immunol,* 9**,** 995.

MALISSEN, B., TAMOUTOUNOUR, S. & HENRI, S. 2014. The origins and functions of dendritic cells and macrophages in the skin. *Nat Rev Immunol,* 14**,** 417-28.

MALYSHKINA, A., LITTWITZ-SALOMON, E., SUTTER, K., ZELINSKYY, G., WINDMANN, S., SCHIMMER, S., PASCHEN, A., STREECK, H., HASENKRUG, K. J. & DITTMER, U. 2017. Fas Ligand-mediated cytotoxicity of CD4+ T cells during chronic retrovirus infection. *Sci Rep,* 7**,** 7785.

MANTOVANI, A. & SICA, A. 2010. Macrophages, innate immunity and cancer: balance, tolerance, and diversity. *Curr Opin Immunol,* 22**,** 231-7.

MARTENS, A., WISTUBA-HAMPRECHT, K., GEUKES FOPPEN, M., YUAN, J., POSTOW, M. A., WONG, P., ROMANO, E., KHAMMARI, A., DRENO, B., CAPONE, M., ASCIERTO, P. A., DI GIACOMO, A. M., MAIO, M., SCHILLING, B., SUCKER, A., SCHADENDORF, D., HASSEL, J. C., EIGENTLER, T. K., MARTUS, P., WOLCHOK, J. D., BLANK, C., PAWELEC, G., GARBE, C. & WEIDE, B. 2016. Baseline Peripheral Blood Biomarkers Associated with Clinical Outcome of Advanced Melanoma Patients Treated with Ipilimumab. *Clin Cancer Res,* 22**,** 2908-18.

MARTIN-OROZCO, N., MURANSKI, P., CHUNG, Y., YANG, X. O., YAMAZAKI, T., LU, S., HWU, P., RESTIFO, N. P., OVERWIJK, W. W. & DONG, C. 2009. T helper 17 cells promote cytotoxic T cell activation in tumor immunity. *Immunity,* 31**,** 787-98.

MARZO, A. L., KINNEAR, B. F., LAKE, R. A., FRELINGER, J. J., COLLINS, E. J., ROBINSON, B. W. & SCOTT, B. 2000. Tumor-specific CD4+ T cells have a major "post-licensing" role in CTL mediated anti-tumor immunity. *J Immunol,* 165**,** 6047-55.

MARZO, A. L., KLONOWSKI, K. D., LE BON, A., BORROW, P., TOUGH, D. F. & LEFRANCOIS, L. 2005. Initial T cell frequency dictates memory CD8+ T cell lineage commitment. *Nat Immunol,* 6**,** 793-9.

MATSUSHITA, H., VESELY, M. D., KOBOLDT, D. C., RICKERT, C. G., UPPALURI, R., MAGRINI, V. J., ARTHUR, C. D., WHITE, J. M., CHEN, Y. S., SHEA, L. K., HUNDAL, J., WENDL, M. C., DEMETER, R., WYLIE, T., ALLISON, J. P., SMYTH, M. J., OLD, L. J., MARDIS, E. R. & SCHREIBER, R. D. 2012. Cancer exome analysis reveals a T-cell-dependent mechanism of cancer immunoediting. *Nature,* 482**,** 400-4.

MATSUZAKI, J., TSUJI, T., LUESCHER, I., OLD, L. J., SHRIKANT, P., GNJATIC, S. & ODUNSI, K. 2014. Nonclassical antigen-processing pathways are required for MHC class II-restricted direct tumor recognition by NY-ESO-1-specific CD4(+) T cells. *Cancer Immunol Res,* 2**,** 341-50.

MATSUZAKI, J., TSUJI, T., LUESCHER, I. F., SHIKU, H., MINENO, J., OKAMOTO, S., OLD, L. J., SHRIKANT, P., GNJATIC, S. & ODUNSI, K. 2015. Direct tumor recognition by a human CD4(+) T-cell subset potently mediates tumor growth inhibition and orchestrates anti-tumor immune responses. *Sci Rep,* 5**,** 14896.

MAURI, D. N., EBNER, R., MONTGOMERY, R. I., KOCHEL, K. D., CHEUNG, T. C., YU, G. L., RUBEN, S., MURPHY, M., EISENBERG, R. J., COHEN, G. H., SPEAR, P. G. & WARE, C. F. 1998. LIGHT, a new member of the TNF superfamily, and lymphotoxin alpha are ligands for herpesvirus entry mediator. *Immunity,* 8**,** 21-30.

MCLACHLAN, J. B., CATRON, D. M., MOON, J. J. & JENKINS, M. K. 2009. Dendritic cell antigen presentation drives simultaneous cytokine production by effector and regulatory T cells in inflamed skin. *Immunity,* 30**,** 277-88.

MENG, S., TRIPATHY, D., FRENKEL, E. P., SHETE, S., NAFTALIS, E. Z., HUTH, J. F., BEITSCH, P. D., LEITCH, M., HOOVER, S., EUHUS, D., HALEY, B., MORRISON, L., FLEMING, T. P., HERLYN, D., TERSTAPPEN, L. W., FEHM, T., TUCKER, T. F., LANE, N., WANG, J. & UHR, J. W. 2004. Circulating tumor cells in patients with breast cancer dormancy. *Clin Cancer Res,* 10**,** 8152-62.

MEYER, C., CAGNON, L., COSTA-NUNES, C. M., BAUMGAERTNER, P., MONTANDON, N., LEYVRAZ, L., MICHIELIN, O., ROMANO, E. & SPEISER, D. E. 2014. Frequencies of circulating MDSC correlate with clinical outcome of melanoma patients treated with ipilimumab. *Cancer Immunol Immunother,* 63**,** 247-57.

MEYER, C., SEVKO, A., RAMACHER, M., BAZHIN, A. V., FALK, C. S., OSEN, W., BORRELLO, I., KATO, M., SCHADENDORF, D., BANIYASH, M. & UMANSKY, V. 2011. Chronic inflammation promotes myeloid-derived suppressor cell activation blocking antitumor immunity in transgenic mouse melanoma model. *Proc Natl Acad Sci U S A,* 108**,** 17111-6.

MIKLOSKA, Z. & CUNNINGHAM, A. L. 1998. Herpes simplex virus type 1 glycoproteins gB, gC and gD are major targets for CD4 T-lymphocyte cytotoxicity in HLA-DR expressing human epidermal keratinocytes. *J Gen Virol,* 79 (Pt 2)**,** 353-61.

MINTZ, B. & SILVERS, W. K. 1993. Transgenic mouse model of malignant skin melanoma. *Proc Natl Acad Sci U S A,* 90**,** 8817-21.

MONTFORT, A., COLACIOS, C., LEVADE, T., ANDRIEU-ABADIE, N., MEYER, N. & SEGUI, B. 2019. The TNF Paradox in Cancer Progression and Immunotherapy. *Front Immunol,* 10**,** 1818.

MORRISON, A. H., DIAMOND, M. S., HAY, C. A., BYRNE, K. T. & VONDERHEIDE, R. H. 2020. Sufficiency of CD40 activation and immune checkpoint blockade for T cell priming and tumor immunity. *Proc Natl Acad Sci U S A,* 117**,** 8022-8031.

MOTZ, G. T., SANTORO, S. P., WANG, L. P., GARRABRANT, T., LASTRA, R. R., HAGEMANN, I. S., LAL, P., FELDMAN, M. D., BENENCIA, F. & COUKOS, G. 2014. Tumor endothelium FasL establishes a selective immune barrier promoting tolerance in tumors. *Nat Med,* 20**,** 607-15.

MUMBERG, D., MONACH, P. A., WANDERLING, S., PHILIP, M., TOLEDANO, A. Y., SCHREIBER, R. D. & SCHREIBER, H. 1999. CD4(+) T cells eliminate MHC class II-negative cancer cells in vivo by indirect effects of IFN-gamma. *Proc Natl Acad Sci U S A,* 96**,** 8633-8.

MURANSKI, P., BONI, A., ANTONY, P. A., CASSARD, L., IRVINE, K. R., KAISER, A., PAULOS, C. M., PALMER, D. C., TOULOUKIAN, C. E., PTAK, K., GATTINONI, L., WRZESINSKI, C., HINRICHS, C. S., KERSTANN, K. W., FEIGENBAUM, L., CHAN, C. C. & RESTIFO, N. P. 2008. Tumor-specific Th17-polarized cells eradicate large established melanoma. *Blood,* 112**,** 362-73.

NAKAMURA, K., YOSHIKAWA, N., YAMAGUCHI, Y., KAGOTA, S., SHINOZUKA, K. & KUNITOMO, M. 2002. Characterization of mouse melanoma cell lines by their mortal malignancy using an experimental metastatic model. *Life Sci,* 70**,** 791-8.

NAREZNOI, D., KONIKOV-ROZENMAN, J., PETUKHOV, D., BREUER, R. & WALLACH-DAYAN, S. B. 2020. Matrix Metalloproteinases Retain Soluble FasL-mediated Resistance to Cell Death in Fibrotic-Lung Myofibroblasts. *Cells,* 9.

NAUMOV, G. N., MACDONALD, I. C., WEINMEISTER, P. M., KERKVLIET, N., NADKARNI, K. V., WILSON, S. M., MORRIS, V. L., GROOM, A. C. & CHAMBERS, A. F. 2002. Persistence of solitary mammary carcinoma cells in a secondary site: a possible contributor to dormancy. *Cancer Res,* 62**,** 2162-8.

NISHIDA, S., YOSHIOKA, S., KINOSHITA-KIMOTO, S., KOTANI, M., TSUBAKI, M., FUJII, Y., TOMURA, T. T. & IRIMAJIRI, K. 2003. Pretreatment with PKC inhibitor triggers TNF-alpha induced apoptosis in TNF-alpha-resistant B16 melanoma BL6 cells. *Life Sci,* 74**,** 781-92.

NISHIMURA, T., IWAKABE, K., SEKIMOTO, M., OHMI, Y., YAHATA, T., NAKUI, M., SATO, T., HABU, S., TASHIRO, H., SATO, M. & OHTA, A. 1999. Distinct role of antigen-specific T helper type 1 (Th1) and Th2 cells in tumor eradication in vivo. *J Exp Med,* 190**,** 617-27.

NORTHROP, J. K., THOMAS, R. M., WELLS, A. D. & SHEN, H. 2006. Epigenetic remodeling of the IL-2 and IFN-gamma loci in memory CD8 T cells is influenced by CD4 T cells. *J Immunol,* 177**,** 1062-9.

NUMASAKI, M., FUKUSHI, J., ONO, M., NARULA, S. K., ZAVODNY, P. J., KUDO, T., ROBBINS, P. D., TAHARA, H. & LOTZE, M. T. 2003. Interleukin-17 promotes angiogenesis and tumor growth. *Blood,* 101**,** 2620-7.

O'SULLIVAN, T., SADDAWI-KONEFKA, R., VERMI, W., KOEBEL, C. M., ARTHUR, C., WHITE, J. M., UPPALURI, R., ANDREWS, D. M., NGIOW, S. F., TENG, M. W., SMYTH, M. J., SCHREIBER, R. D. & BUI, J. D. 2012.

Cancer immunoediting by the innate immune system in the absence of adaptive immunity. *J Exp Med,* 209**,** 1869-82.

OCHSENBEIN, A. F., SIERRO, S., ODERMATT, B., PERICIN, M., KARRER, U., HERMANS, J., HEMMI, S., HENGARTNER, H. & ZINKERNAGEL, R. M. 2001. Roles of tumour localization, second signals and cross priming in cytotoxic T-cell induction. *Nature,* 411**,** 1058-64.

OH, D. Y., KWEK, S. S., RAJU, S. S., LI, T., MCCARTHY, E., CHOW, E., ARAN, D., ILANO, A., PAI, C. S., RANCAN, C., ALLAIRE, K., BURRA, A., SUN, Y., SPITZER, M. H., MANGUL, S., PORTEN, S., MENG, M. V., FRIEDLANDER, T. W., YE, C. J. & FONG, L. 2020. Intratumoral CD4(+) T Cells Mediate Anti-tumor Cytotoxicity in Human Bladder Cancer. *Cell*.

ONDA, M., KOBAYASHI, K. & PASTAN, I. 2019. Depletion of regulatory T cells in tumors with an anti-CD25 immunotoxin induces CD8 T cell-mediated systemic antitumor immunity. *Proc Natl Acad Sci U S A,* 116**,** 4575-4582.

ORTIZ, M. L., KUMAR, V., MARTNER, A., MONY, S., DONTHIREDDY, L., CONDAMINE, T., SEYKORA, J., KNIGHT, S. C., MALIETZIS, G., LEE, G. H., MOORGHEN, M., LENOX, B., LUETTEKE, N., CELIS, E. & GABRILOVICH, D. 2015. Immature myeloid cells directly contribute to skin tumor development by recruiting IL-17-producing CD4+ T cells. *J Exp Med,* 212**,** 351-67.

OSSENDORP, F., MENGEDE, E., CAMPS, M., FILIUS, R. & MELIEF, C. J. 1998. Specific T helper cell requirement for optimal induction of cytotoxic T lymphocytes against major histocompatibility complex class II negative tumors. *J Exp Med,* 187**,** 693-702.

OTT, P. A., HU, Z., KESKIN, D. B., SHUKLA, S. A., SUN, J., BOZYM, D. J., ZHANG, W., LUOMA, A., GIOBBIE-HURDER, A., PETER, L., CHEN, C., OLIVE, O., CARTER, T. A., LI, S., LIEB, D. J., EISENHAURE, T., GJINI, E., STEVENS, J., LANE, W. J., JAVERI, I., NELLAIAPPAN, K., SALAZAR, A. M., DALEY, H., SEAMAN, M., BUCHBINDER, E. I., YOON, C. H., HARDEN, M., LENNON, N., GABRIEL, S., RODIG, S. J., BAROUCH, D. H., ASTER, J. C., GETZ, G., WUCHERPFENNIG, K., NEUBERG, D., RITZ, J., LANDER, E. S., FRITSCH, E. F., HACOHEN, N. & WU, C. J. 2017. An immunogenic personal neoantigen vaccine for patients with melanoma. *Nature,* 547**,** 217-221.

OVERWIJK, W. W. & RESTIFO, N. P. 2001. B16 as a mouse model for human melanoma. *Curr Protoc Immunol,* Chapter 20**,** Unit 20 1.

PALUSKIEVICZ, C. M., CAO, X., ABDI, R., ZHENG, P., LIU, Y. & BROMBERG, J. S. 2019. T Regulatory Cells and Priming the Suppressive Tumor Microenvironment. *Front Immunol,* 10**,** 2453.

PAN, X. Q. 2012. The mechanism of the anticancer function of M1 macrophages and their use in the clinic. *Chin J Cancer,* 31**,** 557-63.

PAPALEXI, E. & SATIJA, R. 2018. Single-cell RNA sequencing to explore immune cell heterogeneity. *Nat Rev Immunol,* 18**,** 35-45.

PARK, C. O., FU, X., JIANG, X., PAN, Y., TEAGUE, J. E., COLLINS, N., TIAN, T., O'MALLEY, J. T., EMERSON, R. O., KIM, J. H., JUNG, Y., WATANABE, R., FUHLBRIGGE, R. C., CARBONE, F. R., GEBHARDT, T., CLARK, R. A., LIN, C. P. & KUPPER, T. S. 2018. Staged development of long-lived T-cell receptor alphabeta TH17 resident memory T-cell population to Candida albicans after skin infection. *J Allergy Clin Immunol,* 142**,** 647-662.

PARK, I. A., HWANG, S. H., SONG, I. H., HEO, S. H., KIM, Y. A., BANG, W. S., PARK, H. S., LEE, M., GONG, G. & LEE, H. J. 2017. Expression of the MHC class II in triple-negative breast cancer is associated with tumor-infiltrating lymphocytes and interferon signaling. *PLoS One,* 12**,** e0182786.

PARK, S. L., BUZZAI, A., RAUTELA, J., HOR, J. L., HOCHHEISER, K., EFFERN, M., MCBAIN, N., WAGNER, T., EDWARDS, J., MCCONVILLE, R., WILMOTT, J. S., SCOLYER, R. A., TUTING, T., PALENDIRA, U., GYORKI, D., MUELLER, S. N., HUNTINGTON, N. D., BEDOUI, S., HOLZEL, M., MACKAY, L. K., WAITHMAN, J. & GEBHARDT, T. 2019. Tissue-resident memory CD8(+) T cells promote melanoma-immune equilibrium in skin. *Nature,* 565**,** 366-371.

PAUL, S. & LAL, G. 2017. The Molecular Mechanism of Natural Killer Cells Function and Its Importance in Cancer Immunotherapy. *Front Immunol,* 8**,** 1124.

PEPPER, M., PAGAN, A. J., IGYARTO, B. Z., TAYLOR, J. J. & JENKINS, M. K. 2011. Opposing signals from the Bcl6 transcription factor and the interleukin-2 receptor generate T helper 1 central and effector memory cells. *Immunity,* 35**,** 583-95.

PEREZ-DIEZ, A., JONCKER, N. T., CHOI, K., CHAN, W. F., ANDERSON, C. C., LANTZ, O. & MATZINGER, P. 2007. CD4 cells can be more efficient at tumor rejection than CD8 cells. *Blood,* 109**,** 5346-54.

POOLEY, J. L., HEATH, W. R. & SHORTMAN, K. 2001. Cutting edge: intravenous soluble antigen is presented to CD4 T cells by CD8- dendritic cells, but cross-presented to CD8 T cells by CD8+ dendritic cells. *J Immunol,* 166**,** 5327-30.

POSTOW, M. A., CHESNEY, J., PAVLICK, A. C., ROBERT, C., GROSSMANN, K., MCDERMOTT, D., LINETTE, G. P., MEYER, N., GIGUERE, J. K., AGARWALA, S. S., SHAHEEN, M., ERNSTOFF, M. S., MINOR, D., SALAMA, A. K., TAYLOR, M., OTT, P. A., ROLLIN, L. M., HORAK, C., GAGNIER, P., WOLCHOK, J. D. & HODI, F. S. 2015. Nivolumab and ipilimumab versus ipilimumab in untreated melanoma. *N Engl J Med,* 372**,** 2006-17.

PURWAR, R., SCHLAPBACH, C., XIAO, S., KANG, H. S., ELYAMAN, W., JIANG, X., JETTEN, A. M., KHOURY, S. J., FUHLBRIGGE, R. C., KUCHROO, V. K., CLARK, R. A. & KUPPER, T. S. 2012. Robust tumor immunity to melanoma mediated by interleukin-9-producing T cells. *Nat Med,* 18**,** 1248-53.

QIN, Z. & BLANKENSTEIN, T. 2000. CD4+ T cell--mediated tumor rejection involves inhibition of angiogenesis that is dependent on IFN gamma receptor expression by nonhematopoietic cells. *Immunity,* 12**,** 677-86.

QUEZADA, S. A., SIMPSON, T. R., PEGGS, K. S., MERGHOUB, T., VIDER, J., FAN, X., BLASBERG, R., YAGITA, H., MURANSKI, P., ANTONY, P. A., RESTIFO, N. P. & ALLISON, J. P. 2010. Tumor-reactive CD4(+) T cells

develop cytotoxic activity and eradicate large established melanoma after transfer into lymphopenic hosts. *J Exp Med,* 207**,** 637-50.

RAZA, A., MERHI, M., INCHAKALODY, V. P., KRISHNANKUTTY, R., RELECOM, A., UDDIN, S. & DERMIME, S. 2020. Unleashing the immune response to NY-ESO-1 cancer testis antigen as a potential target for cancer immunotherapy. *J Transl Med,* 18**,** 140.

READ, J., WADT, K. A. & HAYWARD, N. K. 2016. Melanoma genetics. *J Med Genet,* 53**,** 1-14.

REINHARDT, R. L., BULLARD, D. C., WEAVER, C. T. & JENKINS, M. K. 2003. Preferential accumulation of antigen-specific effector CD4 T cells at an antigen injection site involves CD62E-dependent migration but not local proliferation. *J Exp Med,* 197**,** 751-62.

RODIG, S. J., GUSENLEITNER, D., JACKSON, D. G., GJINI, E., GIOBBIE-HURDER, A., JIN, C., CHANG, H., LOVITCH, S. B., HORAK, C., WEBER, J. S., WEIRATHER, J. L., WOLCHOK, J. D., POSTOW, M. A., PAVLICK, A. C., CHESNEY, J. & HODI, F. S. 2018. MHC proteins confer differential sensitivity to CTLA-4 and PD-1 blockade in untreated metastatic melanoma. *Sci Transl Med,* 10.

ROSENBERG, S. A. 2014. IL-2: the first effective immunotherapy for human cancer. *J Immunol,* 192**,** 5451-8.

RUSSELL, J. H. & LEY, T. J. 2002. Lymphocyte-mediated cytotoxicity. *Annu Rev Immunol,* 20**,** 323-70.

RYAN, A. E., SHANAHAN, F., O'CONNELL, J. & HOUSTON, A. M. 2005. Addressing the "Fas counterattack" controversy: blocking fas ligand expression suppresses tumor immune evasion of colon cancer in vivo. *Cancer Res,* 65**,** 9817-23.

SAHIN, U., DERHOVANESSIAN, E., MILLER, M., KLOKE, B. P., SIMON, P., LOWER, M., BUKUR, V., TADMOR, A. D., LUXEMBURGER, U., SCHRORS, B., OMOKOKO, T., VORMEHR, M., ALBRECHT, C., PARUZYNSKI, A., KUHN, A. N., BUCK, J., HEESCH, S., SCHREEB, K. H., MULLER, F., ORTSEIFER, I., VOGLER, I., GODEHARDT, E., ATTIG, S., RAE, R., BREITKREUZ, A., TOLLIVER, C., SUCHAN, M., MARTIC, G., HOHBERGER, A., SORN, P., DIEKMANN, J., CIESLA, J., WAKSMANN, O., BRUCK, A. K., WITT, M., ZILLGEN, M., ROTHERMEL, A., KASEMANN, B., LANGER, D., BOLTE, S., DIKEN, M., KREITER, S., NEMECEK, R., GEBHARDT, C., GRABBE, S., HOLLER, C., UTIKAL, J., HUBER, C., LOQUAI, C. & TURECI, O. 2017. Personalized RNA mutanome vaccines mobilize poly-specific therapeutic immunity against cancer. *Nature,* 547**,** 222-226.

SAKAI, S., KAUFFMAN, K. D., SCHENKEL, J. M., MCBERRY, C. C., MAYER-BARBER, K. D., MASOPUST, D. & BARBER, D. L. 2014. Cutting edge: control of Mycobacterium tuberculosis infection by a subset of lung parenchyma-homing CD4 T cells. *J Immunol,* 192**,** 2965-9.

SALLUSTO, F., LENIG, D., FORSTER, R., LIPP, M. & LANZAVECCHIA, A. 1999. Two subsets of memory T lymphocytes with distinct homing potentials and effector functions. *Nature,* 401**,** 708-12.

SALLUSTO, F., LENIG, D., FORSTER, R., LIPP, M. & LANZAVECCHIA, A. 2014. Pillars article: two subsets of memory T lymphocytes with distinct homing potentials and effector functions. Nature. 1999. 401: 708-712. *J Immunol,* 192**,** 840-4.

SASHCHENKO, L. P., DUKHANINA, E. A., SHATALOV, Y. V., YASHIN, D. V., LUKYANOVA, T. I., KABANOVA, O. D., ROMANOVA, E. A., KHAIDUKOV, S. V., GALKIN, A. V., GNUCHEV, N. V. & GEORGIEV, G. P. 2007. Cytotoxic T lymphocytes carrying a pattern recognition protein Tag7 can detect evasive, HLA-negative but Hsp70-exposing tumor cells, thereby ensuring FasL/Fas-mediated contact killing. *Blood,* 110**,** 1997-2004.

SCHENKEL, J. M. & MASOPUST, D. 2014. Tissue-resident memory T cells. *Immunity,* 41**,** 886-97.

SCHIETINGER, A., PHILIP, M., LIU, R. B., SCHREIBER, K. & SCHREIBER, H. 2010. Bystander killing of cancer requires the cooperation of CD4(+) and CD8(+) T cells during the effector phase. *J Exp Med,* 207**,** 2469-77.

SCHMID-BURGK, J. L., HONING, K., EBERT, T. S. & HORNUNG, V. 2016. CRISPaint allows modular base-specific gene tagging using a ligase-4-dependent mechanism. *Nat Commun,* 7**,** 12338.

SCHMIDT, A., OBERLE, N. & KRAMMER, P. H. 2012. Molecular mechanisms of treg-mediated T cell suppression. *Front Immunol,* 3**,** 51.

SHANKARAN, V., IKEDA, H., BRUCE, A. T., WHITE, J. M., SWANSON, P. E., OLD, L. J. & SCHREIBER, R. D. 2001. IFNgamma and lymphocytes prevent primary tumour development and shape tumour immunogenicity. *Nature,* 410**,** 1107-11.

SHARONOV, G. V., SEREBROVSKAYA, E. O., YUZHAKOVA, D. V., BRITANOVA, O. V. & CHUDAKOV, D. M. 2020. B cells, plasma cells and antibody repertoires in the tumour microenvironment. *Nat Rev Immunol,* 20**,** 294-307.

SHEDLOCK, D. J. & SHEN, H. 2003. Requirement for CD4 T cell help in generating functional CD8 T cell memory. *Science,* 300**,** 337-9.

SHIMIZU, M., FONTANA, A., TAKEDA, Y., YAGITA, H., YOSHIMOTO, T. & MATSUZAWA, A. 1999. Induction of antitumor immunity with Fas/APO-1 ligand (CD95L)-transfected neuroblastoma neuro-2a cells. *J Immunol,* 162**,** 7350-7.

SHIMIZU, M., FONTANA, A., TAKEDA, Y., YOSHIMOTO, T., TSUBURA, A. & MATSUZAWA, A. 2001. Fas/Apo-1 (CD95)-mediated apoptosis of neutrophils with Fas ligand (CD95L)-expressing tumors is crucial for induction of inflammation by neutrophilic polymorphonuclear leukocytes associated with antitumor immunity. *Cell Immunol,* 207**,** 41-8.

SHIOW, L. R., ROSEN, D. B., BRDICKOVA, N., XU, Y., AN, J., LANIER, L. L., CYSTER, J. G. & MATLOUBIAN, M. 2006. CD69 acts downstream of interferon-alpha/beta to inhibit S1P1 and lymphocyte egress from lymphoid organs. *Nature,* 440**,** 540-4.

SHKLOVSKAYA, E., TERRY, A. M., GUY, T. V., BUCKLEY, A., BOLTON, H. A., ZHU, E., HOLST, J. & FAZEKAS DE ST. GROTH, B. 2016. Tumour-specific CD4 T cells eradicate melanoma via indirect recognition of tumour-derived antigen. *Immunol Cell Biol,* 94**,** 593-603.

SIMON, A. K., GALLIMORE, A., JONES, E., SAWITZKI, B., CERUNDOLO, V. & SCREATON, G. R. 2002. Fas ligand breaks tolerance to self-antigens and induces tumor immunity mediated by antibodies. *Cancer Cell,* 2**,** 315-22.

SMYTH, M. J., CRETNEY, E., TAKEDA, K., WILTROUT, R. H., SEDGER, L. M., KAYAGAKI, N., YAGITA, H. & OKUMURA, K. 2001a. Tumor necrosis factor-related apoptosis-inducing ligand (TRAIL) contributes to interferon gamma-dependent natural killer cell protection from tumor metastasis. *J Exp Med,* 193**,** 661-70.

SMYTH, M. J., CROWE, N. Y. & GODFREY, D. I. 2001b. NK cells and NKT cells collaborate in host protection from methylcholanthrene-induced fibrosarcoma. *Int Immunol,* 13**,** 459-63.

SMYTH, M. J., KRASOVSKIS, E. & JOHNSTONE, R. W. 1998. Fas ligand-mediated lysis of self bystander targets by human papillomavirus-specific CD8+ cytotoxic T lymphocytes. *J Virol,* 72**,** 5948-54.

STALDER, T., HAHN, S. & ERB, P. 1994. Fas antigen is the major target molecule for CD4+ T cell-mediated cytotoxicity. *J Immunol,* 152**,** 1127-33.

STANKOVIC, S., HARPUR, C. M., MACLEOD, B. L., WHITNEY, P. G., GEBHARDT, T. & BROOKS, A. G. 2015. Limited Internodal Migration of T Follicular Helper Cells after Peripheral Infection with Herpes Simplex Virus-1. *J Immunol,* 195**,** 4892-9.

STEIMLE, V., SIEGRIST, C. A., MOTTET, A., LISOWSKA-GROSPIERRE, B. & MACH, B. 1994. Regulation of MHC class II expression by interferon-gamma mediated by the transactivator gene CIITA. *Science,* 265**,** 106-9.

STEINERT, E. M., SCHENKEL, J. M., FRASER, K. A., BEURA, L. K., MANLOVE, L. S., IGYARTO, B. Z., SOUTHERN, P. J. & MASOPUST, D. 2015. Quantifying Memory CD8 T Cells Reveals Regionalization of Immunosurveillance. *Cell,* 161**,** 737-49.

STRAUSS, D. C. & THOMAS, J. M. 2010. Transmission of donor melanoma by organ transplantation. *Lancet Oncol,* 11**,** 790-6.

SUN, J. C., WILLIAMS, M. A. & BEVAN, M. J. 2004. CD4+ T cells are required for the maintenance, not programming, of memory CD8+ T cells after acute infection. *Nat Immunol,* 5**,** 927-33.

SVANE, I. M., ENGEL, A. M., NIELSEN, M. B., LJUNGGREN, H. G., RYGAARD, J. & WERDELIN, O. 1996. Chemically induced sarcomas from nude mice are more immunogenic than similar sarcomas from congenic normal mice. *Eur J Immunol,* 26**,** 1844-50.

TAKEDA, K., HAYAKAWA, Y., SMYTH, M. J., KAYAGAKI, N., YAMAGUCHI, N., KAKUTA, S., IWAKURA, Y., YAGITA, H. & OKUMURA, K. 2001. Involvement of tumor necrosis factor-related apoptosis-inducing ligand in surveillance of tumor metastasis by liver natural killer cells. *Nat Med,* 7**,** 94-100.

TAKEUCHI, A. & SAITO, T. 2017. CD4 CTL, a Cytotoxic Subset of CD4(+) T Cells, Their Differentiation and Function. *Front Immunol,* 8**,** 194.

TAMOUTOUNOUR, S., GUILLIAMS, M., MONTANANA SANCHIS, F., LIU, H., TERHORST, D., MALOSSE, C., POLLET, E., ARDOUIN, L., LUCHE, H., SANCHEZ, C., DALOD, M., MALISSEN, B. & HENRI, S. 2013. Origins and functional specialization of macrophages and of conventional and monocyte-derived dendritic cells in mouse skin. *Immunity,* 39**,** 925-38.

TAYLOR, C. T. & COLGAN, S. P. 2017. Regulation of immunity and inflammation by hypoxia in immunological niches. *Nat Rev Immunol,* 17**,** 774-785.

TCHAO, N. K. & TURKA, L. A. 2012. Lymphodepletion and homeostatic proliferation: implications for transplantation. *Am J Transplant,* 12**,** 1079-90.

TEIJARO, J. R., TURNER, D., PHAM, Q., WHERRY, E. J., LEFRANCOIS, L. & FARBER, D. L. 2011. Cutting edge: Tissue-retentive lung memory CD4 T cells mediate optimal protection to respiratory virus infection. *J Immunol,* 187**,** 5510-4.

TENG, M. W., SWANN, J. B., KOEBEL, C. M., SCHREIBER, R. D. & SMYTH, M. J. 2008. Immune-mediated dormancy: an equilibrium with cancer. *J Leukoc Biol,* 84**,** 988-93.

TOBIN, D. J. 2011. The cell biology of human hair follicle pigmentation. *Pigment Cell Melanoma Res,* 24**,** 75-88.

TRAN, E., TURCOTTE, S., GROS, A., ROBBINS, P. F., LU, Y. C., DUDLEY, M. E., WUNDERLICH, J. R., SOMERVILLE, R. P., HOGAN, K., HINRICHS, C. S., PARKHURST, M. R., YANG, J. C. & ROSENBERG, S. A. 2014. Cancer immunotherapy based on mutation-specific CD4+ T cells in a patient with epithelial cancer. *Science,* 344**,** 641-5.

TUBO, N. J., PAGAN, A. J., TAYLOR, J. J., NELSON, R. W., LINEHAN, J. L., ERTELT, J. M., HUSEBY, E. S., WAY, S. S. & JENKINS, M. K. 2013. Single naive CD4+ T cells from a diverse repertoire produce different effector cell types during infection. *Cell,* 153**,** 785-96.

UMANSKY, V. & SEVKO, A. 2012. Overcoming immunosuppression in the melanoma microenvironment induced by chronic inflammation. *Cancer Immunol Immunother,* 61**,** 275-82.

VAN LEEUWEN, E. M., REMMERSWAAL, E. B., VOSSEN, M. T., ROWSHANI, A. T., WERTHEIM-VAN DILLEN, P. M., VAN LIER, R. A. & TEN BERGE, I. J. 2004. Emergence of a CD4+CD28- granzyme B+, cytomegalovirus-specific T cell subset after recovery of primary cytomegalovirus infection. *J Immunol,* 173**,** 1834-41.

VEGRAN, F., BERGER, H., BOIDOT, R., MIGNOT, G., BRUCHARD, M., DOSSET, M., CHALMIN, F., REBE, C., DERANGERE, V., RYFFEL, B., KATO, M., PREVOST-BLONDEL, A., GHIRINGHELLI, F. & APETOH, L. 2014. The transcription factor IRF1 dictates the IL-21-dependent anticancer functions of TH9 cells. *Nat Immunol,* 15**,** 758-66.

VELDHOEN, M., UYTTENHOVE, C., VAN SNICK, J., HELMBY, H., WESTENDORF, A., BUER, J., MARTIN, B., WILHELM, C. & STOCKINGER, B. 2008. Transforming growth factor-beta 'reprograms' the differentiation of T helper 2 cells and promotes an interleukin 9-producing subset. *Nat Immunol,* 9**,** 1341-6.

VERCAMMEN, D., BROUCKAERT, G., DENECKER, G., VAN DE CRAEN, M., DECLERCQ, W., FIERS, W. & VANDENABEELE, P. 1998. Dual signaling of the Fas receptor: initiation of both apoptotic and necrotic cell death pathways. *J Exp Med,* 188**,** 919-30.

VILLIKKA, K. & PYRHONEN, S. 1996. Cytokine therapy of malignant melanoma. *Ann Med,* 28**,** 227-33.

VINAY, D. S., RYAN, E. P., PAWELEC, G., TALIB, W. H., STAGG, J., ELKORD, E., LICHTOR, T., DECKER, W. K., WHELAN, R. L., KUMARA, H., SIGNORI, E., HONOKI, K., GEORGAKILAS, A. G., AMIN, A., HELFERICH, W. G., BOOSANI, C. S., GUHA, G., CIRIOLO, M. R., CHEN, S., MOHAMMED, S. I., AZMI, A. S., KEITH, W.

N., BILSLAND, A., BHAKTA, D., HALICKA, D., FUJII, H., AQUILANO, K., ASHRAF, S. S., NOWSHEEN, S., YANG, X., CHOI, B. K. & KWON, B. S. 2015. Immune evasion in cancer: Mechanistic basis and therapeutic strategies. *Semin Cancer Biol,* 35 Suppl**,** S185-S198.

VON KARSTEDT, S., MONTINARO, A. & WALCZAK, H. 2017. Exploring the TRAILs less travelled: TRAIL in cancer biology and therapy. *Nat Rev Cancer,* 17**,** 352-366.

WALLACE, M. E., KEATING, R., HEATH, W. R. & CARBONE, F. R. 1999. The cytotoxic T-cell response to herpes simplex virus type 1 infection of C57BL/6 mice is almost entirely directed against a single immunodominant determinant. *J Virol,* 73**,** 7619-26.

WANG, J. C. & LIVINGSTONE, A. M. 2003. Cutting edge: CD4+ T cell help can be essential for primary CD8+ T cell responses in vivo. *J Immunol,* 171**,** 6339-43.

WANG, S., BOONMAN, Z. F., LI, H. C., HE, Y., JAGER, M. J., TOES, R. E. & NIEDERKORN, J. Y. 2003. Role of TRAIL and IFN-gamma in CD4+ T cell-dependent tumor rejection in the anterior chamber of the eye. *J Immunol,* 171**,** 2789-96.

WATANABE, R., GEHAD, A., YANG, C., SCOTT, L. L., TEAGUE, J. E., SCHLAPBACH, C., ELCO, C. P., HUANG, V., MATOS, T. R., KUPPER, T. S. & CLARK, R. A. 2015. Human skin is protected by four functionally and phenotypically discrete populations of resident and recirculating memory T cells. *Sci Transl Med,* 7**,** 279ra39.

WCULEK, S. K., CUETO, F. J., MUJAL, A. M., MELERO, I., KRUMMEL, M. F. & SANCHO, D. 2020. Dendritic cells in cancer immunology and immunotherapy. *Nat Rev Immunol,* 20**,** 7-24.

WELLING-WEBSTER, S., SCHEFFER, A. J. & WELLING, G. W. 1991. B and T cell epitopes of glycoprotein D of herpes simplex virus type 1. *FEMS Microbiol Immunol,* 3**,** 59-68.

WHITBECK, J. C., PENG, C., LOU, H., XU, R., WILLIS, S. H., PONCE DE LEON, M., PENG, T., NICOLA, A. V., MONTGOMERY, R. I., WARNER, M. S., SOULIKA, A. M., SPRUCE, L. A., MOORE, W. T., LAMBRIS, J. D., SPEAR, P. G., COHEN, G. H. & EISENBERG, R. J. 1997. Glycoprotein D of herpes simplex virus (HSV) binds directly to HVEM, a member of the tumor necrosis factor receptor superfamily and a mediator of HSV entry. *J Virol,* 71**,** 6083-93.

WILK, M. M., MISIAK, A., MCMANUS, R. M., ALLEN, A. C., LYNCH, M. A. & MILLS, K. H. G. 2017. Lung CD4 Tissue-Resident Memory T Cells Mediate Adaptive Immunity Induced by Previous Infection of Mice with Bordetella pertussis. *J Immunol,* 199**,** 233-243.

WIRTH, T. C. & KUHNEL, F. 2017. Neoantigen Targeting-Dawn of a New Era in Cancer Immunotherapy? *Front Immunol,* 8**,** 1848.

WOLKERS, M. C., GERLACH, C., ARENS, R., JANSSEN, E. M., FITZGERALD, P., SCHUMACHER, T. N., MEDEMA, J. P., GREEN, D. R. & SCHOENBERGER, S. P. 2012. Nab2 regulates secondary CD8+ T-cell responses through control of TRAIL expression. *Blood,* 119**,** 798-804.

WONG, S. B., BOS, R. & SHERMAN, L. A. 2008. Tumor-specific CD4+ T cells render the tumor environment permissive for infiltration by low-avidity CD8+ T cells. *J Immunol,* 180**,** 3122-31.

WYLIE, B., SEPPANEN, E., XIAO, K., ZEMEK, R., ZANKER, D., PRATO, S., FOLEY, B., HART, P. H., KROCZEK, R. A., CHEN, W. & WAITHMAN, J. 2015. Cross-presentation of cutaneous melanoma antigen by migratory XCR1(+)CD103(-) and XCR1(+)CD103(+) dendritic cells. *Oncoimmunology,* 4**,** e1019198.

XIE, Y., AKPINARLI, A., MARIS, C., HIPKISS, E. L., LANE, M., KWON, E. K., MURANSKI, P., RESTIFO, N. P. & ANTONY, P. A. 2010. Naive tumor-specific CD4(+) T cells differentiated in vivo eradicate established melanoma. *J Exp Med,* 207**,** 651-67.

YAJIMA, T., HOSHINO, K., MURANUSHI, R., MOGI, A., ONOZATO, R., YAMAKI, E., KOSAKA, T., TANAKA, S., SHIRABE, K., YOSHIKAI, Y. & KUWANO, H. 2019. Fas/FasL signaling is critical for the survival of exhausted antigen-specific CD8(+) T cells during tumor immune response. *Mol Immunol,* 107**,** 97-105.

YAMAMOTO, T. N., LEE, P. H., VODNALA, S. K., GURUSAMY, D., KISHTON, R. J., YU, Z., EIDIZADEH, A., EIL, R., FIORAVANTI, J., GATTINONI, L., KOCHENDERFER, J. N., FRY, T. J., AKSOY, B. A., HAMMERBACHER, J. E., CRUZ, A. C., SIEGEL, R. M., RESTIFO, N. P. & KLEBANOFF, C. A. 2019. T cells genetically engineered to overcome death signaling enhance adoptive cancer immunotherapy. *J Clin Invest,* 129**,** 1551-1565.

YIN, Z. J., JU, B. M., ZHU, L., HU, N., LUO, J., HE, M., FENG, X. Y., LV, X. H., PU, D. & HE, L. 2018. Increased CD4(+)CD25(-)Foxp3(+) T cells in Chinese systemic lupus erythematosus: correlate with disease activity and organ involvement. *Lupus,* 27**,** 2057-2068.

ZAROUR, H. M. 2016. Reversing T-cell Dysfunction and Exhaustion in Cancer. *Clin Cancer Res,* 22**,** 1856-64.

ZERAFA, N., WESTWOOD, J. A., CRETNEY, E., MITCHELL, S., WARING, P., IEZZI, M. & SMYTH, M. J. 2005. Cutting edge: TRAIL deficiency accelerates hematological malignancies. *J Immunol,* 175**,** 5586-90.

ZHANG, S., MA, X., ZHU, C., LIU, L., WANG, G. & YUAN, X. 2016. The Role of Myeloid-Derived Suppressor Cells in Patients with Solid Tumors: A Meta-Analysis. *PLoS One,* 11**,** e0164514.

ZHU, J., POWIS DE TENBOSSCHE, C. G., CANE, S., COLAU, D., VAN BAREN, N., LURQUIN, C., SCHMITT-VERHULST, A. M., LILJESTROM, P., UYTTENHOVE, C. & VAN DEN EYNDE, B. J. 2017. Resistance to cancer immunotherapy mediated by apoptosis of tumor-infiltrating lymphocytes. *Nat Commun,* 8**,** 1404.

ZHU, Z., CUSS, S. M., SINGH, V., GURUSAMY, D., SHOE, J. L., LEIGHTY, R., BRONTE, V. & HURWITZ, A. A. 2015. CD4+ T Cell Help Selectively Enhances High-Avidity Tumor Antigen-Specific CD8+ T Cells. *J Immunol,* 195**,** 3482-9.

ZIEGLER, U. & GROSCURTH, P. 2004. Morphological features of cell death. *News Physiol Sci,* 19**,** 124-8.

Chapter 8:
Appendix

Chapter 8: Appendix

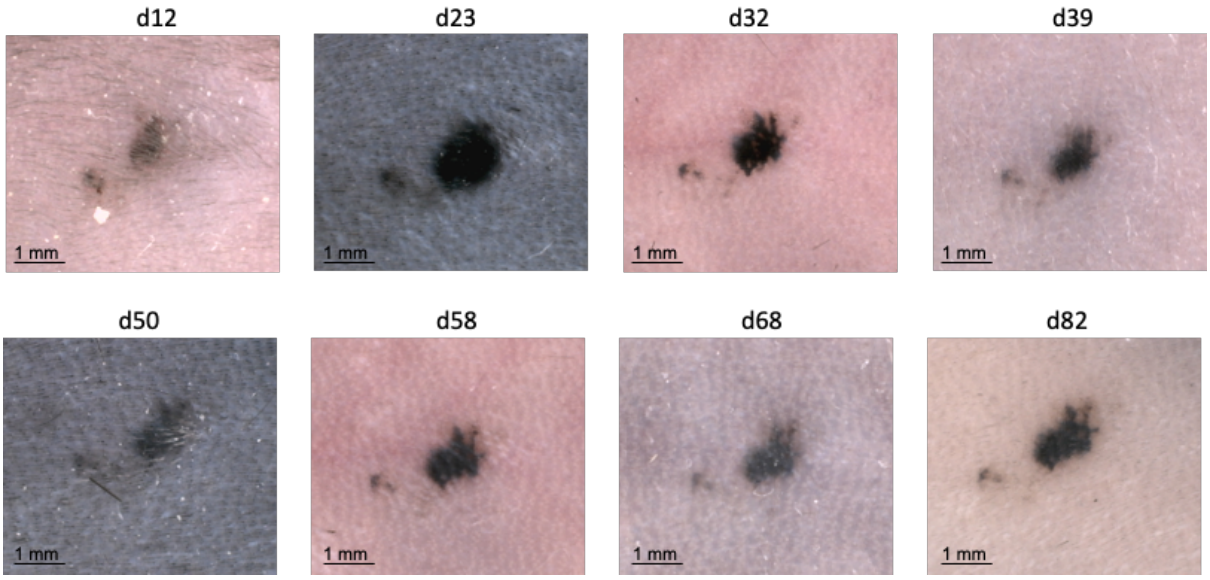

Appendix Figure 1. Photographical evidence of a persistent pigmented lesion at inoculation site.
Data from a C57BL/6 mouse challenged with B16.gD cells (1×10^5 e.c.) following transfer of naïve gDT-II.*Tbx21*$^{-/-}$ cells (1×10^4 i.v.). Photos taken by dermoscopy camera at day (d) p.i. indicated. *Histology not performed.*

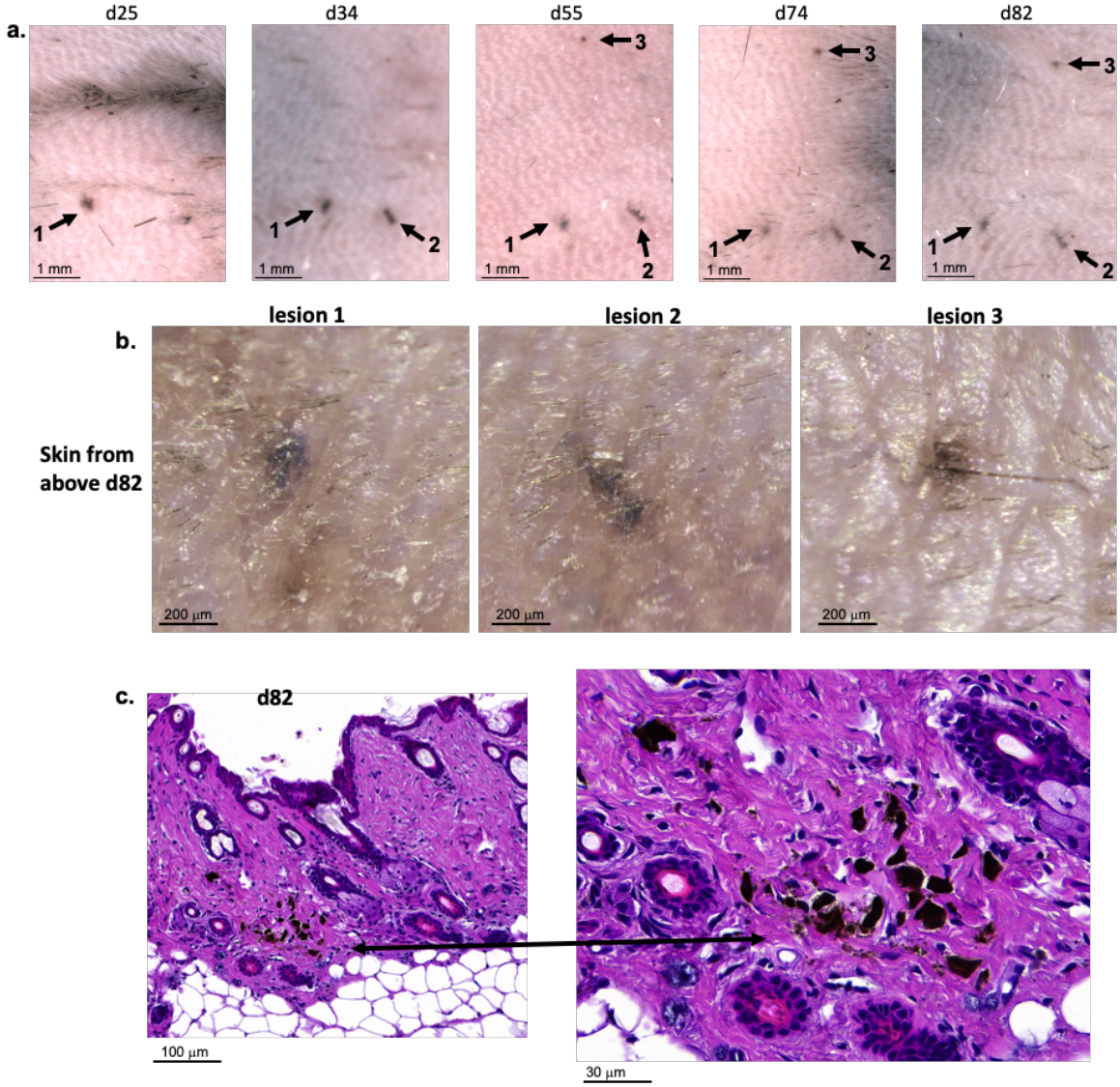

Appendix Figure 2. Photographical and histological evidence of persistent pigmented lesions at inoculation site.
Data from a C57BL/6 mouse challenged with B16.gD cells (1×10^5 e.c.) following transfer of naïve gDT-II.*Tbx21*$^{-/-}$ cells (1×10^4 i.v.). **a,** Photos taken by dermoscopy camera (lesions indicated by arrows) or **b,** by stereo microscope camera at day (d) p.i. indicated. Stereo microscope photos correspond to lesions labelled 1-3 in dermoscopy photos. **c,** H&E stain of skin section containing lesions 1 and 2 at day 82 p.i.

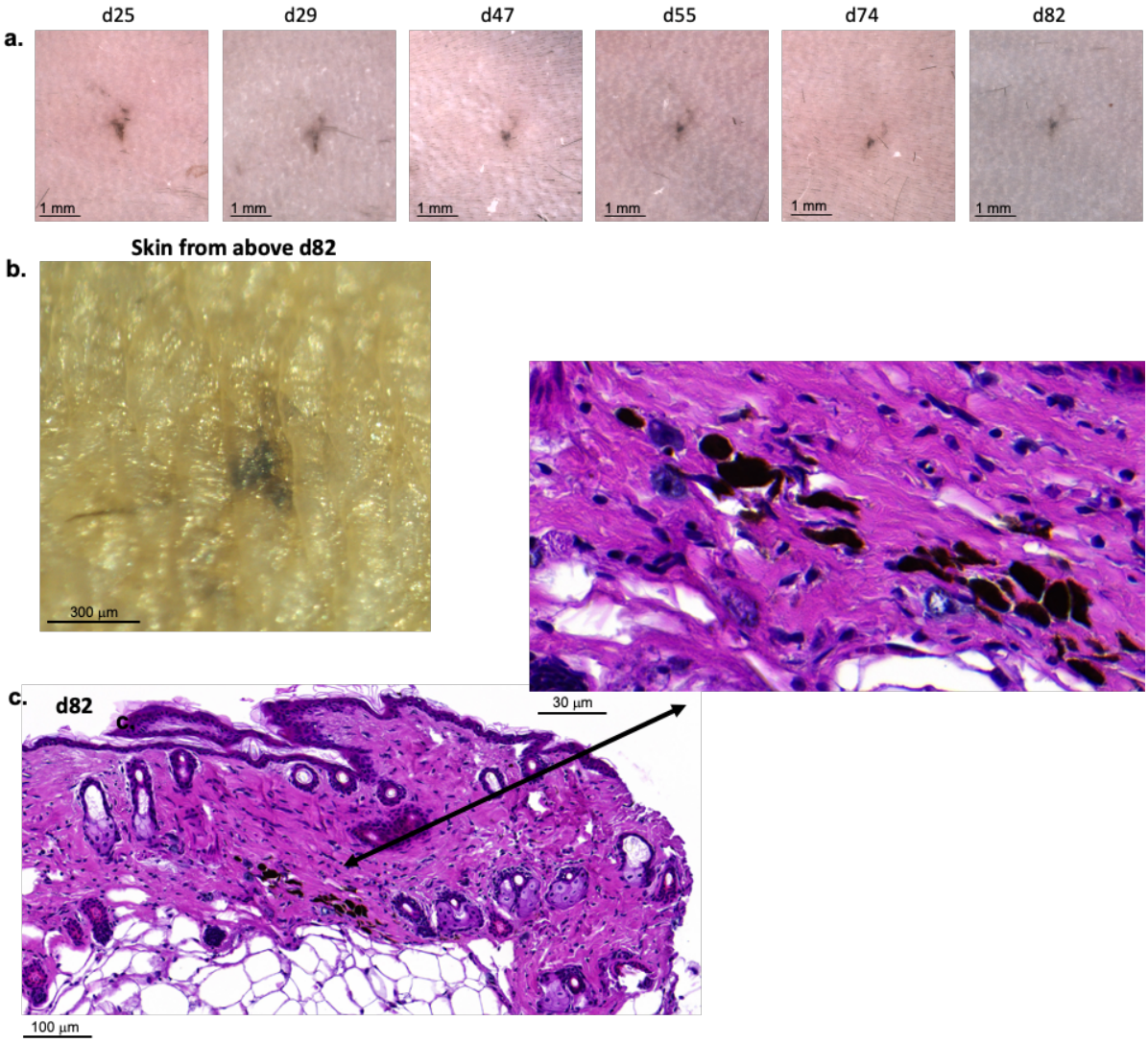

Appendix Figure 3. Photographical and histological evidence of a persistent pigmented lesion at inoculation site.
Data from a C57BL/6 mouse challenged with B16.gD cells (1×10^5 e.c.) following transfer of naïve gDT-II.*Tbx21*$^{-/-}$ cells (1×10^4 i.v.). **a,** Photos taken by dermoscopy camera or **b,** by stereo microscope camera at day (d) p.i. indicated. **c,** H&E stain of skin at day 82 p.i.

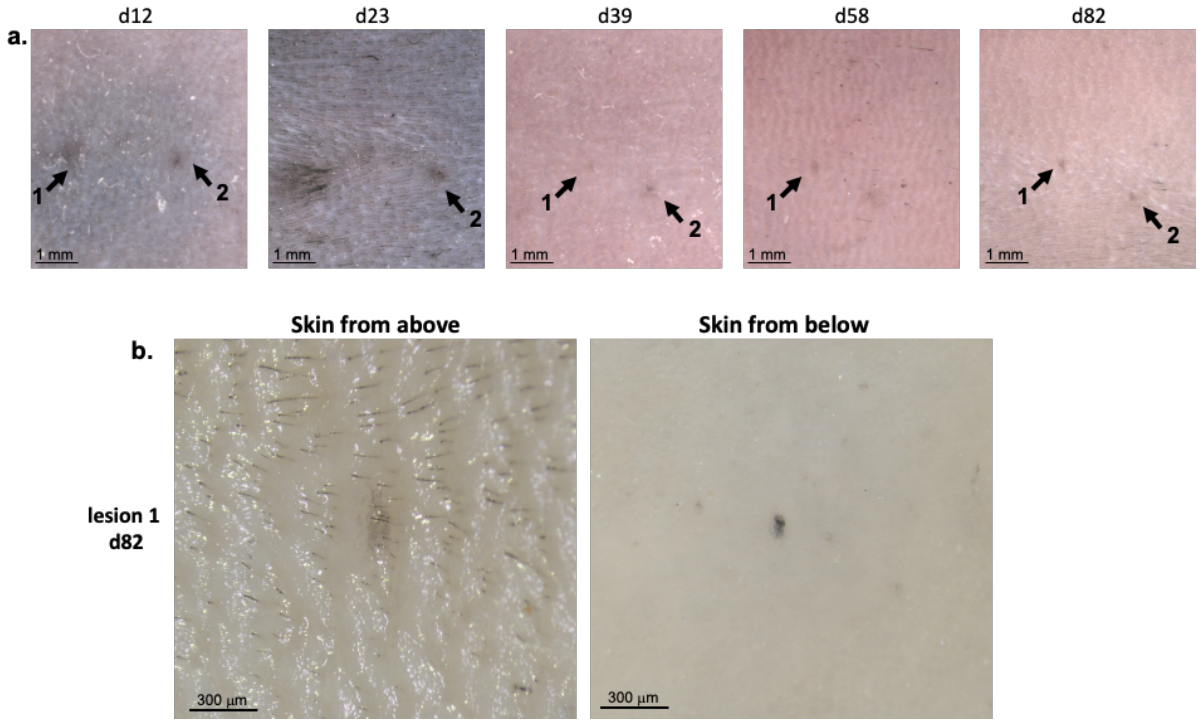

Appendix Figure 4. Photographical evidence of persistent pigmented lesions at inoculation site.
Data from a in a C57BL/6 mouse challenged with B16.gD cells (1×10^5 e.c.) following transfer of naïve gDT-II.*Tbx21*$^{-/-}$ cells (1×10^4 i.v.). **a,** Photos taken by dermoscopy camera (lesions indicated by arrows) or **b,** by stereo microscope camera at day (d) p.i. indicated. Stereo microscope photos are of the lesion labelled 1 in dermoscopy photos. *Histology not performed.*

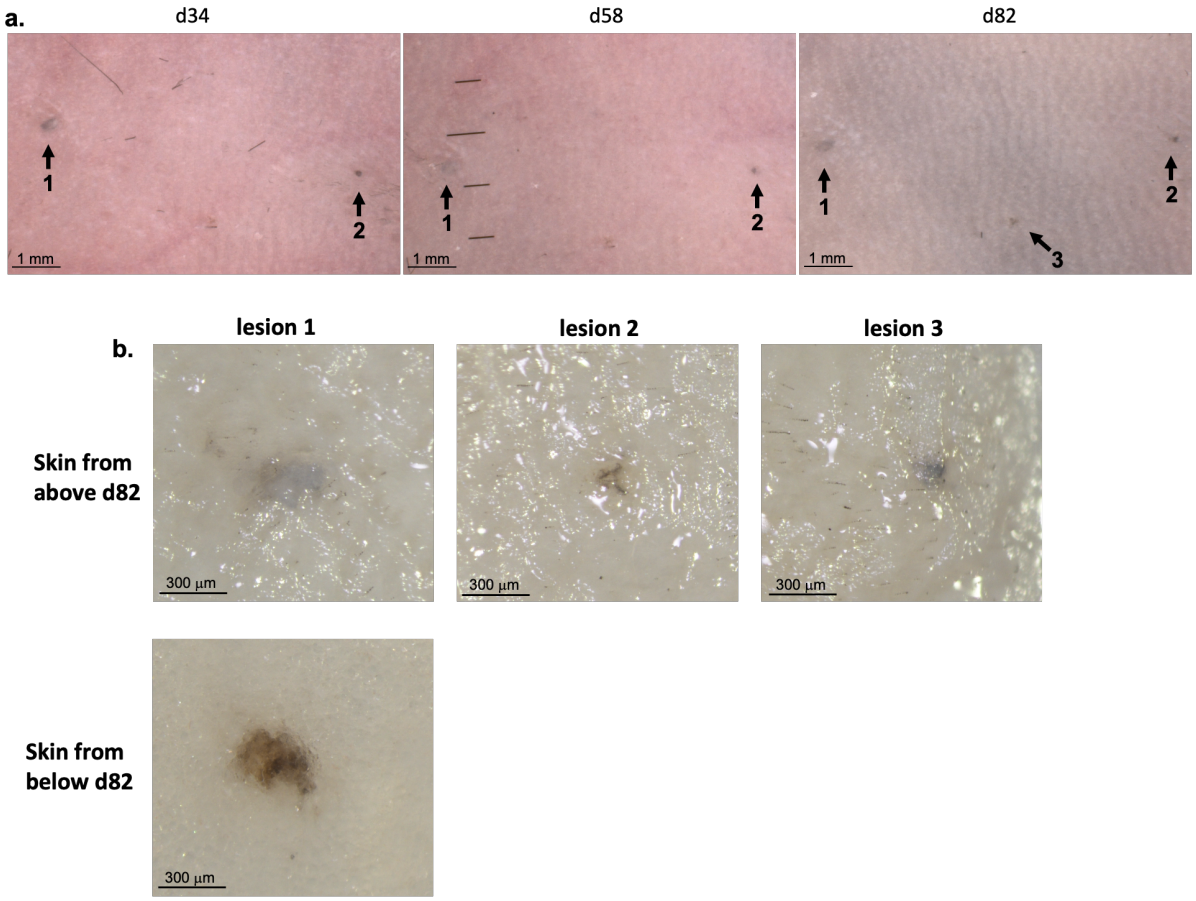

Appendix Figure 5. Photographical evidence of a persistent pigmented lesion at inoculation site.
Data from a C57BL/6 mouse challenged with B16.gD cells (1×10^5 e.c.) following transfer of naïve gDT-II cells (1×10^4 i.v.). **a,** Photos taken by dermoscopy camera (lesions indicated by arrows) or **b,** by stereo microscope camera at day (d) p.i. indicated. Stereo microscope photos correspond to lesions labelled 1-3 in dermoscopy photos. *Histology not performed.*

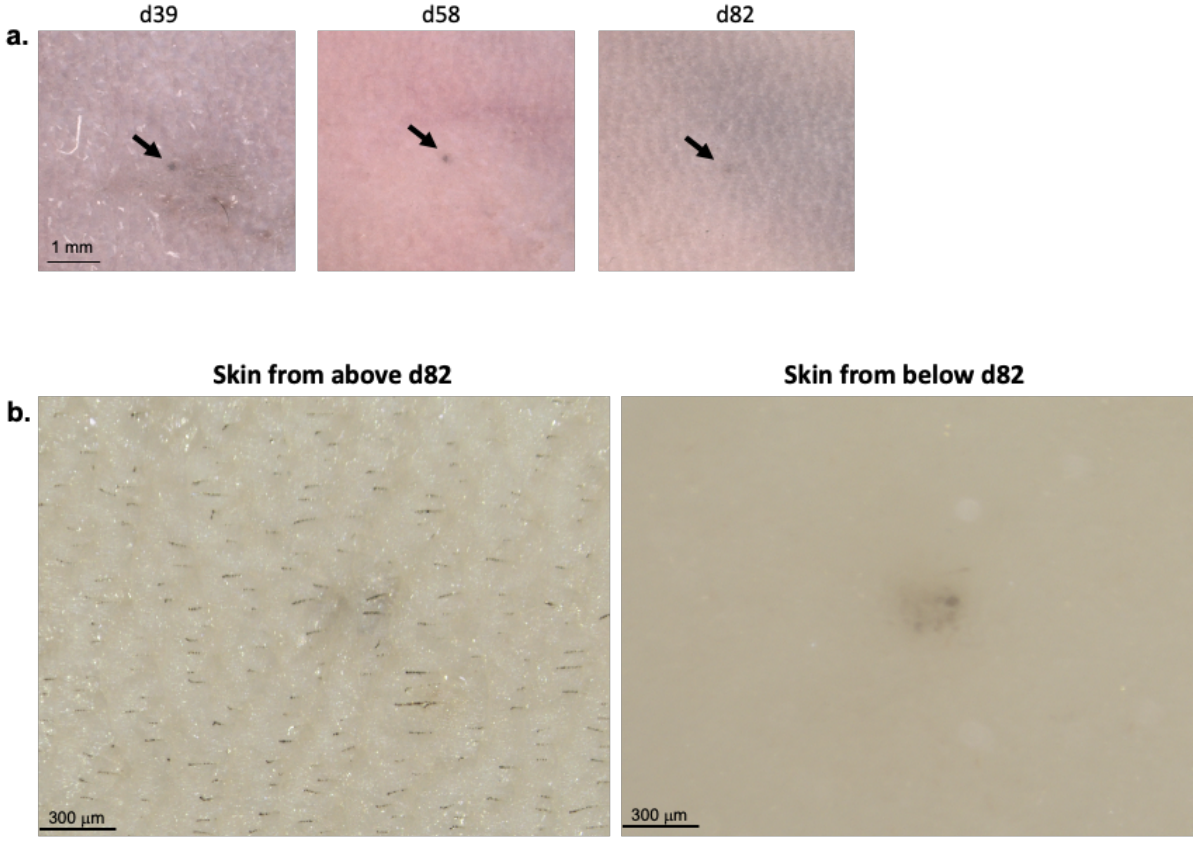

Appendix Figure 6. Photographical evidence of a persistent pigmented lesion at inoculation site.
Data from a C57BL/6 mouse that was challenged with B16.gD cells (1×10^5 e.c.) following transfer of naïve gDT-II cells (1×10^4 i.v.). **a,** Photos taken by dermoscopy camera (lesion indicated by arrows) or **b,** by stereo microscope camera at day (d) p.i. indicated. *Histology not performed.*

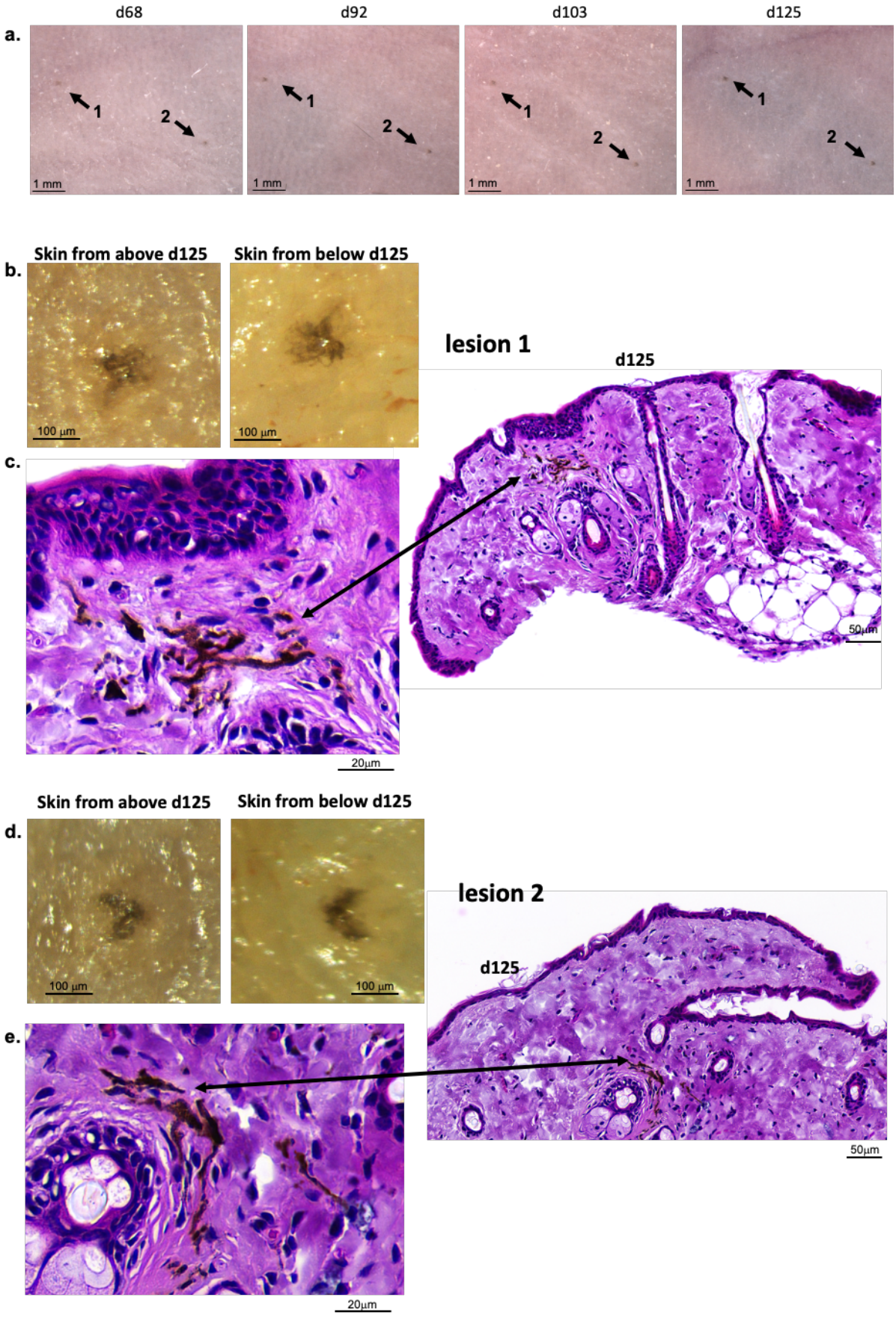
a.
d68
d92
d103
d125
1
2
1 mm
b.
Skin from above d125
Skin from below d125
100 µm
lesion 1
d125
c.
50µm
20µm
d.
Skin from above d125
Skin from below d125
100 µm
lesion 2
d125
e.
50µm
20µm

Appendix Figure 7. Photographical and histological evidence of persistent pigmented lesions at inoculation site.
Data from a *Rag2*$^{-/-}$;*Il2rg*$^{-/-}$ mouse challenged with B16.gD cells (1 × 10^5 e.c.) that received *in vitro* activated gDT-II.*Tbx21*$^{-/-}$ cells (1 × 10^6, i.v.) one week later. **a,** Photos taken by dermoscopy camera at day (d) p.i. indicated. Two lesions (1 and 2) indicated by arrows. **b.** Photos of lesion 1 taken by stereo microscope camera at day 125. **c,** H&E stain of lesion 1 at day 125 p.i.. **d.** Photos of lesion 2 taken by stereo microscope camera at day 125. c. **e,** H&E stain of lesion 2 at day 125 p.i.

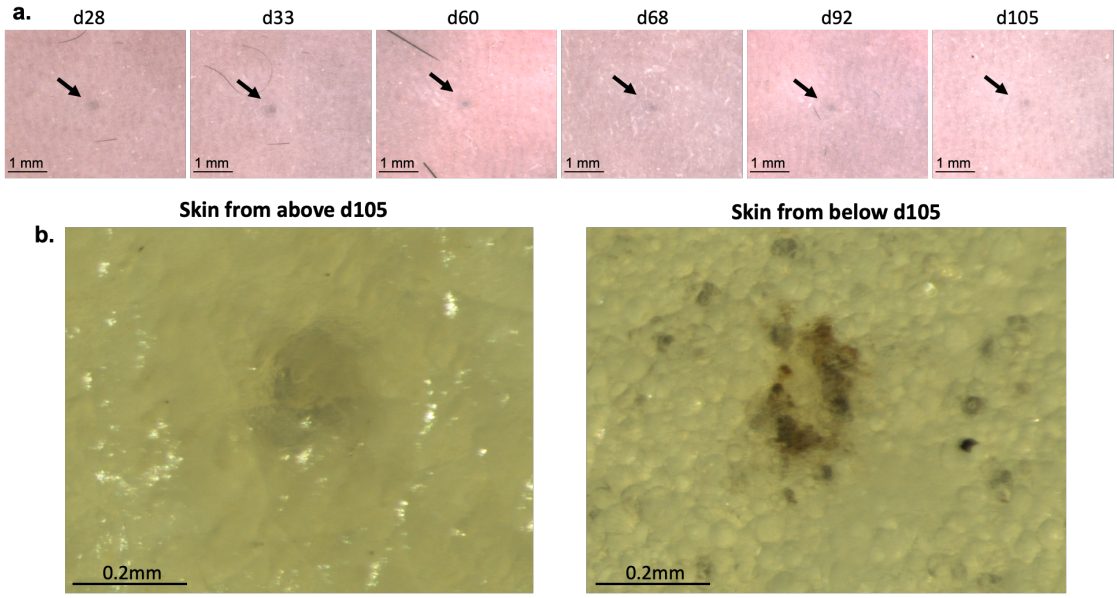

Appendix Figure 8. Photographical evidence of a persistent pigmented lesion at inoculation site.
Data from a *Rag2*$^{-/-}$;*Il2rg*$^{-/-}$ mouse challenged with B16.gD cells (1 × 10^5 e.c.) that received *in vitro* activated gDT-II.*Tbx21*$^{-/-}$ cells (1 × 10^6, i.v.) one week later. **a,** Photos taken by dermoscopy camera (lesion indicated by arrows) or **b,** by stereo microscope camera at day (d) p.i. indicated. *Histology not performed.*

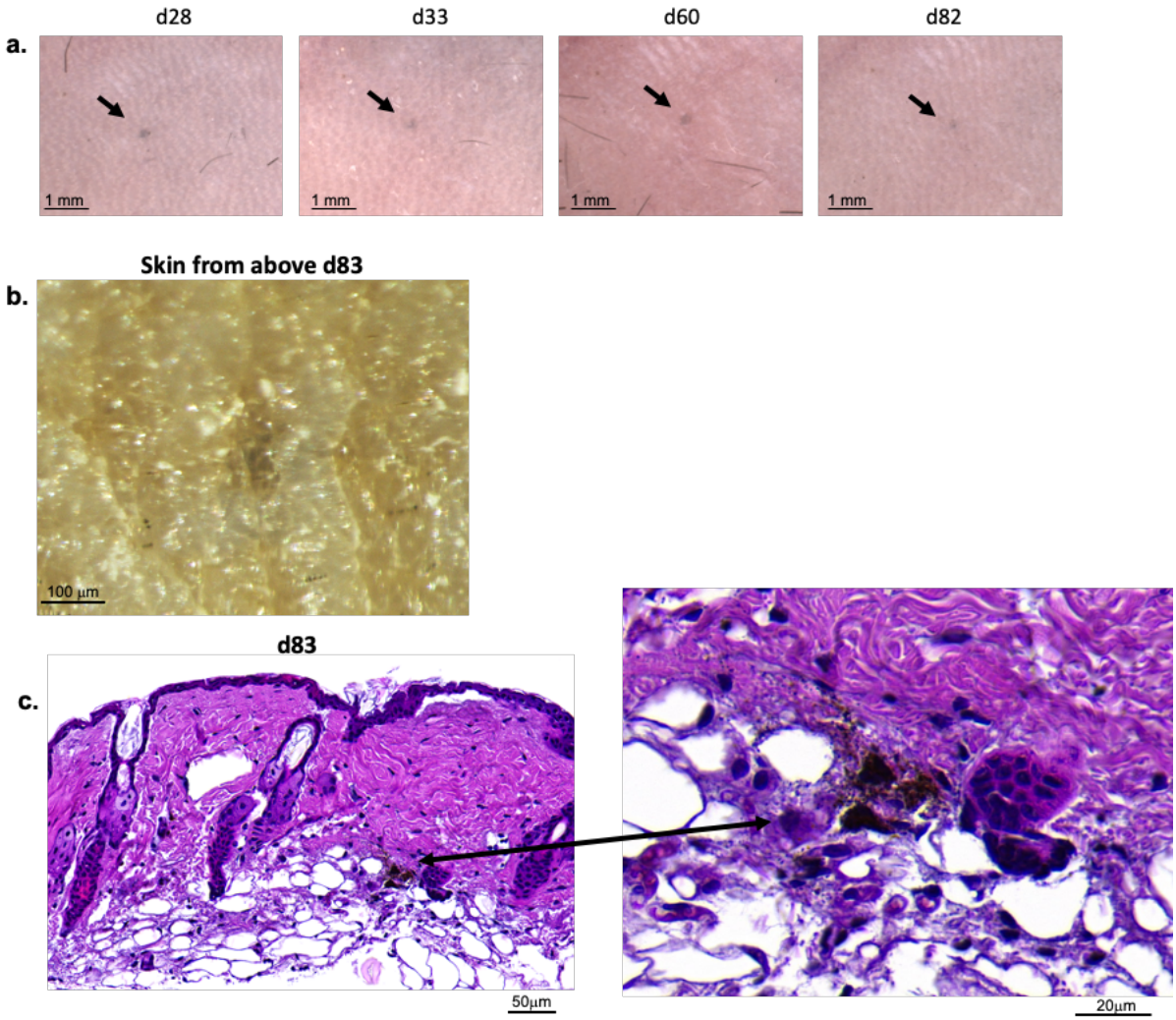

Appendix Figure 9. Photographical and histological evidence of persistent pigmented lesion at inoculation site.
Data from a naïve *Rag2*$^{-/-}$;*Il2rg*$^{-/-}$ mouse challenged with B16.gD cells (1 × 10^5 e.c.). **a,** Photos taken by dermoscopy camera (lesion indicated by arrows) or **b,** by stereo microscope camera at day (d) p.i. indicated. **c,** H&E stain at day 83 p.i.

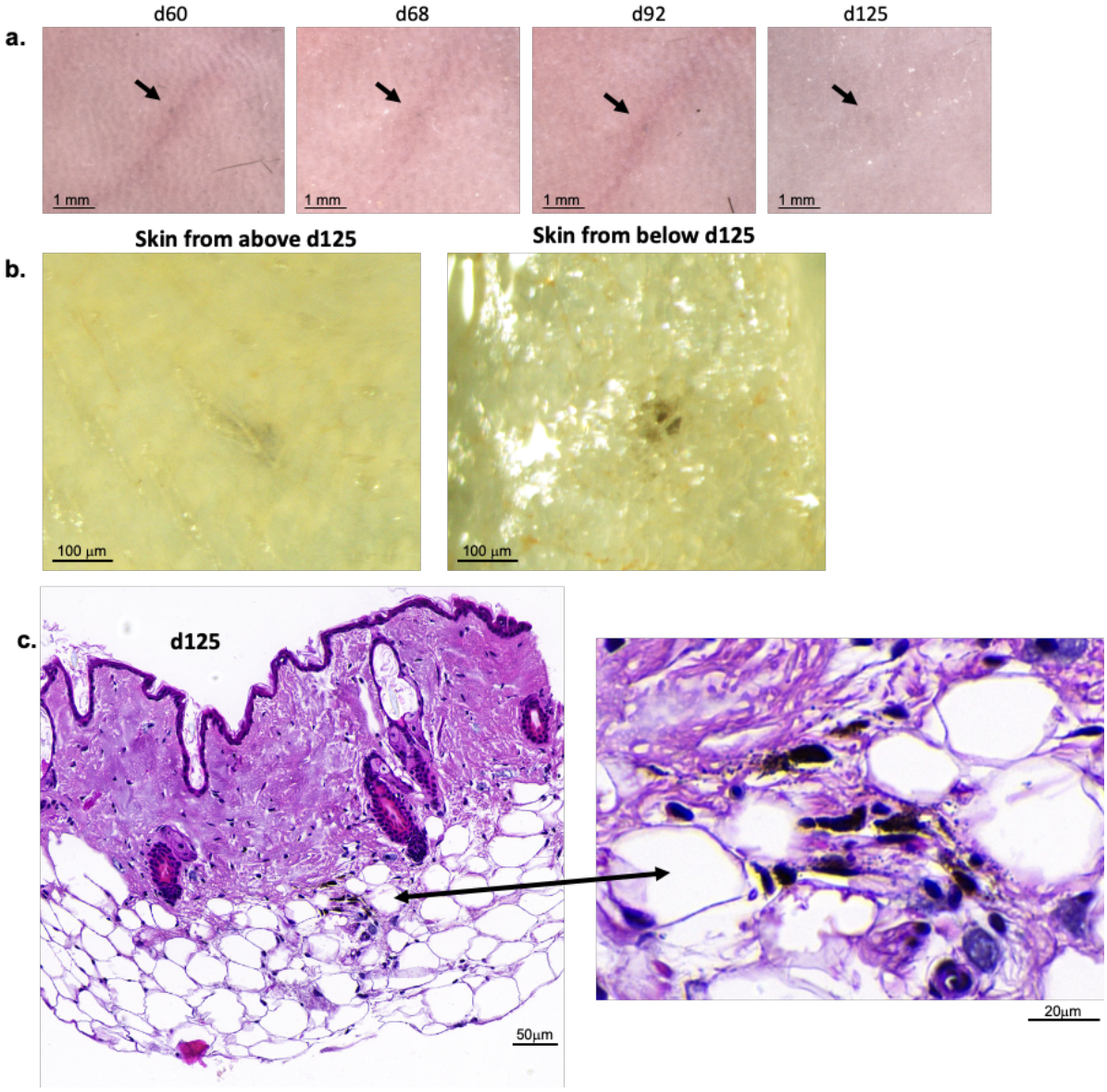

Appendix Figure 10. Photographical and histological evidence of persistent pigmented lesion at inoculation site.
Data from a naïve *Rag2*$^{-/-}$;*Il2rg*$^{-/-}$ mouse challenged with B16.gD cells (1 × 10^5 e.c.). **a,** Photos taken by dermoscopy camera (lesion indicated by arrows) or **b,** by stereo microscope camera at day (d) p.i. indicated. **c,** H&E stain at day 125 p.i.

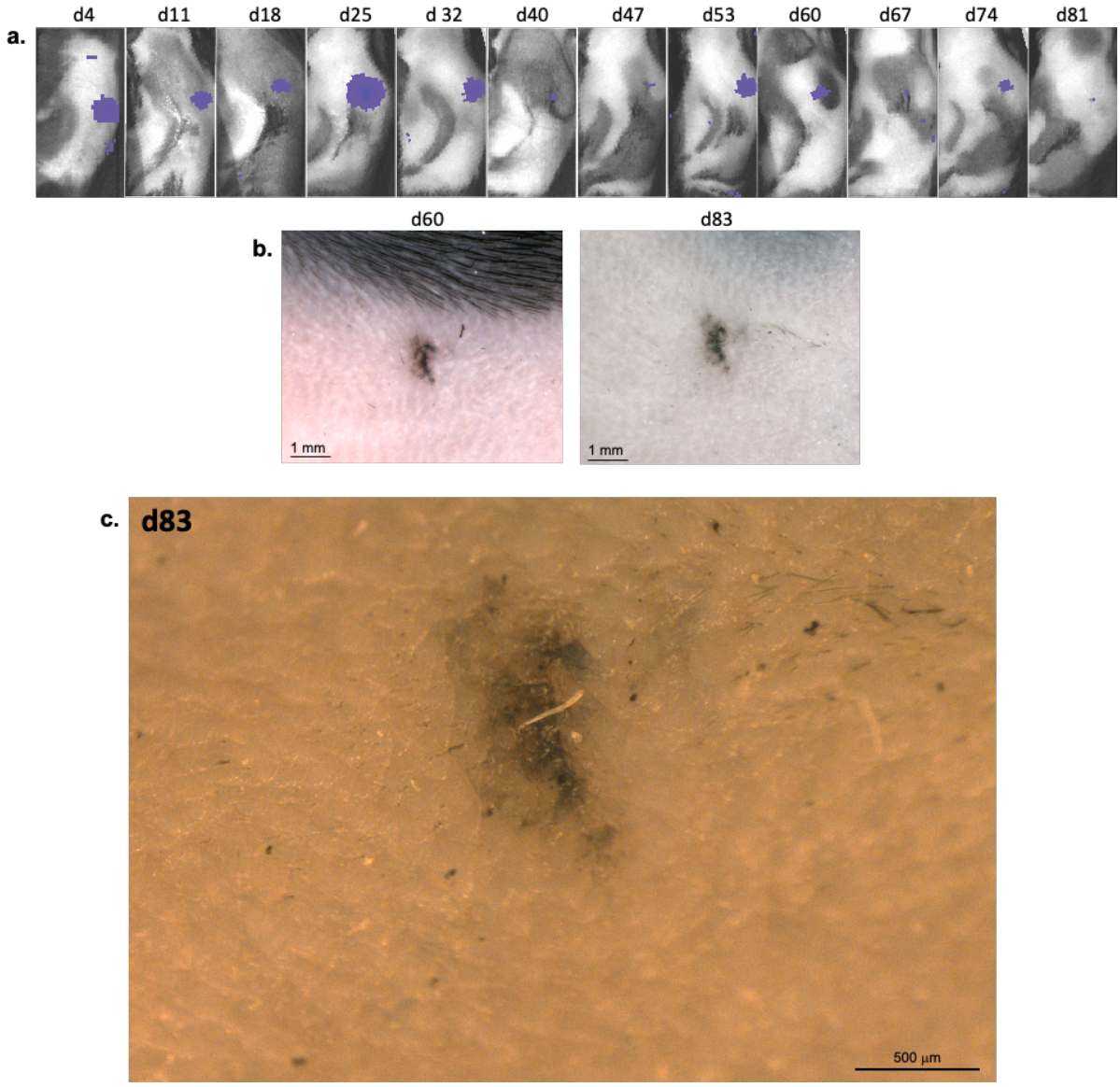

Appendix Figure 11. Persistence of melanoma lesion in a Cd40$^{-/-}$ mouse. *Cd40*$^{-/-}$ mouse inoculated with B16.gD.Luc.mScar (1 × 10^5 e.c.). **a,** Longitudinal monitoring of bioluminescence signals using In Vivo Imaging Software (IVIS). **b,** Photos taken by dermoscopy camera or **c,** by stereo microscope camera. Photos taken on day (d) p.i. indicated. *IVIS imaging performed by David Freestone.*

Appendix Video 1: Tracking T cell priming in the lymph nodes by light-sheet microscopy.
Albino mouse (mouse 1) received 1 × 10^4 naïve gDT-II.GFP cells and was challenged with B16.gD.*Tyr*$^{-/-}$.mCherry cells (1 × 10^5 e.c.) the following day. Images from light-sheet microscopy of lymph nodes (ipsilateral brachial, ipsilateral auxiliary, contralateral inguinal) 8 days p.i.. Green; gDT-II.GFP, white; autofluorescence. *Light-sheet microscopy performed by Teagan Wagner.*
https://doi.org/10.22000/459

Appendix Video 2: Tracking T cell priming in the lymph nodes by light-sheet microscopy.
Albino mouse (mouse 2) received 1 × 10^4 naïve gDT-II.GFP cells and was challenged with B16.gD.*Tyr*$^{-/-}$.mCherry cells (1 × 10^5 e.c.) the following day. Images from light-sheet microscopy of lymph nodes (ipsilateral brachial, ipsilateral auxiliary, contralateral inguinal) 8 days p.i.. Green; gDT-II.GFP, white; autofluorescence. *Light-sheet microscopy performed by Teagan Wagner.*
https://doi.org/10.22000/459

Appendix Video 3: Visualisation of CD4$^+$ T cells and melanoma cells in the skin using two-photon microscopy.
Two-photon microscopy video of the skin at the site of tumor inoculation 8 days p.i. in an albino C57BL/6 mouse. Mouse received 1 × 10^4 naïve gDT-II.GFP cells (green) intravenously, one day prior to e.c. challenge with 1 × 10^5 B16.gD.*Tyr*$^{-/-}$.mCherry cells (red). Second harmonic generation signal (SHG) shown in white and autofluorescence of hair appears yellow/green. *Two-photon microscopy performed in collaboration with Teagan Wagner.*
https://doi.org/10.22000/459

Appendix Video 4: Visualisation of CD4$^+$ T cells and melanoma cells in the skin using two-photon microscopy.
Two-photon microscopy video of the skin at the site of tumor inoculation 8 days p.i. in an albino C57BL/6 mouse. Mouse received 4 × 10^4 naïve gDT-II.GFP cells (green) intravenously, one day prior to e.c. challenge with 1 × 10^5 B16.gD.*Tyr*$^{-/-}$.mCherry cells (red). Second harmonic generation signal (SHG) shown in white and autofluorescence of hair appears yellow/green. *Two-photon microscopy performed in collaboration with Teagan Wagner.*
https://doi.org/10.22000/459